Towards the identification and characterization of new regulators of fruit tissue morphology

Constance Musseau

THESE

Présentée pour l'obtention du grade de
DOCTEUR DE L'UNIVERSITÉ DE BORDEAUX
École Doctorale des Sciences de la Vie et de la Santé

Spécialité : Biologie Végétale

Par

Constance MUSSEAU

Towards the identification and characterization of new regulators of fruit tissue morphology

-

Vers l'identification et la caractérisation de nouveaux régulateurs de la morphologie des tissus du fruit

Sous la direction de Lucie FERNANDEZ-LOCHU et Frédéric GEVAUDANT
Présentée et soutenue publiquement le 14 Décembre 2018

Direction	Mme. Lucie FERNANDEZ-LOCHU - Chargée de recherche, *INRA Bordeaux*
Président	M. Michel HERNOULD - Professeur, *Université de Bordeaux*
Rapporteurs	M. David BOUCHEZ - Directeur de recherche, *INRA Versailles* M. Jose JIMENEZ-GOMEZ - Chargé de recherche, *INRA Versailles*
Examinateurs	Mme Mathilde CAUSSE - Directrice de recherche, *INRA Avignon* Mme Sabine MÜLLER - Directrice de recherche, *Université de Tübingen* M. Christophe TREHIN - Maître de conférences, *École Nationale Supérieure de Lyon*
Invité	M. Frédéric GEVAUDANT - Maître de conférences, *Université de Bordeaux*

à Pipou,

« *Dans la vie, rien n'est à craindre, tout est à comprendre*. »

Marie Sklodowska-Curie

-

« *In life, nothing is to be feared, everything is to understand*."

Marie Sklodowska-Curie

Remerciements

Je tiens dans un premier temps à adresser mes remerciements aux membres de mon jury, Michel Hernould, David Bouchez, José Jimenez-Gomez, Sabine Müller, Christophe Trehin et Mathilde Causse, d'avoir accepté de juger ce travail de thèse.

Un très grand merci à Lucie Fernandez-Lochu et Frédéric Gévaudant. Merci pour votre bienveillance, votre soutien, votre gentillesse et vos rires pendant ces quatre dernières années. Depuis le stage de Master 2, en passant par le concours de l'école doctorale et les nombreux retournements de situation au cours de ma thèse, vous avez toujours su me soutenir, m'encourager et me motiver. Apprendre le métier de chercheur à vos côtés a été une vraie chance ; j'espère, comme vous, être toujours aussi passionnée, enjouée et excitée par la recherche. Une chose est sûre, vous allez profondément me manquer !

Je voudrais remercier Christian Chevalier et Christophe Rothan d'avoir toujours répondu présents pour m'entraîner aux examens, au concours de l'école doctorale, aux présentations orales et pour les nombreuses discussions autour de mon sujet de thèse. Merci également pour votre aide dans la correction de ce manuscrit. Je remercie aussi Martine Lemaire-Chamley, Nathalie Frangne, Jean-Pierre Renaudin et Catherine Cheniclet pour votre écoute et vos conseils. Je tiens à remercier chaleureusement Joana Jorly, Stéphanie Gadin et Jean-Philippe Mauxion pour le soutien technique, Isabelle Atienzia-Babin et Aurélie Honoré pour l'aide cruciale en serre, Lysiane Brocard et Leslie Bancel-Vallée pour l'aide à la plateforme de microscopie. Merci également à Catherine Deborde et Stephane Merillon pour m'avoir formée à l'extraction des métabolites et l'aide pour l'analyse et l'interprétation des résultats.

Faire une thèse en « garde alternée » dans deux équipes de recherche implique certes, beaucoup de réunions d'équipe, mais s'est avérée être une occasion unique de travailler et d'apprendre à connaître de chouettes personnes ! Merci à Nathalie Gonzalez, Frédéric Delmas, Cécile Brès, Daniel Just, Aline Potier, Johann Petit, Pierre Baldet, Amelia Gaston, Beatrice Denoyes, Edouard Tourdot et tous les autres, pour les conversations sans queue ni tête, les encouragements, les blagues ou les simples sourires dans les couloirs. Vous avez tous, de près ou de loin, contribué à mon épanouissement pendant ces quatre dernières années.

Je tiens également à remercier les chercheurs que j'ai pu rencontrer au cours de mon cursus universitaire et qui m'ont donnée envie de faire ce métier. Je pense notamment à Michel Hernould et à Benjamin

Péret. Je voudrais remercier l'équipe de recherche de Sabine Müller à l'université de Tübingen, pour m'avoir accueillie dans son laboratoire pendant trois mois. J'ai énormément appris pendant ce séjour et je suis plus déterminée que jamais à abandonner la tomate au profit d'*Arabidopsis thaliana*.

Merci à mes compagnons de bureau Paul, Isma, Alice, Jiao-Jiao, qui ont rendu la thèse plus fun et bien plus encore !

Bien sûr, toute ma gratitude revient à mes parents. Merci de m'avoir laissée libre de mes choix et de m'avoir toujours encouragée. J'espère vous rendre fiers et surtout, j'espère qu'un jour vous comprendrez ce que je fais dans la vie ! Travailler dans la tomate n'est pas un métier ! Merci à mes grandes sœurs Elodie et Laura et à mon grand frère Antoine pour les encouragements : « Si Antoine l'a fait, tu peux le faire ! ». Merci à mes chères amies Marie, Elodie et Justine qui me suivent depuis le lycée. Merci pour votre soutien dans les moments difficiles, et même si vous êtes loin, les émojis chat et hibou, ça aide beaucoup ! Enfin, il n'y a pas de mots assez forts pour exprimer toute ma reconnaissance envers mon amoureux Valentin qui, en plus de m'avoir supportée pendant ces trois années de thèse, m'a toujours soutenue et épaulée. Je n'en serais certainement pas là sans toi. Allez viens, on s'en va en Amérique !

Abstract of the thesis

The fruit is a plant specific organ offering a suitable environment for seed maturation and proper embryo development. Using the large fruit natural diversity, human domestication and selection have clearly triggered changes in fruit size and morphology within the same species. Previous studies aimed at understanding the genetic basis of fruit size and fruit shape variations and allowed identifying six QTLs and their underlying genes, mainly involved in cell division and stem cell identity during flower and early fruit development. These genes explain up to 71% of the fruit size and shape variation observed in the cultivated tomato. However, these few genes are unlikely to represent the entire repertoire of regulators involved in the fruit morphology determination. In this context, the main objective of my PhD work was to identify new regulators of fruit tissue morphology in tomato and understand their role during fruit growth.

First, I finalized the genetic screen of a tomato EMS mutant collection as to select mutants exhibiting strong and stable alterations in fruit size and tissue morphology. This multi-scale phenotyping revealed that fruit growth in these EMS mutants is controlled by two major processes: 1) an isotropic pericarp cell expansion associated with a proportional growth of all fruit tissues, and 2) an anisotropic cell expansion boosting pericarp growth only (Musseau *et al.*, 2017). Then, I selected two mutants with opposite anisotropic cell expansion direction inducing drastic alterations of pericarp thickness, without altering the final fruit size. The P30A9 mutant developed a very thick pericarp contrary to the P3D3 mutant characterized by a thin pericarp.

The thick pericarp phenotype in P30A9 is associated with an increase in pericarp cell volume and a higher proportion of nuclei with high ploidy levels. As a response to compensate the reduction in fruit growth observed at 15 DPA, the ploidy level in pericarp cells of P30A9 increased between 15 to 20 DPA, together with a rapid increase in cell volume that triggers fruit growth as to reach a normal fruit size. To identify the gene underlying this phenotype, I developed the mapping-by-sequencing strategy for P30A9, from the generation of a F2 segregant population to the recombinant analysis of the candidate regions. This work revealed a range of phenotypic expression of the pericarp thickness in the F2 segregant population possibly involving incomplete penetrance, variable expressivity and/or additive genetic effects. Despite these difficulties, I highlighted different genetic regions associated with pericarp morphology modification in P30A9, including a region of around 20 cM on chromosome 10, supposedly causing the extreme

increase in pericarp thickness observed in P30A9. In depth phenotypic and genetic analyses are further required to unravel the genetic complexity of P30A9.

Last, I initiated the functional characterization of the Guanylate-Binding Protein (GBP), which is mutated in P3D3. GBP is a large GTP binding protein that has never been described in plants and belongs to the DYNAMIN protein superfamily. Plant DYNAMIN proteins have been shown to participate in many cellular processes such as cytokinesis and endocytosis. The strong reduction in pericarp thickness of P3D3 is concomitant to reduced cell size and ploidy levels. Pericarp in P3D3 fruits exhibited late and extreme defects with the occurrence of cell division patterns once no more divisions take place in the pericarp, as well as aberrant polyploid nucleus morphology. Both tomato and *Arabidopsis* GBP proteins are localized in precise nuclear regions. Interestingly, CRISPR mutants generated in Arabidopsis and tomato are both characterized by a strong reduction in lateral root growth, a classical feature of mutants impaired in mitosis. This functional characterization suggests a role for GBP in the fine control of cell division in the pericarp.

Résumé de la thèse

Le fruit est un organe spécifique de la plante offrant un environnement propice à la maturation des graines et au développement de l'embryon. En utilisant la diversité naturelle des fruits, la domestication humaine et la sélection ont entraîné de profonds changements de la taille du fruit et de la morphologie des tissus, au sein de la même espèce. De précédentes recherches, visant à comprendre la base génétique de ces variations, ont permis d'identifier six QTLs et leurs gènes sous-jacents, principalement impliqués dans la division cellulaire et l'identité des cellules souches, au cours du développement précoce de la fleur et du fruit. Ces gènes expliquent, à eux seuls, jusqu'à 71% des variations de tailles et de formes du fruit observées chez la tomate cultivée. Cependant, il est évident que ces quelques gènes ne contrôlent pas toute la diversité de morphologie observée. De plus, les mécanismes cellulaires et moléculaires par lesquels la morphologie des tissus du fruit est définie restent imprécis. Dans ce contexte, l'objectif principal de ma thèse est d'identifier de nouveaux régulateurs de la morphologie des tissus du fruit chez la tomate et de comprendre leur rôle pendant la croissance du fruit.

Pour cela, j'ai dans un premier temps finalisé le criblage génétique d'une collection de mutants EMS de tomates, afin de sélectionner des mutants présentant des altérations de taille et de morphologie du fruit. Cette étude a révélé que la croissance des fruits chez ces mutants EMS est contrôlée par deux processus principaux: 1) une expansion isotrope des cellules du péricarpe associée à une croissance proportionnelle de tous les tissus du fruit, et 2) une expansion anisotrope des cellules stimulant la croissance du péricarpe uniquement (Musseau *et al.*, 2017). A la suite de cette étude, j'ai sélectionné deux mutants de tomate présentant une direction d'expansion anisotrope opposée, ainsi que des modifications drastiques de l'épaisseur du péricarpe, sans modification de la taille finale du fruit. Ces deux mutants, le mutant P30A9 caractérisé par un péricarpe très épais et le mutant P3D3 caractérisé par un péricarpe fin, font l'object de la suite de ma thèse. Par une caractérisation phénotypique au cours de la croissance du fruit, j'ai montré que le péricarpe épais chez le mutant P30A9 est associé à une augmentation du volume des cellules du péricarpe et à une proportion plus importante de noyaux de niveaux de ploïdie élevés (128C et 256C). En réponse à la réduction de croissance du fruit observée à 15 DPA, une augmentation du niveau de ploïdie dans les cellules du péricarpe entre 15 et 20 DPA déclenche une augmentation rapide du volume cellulaire et de la croissance du fruit, pour atteindre la taille finale du fruit attendue. Afin d'identifier le gène sous-jacent à ce phénotype d'intérêt, j'ai développé la stratégie de cartographie par séquençage pour le mutant P30A9, depuis la génération de la population en ségrégation jusqu'à l'analyse de recombinants

des régions candidates. Ce travail a révélé une gamme d'expressions du phénotype dans la population en ségrégation, pouvant impliquer une pénétrance incomplète, une expressivité variable ou des effets génétiques additifs. Malgré ces difficultés, j'ai mis en évidence différentes régions associées à la modification de la morphologie du péricarpe chez le mutant P30A9, dont une région d'une vingtaine de cM sur le chromosome 10. Des analyses phénotypiques et génétiques approfondies sont nécessaires afin de comprendre la complexité génétique de P30A9 et d'identifier la mutation causale.

Enfin, j'ai initié la caractérisation fonctionnelle de la Guanylate Binding Protein (GBP), qui est mutée chez le mutant P3D3. La GBP est une grosse GTP binding protein qui n'a jamais été décrite chez les plantes et qui fait partie de la famille des DYNAMIN. Il a été démontré que les DYNAMIN participent à de nombreux processus cellulaires chez les plantes, tels que la cytokinèse et l'endocytose. La forte réduction d'épaisseur du péricarpe caractéristique du mutant P3D3 est associée à la réduction de taille des cellules du péricarpe et du niveau de ploïdie de leurs noyaux. Le péricarpe présente également des défauts tardifs et extrêmes d'organisation cellulaire, avec notamment l'apparition tardive de plans de division et une morphologie de noyau polyploïde aberrante. Afin d'approfondir l'étude de cette protéine, j'ai étudié en parallèle son rôle dans les modèles tomate et *Arabidopsis thaliana*. Les GBPs de tomate et d'*Arabidopsis* sont localisées dans des zones précises du noyau. De plus, les mutants CRISPR générés chez *Arabidopsis* et chez la tomate se caractérisent tous deux par une forte réduction de la croissance des racines latérales, classiquement retrouvée chez les mutants altérés dans la mitose. Cette caractérisation fonctionnelle suggère que la GBP joue un rôle dans le contrôle précis des divisions cellulaires dans le péricarpe.

Host laboratory

This thesis was financed by the French Ministry of National Education, Higher Education and Research. It was done under the supervision of Lucie Fernandez-Lochu and Frédéric Gévaudant, within the team “Fruit Organogenesis and Endoreduplication”, directed by Christian Chevalier, and “Functional Genomic of Fruit Development” directed by Martine Lemaire-Chamley, parts of the UMR 1332 Fruit Biology and Pathology at INRA Bordeaux-Aquitaine.

Table of contents

Part II: Functional characterization of the Guanylate Binding Protein: case of P3D3 mutant

Results

Discussion

List of abbreviations

- Protein

ABP	ACTIN-BINDING PROTEIN
AG	AGAMOUS
APC	ANAPHASE-PROMOTING COMPLEX
ARP	ACTIN-RELATED PROTEIN
AUR	AURORA
CAK	CDK-ACTIVATING KINASE
CDK	CYCLIN DEPENDANT KINASE
CNR1	CELL NUMBER REGULATOR 1
CLV	CLAVATA
CYC	CYCLIN
DYN	DYNAMIN
FAS	FASCIATED
FW2.2	FRUIT WEIGHT 2.2
FW2.3	FRUIT WEIGHT 3.2
GBP	GUANYLATE BINGIN PROTEIN
KLCR1	KINESIN LIGHT CHAIN-RELATED PROTEIN-1
LC	LOCULE NUMBER
MAP	MICROTUBULE-ASSOCIATED PROTEIN
MIF	MITOSIS-INDUCING FACTOR
OFP	OVATE FAMILY PROTEIN
OV	OVATE
SIM	SIAMESE
SPR	SPIRAL
SMR	SIAMESE RELATED
TAN	TANGLED
TON	TONNEAU
TOR	TORTIFOLIA
WUS	WUSCHEL
YAB	YABBY

- Unit of measure

°C	Degree Celsius
OD	Optical Density
cm	Centimeter

g	Gram
h	Hour
L	Liter
M	Mole
min	Minute
v/v	Volume/Volume
w/v	Weight/Volume
bp	Base pair
s	Second

- Others

AA	Amino Acid
ABD	Actin-Binding Domain
ACT	Actin
ADP, ATP	Adenosine 5’ di/triphosphate
ADZ	Actin-Depleted Zone
AS	Antisens
BY-2	Bright Yellow 2
Chr	Chromosome
CDS	Cortical Division Site
CDZ	Cortical Division Zone
CRISPR	Clustered Regularly Interspaced Short Palindromic Repeats
Ct	Control
DAPI	4',6-diamidino-2-phénylindole
DAS	Days After Seedlings
DNA	Deoxyribonucleic acid
DP	Read Depth
cDNA	complementary Deoxyribonucleic acid
gDNA	genomic Deoxyribonucleic acid
DNAse I	Deoxy ribonuclease I
DPA	Days post anthesis
dNTP	Deoxy nucleotide 5’ triphosphate (dATP, dCTP, dGTP, dTTP)
EDTA	Ethylene diamine tetra acetic
ER	Endoreduplication Factor
FAA	Formaldehyde Acetic Acid
FRET	Fluorescence Resonant Energy Transfer
GDP	Guanosine diphosphate
GFP	Green Fluorescent Protein
GMPc	Guanosine monophosphate cyclic
GTP	Guanosine triphosphate

GTPase	Guanosine triphosphate hydrolase
INDELs	Insertions, deletions
IP	Propidium iodide
KO	Knocked-out
LD	Linkage Desequilibrium
mQ	MilliQ
MBD	Microtubule-Binding Domain
MBS	Mapping-by-sequencing
MS	Murashige and Skoog medium
MT	Micro-Tom
MTs	Microtubules
MUT	Mutant
NGS	Next-Generation Sequencing
OE	Overexpression
ORF	Open reading frame
PBS	Phosphate buffer saline
PCA	Principal Component Analysis
PCR	Polymerase Chain Reaction
qPCR	quantitative PCR
PI	Ploidy Index
PBB	Preprophase band
QTLs	Quantitative Trait Locus
RFP	Red Fluorescent Protein
RNA	Ribonucleic acid
mRNA	messenger RNA
RNAi	RNA interference
RNAseq	RNA sequencing
rpm	Rotation per minute
RT-PCR	Reverse-transcription PCR
SD	Standard deviation
SDS	Sodium dodecyl sulfate
SEM	Scanning Electron Microscopy
SgRNA	Single guide RNA
SNP	Single nucleotide polymorphism
TBS	Tris buffer saline
TIBA	2,3,5-triiodobenzonic acid
TPMT	Transmitted light detector
TRM	TONNEAU RECRUITING MOTIF
WT	Wild type
WGS	Whole Genome Sequencing
YFP	Yellow fluorescent protein

Chapter I

–

INTRODUCTION

I. Fruit tissue morphology

The fruit is a plant specific organ that protects ovule and seed during embryo development, and ensure seed dispersal after maturation. The fruit appeared during the Cretaceous around 100–125 million years ago and is an evolutionary innovation that accounts for a significant part of the durability of the Angiosperms throughout the ages. Fruits from different taxa are diverse in structure because during the course of evolution plant species have developed a variety of strategies for seed dispersal to maximize the distribution and success of the progeny. Some plant species use fruit structures to provide a mechanical device for seed dispersal, while other species are dependent on the consumption of the fleshy fruit tissues to act as an agent of seed dissemination. Besides of being an asset to the plant, the fruit provides food and natural resources for animal and human diet, as a major source of fibers, sugars, vitamins and antioxidants.

I.a. Diversity of fruit morphology among the Angiosperms

- *Natural diversity in fruit size, shape and tissue morphology*

Angiosperms have developed many different fruit types with a very wide diversity of fruit size, form and composition, and of seed and fruit dispersion mechanisms. These mechanisms range from the small, nondehiscent achene dry fruit dispersed by the wind, to the large, fleshy, and juicy berry and drupe fruits, which have to be eaten by animals, such as mammals or birds for seed dispersion and germination. Classification systems for mature fruits take into account the number of carpels constituting the original ovary (simple versus aggregate or multiple fruits), the dehiscence mode (dehiscence versus indehiscence), and the dryness versus fleshiness of the pericarp (Figure 1).

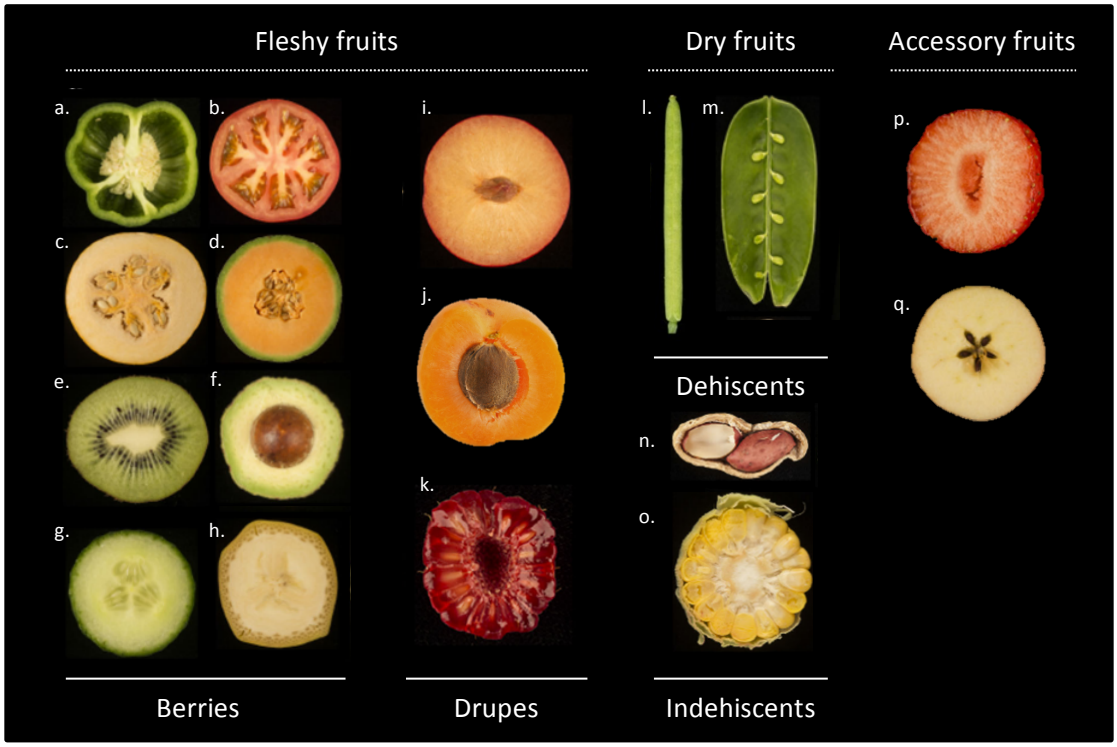

Figure 1: **Natural diversity for fruit tissue morphology observed in nature.** Adapted from Łangowski et al., 2016. a. Transversal section of a pepper. b. Transversal section of a tomato. c. Transversal section of a pumpkin. d. Transversal section of a melon. e. Transversal section of a kiwi. f. Transversal section of an avocado. g. Transversal section of a cucumber. h. Transversal section of a banana. i. Cross section of a plum. j. Cross section of a apricot. k. Cross section of a multiple-fruited raspberry. l. A silique of *Arabidopsis thaliana*. m. Opened pods of a pea. n. Opened pods of a peanut. o. Cross section of the corncob and kernels. p. Cross section of a strawberry, containing achene. q. Cross section of an apple.

- Simple fruits develop from a single or fused carpels (such as the tomato (Figure 1.b)), while aggregate or multiple fruits consist of several separate carpels (such as the raspberries (Figure 1.k) or develop from more than one flower and represent a whole inflorescence (such as the pineapple (Figure 1.o)), respectively.
- Fruit pericarp is either fleshy or dry (Figure 1). Fleshy fruits are characterized by a pericarp that develops into succulent tissues. The fleshy pericarp is made of living cells, having a great capacity to grow. Fleshy fruits represent a major part of human diet, because of their high content in water and organic compounds, such as sugars and vitamins (Azzi *et al.*, 2015). Dry fruits are characterized by a dry pericarp, made up of dead cells at maturity (like *Arabidopsis thaliana* (Figure 1.l) or rapeseed). Dry fruits include the legumes, cereal grains, capsulate fruits, and nuts.
- Fleshy fruits are either berries or drupes depending if the seeds are free or included in a kernel, respectively. Berries are multiple-seeded simple fruits developed from one carpel (apocarpous) or from compound carpels (syncarpous). In drupes, there is usually only one seed per carpel or locule. Some fruits are classified as accessory fleshy fruits or pseudocarpic fruits, because the fleshy parts are not derived from the ovaries, but derived from accessory tissue like hypanthium (tissue composed of fused petals, sepals, and stamens) or the receptacle (Figure 3). As an example, pomes are fruits of Rosaceae family, which develop from an adnate hypanthium (apples and pears).
- Dry fruits are dehiscent, if the pericarp splits at maturity and releases the seeds (as the pea (Figure 1.m)), or indehiscent if the fruit does not open at maturity and the pericarp remains intact when the fruit is shed from the plant (as the maize caryopses (Figure 1.o)). The three principal types of dehiscent fruits are follicles, pods, and capsules.

All these different properties subsequently lead to a huge variety of fruit size and fruit shape and fruit tissue morphology (Łangowski, Stacey & Østergaard, 2016).

- *Diversity of morphology upon the human domestication and selection*

As fleshy fruits are one of the main parts of the human consumption, fleshy fruit species are subjected to major agricultural production, which rely on permanent selection and improvement in yield and quality. Human domestication and selection of fruit has clearly induced phenotypic changes in fruit size and

a. b.

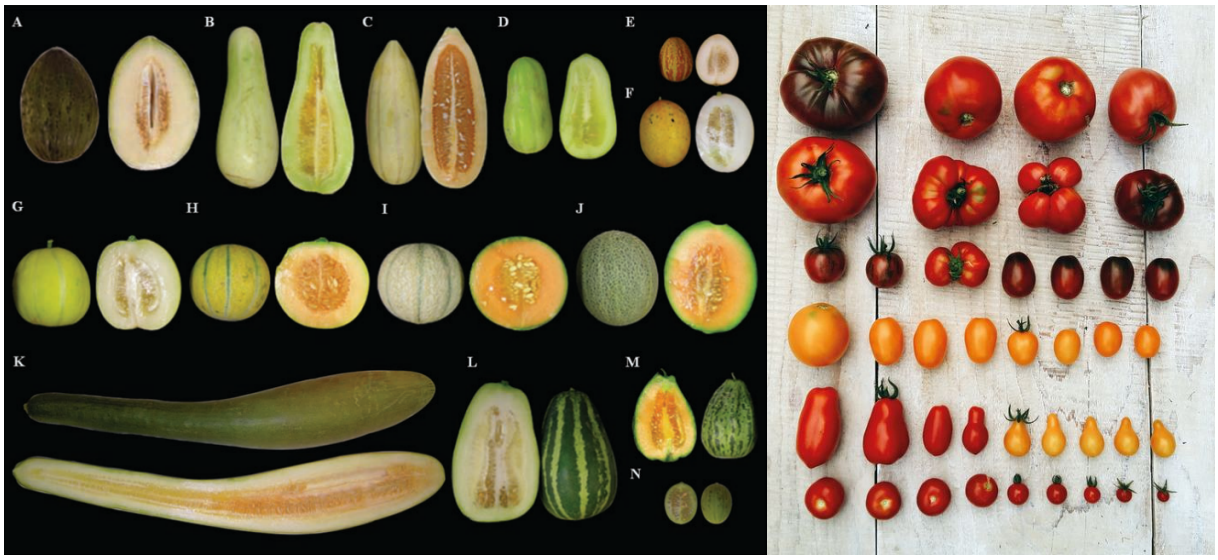

Figure 2: **Diversity of fruit size and shape within the same specie**. a. Fruits of several melon (*Cucumis melo*) cultivars from Pitrat *et al.*, 2008. b. Fruits of several tomato (*Solanum lycopersicum*) cultivars (Image from *sonjalazukic/Getty)*

morphology, creating a broad diversity of fruit shapes within the same species (Tanksley, 2004). As an example, *Solanum pimpinellifolium,* the wild ancestor of the modern tomato *Solanum lycopersicum* produces two-loculed fruits weighing only few grams mainly containing seeds, whereas some varieties of the modern cultivated tomato plants are able to produce fruits that contain many locules. These latter can reach more than a 100-fold the size of the wild species (Grandillo *et al.*, 1999). Modern tomato accessions also exhibit variations in fruit shape in addition to the classical round shapes. Eight shape categories are described in cultivated tomato: flat, ellipsoid, rectangular, oxheart, heart, long, obovoid, and round (Rodríguez *et al.*, 2011) (Figure 2.b). These variations of fruit size and morphology between wild and domesticated species are also found in the melon *Cucumis melo*. Wild melon fruits are small (3 to 6 cm in diameter, weighing less than 50 g), round or oval with a very thin and bitter-tasting mesocarp, while domesticated species can reached up very large fruit size (weighting more than 10 kg), and fruit shape varies from slightly flat, ellipsoid, obovoid, round, and long to extremely long (Monforte *et al.*, 2013) (Figure 2.a). Diversity in fruit morphology was also increased within dry fruit species of agronomical interest, such as maize and wheat. The genetic manipulations of the model plant *Arabidopsis thaliana* and other members of the Brassicaceae family also induce strong variations in size and shape (Łangowski *et al.*, 2016).

I.b. Fruit tissue morphology is established during early fruit development

Fruit development begins following successful fertilization of the ovules in the flowers and occurs concomitantly with that of the developing seeds. The overall final fruit morphology together with the fruit tissue morphology is tightly linked to the flower morphology. Furthermore, the developmental fates of each cell or group of cells, inside the fruit tissue, greatly determine their morphology.

- *Link between the flower anatomy and the final fruit morphology*

Fruits develop from carpels, which originate from floral meristems. Inflorescential or floral meristems initiate from axillary meristems, through complex regulatory networks that enable the transition from vegetative to reproductive development, strongly dependent on both environmental (photoperiod and vernalization) and endogenous signals (hormonal pathways) (Boss *et al.*, 2004). In turn, floral meristems

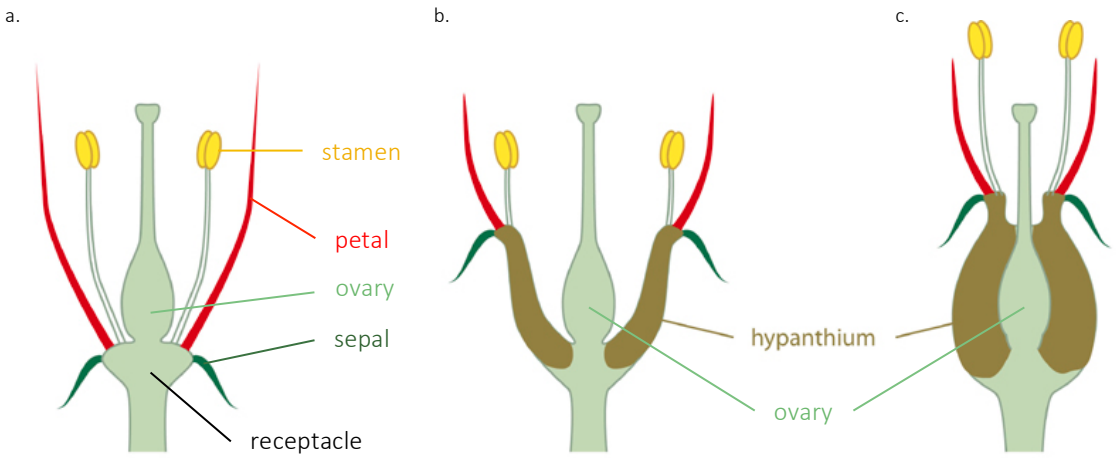

Figure 3: **Diversity in the flower anatomy**. a. Hypogynous flower's structure. The base of the petals, sepals, and stamens are not fused and arise from the receptacle below the ovary (superior ovary). b. Perigynous flower's structure. The basal portions of the petals, sepals, and stamens are fused into the hypanthium tissue and form a detached structure around the ovary (inferior ovary). c. Epigynous flower's structure. The hypanthium tissue is attached to the ovary. The ovary is inferior (below the petals, sepals and stamens).

give rise to floral organs producing flowers with a tremendous diversity of form, size and color but a conserved basic floral structure. A complete flower is composed of four organs attached to the floral stalk by a receptacle. From the base of the receptacle upward these four organs are the sepals, petals, stamens, and carpels. The position of the carpel relative to the sepals, petals, and stamens is an important determinant of fruit morphology and the extent to which fruit development is dependent upon seed development. Flowers can be grouped into the three categories, which describe the position of the ovary relative to other floral organs (superior or inferior), and the presence or absence of a hypanthium: perigynous, epigynous or hypogynous flowers (Figure 3). The anatomy of these three flower types leads to structural differences of fruit morphology, following fertilization. Thus, the broad range of variation in the morphology and structure of the floral organs within the Angiosperms gives rise to a similarly broad range in the morphology and structure of the future fruit.

- *Flower fertilization and the beginning of fruit differentiation*

At anthesis, pollen grains land and germinate at the apical stigma and pollen tubes grow through the style and ovary to deliver the male gametophyte and fertilize the ovules. The number of cells formed in the ovary wall before anthesis is an important determinant of the potential final size in many fruits. Next, fruit set is defined by the double fertilization occurring in ovules and the following differentiation and growth of carpels and ovules (Gillaspy *et al.*, 1993). During this crucial step, the future fruit tissues are setting up. The number of cells within the carpel at fruit set will determine the final fruit size, thus ovary and mature fruit sizes are positively correlated (Tanksley, 2004). However, certain plants, mostly cultivated varieties, spontaneously produce fruits in the absence of pollination and fertilization, defined as parthernocarpy. Fruit development, without fertilization, leads to seedless fruits, as can be the case for bananas, oranges, and cucumbers.

- *Fruit tissue formation during fruit development*

Fruit development is generally defined as the succession of three main developmental periods: the fruit set, the fruit growth and the fruit ripening. Fruit growth is by far the longest phase of fruit development. It ranges from one week for *Arabidopsis thaliana*, 3 to 5 weeks for strawberry, 5 to 8 weeks for tomato, to 60 weeks for many citrus fruits with an average of 15 weeks for most fleshy fruits (Coombe, 1976). Two distinctive types of fruit growth behavior have been reported depending on the fruit specie: a sigmoidal

growth pattern in most species including tomato, and a double-sigmoidal growth pattern in few-seeded-fruit, such as drupes and some berries (grape), which involves two successive phases of growth (Bourdon *et al.*, 2010; Coombe, 1976). Following fruit growth, the ripening process prepares the fruit ready for dissemination. This involves color changes and tissue softening processes and/or dehiscence to release seed. In the case of fleshy fruits, the ripening is defined among others, by the accumulation of organic compounds, such as sugars, organic acids, pigments, flavors, aromas, and vitamins.

As other multi-cellular organs, fruit is a multidimensional organ, in which temporal variation and spatial distribution of growth determine the final shape and size (Kalve *et al.*, 2014). In addition, fruit growth involves the tight coordination between the different cell types that comprise each fruit tissue. Fruit development includes key developmental processes such as differentiation, proliferation and growth. Growth reflects quantitative differences during development, while differentiation describes qualitative changes. Differentiation involves changes in morphology usually related to a functional specialization. It generally affects cell populations that differentiate simultaneously, resulting in the realization of different tissues. Each cell acquires a firmness, a structure and a physiology, characteristic of each kind of tissue. Thus, each tissue composing a fruit can have a different strategy of differentiation. Cell differentiation can occur at different levels and ranks, from macroscopic shape changes due to changes in internal structures, to biochemical variations. Biochemical differentiation involves a broad spectrum of metabolic products. Several signals may be at the origin of cell differentiation, including chemical substances, phytohormones, or mechanical stimuli. The genetic factor remains decisive.

The term “growth” is used to define the gain in terms of volume due to both cell division and cell expansion processes. Fruit growth is often understood as the succession of a period of intense cell divisions, followed by a period of cell expansion, but at the tissue level these two cellular mechanisms occur simultaneously over a short period of time. Growth and proliferation are negotiated within and between cells, rather than imposed on cells across tissues (Sablowski, 2016). Although the growth in volume of many fruits is mainly due to cell expansion (Coombe, 1976), the number and orientation of cellular divisions (periclinal or anticlinal) also contribute to the control of the final size of the fruit. Spatial and temporal regulations of these two major processes by external signals, such as the nutrient availability, hormones and the localized expression of transcription factors, are critical and contribute mainly to the overall final size and shape of the fruit (Bourdon *et al.*, 2010; Van der Knaap & Østergaard, 2018).

In conclusion, not all cells are synchronous in their differentiation, which explains the complexity of the fruit tissues with shared and heterogeneous cell behavior within the same cell layer (Sablowski, 2016). These cellular developmental specifications have been addressed in tomato fruit. Indeed, Renaudin *et al*. (2017) have shown that each cell layer inside the tomato pericarp displays a specific pattern of growth. The difference in growth rate and fate between pericarp outer and inner cell layers contributes to the overall final tomato fruit size. However, among the vast array of fruit tissue morphologies that exist in nature, and within the same species, the mechanisms by which growth is oriented and coordinated to generate this diversity of forms remain to be understood.

II. Cellular and molecular mechanisms involved in fleshy fruit tissue morphology

Fruit tissue morphology depends on three mains cellular parameters: the number of cells inside the tissue, the size of the cells and the shape of the cells. As previously mentioned, the number and type of cell divisions (periclinal and anticlinal), in addition to the relationship between cell division and cell expansion are important for determining the final shape and size of the fruit.

Cell divisions depend on the regulation and progression of the mitotic cell cycle, allowing the increase in cell number inside the tissue. Cell expansion may results from two different processes: cell expansion by the increase in cytoplasmic volume and cell expansion through vacuolation, both allowing cell enlargement. Furthermore, the orientation of cell division and cell expansion, which is determinant for tissue morphology, is closely dependent on the mechanical forces inside the cell, applied by the microtubule and actin cytoskeletons.

In the following part, I will review the complex cellular and molecular networks that control these three processes and intend to understand their impact on fruit tissue morphology.

II.a. Cell divisions: definition of the cell number inside a tissue

Cell divisions lead to the increase in cell number inside a tissue or an organ. The cell cycle is defined by series of molecular events leading to the transmission of the genetic information from one mother cell to two identical daughter cells. The plant cell cycle is divided into four distinct phases (Figure 4):

- the G1 phase, characterized by a 2C nuclear DNA content, during which the cell is getting ready to replicate its DNA content,
- the S phase during which DNA is synthesized,
- the G2 phase, characterized by a 4C nuclear DNA content, during which the cell is getting ready to divide into two daughter cells,

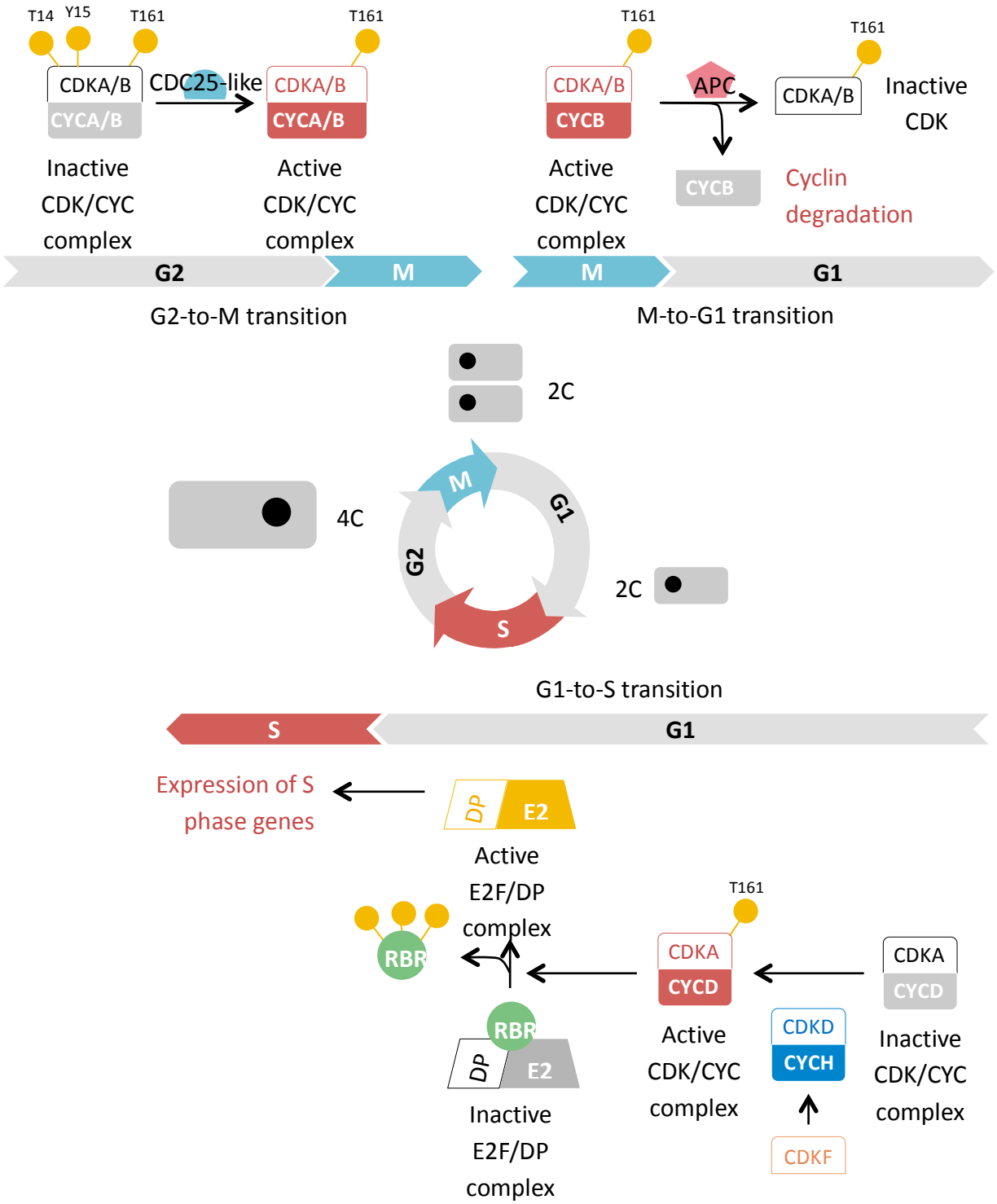

Figure 4: **Progression and regulation of the classical cell cycle.** Adapted from Inzé and De veylder 2006. Inactive proteins and complex are in black and grey, active proteins and complex are in colors. P highlights the phosphorylation site.

- the M phase corresponding to the mitosis, during which the cell organizes and separates the chromosomes correctly. After the two daughter cells separate the chromosomes and build new nuclei, they finally divide their cytoplasm by cytokinesis and form two distinct cells.

- *Cell cycle progression and regulation*

The cell cycle is a widespread phenomenon among eukaryotes and has been extensively studied in both animal and plant cells, highlighting numerous common molecular regulators. The progression through the cell cycle depends on the activity of regulatory enzymatic complexes known as Cyclin-Dependent Kinases (CDK) – cyclin (CYC) complexes (Inzé and De Veylder, 2006). Different CDK-cyclin complexes govern the cell cycle progression at the key transition points G1-to-S, G2-to-M and M-to-G1 (Figure 4). The catalytic CDK subunit is responsible for recognizing the target motif of the substrate proteins, while the cyclin allows discriminating distinct protein substrates (Inzé and De Veylder, 2006; Francis, 2007). The activity of these regulatory complexes is required to trigger the onset of the DNA replication and the mitosis phases.

Cyclin-dependent kinases have been extensively described in mammalians cells, highlighting the major role of two CDKs, named CDK4 and CDK6. Although the cell cycle genes are highly conserved in higher eukaryotes, there are fundamental differences between plant and animal cells, involving plant-specific regulatory pathways. Six families of CDKs (CDKA to CDKF) are known in plants, of which the two keys CDKA and CDKB are the most prominent (Inzé and De Veylder, 2006). CDKA is the unique CDK governing the G1-to-S transition, whereas the G2-to-M and M-to-G1 is probably controlled by both CDKA and CDKB. The specific function of the two CDKs depends on their PSTAIRE hallmark that is present in CDKAs and similar as the animal PSTAIRE motif. In contrast, this motif is replaced by either plant-specific PPTALRE or PPTTLRE hallmarks, in the subgroups CDKB1 and CDKB2 respectively (Joubès *et al.*, 1999; Porceddu *et al.*, 2001; Vandepoele *et al.*, 2002). Genome-wide expression analysis in the tobacco Bright Yellow-2 (BY-2) cells revealed that CDKB1 and CDKB2 have slightly different timing in cell cycle phase-dependent transcription. CDKB1 transcripts accumulate during S, G2, and M phases, whereas CDKB2 expression is specific to the G2 and M phases (Breyne *et al.*, 2002).

CDKs activity is regulated by phosphorylation of the residue threonine 161 (T161) (Figure 4) dependent on the activity of CDK-activating kinases (CAKs) (Inzé and De Veylder, 2006; Harashima *et al.*, 2007). Two functional groups of CAKs have been described in *Arabidopsis thaliana*, named CDKD and CDKF (Figure 4). The phosphorylation of the CDK by the CAKs induces a conformational change allowing proper recognition

of the CDK substrates. Defects in CDK activities have been shown to impact many cellular processes in plants. As an example, CDKA deficiency in *Arabidopsis thaliana cdka;1* dominant negative mutant (also called *cdc2* mutant, because plant CDKAs are homologous of yeast CDC2) blocks the cell cycle progression that is required for male gametogenesis. As a result *cdc2* mutant failed to undergo the second mitosis and only one pollen is produced instead of two, while the loss-of-function mutation of CDKA;1 results in lethality of the male gametophyte (Iwakawa *et al.*, 2006; Nowack *et al.*, 2006). Plants that overexpress a dominant negative allele of CDKB1;1 have abnormal stomata and a decreased number of stomatal complexes, because of the inhibition of stomatal precursors divisions (Boudolf *et al.*, 2004). Furthermore, downregulation of the CDK-activating kinase CDKF results in the reduction of CDK activity and cessation of cell division, causing the premature differentiation of initial cells in the root meristem (Umeda *et al.*, 2000). In rice, the overexpression of the CDK-activating kinase CDKD accelerated S-phase progression and the overall growth rate of suspension cells (Fabian-Marwedel *et al.*, 2002).

CDKs activity is also strictly dependent on their association to the cyclin moiety. Plants contain many more cyclins than in any other organisms (Vandepoele *et al.*, 2002). At least, 49 cyclins have been found in *Arabidopsis thaliana*, which can be divided into 10 types and show different expression patterns during the cell cycle, reflecting their various putative functions : cyclins A and B help to drive cells into mitosis, while cyclins C, D and E are responsible for the entry into the S phase (Zhang *et al.*, 2013). Indeed, antisense expression of tobacco CYCA alters embryo formation and callus regeneration (Yu *et al.*, 2003) whereas the overexpression of Arabidopsis CYCD in transgenic tobacco plants stimulates the progression through G1 in roots and shoots, leading to a faster growth (Cockcroft *et al.*, 2000). D-type cyclins can trigger the G1-to-S transition through activation of the RBR/E2F-DP pathway (Figure 4). Activated CDKA-CYCD complex will induce the hyper-phosphorylation of the retinoblastoma-related protein (RBR) and leads to the release of sequestered E2F promoter-binding factor (E2F) required to drive the expression of many genes necessary for the entry into of the S phase (Figure 4) (Boniotti & Gutierrez, 2001; Gutierrez *et al.*, 2002). Inactivation of the RBR/E2F-DP pathway in *Arabidopsis rbr* knock-out mutants causes sterility because of excessive nuclear division in the mature female gametophyte (Ebel *et al.*, 2004). In addition to the canonical E2F proteins, plants and mammals have atypical E2F factors (Lammens *et al.*, 2009). In *Arabidopsis thaliana*, three atypical E2F factors have been identified, E2Fd/DEL2, E2Fe/DEL1 and E2Ff/DEL3, which competitively inhibit the transcription of genes controlled by canonical E2Fs. Furthermore, the progression within the cell cycle depends on the post-translational control of the CDK activity, via inhibitory phosphorylation involving the WEE1 kinase in response to genotoxic stress (De Schutter *et al.*, 2007; Cools *et al.*, 2011), and the selective degradation of the cyclin subunits, which is

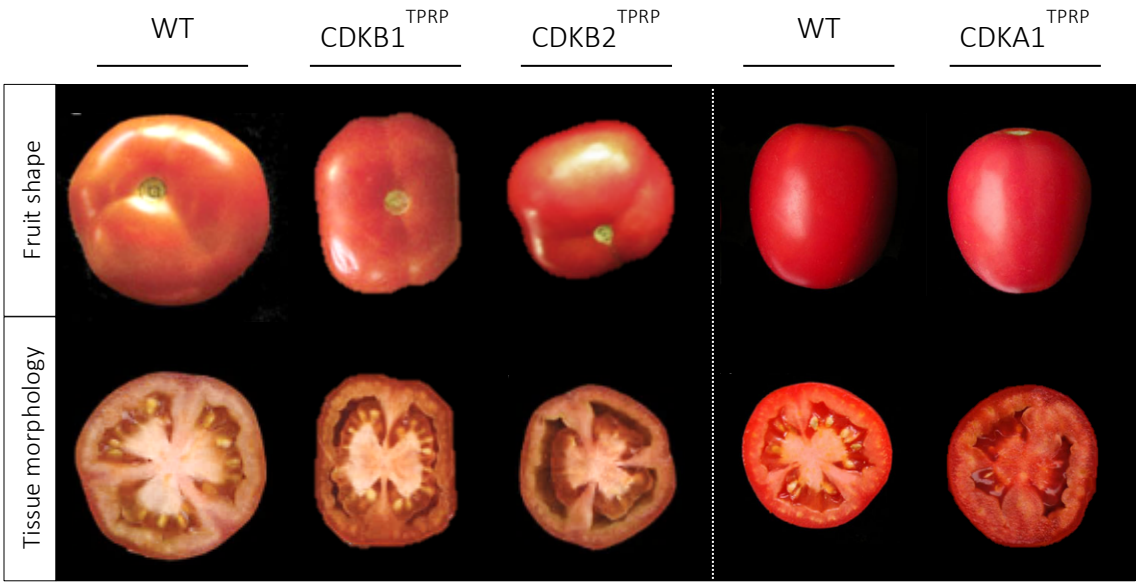

Figure 5: **Tomato mutants overexpressing CDKA and CDKB.** Adapted from Czerednik *et al.,* 2012 and Czerednik *et al.,* 2015. TPRP is a fruit-specific promoter.

triggered by the E- Ubiquitin ligase Anaphase-Promoting Complex (APC) (Heyman and De Veylder, 2012) (Figure 4).

CDK-Cyclin activities are essential for the cell cycle progression resulting proper cell division, inside a tissue. Deregulation of these complex regulatory pathways alters many developmental processes involved in plant organ morphogenesis, including fruit development and morphology.

- *Alterations of the cell cycle affect fruit tissue morphology*

The function of cell cycle regulatory genes and their relation with fruit size and morphology have been studied mainly in tomato. It was shown that CDKB genes are highly expressed up to 15 days after anthesis while their expression decreases thereafter, suggesting that CDKBs play an important role during the cell division phase (Joubès *et al.*, 2001; Czerednik *et al.*, 2012). In contrast, the tomato CDKA1 is expressed at later stages of development until the mature green stage (Joubès *et al.*, 1999). When specifically overexpressed in the fruit, CDKB1 and CDKB2 can alter fruit morphology. Transgenic fruits are smaller, with irregular form, have a reduced cell layers number and a thinner pericarp than the control non-transgenic fruits (Czerednik *et al.*, 2012) (Figure 5). In contrast, transgenic tomato fruits overexpressing CDKA1 are characterized by changes in fruit tissues morphology without affecting the final fruit size. Indeed, transgenic fruits have similar diameter and weight than the wild-type fruits, but significantly thicker pericarp compared with the control fruits, associated with an increase in cell division and cell expansion (Figure 5) (Czerednik *et al.*, 2015).

Cell cycle determines the final number of cells inside the fruit and therefore represents an essential parameter of fruit organogenesis. Alterations in the cell cycle and its complex regulation therefore directly impact tomato fruit size.

II.b. Cell expansion: definition of the final cell size

In eukaryotes, cell enlargement is managed by two processes: cell expansion through vacuolation and cell expansion by the increase in cytoplasmic volume. Cell expansion through vacuolation is a particular property of plant cells because of their large vacuolar compartment, and it leads to an increase in cell volume by more than one hundred-fold. Cell expansion through vacuolation starts once cells have stop dividing, and start to differentiate (Bourdon *et al.*, 2010; Sugimoto-Shirasu & Roberts, 2003). Cell expansion by a cytoplasmic volume increase is driven by endoreduplication and is responsible for a rapid but moderate increases in cell volume, by less than ten-fold (Sugimoto-Shirasu and Roberts, 2003).

II.b.1. Cell expansion through vacuolation

In plant cells, the most intense increase in cell size is achieved by dramatic expansion of the vacuole. The vacuole is a membrane-bound organelle which is filled with water containing inorganic and organic molecules including enzymes. Most mature plant cells have one large vacuole that typically occupies more than 30% of the cell volume, and that can occupy as much as 80% of the cell volume in fleshy fruits. In that case, the cytoplasm is restricted to a thin layer in the cell cortex and around the nucleus.

Because most of the cell volume is occupied by a large central vacuole, it has been postulated that fruit growth mainly depends on osmotic-driven enlargement of vacuoles, thereby giving the fruit its fleshy characteristics (Kost and Chua, 2002). In tomato fruit, the vacuolar and cytoplasmic volume fractions within cells change with time. During the cell division phase, the vacuole expands from 20 to 75%, whereas the cytoplasm shrank from 65 to 10% of the cell volume. The expansion phase is associated with tremendous water flow and sugar transport into the vacuole (Beauvoit *et al.*, 2014). Other important cellular mechanisms are therefore critical for the cell expansion, as the balance between turgor pressure and the resistance of the cell walls to tensile stress (Sablowski, 2016; Szymanski & Staiger, 2018). The close coordination of these processes also responds to external signals, such as nutrient availability and environmental stress and to internal signaling, such hormones and transcription factors. However, little is known about the control of this coordination and which one(s) is determinant for fruit tissue morphology.

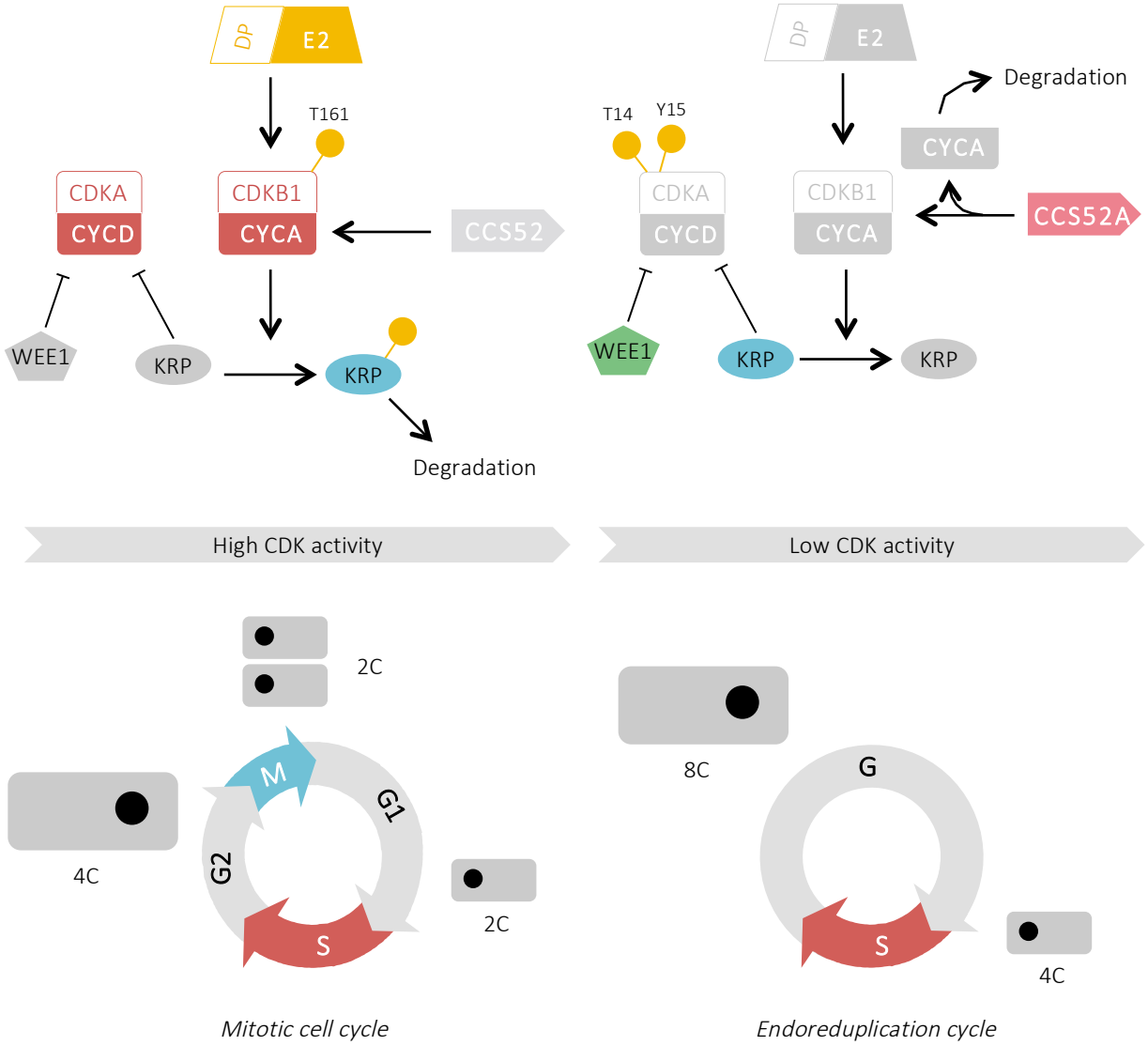

Figure 6: **Transition from the cell cycle to the endoreduplication cycle**. Adapted from Inzé and De Veylder, 2006. Inactive proteins and complexes are in black and grey, active proteins and complexes are in colors. Yellow circles highlight the phosphorylation site.

II.b.2. Cell expansion through endoreduplication

Many plant cells present a modified cell cycle, characterized by continuous DNA replication without mitosis. This modified cell cycle is called the endoreduplication cycle or endocycle and results in the increase of nuclear ploidy and the production of chromosomes with 2^n chromatids, without any change in the chromosome number (Chevalier *et al.*, 2014). Endoreduplication is a widespread phenomenon in plants, and is estimated to occur in over 90% of angiosperms (Joubès & Chevalier, 2000). Endopolyploidy resulting from endoreduplication, varies among plant species and within the same species depending on the organ, the tissue or the cellular type (Barow, 2006). In *Arabidopsis thaliana*, endoreduplication occurs in most organs and tissues (root, hypocotyl, leaf and sepal for example). However, endoreduplication is rarely observed in tobacco and rice. The onset of the endocycle often characterizes the switch between cell proliferation and differentiation, as observed during hypocotyl elongation, trichome growth and leaf development (Inzé and De Veylder, 2006). In addition, endoreduplication is concomitant with the cell expansion phase during fruit growth. Nevertheless, there is no clear-cut relationship between endoreduplication and cell growth, in many plant organs and tissues (Joubès & Chevalier, 2000).

- *Transition from cell cycle to endoreduplication cycle*

The decision of a cell to undergo endoreduplication cycle depends on the expression of a cellular factor called the Mitosis-Inducing Factor (MIF). The absence or reduced activity of this MIF is sufficient to drive cells into the endoreduplication cycle. It has been shown that CDKB1 is a MIF because CDKB1 is highly expressed in dividing cells and is down-regulated at the onset of endoreduplication (Figure 6) (Inzé and De Veylder, 2006). Indeed, the activity of CDKB1 triggers cells to enter into mitosis and its absence of activity induces endoreduplication activity (Boudolf *et al.*, 2004). The control of CDKB1 activity depends on its interaction with the A2-type cyclin CYCA2. The co-overexpression of both CDKB1 and its regulatory unit CYCA2 induces ectopic cell divisions and inhibition of endoreduplication in *Arabidopsis* pavement cells (Boudolf *et al.*, 2009). The required decrease of CDK–CYC complex activity, in order to exit from mitosis, occurs upon the proteolytic destruction of the cyclin. This involves a specific E3-type ubiquitin ligase named the Anaphase-Promoting Complex/Cyclosome (APC/C) which is activated through its association with the Cell-Cycle Switch 52 (CCS52) protein (Heyman and De Veylder, 2012) (Figure 6). Indeed, when overexpressed in yeast, CCS52A triggered cell division arrest through the degradation of mitotic cyclin CYCA (Cebolla *et al.*, 1999). Furthermore, it was shown that the overexpression of CCS52A has a great impact on organ size and ploidy levels in *Arabidopsis* transgenic plants which is dependent on the

expression level (Baloban *et al.*, 2013). The rice *ccs52a* mutant also fails to undergo endoreduplication cycles during rice endosperm development (Su'udi *et al.*, 2012). The reduction in CDK-CYC complexes activity is also mediated by the CDK inhibitory proteins ICKs/KRPs. The abundance of the Kip-Related Protein (KRP) is controlled through CDKB1 phosphorylation inducing proteasome degradation, and KRP binds specifically to CDKA and represses its activity (Figure 6). Indeed, the accumulation of KRP in a dominant negative mutant of CDKB1 represses CDKA activity and induces an increase in ploidy level in *Arabidopsis* leaves (Verkest *et al.*, 2005; De Veylder *et al.*, 2001). Mitotic CDK activity is also negatively regulated by WEE1, by the inhibitory phosphorylation of the threonine 14 (T14) and the tyrosine 15 (Y15)residues (Figure 6) (Chevalier *et al.*, 2014). Primary WEE1 function is to block the CDK–CYC complexes activity during S phase, unless possible DNA damages resulting from DNA replication have been corrected (De Schutter *et al.*, 2007). Although WEE1 loss of function seems to have no strike impact on cell cycle or endoreduplication in *Arabidopsis thaliana* mutants (De Schutter *et al.*, 2007; Cools *et al.*, 2011). The ectopic down-regulation of WEE1 in tomato transgenic plants led to a significant reduction in cell size, together with a strong reduction in ploidy levels (Gonzalez *et al.*, 2007). Thus, the CDKA phosphorylation status controlled by WEE1 appears to be an important mode of regulation of endoreduplication during tomato fruit development.

Furthermore, the SIM and SMR family CDK inhibitors provide another mechanism that regulates CDK activity at the onset of endocycle. An *Arabidopsis sim* mutant develops multicellular trichomes with decreased ploidy levels (Walker *et al.*, 2000) and the overexpression of SIM generates greatly enlarged cells with increased ploidy levels (Churchman *et al.*, 2006). Similarly, SMR1 is involved in initiating endoreduplication during development of giant cells in the *Arabidopsis* sepal epidermis (Roeder *et al.*, 2010). The endoreduplication level and the morphology of trichomes are normal in the *smr1* mutant, indicating that each SIM-related CDK inhibitor may control endoreduplication in a particular development context.

- *The role of endoreduplication in cell size definition*

The role of endoreduplication in organ and cell growth has long been and still is debated in the literature, and many putative role of endoreduplication have been proposed, notably in determining cell size inside a tissue. As described according to the "karyoplasmic ratio theory" (Sugimoto-Shirasu and Roberts, 2003), the cytoplasmic volume is adjusted with respect to the DNA content of the nucleus, suggesting that DNA

Figure 7: **Tomato mutants presenting defects in endoreduplication.** Adapted from Chevalier *et al.,* 2014. AS means anti-sens. OE means over-expression.

content positively impacts the determination of cell size. Therefore, endoreduplication could be a key regulator of cell size by determining the DNA content inside the nucleus. Indeed, many plant species and tissues show a positive correlation between the level of ploidy and the cell size. In *Arabidopsis thaliana*, endoreduplication is associated with an increase in cell size, in the leaves epidermal cells and the elongated hypocotyl (Cebolla *et al.*, 1999; Dewitte *et al.*, 2003; Gendreau *et al.*, 1997; Melaragno, Mehrotra, & Coleman, 1993; Wang *et al.*, 2000). Environmental stresses like water deficit were shown to reduce the ploidy level in correlation with a reduction in cell size, in *Arabidopsis* leaves (Cookson *et al.*, 2006). Endoreduplication is also a key regulator of trichome growth and its deregulation alters the number of trichomes branches (Schnittger *et al.*, 2002; Walker *et al.*, 2000), as previously mentioned.

Nevertheless, some counter examples in which ploidy level does not seem to be associated with the cell size exists. *Arabidopsis* transgenic plants that overexpress previously described cell cycle regulators are characterized by a decrease in ploidy level without associated cell-size reduction (De Veylder *et al.*, 2001; Schnittger *et al.*, 2003; De Veylder *et al.*, 2002). In the maize endosperm, which display high ploidy levels (up to 192C), alterations of endoreduplication in a dominant negative mutant of CDKA did not induce any changes in endosperm cell size (Leiva-Neto *et al.*, 2004). Additionally, cell size was dramatically increased in response to shade treatment, despite a decrease in the ploidy level (Cookson *et al.*, 2006). On the contrary, in the *Arabidopsis* hypocotyl, light exerted a negative effect on endoreduplication and cell size (Gendreau *et al.*, 1997). These findings suggest that endoreduplication is not the only mechanism involved in cell size determination in plants. Recently, Katagiri *et al.*, 2016 proposed that the correlation between endoreduplication and cell volume is dependent on the cell identity.

- *Correlation between endoreduplication and fruit growth*

In tomato fruit, the increase in ploidy level is concomitant with the beginning of cell expansion and can reach 512C in pericarp cells (Joubes *et al.*, 1999; Cheniclet *et al.*, 2005). By comparing over 20 tomato lines, a strong, positive correlation was demonstrated between the ploidy level inside the pericarp, the mean pericarp cell size and the final fruit diameter (Cheniclet *et al.*, 2005). These data strongly suggest that endoreduplication is a driver of cell expansion in tomato fruit. Endoreduplication is such an important process during tomato fruit development that alterations in the expression of cell cycle regulatory genes affect both cell and fruit sizes. The down-regulation of *CCS52A* and *WEE1* in tomato plants causes a reduction of fruit size that correlates with a decrease in mean cell size and ploidy level (Figure 7)

(Gonzalez *et al.*, 2007; Mathieu-Rivet *et al.*, 2010). In contrast, the final fruit size was not modified when the endoreduplication was decreased, in transgenic tomato fruits overexpressing KRP (Figure 7) (Nafati *et al.*, 2011). The comparison of the ploidy levels of different fruits also revealed no clear-cut relationship between endoreduplication and fruit size. For example, fruit displaying no endoreduplication, like kiwi and grape are still able to produce very big cells, whereas small cells are observed in fruit displaying endoreduplication like strawberry and peach (Bourdon *et al.*, 2010). Thus, the ability to develop very large fruit cells is not restricted to endopolyploidizing fruits. Interestingly, it was reported that the endocycle number is higher in fleshy fruit species, which develop rapidly. Plant species, for which fruit development lasts for a longer time, display low level of endoreduplication (Chevalier *et al.*, 2011). It suggests that endoreduplication may be a driver of cell expansion to go with rapid fruit growth.

Although the role of endoreduplication in cell size determination is still challenged, deregulation of endoreduplication clearly showed that this cellular process has an important role in the pericarp cell size definition and in tomato fruit size consequently.

II.c. The cytoskeleton: mechanical forces driving cell division and cell expansion

As previously mentioned, fruit tissue morphology is tightly dependent on the orientation of the cell division and cell expansion processes. Plant cytoskeleton plays a pivotal role in many cellular processes, such as cell growth, by defining the orientation of cell division and cell expansion inside a tissue. At the tissue scale, orientation of cell division and cell expansion and their coordination is highly regulated to accomplish correct organ growth (Armour *et al.*, 2015; Hervieux *et al.*, 2016; Van der Knaap *et al.*, 2014). The role of cytoskeleton in this orientation is crucial and involves arrays of actins and microtubules (de Keijzer *et al.*, 2014; Hussey *et al.*, 2006). In addition to offer structure and support for the cell, the cytoskeleton provides an internal network allowing the transport of proteins and organelles within the cell. Like in other eukaryote cells, the plant actin cytoskeleton exists in two states, as monomeric or globular actin (G-actin) and as filaments (F-actin). Actin cytoskeleton dynamic depends on the transition between these two states, and is tightly regulated in time and space by a large number of signaling and the activity of actin-binding proteins (ABPs) (Lee and Dominguez, 2010). Microtubules are cytoskeletal structures forming cylindrical tubes composed of α- and β-tubulin heterodimer subunits.

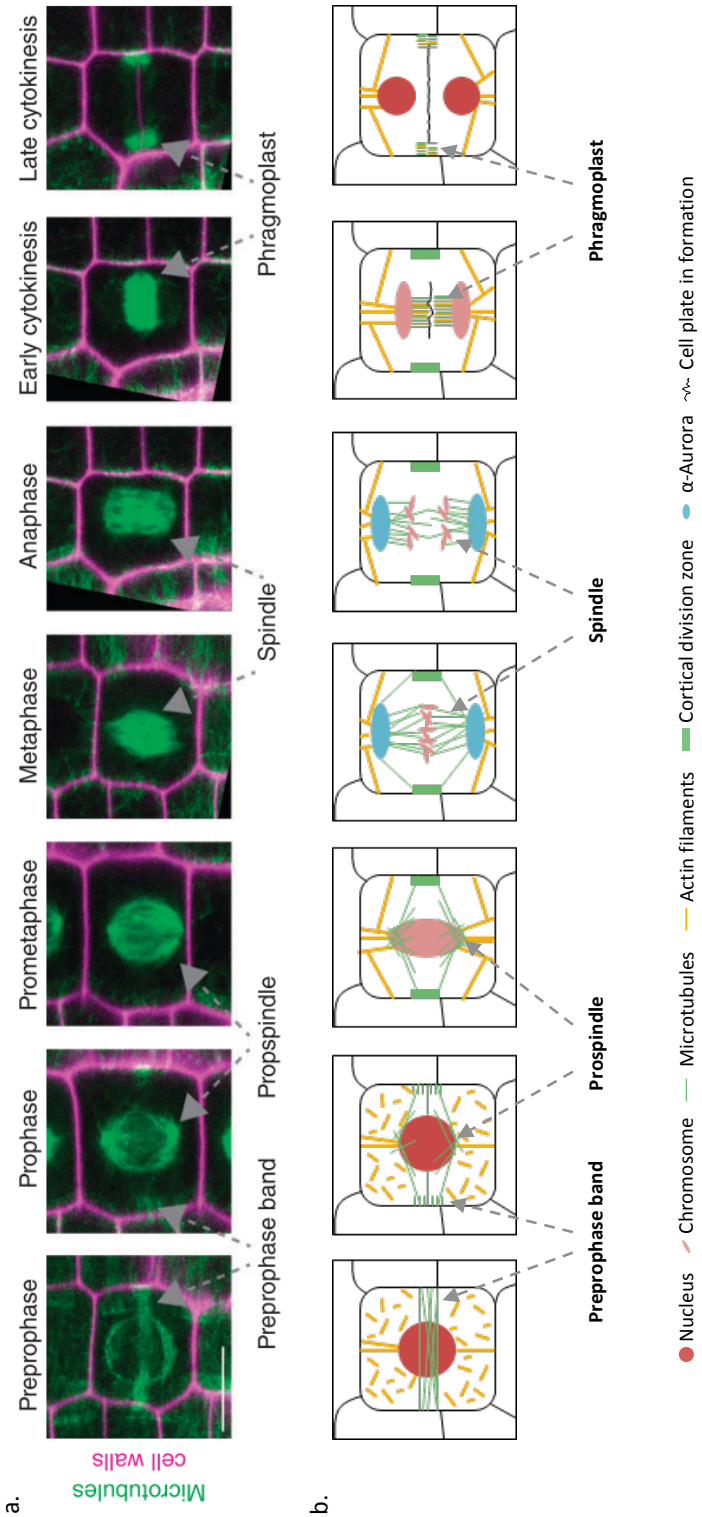

Figure 8: **Microtubule and actin cytoskeletal remodeling during cytokinesis**. a. Micrographs of the microtubule arrays during plant cell division from Lipka, Herrman and Müller, 2015. b. Schematic illustration of the cytoskeletal remodeling during mitosis.

- *Orientation of the cell division plans*

In contrast to animal cells, plant cells are constrained by the rigid cell wall surrounding them, which prevents them to migrate. Consequently, local cell division parameters, such as the cell division plane orientation, contribute to the organ/tissue organization and final morphology. Cell division orientation is visible during cytokinesis but is defined earlier at the beginning and all along mitosis. Plant mitosis is divided into five major stages: the prophase, the metaphase, the anaphase, the telophase and the cytokinesis (Figure 8). During mitosis, the chromosomes, which are already duplicated, condense (preprophase and prophase) and attach to spindle fibers (prometaphase and metaphase), that pull one copy of each chromosome to opposite sides of the cell (anaphase). Following anaphase, nuclear envelop is reforming around each nucleus (telophase) and cytokinesis is necessary for completing cell division and form a new cell wall (Figure 8.a).

During mitosis, the cytoskeleton remodels and plays a critical role for successful orientated cell division plans (Figure 8.b). In addition to other eukaryote cells, plants have developed two unique microtubule structures involved in the selection and maintenance of the division plane and in the formation of the cell plate: the preprophase band and the phragmoplast (Figure 8) (Keijzer *et al.*, 2014; Lipka *et al.*, 2015).

- The preprophase band (PPB) is a remarkable dense ring-like structure of microtubules, outlining the cell periphery of the future division plane. PPB is setting up at the G2/M phase by a change of microtubule dynamics. The formation of the PPB also involves the recruitment of landmark proteins that remain in the cortical division zone (CDZ), where cell plate attachment takes place with the parental cell wall (Lipka *et al.*, 2015; Van Damme *et al.*, 2007). The PPB is removed before chromosome segregation and cytokinesis (Figure 8.b). The PPB is thought to be a crucial determinant for the nuclear positioning, the bipolar spindle formation, and the division plane determination (Van Damme, 2009).
- The phragmoplast, which is a complex assembly of microtubules, emerges from the area previously occupied by the PPB and expands toward the cell periphery, guided by microtubules (Figure 8). The phragmoplast guides Golgi-derived vesicles containing cell wall synthesis enzymes, to the center of the cell in order to construct the new cell wall. It physically partitions daughter cell content by synthesis of the new cell plate (Van Damme *et al.*, 2007).

Thus, microtubules (MTs) are the main driver of mitosis by defining the plane or the future cell plate and forming the chromosome spindle. The actin cytoskeleton is also involved in determining the division zone and cell plate guidance. Indeed, actin filaments are present in the PPB and phragmoplast structures and could contribute to the organization of the MTs. When the PPB disappears during metaphase, cortical actin is also degraded, leaving behind an actin-depleted zone (ADZ) that is used as a negative marker of the CDZ (Van Damme *et al.*, 2006). Furthermore, treatment with auxin transport inhibitors (2,3,5-triiodobenzonic acid (TIBA) or jasplakinolide) alters cortical actin microfilament patterning and correlates with oblique mitotic spindles in BY-2 cells (Kojo *et al.*, 2013). Although mutations in actin or treatments with actin drugs do not have dramatic effects on cell division, actin cytoskeleton is still believed to have a role in the PPB positioning, in a more subtle way (Lipka *et al.*, 2015; Van Damme *et al.*, 2007). However, its real implication is far from being totally understood.

- Alterations for division plans in plants

Therefore, the organization of the MTs is a critical parameter for cell plate positioning during cytokinesis. Mutants impaired in PPB formation present altered cell division orientation. *Arabidopsis trm* (TON1 Recruiting Motif) mutant shows defects in cell division orientation, because of the PPB disruption. It was shown that the TRM protein superfamily plays a role in complex assembly and targeting to the cytoskeleton (Schaefer *et al.*, 2017). In the same way, the *Arabidopsis* double knockout mutant *pok1pok2* presents aberrant cell wall orientation because of defects in phragmoplast guidance (Lipka *et al.*, 2015; Müller *et al.*, 2006). It was suggested that POKs are involved in the positioning of the PPB by maintaining downstream identity markers (Lipka and Müller, 2014). The PPB establishment and maintenance is therefore essential for proper cell division orientation.

The overexpression of the *Arabidopsis* AtAurora3 in BY-2 cells, that is believed to be implicated in the control of microtubule dynamics, also leads to unusual cell division patterns with abnormal division orientations and spindle formation defects (Kawabe *et al.*, 2005). Aurora proteins are serine-threonine protein kinases, highly conserved in all eukaryote cells. In plants, two subfamilies of Aurora have been described α-Aurora (Aurora 1 and Aurora 2) and β-Aurora (Aurora 3) which are differentially localized throughout mitosis (Figure 8.b) (Demidov *et al.*, 2005; Weimer *et al.*, 2016). Inhibition of the plant Aurora kinase induces aberrant kinetochore-microtubule attachment and aberrant cell division orientation, suggesting that the plant Aurora kinase regulates kinetochore-microtubule attachment during

chromosome alignment (Kurihara *et al.*, 2008). Furthermore, the *Arabidopsis aur1aur2* double mutant is hallmarked by the occurrence of periclinal-like instead of anticlinal pericycle divisions at the onset of lateral root formation, leading to strongly reduced lateral roots (Figure 8.b) (Van Damme *et al.*, 2011). This also suggests that the plant Aurora kinases may be involved in orienting cell divisions, through the regulation of microtubule dynamics.

- *Direction of cell expansion*

Cell expansion could be diffuse (isotropic) or oriented (anisotropic). Isotropic growth takes place when the rates of expansion are equal in all the directions, in contrast to anisotropic growth for which the rates of expansion are in different directions (Ivakov and Persson, 2013). Both growing behavior are defined by different cytoskeleton behavior. Indeed, in the case of a diffuse growth, the cytoskeleton fibbers randomly arrange inside the cell, while they organize and specifically orientate in the case of a directed growth.

Plant cells contain cortical actin filaments that are in close proximity to the plasma membrane, pushing it against the cell wall. Actin filaments are commonly observed throughout the cytoplasm in growing plant cells, providing a scaffold that positions the endoplasmic reticulum and supports long-distance organelle transport. The efficient transport of materials throughout the cell by the F-actin is thus critical for cell growth and cell wall synthesis (Ivakov & Persson, 2013; Szymanski *et al.*, 1999). During anisotropic growth, cytoskeleton is a determining factor of the cell expansion direction because it ensures the transport of the vesicle from the Golgi network to the cell wall, where the directed growth might happen.

Cytoskeleton organization during cell expansion has been mainly described in tip-growing plant cells such as trichomes, root hairs and pollen tubes. *Arabidopsis* trichomes are used as unicellular systems to study anisotropic cell expansion in relation with the actin cytoskeleton. Indeed, the pattern of F-actin organization correlates with the different states of trichome cell elongation. Actin cytoskeleton is diffuse at early stages of trichome development and organizes into thicker bundles aligned along the growth axis during trichome maturation (Figure 9.a). Disruption of F-actin organization by a treatment with cytochalasin D, causes a distorted trichome phenotype, due to the absence of actin dependent growth signal at the tip of trichome branches (Sambade *et al.*, 2014; Szymanski *et al.*, 1999). Furthermore, both *Arabidopsis act2* and *act8* knock-down mutants, defective in ACTIN2 and ACTIN8 isoform expression respectively, have defects in root hair elongation. The phenotype is more severe in the *act2;act8* double mutant, which is characterized by no elongation of any root hairs (Ringli *et al.*, 2002). During *Lilium*

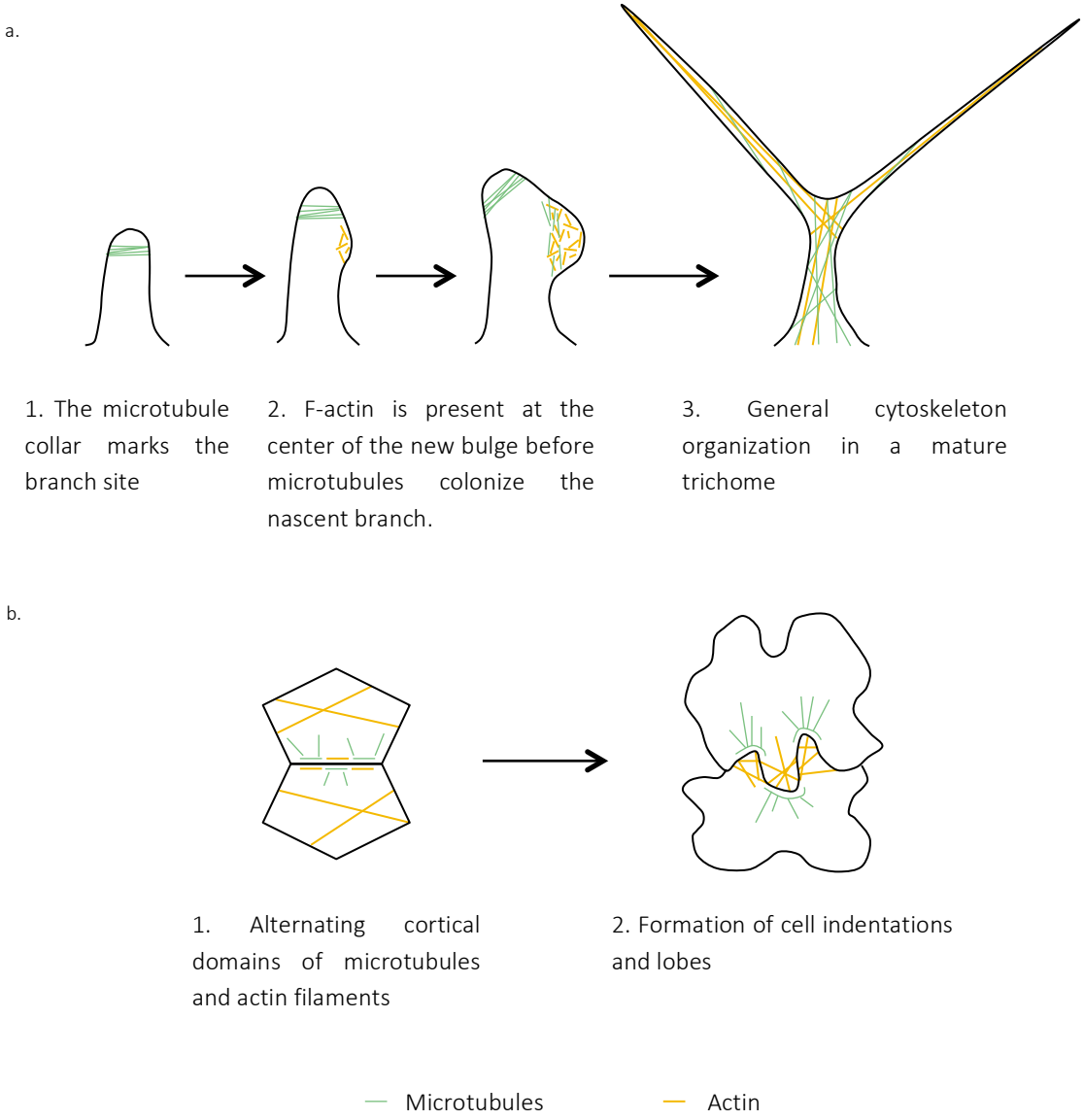

Figure 9: **Examples of microtubule and actin cytoskeletal organization for cell expansion.** a. Anisotropic expansion during trichome development. b. Multi-polar expansion during the development of leaf pavement cells. Adapted from Szymanski *et al.*, 2009 and Sambade *et al.*, 2014.

longifloru pollen tube elongation, cytochalasin D causes immediate arrest of membrane trafficking, in correlation with the reorganization into randomly oriented F-actin, resulting in the arrest of the pollen tube growth (Hörmanseder *et al.*, 2005). Thus, the reorganization of actin cytoskeleton is necessary to initiate and maintain oriented growth in many cell types.

Microtubule organization is also playing an important part in regulating the direction of cell expansion by directing the orientation of the cellulose microfibrils (Baskin, 2001). Various mutants with defects in microtubule organization or stability have defects in establishing anisotropic expansion (Ivakov and Persson, 2013). As an example, the Arabidopsis *tortifolia1* (*tor1*) and *spiral2* (*spr2*) mutants are defective in directional cell elongation for longitudinally expanding organs such as root, hypocotyl, stem, petiole, and petal. TOR1 and SPR2 are microtubule-associated proteins (MAP) that are required for proper microtubule organization (Buschmann *et al.*, 2004; Shoji *et al.*, 2004). So, microtubule cytoskeleton is also involved in the control of anisotropic growth, in many plant organs.

- *Coordination of the actin and microtubule cytoskeleton to define spatial and temporal growth*

In many plant cell types, the tight coordination between actin and microtubule cytoskeletons is thought to be central in directing cell elongation and shape. In plant cells using a diffuse growth mechanism, the microtubule and actin cytoskeletons also work cooperatively to maintain cell wall mechanical properties and spatial heterogeneity that support long-term, irreversible cell expansion.

In *Arabidopsis* leaf pavement cells, interactions between the two cytoskeleton components are required for their complex multi-polar growth (Ivakov and Persson, 2013). The convex sides of the pavement cell lobes contain cortical domains of microtubules while the concave sides of the lobes are defined by localized concentration of actin filaments (Figure 9.b) (Szymanski & Cosgrove, 2009; Yanagisawa *et al.*, 2015). Both microtubule and actin cytoskeletons are also required for growth of the *Arabidopsis* leaf trichome branches. At the beginning of trichome development, the unbranched trichome elongates mainly by tip growth, thanks to a microtubule collar. After branching, trichomes expand along the whole cell axis by diffuse growth. To give birth to a new branch, F-actin is localized at the center of the new bulge and then microtubules localized to the nascent branch (Figure 9.a). Treatments with both actin-destabilizing and microtubule-destabilizing drugs show different effects on trichome growth, suggesting a distinct and stage-specific requirement for actin- and microtubule-dependent function, during trichome morphogenesis. The microtubule-destabilizing drug oryzalin inhibits the onset of cell polarization, and

cytochalasin D inhibits the maintenance of cell shape later during trichome morphogenesis, but both are essential for normal trichome directed expansion (Sambade *et al.*, 2014; Szymanski *et al.*, 1999).

- *Importance of cell division and cell expansion orientation for plant organ morphology*

Mis-orientation of the cell division can have dramatic effects on plant organ morphogenesis. As an example, *ttp Arabidopsis* mutant that is impaired in the PPB formation, fails to develop normally, because of the mis-positioning of the division plane during the embryo development (Spinner *et al.*, 2013; Schaefer *et al.*, 2017). The maize TANGLED mutant *tan1* is characterized by abnormal leaf cell shape, short stature and rough textured leaves because the phragmoplast fails to be directed to the former PPB site. Thus, phragmoplast guidance and division plane orientation have direct effect on maize leaf morphology (Martinez *et al.*, 2017; Smith *et al.*, 2001). The *Arabidopsis* double knockout mutant *pok1pok2* displays severe developmental defects, such as smaller cotyledons, shorter and wider roots and hypocotyls, because of multiple mis-oriented cell walls during embryo and root development. POK1 and POK2 have been found to control the phragmoplast guidance, in association with the MTs cytoskeleton (Lipka *et al.*, 2015; Mueller, Han and Smith, 2006).

The spatial and temporal control of cell division and cell expansion and the coordination of both processes together with cytoskeleton remodeling remain poorly investigated in fleshy fruits. The identification of regulators and the study of their role at sub-cellular, cellular and tissue level is a requirement to decipher and understand fleshy fruit growth.

III. Fruit tissue morphology in tomato

III.a. Tomato as a plant model for fleshy fruit

Tomato has served as the primary model for fleshy fruit development and ripening (Giovannoni, 2007). Tomato (*Solanum lycopersicum*) belongs to the Solanaceae family and is the second most cultivated plant and the first most cultivated fruit in the world. First, tomato presents a wide range of fruit color, size, shape and morphology, which makes it a nice model to study fruit development. Mean fruit weights can ranged from 3 to 500 g, mainly depending on the number of carpellar locules, which varied from two to 22 (Cheniclet *et al.*, 2005). Fruit tissue morphology is also extremely diverse in tomato, notably comparing processing and cultivated tomato (Rodríguez *et al.*, 2011).

A large repertory of genetic resources is available in tomato including wild, domesticated and cultivated species, together with various core collections, including MAGIC one to support genetic studies (Pascual *et al.*, 2015). Due to the emergence of the use of tomato as a plant model for fleshy fruit species, efforts have been made during the last 10 years, to develop many tools and resources in this species. In particular, induced mutant collections were developed in various genetic backgrounds (Gady *et al.*, 2009; Gupta *et al.*, 2017; Just *et al.*, 2013; Menda *et al.*, 2004; Minoia *et al.*, 2016; Saito *et al.*, 2011), to create large collections of new genetic and phenotypic diversity, which were useful resources for reverse genetic approaches. These collections are today also used in direct genetics approaches thanks to the availability of the tomato genome and to the rise of the NGS technologies which reduces the time and financial costs of these approaches. Since, 2012, the annotated Heinz reference genome was published (Tomato Genome Consortium, 2012) and resequencing of many genomes are today available including new reference genomes of wild species and Micro-Tom.

Last but not least, tomato displays a highly favorable biology for laboratory research with a short life cycle, an easy growth in open fields and in greenhouses, a high multiplication rate, the facility of plant reproduction (usually by self-pollination but easiness to realize crosses) and the existence of well-established genetic transformation protocols.

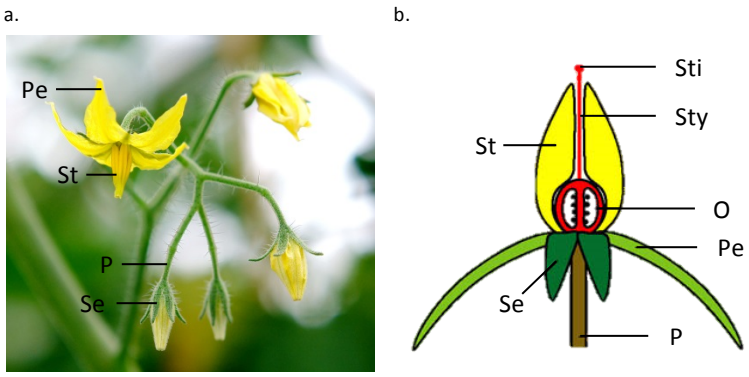

Figure 10: **Tomato flower anatomy**. a. Tomato flowers. b. Schematic representation of a tomato flower from Jussieu university website. Sti, Stigma; Sty, Style; St, Stamen; O, Ovary; Pe Petal; Se, Sepal; P, Pedicel.

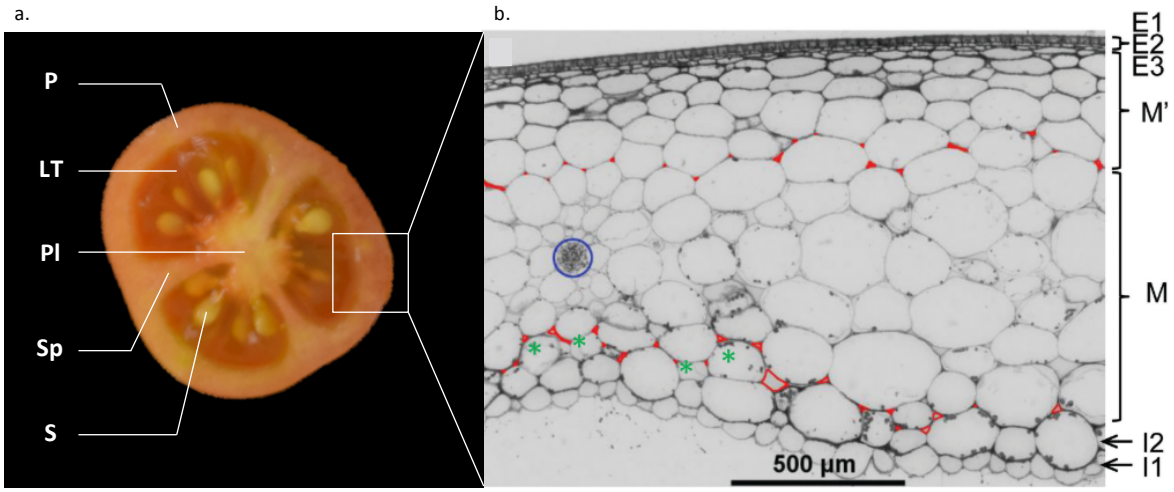

Figure 11: Tomato fruit tissues. a. Equatorial section of a Micro-Tom tomato fruit. P, Pericarp; LT, Locular Tissue; Pl, Placenta; Sp, Septum; S, Seeds. b. Structure of tomato pericarp at breaker stage from Renaudin *et al.* (2017). E1, outer epidermis; E2 and E3, two cell layers below E1; M, around 4 cell layers inside the mesocarp; M', cell layers formed after anthesis mostly from divisions of E2 and E3; I2 and I1, cell layers of the inner epidermis.

III.b. Fruit tissue types and development

- *From the flower to the fruit*

In most of tomato cultivars, tomato flowers are actinomorphic with pentameric symmetry. The calyx (all the sepals) have five green sepals that persist after fertilization at the base of the fruit, the corolla (all the petals) have five bright yellow petals fused at the base, and the androcea (all the stamens) five stamens, whose elongated anthers form a cone constricted around the pistil (Figure 10). The stamens have an introrse dehiscence, which allows the pollen to be released in the inner side of the flower. The gynoecium consists of at least two or three fused carpels. At flowering time, the calyx and the corolla are completely open and the anther blossoms to release the pollen, allowing fertilization. After fertilization, the ovary will evolve to give the fruit, which is composed of different tissues (Figure 11.a):

- The external pericarp, mostly referred as the main fleshy part of the fruit, is divided into three zones, the outermost exocarp, the mesocarp in the center and the endocarp the most inside,
- The radial pericarp or septa, corresponds to the melting zone of the lateral wall of the carpels in the ovary,
- The placenta is part of the wall of the ovary or the fruit, where are inserted the seeds and it surrounds the columella which constitutes the central axis of the fruit (regrouping the vascular tissues coming from the vegetative part of the plant),
- The locular tissue or gel, which develops from the placenta after fertilization and surrounds the seeds,
- The seeds, which develops from the ovules.

Fruit development starts with a period of intense cell division and cell expansion (Renaudin *et al.*, 2017), that led notably to the gradual increase in pericarp thickness. Cell division lasts approximately 10 days, depending on the tomato cultivar; whereas cell expansion continues all along fruit development in the exocarp to support the huge increase of fruit size (Figure 12). During pericarp growth occurs also an increase of ploidy levels due to endoreduplication (Cheniclet *et al.*, 2005; Joubes *et al.*, 1999). After reaching almost its final size, the fruit acquires its ability to ripen (Mature Green stage) and starts the ripening phase (Figure 12), tightly synchronized with seed maturation to ensure proper dispersal of the progeny (Giovannoni *et al.*, 2017). As such, fruit ripening is a complex process whose purpose is to make the fruit attractive by promotion of its consumption by organisms that will facilitate the release and

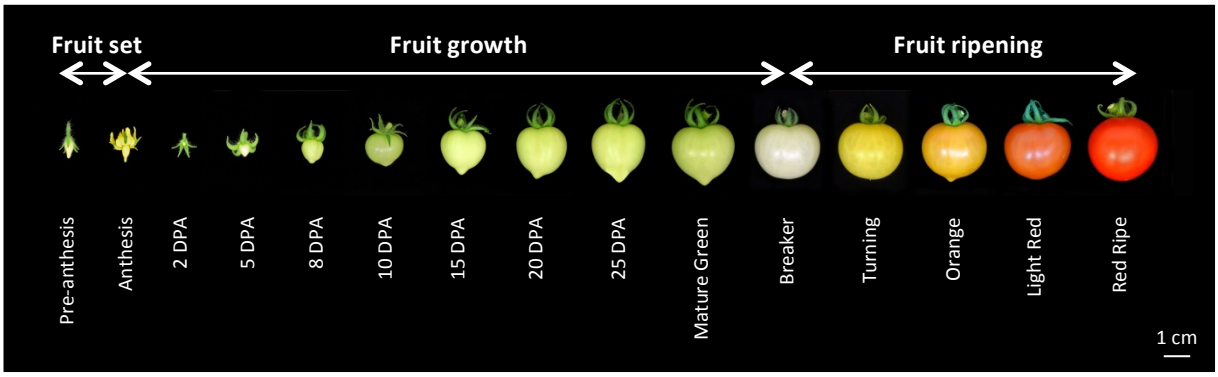

Figure 12: **Tomato fruit development from fruit set to the end of ripening.**

dissemination of the seeds. This process is genetically programmed and involves biochemical, physiological and structural upheavals in all fruit tissues which result in changes in color, firmness, nutritional content, and in aroma production (Klee and Giovannoni, 2011).

- *The Pericarp tissue*

The pericarp has been the subject of most studies addressing fruit growth. After fertilization, the ovary wall differentiates into a pericarp, which is structured into three areas: the exocarp, the mesocarp and the endocarp (Figure 11). The exocarp or skin, which is in contact with fruit external environment, comprises the external epidermis cell layer and the neighboring collenchymatous cell layers. The exocarp is covered with a cuticle, a lipophilic layer composed of a cutin polyester filled with waxes that thickens with age (Martin and Rose, 2013). The mesocarp, an intermediate tissue, is a parenchyma formed of large polyploid cells with large vacuoles, crossed by vascular tissues. Mesocarp cells also have many chloroplasts that allow the fruit producing about 20% of photosynthesis of its photoassimilates. Finally, the endocarp, which is the innermost pericarp layer, is made of a unique cell layer and is believed to be covered by a cuticle layer alike the external pericarp (Matas *et al.*, 2011) (Figure 11.a).

A recent work performed in Wva106 tomato cultivar, precisely described the fate of the ovary cell layers after fertilization during the early phase of fruit development (Renaudin *et al.*, 2017). In this cultivar, the ovary wall at anthesis is made up of nine cell layers which include both outer epidermis (E1) and inner epidermis (I1), two outer (E2 and E3) and one inner (I2) sub-epidermal cell layers, and four rows of central mesocarp cells (M) surrounding vascular bundles (Figure 11.b). During the cell division phase, both periclinal and anticlinal cell divisions specifically occur depending on the pericarp cell layer: periclinal cell divisions mainly result in the increase in cell layer number (which increase the pericarp thickness), while anticlinal cell divisions (which increase the cell number in a given layer) result in the increase in the fruit surface. Anticlinal cell divisions were by far the most numerous in the pericarp, especially in the outer E1 epidermal cell layer. High levels of periclinal cell divisions were present only in E2 and E3 sub-epidermal cell layers and give birth to new cell layers (M' cells) (Figure 11.b). The lowest mitotic activity was found in M and M' cell layers, mostly with periclinal or oblique cell divisions (Renaudin *et al.*, 2017). Each pericarp cell layer also displays a specific pattern of cell number variation and cell expansion. E1 and E2 cell layers display an increase in cell layer, while the mean cell number in one M cell layer remains unchanged. M cells continuously expanded and did not show any axis of preferential expansion. I2 cell layer behavior

looks like that of M cells, with nearly no increase in cell number and a huge cell expansion (Renaudin *et al.*, 2017). At the moment, this reference work on tomato cultivar Wva106 cannot be generalized to other tomato cultivars, since pericarp tissue presents a great variability of size relative to fruit size, thickness and morphology, particularly between processing and non-processing tomatoes (Cheniclet *et al.*, 2005; Rodríguez *et al.*, 2011).

III.c. Identification of fruit growth regulators using natural diversity

So far, previous studies have provided valuable insights into the genetic basis of fruit size and shape variations in tomato by studying, the natural diversity available in tomato which includes, domesticated tomato, spontaneous mutants and wild relatives. These forward genetic studies revealed six quantitative trait loci (QTLs) and their underlying genes, which are involved in fruit size and shape variations in tomato (Monforte *et al.*, 2013; Van der Knaap & Østergaard, 2018): *FW2.2*, *FW3.2*, *LOCULE NUMBER*, *FASCIATED*, *OVATE* and *SUN* (Table 1).

- *FW2.2* (*FRUIT WEIGHT 2.2*) is described as a major QTL involved in 30% of the fruit weight variation between the wild-type and domesticated tomato species. *fw2.2* also represents a key transition during domestication because wild species contain the small-fruit allele, whereas tomato cultivars contain the large-fruit allele for the locus (Frary *et al.*, 2000). Indeed, the large- and small-fruited alleles of *fw2.2* show differences in transcription timing by a week, and this hetero-chronic expression of *fw2.2* accounts for the fruit mass variation between wild and domesticated tomato species (Cong *et al.*, 2002; Frary *et al.*, 2000). *fw2.2* transcripts are inversely associated with the amount of cell division in the fruit. Therefore, *fw2.2* is speculated to be a negative regulator of fruit-growth by negatively regulating cell division during tomato fruit development (Cong *et al.*, 2002). Furthermore, *fw2.2* influences the 2D- and 3D cell division patterns in the pericarp without affecting fruit shape (Liu *et al.*, 2003). Functional characterization of FW2.2 revealed that the protein accumulates at the plasma membrane and might interact with the regulatory subunit of CDKII kinase, which is known to be involved in cell cycle regulation (Cong and Tanksley, 2006). Cell Number Regulator 1 (CNR1), a putative ortholog of *fw2.2* locus in maize was found to have a role in cell division, impacting plant development (Guo *et al.*, 2010). The accumulation of *Pafw2.2*-

Locus	Mutation type	Underlying gene	Putative function of the protein	Mutation effect on fruit size and shape
fw2.2	SNP in the promoter of the gene	*CNR*, Cell Number Regulator	Negative regulator of fruit growth Protein may be located at the plasma membrane Possible interaction with CDKII kinase	Reduced size of tomato fruit, with reduced cell divisions
fw3.2	SNP in the promoter of the gene	*KLUH* / CYP450 cytochrome P450	Cytochrome P450 of the 78A class	Reduced size of tomato fruit No effect in fruit shape
LC, Locule Number	Two intergenic SNPs, located downstream *WUSCHEL*	*WUS*	Homeobox transcription factor Required to maintain stem cell identity in apical meristem	Increased locule number
FAS, Fasciated	294 kb inversion	*CLV3* promoter	Maintenance of meristem activity	Flat fruit phenotype
OVATE	Single mutation causing a premature stop codon	OFP, Ovate Family Protein	Suppressor of plant growth Putative interaction with TRM/TON1 involved in PPB formation	Pear-schaped fruit Abnormal plant growth
SUN	25 kb duplication from another chromosome	IQD, CaM binding protein	Positive regulator of growth	Pear-schaped fruit

Table 1: **Loci involved in tomato fruit size and shape variations**

like gene, encoding a FW2.2-like protein in avocado, negatively correlates with fruit cell division, suggesting a conserved function between the avocado and tomato FW2.2 proteins (Dahan *et al.*, 2010). However, the precise role of FW2.2 in tomato fruit size control remains largely unknown.

- *FW3.2* (*FRUIT WEIGHT 3.2*) is involved in 19% of the fruit mass variation in an F2 segregant population from a cross between the cultivated tomato cultivar Yellow Stuffer and a tomato wild species (Van der Knaap & Tanksley, 2003), with no effect on fruit shape. *fw3.2* locus corresponds to a 51,4 kb region comprising seven candidate genes (Zhang *et al.*, 2012). Among these candidate genes, *SlKLUH* that encodes a cytochrome P450 (CYP78A) is the most probable candidate because it has been shown to control organ size in *Arabidopsis thaliana* (Zhang *et al.*, 2012). Other members of the CYP78A class, to which SlKLUH/FW3.2 belongs, are known to regulate flower, leaf, seed, embryo and endosperm size in *Arabidopsis*, moss and rice (Van der Knaap *et al.*, 2014). Interestingly, putative pepper and melon orthologs of *SlKLUH* are associated with larger fruit, suggesting a possible conserved role of the cytochrome P450 family in the domestication processes in fruit (Chakrabarti *et al.*, 2013; Monforte *et al.*, 2013; Zhu *et al.*, 2018). This gene is responsible of extra cell divisions which lead to enlarge fruit and a concomitant delay in ripening (Chakrabarti *et al.*, 2013). Like fw2.2 locus, function of fw3.2 is still largely underexplored.

- *LOCULE NUMBER* (*LC*) is a natural mutation that was fine-mapped to a 1,6 kb noncoding region between two putative candidate genes, *WUSCHEL* (*WUS*) and a gene encoding a WD40 repeat protein. Association mapping led to the identification of two single nucleotide polymorphisms located 1080 bp downstream of the putative tomato ortholog of *WUS* (Muños *et al.*, 2011). *WUS* is a likely candidate to be *LC* because it encodes a homeodomain transcription factor that is required for maintaining the stem cell identity in the apical meristem of *Arabidopsis thaliana*. Indeed, the increase in *WUS* expression leads to the increase in floral organ number, which is similar to the phenotype found in the *lc* mutant in tomato (Mayer *et al.*, 1998). Furthermore, the two SNPs located downstream of *SlWUS* are located in a putative tomato CArG cis-regulatory element that might regulate the expression of *SlWUS* (Rodríguez-Leal *et al.*, 2017). The loss-of-function of *lc* then leads to the increase in the *SlWUS* expression and causes the maintenance of stem cell, resulting in the increase in

locule number (van der Knaap *et al.*, 2014). Indeed, engineering the CArG element by CRISPR/Cas9 system has recently been shown to modify fruit weight (Rodríguez-Leal *et al.*, 2017).

- *FASCIATED* (*FAS*) is the second natural mutation that exhibits a synergic effect on meristem size and the locule number with *LC*. *FAS* was initially fine mapped on chromosome region where there is a 294 kb inversion with the first intron of a member of the YABBY family (Huang & Van der Knaap, 2011; Van der Knaap *et al.*, 2014). YABBY family members are transcription factors that control polarity and cell fate in plant meristems. YABBY proteins function redundantly with other polarity proteins and are required to establish the proper boundaries within the meristem and developing organ primordia. Therefore, until recently, the *FAS* mutation was believed to be responsible for flat tomatoes with increased locule number, because of the down regulation of the *YABBY* gene during flower development (Barrero *et al.*, 2006; Cong, Barrero, & Tanksley, 2008). Actually, additional investigations showed that *CLAVATA3* (*SlCLV3*) underlies the FAS phenotype (Xu *et al.*, 2015). Interestingly, SlCLV3 interacts with SlWUS in the CArG element harboring two SNPs responsible for the *lc* mutation (Muños *et al.*, 2011; Rodríguez-Leal *et al.*, 2017). CLV3 activity induces a signaling cascade that restricts *WUS* expression to prevent stem cell over proliferation and, through negative feedback, WUS promotes *CLV3* expression to limit its own activity (Schoof *et al.*, 2000).

- *OVATE* (*OV*) was fine mapped to chromosome 2 and a single mutation, leading to a premature stop codon in a newly defined class of plant proteins Ovate Family Proteins (OFP) (Liu *et al.*, 2002). The *ovate* mutation results in the transition of tomato fruit from round to a pear-shaped phenotype. It is believed that OVATE may regulate the anisotropic growth along the proximal-distal axis at the proximal end of the fruit (Van der Knaap *et al.*, 2014). *OVATE* is expressed in reproductive organs in early stages of flower and fruit development. Overexpression of *OVATE* in tomato induces abnormal plant growth with reduced floral organs and changes in vegetative and floral architecture, suggesting that OVATE is a suppressor of plant growth (Huang *et al.*, 2013; Liu *et al.*, 2002). Yeast-to-Hybrid experiment revealed that the tomato OVATE protein interacts with 11 of the 26 members of the TONNEAU1 Recruiting Motif (TRM) superfamily. TRMs interact with TONNEAU1a (TON1a),

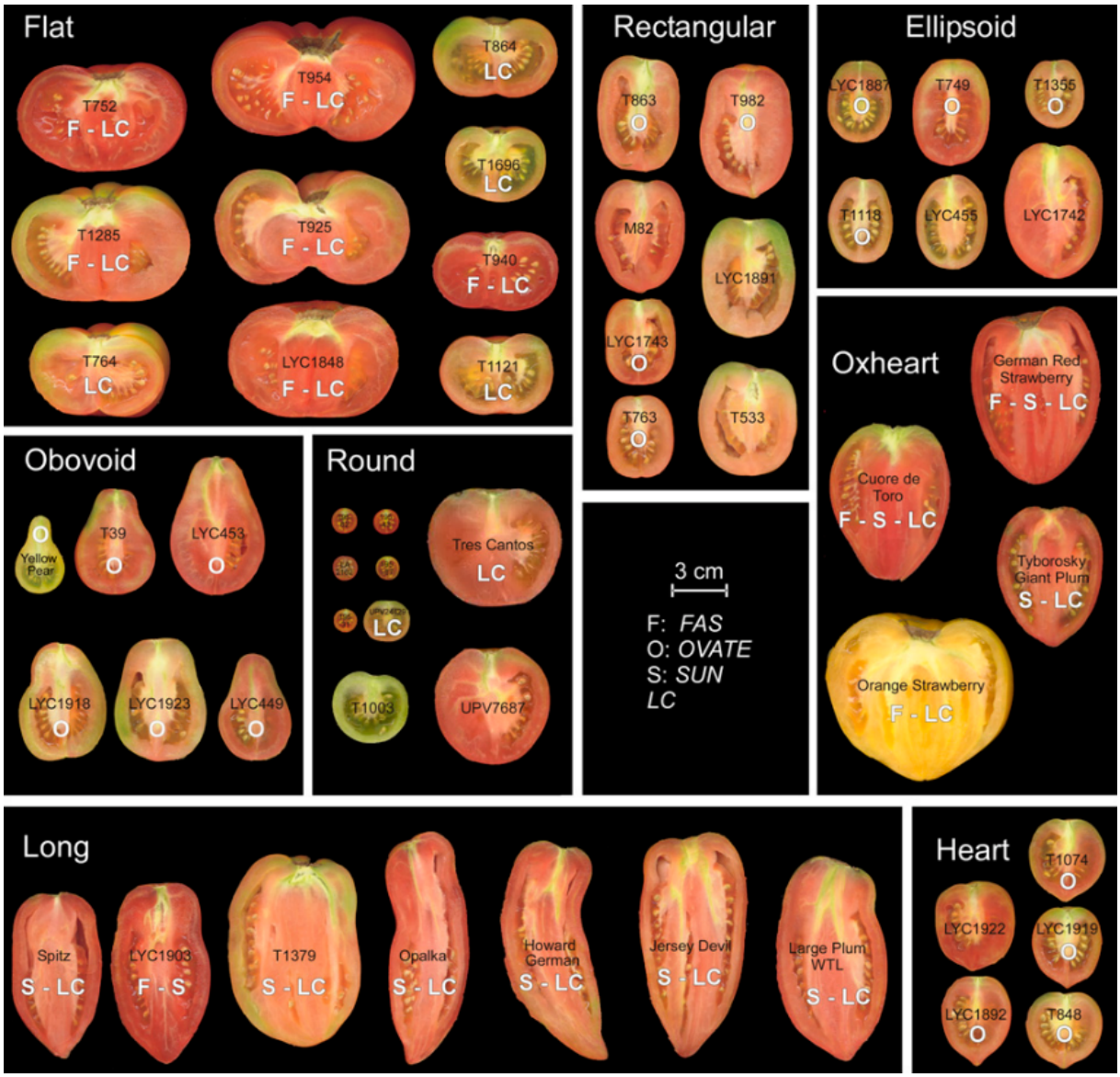

Figure 13: **Diversity in tomato fruit shapes**. From Rodriguez *et al.*, 2011

TON1b and TON2/FASS proteins, which are involved in the preprophase band formation and microtubule array organization (Van der Knaap *et al.*, 2014). According to this result, it is hypothesizes that OVATE is involved in directing the growth of the developing carpels, by interacting with TRMs and microtubules.

- *SUN* locus was fine mapped to the short arm of chromosome 7 and found to encode a member of the IQD family of calmodulin-binding proteins (Van der Knaap *et al.*, 2004; Xiao *et al.*, 2008). The overexpression of *SUN* led to extremely elongated fruit shape, with an increase in cell number along the proximal-distal axis and lower along the medio-lateral axis. SUN is able to redistribute fruit mass, by increasing cell division in the longitudinal axis and decreased cell division in the transverse direction of the fruit (Wu *et al.*, 2011), resulting in modification in fruit shape. *Arabidopsis* IQD1 was shown to interact with CaM/CMLs and Kinesin Light Chain-Related protein-1 (KLCR1), which is involved in transports of vesicles, organelles, mRNA-protein complexes along microtubules. This result suggests that AtIQD1 may act as a scaffold protein recruiting cargo to kinesin motors for directional transport along microtubules (Bürstenbinder *et al.*, 2013; Van der Knaap *et al.*, 2014). However, it is still unknown if SUN plays the same role as AtIQD1 in the regulation of the directional transport inside the cell.

Interestingly, the current diversity of fruit morphology among the tomato cultivars can be explained by modifications at four of these QTLs : *LC, FAS, OV* and *SUN* (Van der Knaap *et al.*, 2014). Rodríguez *et al.*, (2011) was able to determine the frequency by which their mutant alleles are found by comparing 368 tomato accessions (Figure 13). According to this study, the mutant allele of *OVATE* is found in all obovoid, 83% of the ellipsoid, 59% of the rectangular and 48% of the oxheart tomatoes. The mutant allele of *LC* is found at 82% and 63% in flat and long tomatoes, respectively. Most of the long and oxheart tomatoes carry the mutant allele of *SUN*. Individually, the alleles of the major genes *SUN, OVATE, LC*, and/or *FAS* explain up to 71% of the fruit shape variations in cultivated tomato (Rodríguez *et al.*, 2011).

To date, there has been strong progress in the understanding of the variation of fruit shape, and notably the tight coordination of the cell divisions resulting in different tomato forms, in the cultivated tomato. These variations involve few genes. Beyond the shape of the fruit, the fruit tissues morphology is also an important trait of quality that remains poorly studied. No specific regulator of fruit tissue morphology is

known so far and the molecular and cellular understandings underlying this character remain elusive. The functional characterization of new regulators of fruit morphology is greatly needed in order to better understand pathways regulating the final dimensions of the fruit.

III.d. Identification of new fruit growth regulators using induced diversity

As previously described, some regulators of cell division and cell expansion in tomato have been showed to have an impact on tomato fruit size and shape. Deregulations of the mitotic cell cycle and endoreduplication affect tomato fruit development, by modifying the final cell number and cell size inside the pericarp. Many genes involved in cell cycle and endocycle are already well described, thanks to the work done in *Arabidopsis thaliana* and to a lesser extent on *Medicago truncatula*. Reverse genetics strategies allowed the description of their contribution to tomato fruit growth and shape (Bisbis *et al.*, 2006; Chevalier *et al.*, 2014; Czerednik *et al.*, 2012, 2015; Gonzalez *et al.*, 2007; Mathieu-Rivet *et al.*, 2010; Nafati *et al.*, 2011). However, reverse genetics does not offer the possibility to reveal new genes.

To overcome these limitations, mutant collections represent a rich new source of genetic and phenotypic diversity that can be mined to isolate fruit weight or morphology mutants and identify the underlying genes. EMS-induced mutations prove to be efficient to create a large phenotypic diversity in several tomato cultivars (Just *et al.*, 2013; Menda *et al.*, 2004; Saito *et al.*, 2011). High genetic diversity can be obtained through EMS (ethyl methane sulfonate) mutagenesis that creates point mutations evenly distributed over the genome with a high density. One of the advantages of EMS is that it creates a broad range of alleles within relatively small populations. EMS overcomes the effects of domestication bottleneck by potentially creating all the genetic and phenotypic diversity possible in the same genetic background. In this context, mutant collection allows studying, the variation of traits of interest in quasi isogenic backgrounds (at the exception of the EMS mutations created). Combined with the current advances in whole genome sequencing based mapping-by-sequencing strategy (Garcia *et al.*, 2016), it is now much easier to identify allelic variants underlying phenotypes of interests, as previously shown for cutin-deficient mutants (Petit *et al.*, 2014; Petit *et al.*, 2016) and fruit number and yield mutants (Soyk *et al.*, 2017). This strategy seems promising for the identification of new regulators of fruit tissue morphology in tomato.

Chapter II

–

CONTEXT & OBJECTIVES

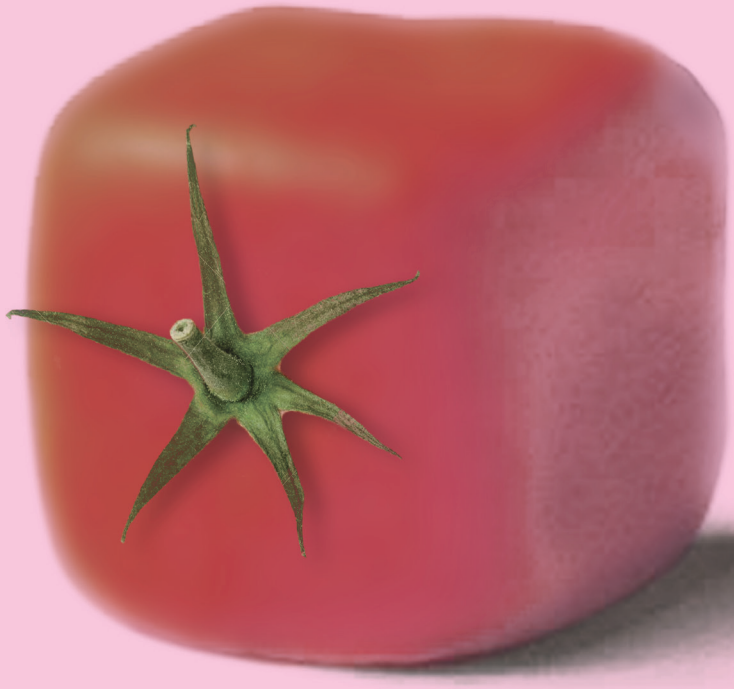

I. Context of the thesis and preliminary works

The use of natural diversity including wild and cultivated tomato in forward genetic approaches or the study of candidate genes through reverse genetics, only allowed identify and characterize a dozen of genes involved in fruit size and fruit shape determination. There is a clear need for the identification of new regulators of fruit growth for a better understanding of the key genetic, cellular and molecular events involved. In this context, one of the main objectives of my thesis is to identify new genetic factors and characterize their function during fruit growth.

With the aim to identify new regulators of tomato fruit growth, a preliminary screening of our Micro-Tom EMS mutant collection was conducted before the beginning of my PhD to identify phenotypes of interest. MicroTom is a miniature tomato cultivar particularly suitable for large-scale mutant screen, due to its small size (10–20 cm tall), short life cycle (70–90 days) and high density culture (Carvalho *et al.*, 2011; Emmanuel and Levy, 2002). We focused on fruit size modifications and on fruit tissue morphology alterations, as this last parameter is highly important for final fruit traits and quality and were not previously studied in tomato. I participated in this screening during my Master 2 internship, during which I characterized six EMS mutants, at the organ, tissue and cellular levels. I also checked if the phenotype of interest in these mutants segregated as a Mendelian trait, by characterizing the F2 segregant individuals.

Data from this study were included in a scientific paper, describing the mutant screening and highlighting two ways of growth. I also participated in the redaction of this article at the beginning of my PhD. This scientific paper published in Frontiers in Plant Science in 2017, introduces my PhD. project.

frontiers in Plant Science

ORIGINAL RESEARCH
published: 12 June 2017
doi: 10.3389/fpls.2017.00988

Identification of Two New Mechanisms That Regulate Fruit Growth by Cell Expansion in Tomato

Constance Musseau, Daniel Just, Joana Jorly, Frédéric Gévaudant, Annick Moing, Christian Chevalier, Martine Lemaire-Chamley, Christophe Rothan† and Lucie Fernandez†*

UMR 1332 BFP, Institut National de la Recherche Agronomique, University of Bordeaux, Villenave d'Ornon, France

Key mechanisms controlling fruit weight and shape at the levels of meristem, ovary or very young fruit have already been identified using natural tomato diversity. We reasoned that new developmental modules prominent at later stages of fruit growth could be discovered by using new genetic and phenotypic diversity generated by saturated mutagenesis. Twelve fruit weight and tissue morphology mutants likely affected in late fruit growth were selected among thousands of fruit size and shape EMS mutants available in our tomato EMS mutant collection. Their thorough characterization at organ, tissue and cellular levels revealed two major clusters controlling fruit growth and tissue morphogenesis either through (i) the growth of all fruit tissues through isotropic cell expansion or (ii) only the growth of the pericarp through anisotropic cell expansion. These likely correspond to new cell expansion modules controlling fruit growth and tissue morphogenesis in tomato. Our study therefore opens the way for the identification of new gene regulatory networks controlling tomato fruit growth and morphology.

Keywords: EMS, fruit, growth, morphology, mutant, phenotype, tissue, tomato

OPEN ACCESS

Edited by:
Elizabete Carmo-Silva, Lancaster University, United Kingdom

Reviewed by:
Sofia Kourmpetli, Cranfield University, United Kingdom
Barbara Molesini, Department of Biotechnology, India

****Correspondence:***
Lucie Fernandez
lucie.fernandez@inra.fr

† These authors have contributed equally to this work.

Specialty section:
This article was submitted to Plant Physiology, a section of the journal Frontiers in Plant Science

Received: *08 February 2017*
Accepted: *24 May 2017*
Published: *12 June 2017*

Citation:
Musseau C, Just D, Jorly J, Gévaudant F, Moing A, Chevalier C, Lemaire-Chamley M, Rothan C and Fernandez L (2017) Identification of Two New Mechanisms That Regulate Fruit Growth by Cell Expansion in Tomato. Front. Plant Sci. 8:988. doi: 10.3389/fpls.2017.00988

INTRODUCTION

Plant domestication has resulted in profound phenotypic changes in fleshy fruit-bearing species including the increase in fruit yield, sensorial and nutritional quality and shelf-life. Even if domestication led to a drastic reduction of the nucleotide diversity (Doebley et al., 2006), mutations were continuously accumulated in a recent diversification phase following this syndrome, offering opportunities for new phenotypes to arise. As a result, in addition to fruit weight, other major fruit developmental traits have been selected, among which the fruit shape that displays a wide diversity in species such as tomato and pepper (Frary et al., 2000; Paran and van der Knaap, 2007; Rodríguez et al., 2011) and melon (Périn et al., 2002; Monforte et al., 2014).

This diversity has been further exploited in order to fulfill specific needs of fruits for fresh consumption (e.g., table grapes, fresh market tomatoes) and for processing and mechanical harvesting (e.g., wine grapes, processing tomatoes). This improvement highly impacted tissue morphology and cellular characteristics of the fruit. To date, tissue morphology has drawn much less attention than fruit weight or shape, probably because of its inherent complexity. Although tools enabling the comparative description of internal fruit morphology have been published (Rodríguez et al., 2010), the bulky nature of the fruit still requires destructive analyses to score

these traits. As a consequence, very few large scale and detailed studies taking into account fruit tissue morphology, similar to those previously conducted on leaves (Chitwood et al., 2014, 2016), have been published.

Cultivated tomato (*Solanum lycopersicum* L.) stands as the model species for *Solanaceae* and for fleshy fruit biology, especially when investigating the ripening process (Klee and Giovannoni, 2011). It is also an appropriate model to analyze fruit weight and tissue morphology because of the large existing phenotypic diversity. Information have been collected in large databases collecting the phenotype of thousands of tomato varieties found all other the world as well as of wild tomato accessions (TGRC[1]; BreeDB[2]). In addition, considerable genomic data have been generated in the recent years, including the genome sequences of a large number of cultivated tomato varieties and of the wild relatives *S. pimpinellifolium* and *S. pennellii* (Tomato Genome Consortium, 2012; Aflitos et al., 2014; Bolger et al., 2014; Lin et al., 2014). A number of loci controlling fruit weight and shape have been mapped (Tanksley, 2004). Those selected through the domestication and subsequent improvement processes have been identified (Lin et al., 2014) and six genes underlying the major QTLs have been cloned. These include the *fw2.2* and *fw3.2* fruit weight QTLs (Frary et al., 2000; Zhang et al., 2012; Chakrabarti et al., 2013), the *locule-number* and *fasciated* locule number QTLs (Muños et al., 2011; Xu et al., 2015) and the *ovate* and *sun* fruit shape QTLs (Liu et al., 2002; van der Knaap et al., 2004; Xiao et al., 2008) that affect flower meristem, ovary or very early stages of fruit development. Remarkably, regardless of the wide diversity in fruit size and shape observed in cultivated tomato (e.g., as much as 3900 carpel number genotypes described in the BreeDB database), a limited set of allelic variants identified in six genes are involved, alone or in combination, in the major variations in fruit morphology in domesticated tomato (van der Knaap et al., 2014). Indeed, the alleles of the major genes SUN, OVATE, LC, and/or FAS individually explain up to 71% of the fruit shape variations in cultivated tomato (Rodríguez et al., 2011). Thus, there is a clear need for isolating new regulators of fruit morphology and, as a first step, to identify new fruit growth modules in tomato.

Of special interest are the variations affecting cell enlargement during the expansion stage of the fruit, which remain largely underexplored. Cell expansion contributes the most to the final size of the fruit (Lemaire-Chamley et al., 2005). It is also regulated differentially in the various tissues within the fruit and thereby likely plays a key role in fruit tissue morphology. One key process associated with the cell expansion phase in tomato is endoreduplication that results in the formation of polyploid nuclei. Rather than determining a defined cell size, endoreduplication in tomato offers a potentiality for further cell growth through the adjustment of the cytoplasmic volume with the nuclear DNA content, according to the karyoplasmic ratio theory (Cheniclet et al., 2005; Bourdon et al., 2012). A large set of data resulting from functional analyses of candidate genes controlling the mitotic cycle/endocycle transition highlighted the tight relationship between nuclear ploidy and cell size (see De Veylder et al., 2011; Chevalier et al., 2014 for reviews). However, because they are mostly limited to known candidate genes, reverse genetic strategies can hardly give new insights into poorly characterized developmental processes.

Thus the reduced genetic diversity in cultivated tomato that limits the identification of minor or "hidden" loci as well as the limitations of reverse genetics approaches hamper our comprehension of the late fruit growth modules in tomato. One way to overcome these limitations is to create *de novo* a wide genetic and phenotypic diversity. High genetic diversity can be obtained through EMS (ethyl methanesulfonate) mutagenesis that creates point mutations evenly distributed over the genome. We and others previously generated tomato mutant collections which displayed extensive fruit phenotypic diversity (Menda et al., 2004; Saito et al., 2011; Just et al., 2013) and further showed that a population of few thousand highly mutagenized mutant lines is sufficient to find at least one severe mutation in every single tomato gene (Garcia et al., 2016; Shirasawa et al., 2016). Here we further exploit this diversity to unravel developmental modules determining fruit weight and tissue morphology during the cell expansion phase of the fruit and get insights into the underlying mechanisms.

MATERIALS AND METHODS

Plant Material and Culture

Fruit weight and tissue morphology tomato (*S. lycopersicum* L.) mutants were isolated from a highly mutagenized EMS mutant collection produced in the miniature cv. Micro-Tom as previously described (Just et al., 2013; Petit et al., 2014). In a first step, 35 mutant lines previously identified as fruit size and/or morphology mutants were phenotyped to confirm the observed phenotypic alterations (six plants/mutant line); this was done on M2 or M3 plants. In a second step, each selected mutant line was self-pollinated and M4–M8 plants were used for detailed phenotypic analysis. Mutant phenotypes are therefore considered as fixed because genome homozygosity is in the ∼93 to 99% range. Phenotyping was carried out during 4 years (2012–2015) on tomato plants grown year-round (3–4 cycles/year) in greenhouse in controlled conditions as described in Rothan et al. (2016). In order to take into account the fruit phenotypic plasticity in changing environmental conditions (mainly due to seasonal variations), the non-mutagenized Micro-Tom parental line, thereafter called WT, was cultivated side-by-side with the mutant lines and used as a reference. In addition, for all the lines, the first flower from each inflorescence was removed to take into account the high incidence of abnormal fruits produced by this flower in cv. Micro-Tom. A total of 39 different parameters thoroughly describing the plant development (3), yield components (2), organ (6), tissue morphology (11), cell morphology (8) and nucleus ploidy (9) were used for phenotyping the mutants (Supplementary Table 1). Ovary analyses were performed at anthesis (i.e., fully opened flower) before fruit set. Fruit analyses

[1]http://tgrc.ucdavis.edu/

[2]https://www.eu-sol.wur.nl/

were performed at breaker stage at the onset of ripening. Breaker stage was defined as the first appearance of yellowish traces on the fruit, which takes place at about 30–35 DPA when the fruit has reached its final size. To take into account the likely influence of photoassimilate availability on fruit growth and tissue morphology, most parameters (Supplementary Table 1) were measured in standardized conditions. To this end, fruit load on the plant was reduced to six fruits distributed on two fruit trusses (controlled load) by flower pruning. In addition, to allow comparison between controlled and unrestricted fruit loads, several parameters (Supplementary Table 1) were also measured from plants in which fruit load was left free and allowed to reach up to 20 fruits per plant (unrestricted load). In addition to ovary and fruit phenotypes, plant traits with possible effect on fruit growth (fruit yield, vegetative-to-reproductive phase transition) were also considered.

Determination of Fruit Tissue Morphology

Fruit tissue morphology features were determined from fresh fruit equatorial sections by scoring the proportion of each fruit tissue. Fruit equatorial sections were analyzed using the Tomato Analyser 3.0® software (Rodríguez et al., 2010). Whole fruit, pericarp, radial pericarp, columella and locular tissue area measurements were done according to Sun et al. (2015) (Supplementary Figure 1A). Values given for the proportion of pericarp (%P), radial pericarp (%RP), locular tissue (%LT) and columella (%C) were relative to the whole fruit and were thus independent from the variations in fruit weight observed amongst the various mutants.

Ovary and Fruit Histological Analyses

Fresh equatorial sections of ovaries (30 μm thickness) and breaker fruits (150 μm) were obtained using a vibration microtome (Microm HM 650 V, Thermo Scientific) prior to staining with 0.01% calcofluor or 0.05% toluidine blue (TB). Three to eleven ovaries or fruits were analyzed for each mutant line (Supplementary Table 1). Sections were then observed under an epifluorescence microscope (Zeiss Axiophot, Carl Zeiss) for calcofluor staining or with a stereomicroscope (Olympus SZX16, Olympus) for TB staining. Pericarp measurements were performed on the three layers (exocarp, mesocarp, and endocarp), excluding the vascular bundles.

Average equatorial ovary area (O_A), ovary wall thickness (OW_thick), pericarp thickness (P_thick) and number of pericarp cell layers (Cell_layer) were determined using these sections (Supplementary Figure 1B). Measurements (5 per trait) were done and averaged using the Image-Pro PLUS software (Media Cybernetics, Silver Spring, MD, United States).

These sections were also used to measure the cell area within the ovary wall and the fruit pericarp. Cell segmentation was performed using the CellSeT software (Pound et al., 2012) to optimize automatic cell counting. Area quantification was done using the Image-Pro PLUS software (Supplementary Figure 1C). For area quantification, 100 to 300 cells were observed per section to evaluate the maximum cell area (OWCell_max, PCell_max), the mean cell area (OWCell_mean, PCell_mean) and the average cell area of the 25% larger cells (OWCell_25, PCell_25). The same segmentations were used to evaluate cell shape of the 10 and 25% largest cells by scoring the X/Y cell ratio where (X) corresponds to the adaxial–abaxial and (Y) to the medio-longitudinal axes.

Ploidy Analysis

Cell ploidy quantification was determined by flow cytometry (CyFlow Space, Partec) using pericarp tissue from the fruit equatorial region according to Cheniclet et al. (2005). The relative proportion of each nucleus population (4C to 256C) was calculated together with the Ploidy Index (PI) and the Endoreduplication Factor (EF). Both are commonly used to estimate the mean ploidy level and the average number of endoreduplication cycles, respectively (Bertin et al., 2009). The 2C peaks were not quantified because of their low level in Micro-Tom at breaker stage (L. Fernandez, pers. obs.).

Statistical Analyses

Multivariate and univariate analyses were performed using BioStatFlow application implemented using R packages (v2.7.7 INRA[3]) in order to identify differences and relationships between mutants or traits.

A Volcano plot was used to visualize significant phenotypic variations for fruit weight and pericarp thickness corresponding to the initial criteria used for mutant screening. Data from the different experiments were plotted in a single Volcano plot to insure consistency between the different environmental conditions. Mean comparisons between mutants and the WT were performed using Student's t-test and choosing the false discovery rate (FDR) cut-off of 0.05 (Benjamini and Hochberg, 1995).

Principal component analysis (PCA) was used to have a global view of the data. As some parameters were analyzed over different experiments, for consistency, for each experiment the mutant values were expressed as relative to the WT (ratio between the mean value of the mutant and the mean value of the WT). The data used for PCA corresponded to the average mutant/WT ratios standardized to unit variance.

Clustering of the mutants was performed using correlation coefficients calculated on 24 fruit traits measured in controlled fruit load conditions. Spearman rank correlations were chosen in order to capture non-linear relationships. The correlations between traits were calculated separately for each mutant cluster based on the same fruit parameters together with ovary parameters. Correlations were calculated on the average mutant/WT ratios for each trait and considered significant when P-value < 0.01. Network reconstruction was performed using BioStatFlow application and visualization was done using Cytoscape software v3.1 using spring embedded layout (Shannon et al., 2003).

[3]http://biostatflow.org/

RESULTS

Screening Micro-Tom EMS Mutant Collection for Fruit Weight and Tissue Morphology Mutants

To investigate the induced variations in fruit weight and tissue morphology, we screened a tomato mutant collection previously generated in the miniature cultivar Micro-Tom by EMS mutagenesis. About 3500 M2 mutant lines had previously been phenotyped for over 150 phenotypic traits; within this collection the fruit shape and size diversity observed was found to be considerable (Just et al., 2013). For example, we observed in the collection 1253 multi-locular mutant families. Increased carpel number and fruit shape alterations are indeed of considerable interest to investigate variations in fruit weight and tissue morphology in cultivated tomato (van der Knaap et al., 2014) but may also hinder the existing relationships between different fruit traits (e.g., the link between pericarp cell ploidy and fruit size; Cheniclet et al., 2005). We therefore excluded fruit carpel number mutants and fruit shape mutants (e.g., round, flat, rectangular, ovoid or heart shaped fruits; Supplementary Figure 2) from the analysis. Likewise, as fruit growth patterns are likely modified in the parthenocarpic fruits which often lack locular tissue and in addition are very difficult to multiply (Serrani et al., 2007), strict parthenocarpic mutants were excluded from the analysis. However, mutants with a reduced number of seeds that could be easily maintained through sexual propagation were included in the study. At last, care was also taken to exclude mutants showing major variations in plant height and leaf attributes (number, size, shape, and color), since the carbon status of the plant can considerably impinge on fruit growth.

Phenotypic selection centered on fruit size and pericarp thickness produced, respectively, as many as ∼ 2300 and ∼1000 mutants in the collection. Taking into account the criteria indicated above, 35 mutants were selected and grown in a greenhouse. To investigate the developmental processes involved in tomato fruit growth, 12 mutants displaying robust and stable fruit phenotypes over the different environmental conditions experienced by the plants were then further characterized (**Figure 1**). All these mutants were comparable to the wild type in term of vegetative growth (data not shown).

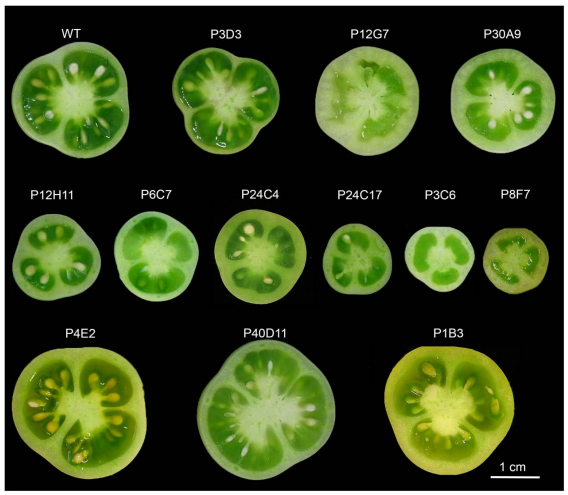

FIGURE 1 | Diversity of fruit weight and tissue morphology of the 12 selected tomato mutants and the wild-type (WT). Fruit equatorial sections around breaker stage show small and large fruits phenotypes as well as thick- and thin-pericarp phenotypes. Locule number and fruit shape in the mutants are similar to the WT. No strict parthenocarpy phenotypes were selected and P12G7, P3C6 and P8F7 produced at least few seeds.

Wild-Type Micro-Tom Fruit Development and Tissue Morphology

To constitute the reference dataset to which all mutant phenotypic data could be subsequently compared, the tissue morphology of ovary and fruit (breaker stage) from cv. Micro-Tom was thoroughly investigated in WT plants. In Micro-Tom the final fruit size is reached after 30–35 days post anthesis (DPA), at breaker stage (**Figure 2A**). From ovary (1 mm diameter) to breaker stage (2.5 cm diameter), the equatorial fruit diameter increases by more than 2000-fold (**Figures 2B,C**) resulting in a mean fruit weight of 3 g (unrestricted load, 20 fruits per plant) to 5–6 g (controlled load, six fruits per plant). Fruit usually comprises three carpels separated by a radial pericarp (RP; 7% of the fruit area in equatorial section) fused to the central axis called columella (C; 11% of the fruit area) (**Figure 2C** and Supplementary Figure 1A). The pericarp (P) that develops from the ovary wall, and the locular tissue (LT) that differentiates from the placenta are the main fruit tissues, representing, respectively, 30 and 50% of the total fruit area in equatorial section (**Figure 2C** and Supplementary Figure 1A). The number of seeds is proportional to the final fruit weight, ca. 5 to 7 seeds per gram of fruit weight.

Starting from the abaxial (external) to the adaxial (internal) side of the fruit, the pericarp is classically subdivided into: (i) the exocarp, which is constituted by the epidermal cell layer and by several layers of small collenchyma cells; (ii) the mesocarp displaying the smaller cells close to the exocarp and to the endocarp while largest cells are located in the inner mesocarp; and (iii) the endocarp constituted of one epidermal cell layer (**Figures 2A,C** and Supplementary Figure 1B). Vascular bundles, which are constituted by very small phloem cells and by xylem cells, are regularly distributed within the mesocarp (**Figure 2C** and Supplementary Figure 1B). The ovary wall (100–120 μm in thickness) is composed of less than 10 cell layers of uniform small cells (**Figure 2B**). The pericarp (2 mm in final thickness) consists of 14 to 17 layers of cells with a mean area of 0.01 mm^2, which show considerable size heterogeneity (**Figure 2C**).

Selected Mutants Exhibit Wide Variations in Fruit Weight, Tissue Morphology, and Cell-Related Traits

Final fruit weight was significantly different from that of WT in three large fruit mutants (P4E2, P1B3, and P40D11) and in six small fruit mutants (P12H11, P24C3, P6C7, P3C6, P24C17, and P8F7) (**Figures 1**, **3**). Among these, the P3C6, P24C17,

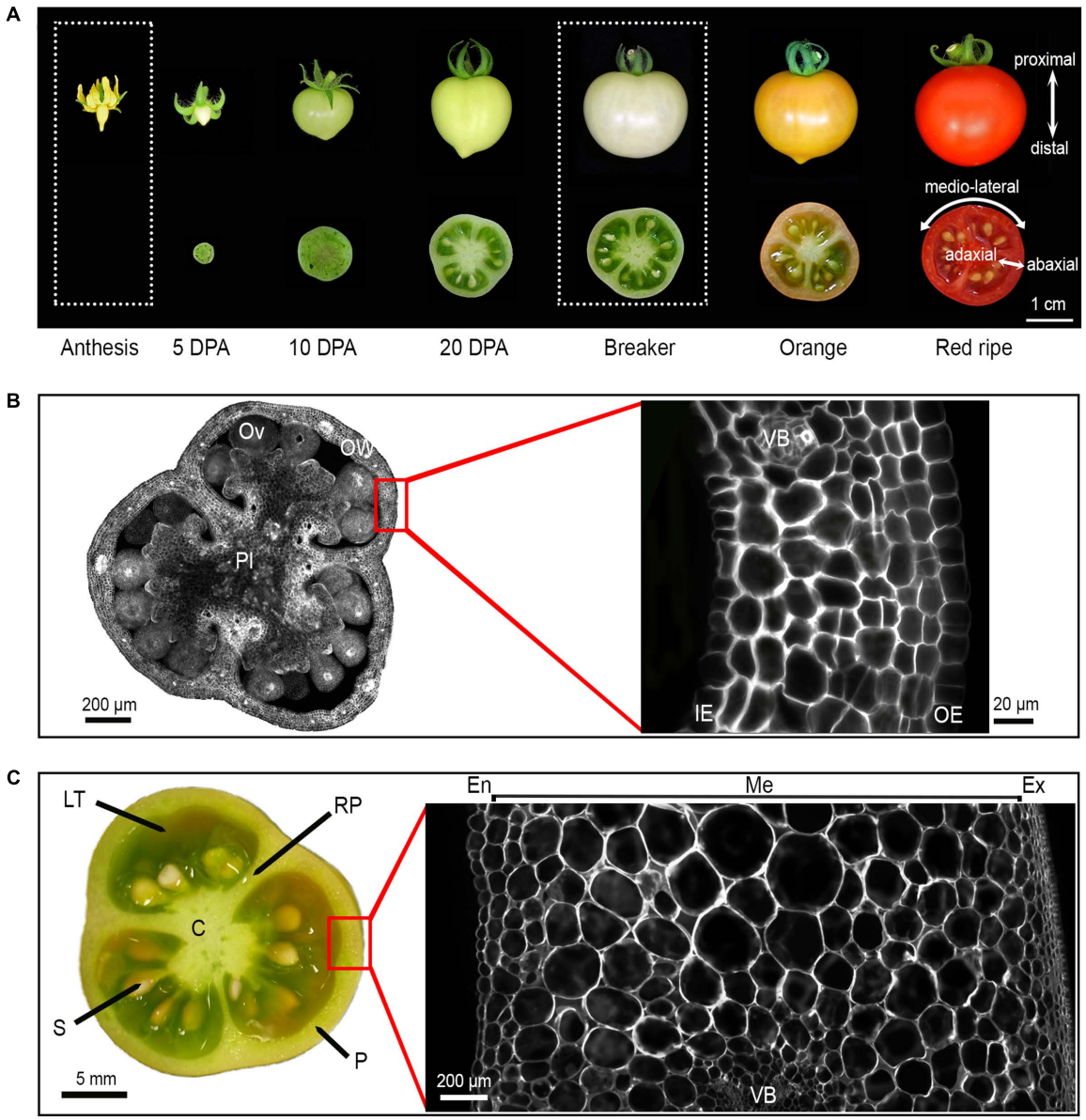

FIGURE 2 | Tomato fruit development and tissue morphology in WT Micro-Tom cultivar. **(A)** Whole fruit and equatorial fruit sections from anthesis to red-ripe stage. The axes of growth: proximal to distal, medio-lateral and abaxial to adaxial are reported. **(B)** Equatorial ovary section and ovary wall section at anthesis stained with calcofluor. **(C)** Equatorial fruit section and pericarp section at breaker stage stained with calcofluor. DPA, Day Post Anthesis; OW, ovary wall; Pl, placenta; Ov, ovule; OE, outer epidermis; IE, inner epidermis, VB, vascular bundle; C, columella; LT, locular tissue; S, seed; RP, radial pericarp; P, pericarp; En, endocarp; Me, mesocarp; Ex, exocarp.

and P8F7 mutants displayed a >2-fold reduction in fruit weight (**Figure 3**). In addition, the P8F7, P24C3, P12G7, and P30A9 mutants produced fruits with a thicker pericarp while the only thin pericarp mutant identified was P3D3 (**Figures 1**, **3**). Noteworthy, although P8F7 and P24C4 were small fruit mutants, their pericarp thickness (P_thick) and percentage of pericarp tissue per fruit (%P) were significantly higher than those of WT (**Figure 3**).

To further investigate the contribution of the various plant, fruit, tissue and cell characteristics to the variations in fruit weight and tissue morphology, we performed a principal component analysis (PCA) based on 37 phenotypic traits scored in the 12 mutants and in WT as a reference (Supplementary Table 1). PC1 clearly separated mutants according to pericarp-related traits, which are opposite to locular tissue-related traits in the PCA (**Figures 4A,B**). In contrast, PC2 separated mutants according to final fruit weight (**Figures 4A,B**). Ovary-related traits such as ovary wall thickness and ovary cell area had limited impact on total variation of PC1 and PC2 (**Figure 4A**). However, ovary wall traits together with nuclear ploidy (4C, 8C, and 64C values)

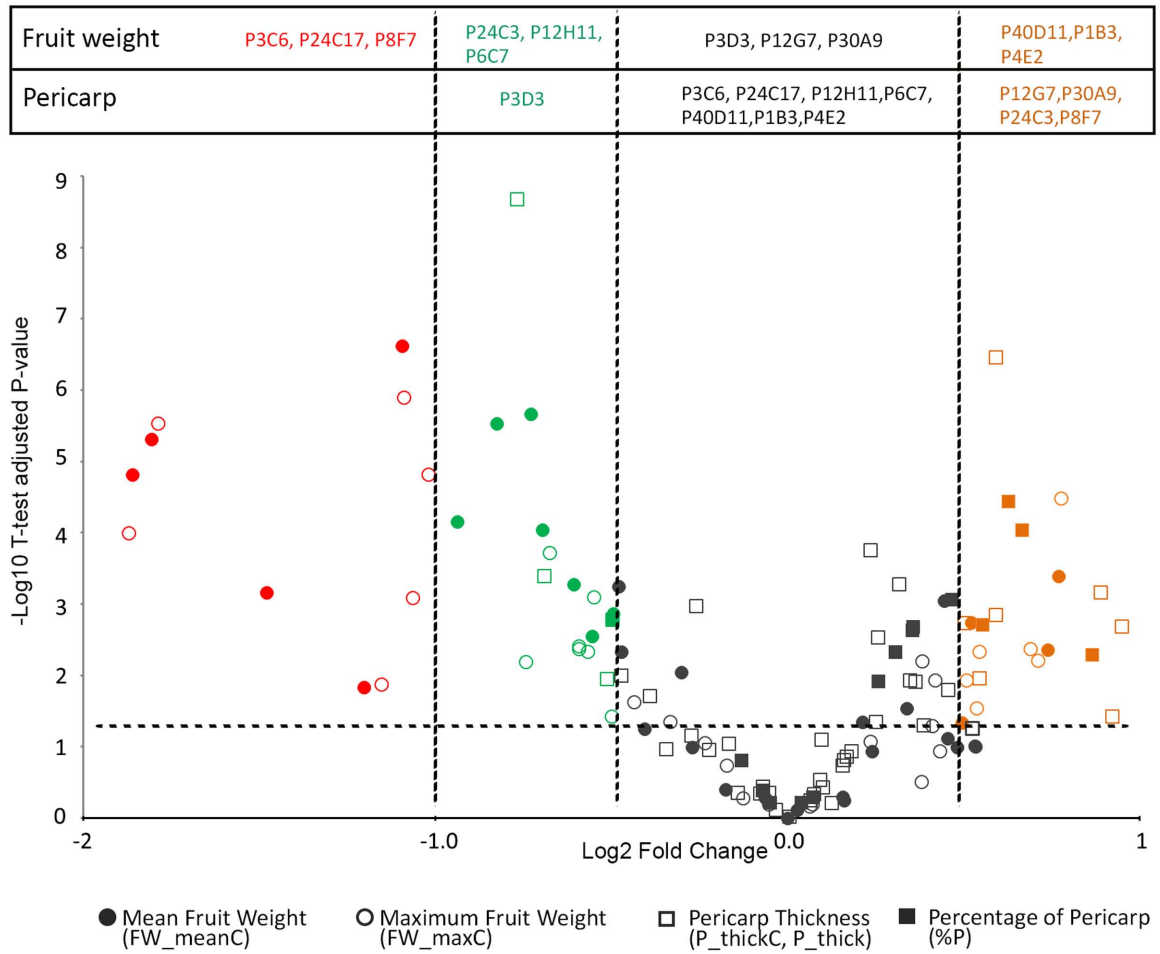

FIGURE 3 | Volcano plot of the variations in fruit weight (FW_meanC and FW_maxC) and pericarp thickness (P_ThickC) or percentage (%P) in the tomato mutants. The Volcano plot combines the magnitude of change plotted on *x*-axis, with the *t*-test significance plotted on *y*-axis indicating the FDR adjusted 0.05 *P*-value threshold. The WT is used as the reference. Log2 Fold change thresholds relative to the WT are indicated using a color code: <–1 (red), >–1 and <–0.5 and (green) and >0.5 (orange).

of pericarp cells accounted for 14.6% of total variance on PC3 (Supplementary Figure 3). Because the plant-related traits scored (Node, FGD, VGD, Supplementary Table 1) poorly contributed to the total variance, they were excluded from further analyses focused on ovary and fruit traits.

Fruit Weight and Tissue Morphology Mutants Group in Only Two Clusters Despite Their Diversity

To further investigate the contribution of each trait to the variations in fruit weight and tissue morphology, we built correlation networks using Spearman correlations between the 24 fruit traits scored in controlled conditions of fruit production (traits underlined in the PCA shown in **Figure 4A**). The correlation network identified positive and negative relationships between the mutants and, rather surprisingly given the large phenotypic diversity observed in the mutants, clearly separated the mutants in only two distinct major clusters (**Figure 5A**). Cluster 1 included the P4E2, P1B3, and P40D11 large fruit mutants negatively correlated to P6C7 and P12H11 small fruit mutants (**Figures 4B**, **5A**). Cluster 2 included the P3C6, P8F7, P24C17, P30A9, P12G7, P24C3, and P3D3 mutants. Cluster 2 mutants are mainly thick pericarp mutants, except for the P3D3 thin pericarp mutant which is negatively correlated to the P24C3 mutant (**Figures 4B**, **5A**). Cluster 1 encompasses fruit weight variations centered on PC2 while cluster 2 is related to pericarp thickness variations centered on PC1 (**Figure 4A**).

We next built, for each mutant cluster, a correlation network between the parameters describing ovary and fruit characteristics. This allowed us to explore their interrelations at organ, tissue and cellular levels and to analyze their contribution to fruit weight and tissue morphology (**Figures 5B,C**). For both clusters, ovary network was independent from fruit network except that ovary wall thickness and cell size were correlated to columella in cluster 1 and to fruit weight in cluster 2 (**Figures 5B,C**). Thus, fruit weight appears as independent from other fruit characteristics and as related to

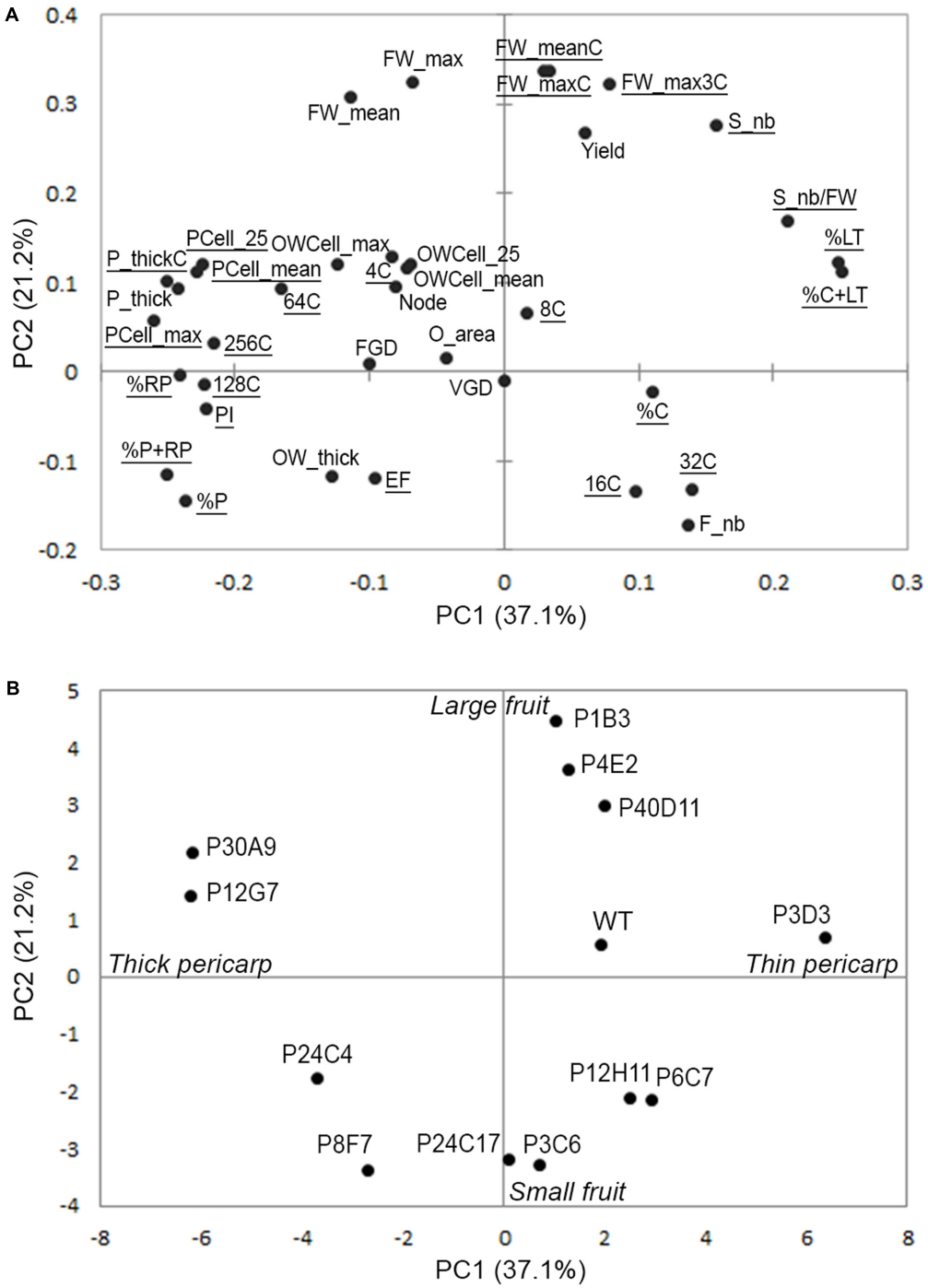

FIGURE 4 | Variability of plant, ovary and fruit traits in the tomato mutants visualized using PCA of 37 traits in 12 mutants and the WT. **(A)** Projection of the 37 phenotypic traits on the first two dimensions PC1 and PC2 explaining 58% of total variance. **(B)** Projection of the mutants and WT on the first two PCs.

pre-anthesis ovary development in cluster 2 (**Figure 5C**). For fruit traits, in cluster 1, positive correlations were observed between fruit weight, % of locular tissue and columella, seed number, pericarp cell size and high ploidy (64C and 128C); negative correlations were observed between these traits and lower ploidy values (16C and 32C) and % of pericarp tissues (**Figure 5B**). The positive correlations between fruit pericarp characteristics (proportion in the fruit, thickness and cell size) and high (128C) to extreme (256C) ploidy levels were the main features of cluster 2; negative correlations were observed between these traits and % of locular tissue and columella (**Figure 5C**).

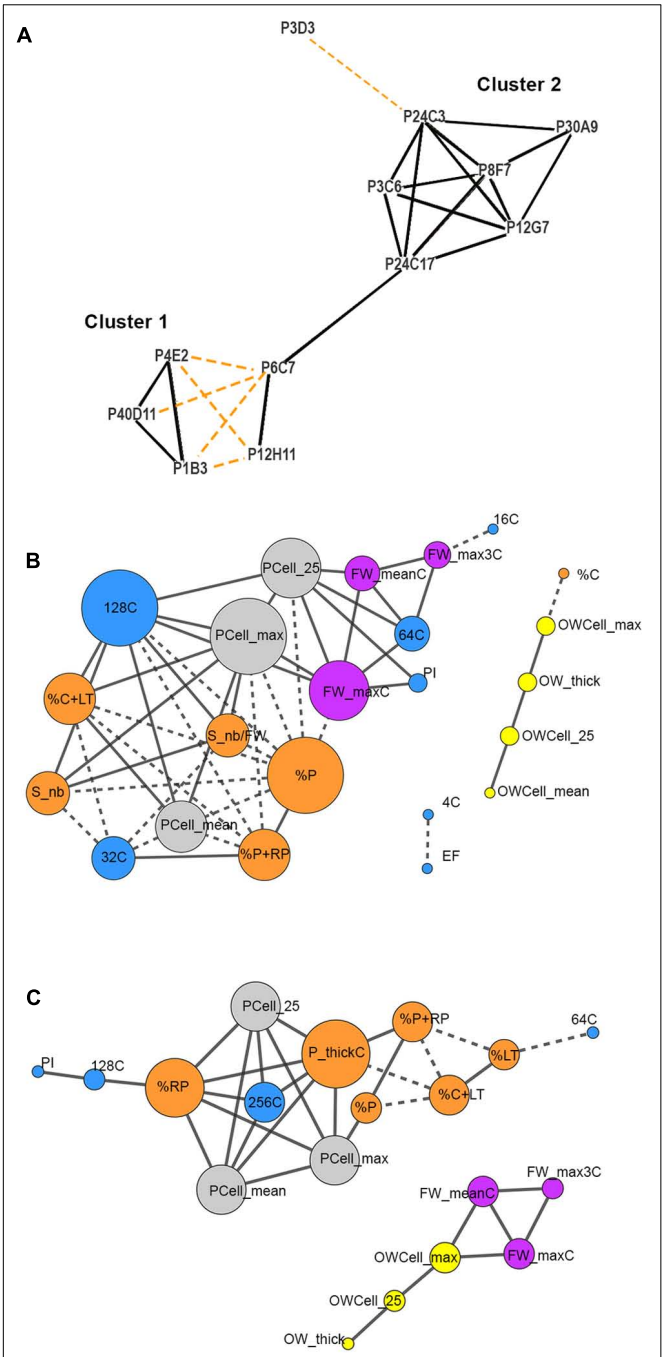

FIGURE 5 | Correlation network analysis of the fruit weight and tissue morphology mutants and of phenotypic traits measured in the tomato mutants. Only significant positive (solid lines) or negative (dashed lines) Spearman rank correlations with **(A)** FDR adjusted *P*-value < 0.01 or **(B,C)** *P*-value < 0.01 are considered in the networks. **(A)** Mutant correlation network based on 24 fruit traits. Mutants whose fruit characteristics have similar trends are clustered together. **(B,C)** Trait correlation networks are represented based on 29 fruit and ovary traits separately for mutant **(B)** cluster 1 and **(C)** cluster 2. A color code is used to distinguish the different subcategories of the phenotypic traits: ovary (yellow), fruit weight (purple), ploidy (blue), cell area (gray), fruit tissue (orange). The size of each node is proportional to the number of correlations with other traits. Phenotypic traits without significant correlations are not reported in the Figure.

Common Fruit Developmental Features Characterize Each Cluster of Mutants

We next focused on main fruit parameters highlighted in the correlation network analysis (**Figures 5B,C**) to investigate more deeply the fruit developmental patterns that characterize the mutants in each cluster. Common features were identified amongst cluster 1 mutants regarding final fruit weight, pericarp cell size and pericarp nuclear ploidy (**Figure 6A**). In this cluster, the relative proportion of the pericarp and of other tissues (locular tissue, radial pericarp, and columella) remained similar to that of the WT, regardless of the final fruit weight (**Figures 6A,B**). Likewise, the seed number remained proportional to fruit weight. Surprisingly, in view of the commonly admitted hypothesis that cell number is a major determinant of fruit weight (Frary et al., 2000), the number of cell layers in the pericarp was barely affected despite the large variation in fruit weight (**Figures 6A,C**). In contrast, the main changes for large fruits were the strong increase in 128C nuclei content and to a lesser extent in 64C nuclei, to which was associated a slight increase in pericarp cell size. The opposite was true for small fruit mutants.

In fruits from cluster 2 mutants, a very different growth pattern was prevailing. In this cluster, fruit weight was either similar to that of the WT or was strongly reduced. However, in contrast to cluster 1, fruit weight reductions were not accompanied by the proportional reduction in all fruit tissues. On the contrary, in all cluster 2 mutants but one (P3D3), the proportion of the pericarp and radial pericarp was substantially increased to reach 40–49% of the fruit tissues (∼30% in WT). Conversely, the proportion of locular tissue was strongly reduced to 27–37% (∼50% in WT), as was the number of seeds (**Figure 6A**). The resulting thick-walled fruits had a bulky and fleshy appearance, reminiscent of processing tomatoes (**Figure 6B**). As already observed for cluster 1 mutants, the number of pericarp cell layers remained largely unaffected. Increased proportion of pericarp tissue in the fruit was associated with increased pericarp thickness and/or pericarp outgrowth in the inner part of the fruit (**Figure 6B**) and with high ploidy values (64C to 256C). Noteworthy, even for the most contrasted P3C6, P8F7, and P24C17 small fruit phenotypes, the pericarp cell area was at least equivalent or higher than that of the WT, while in cluster 1 small fruit phenotypes were associated with smaller pericarp cell area. The thin-pericarp P3D3 mutant, which has the same size as several thick-pericarp mutants displaying high ploidy values, exhibited the opposite trend. Compared to thick-pericarp mutants, the proportions of fruit tissues were inversed (20% of pericarp and 59% of locular tissue) and the fruit had the lowest nuclear ploidy and pericarp cell area values of all the mutants.

Endoreduplication and Cell Size Are Positively Correlated in Both Clusters

Because endopolyploidy is a major determinant of cell expansion and fruit growth in tomato (Cheniclet et al., 2005; Chevalier et al., 2014), we further examined the pericarp nuclear ploidy levels of the mutants. Mutants were classified according to

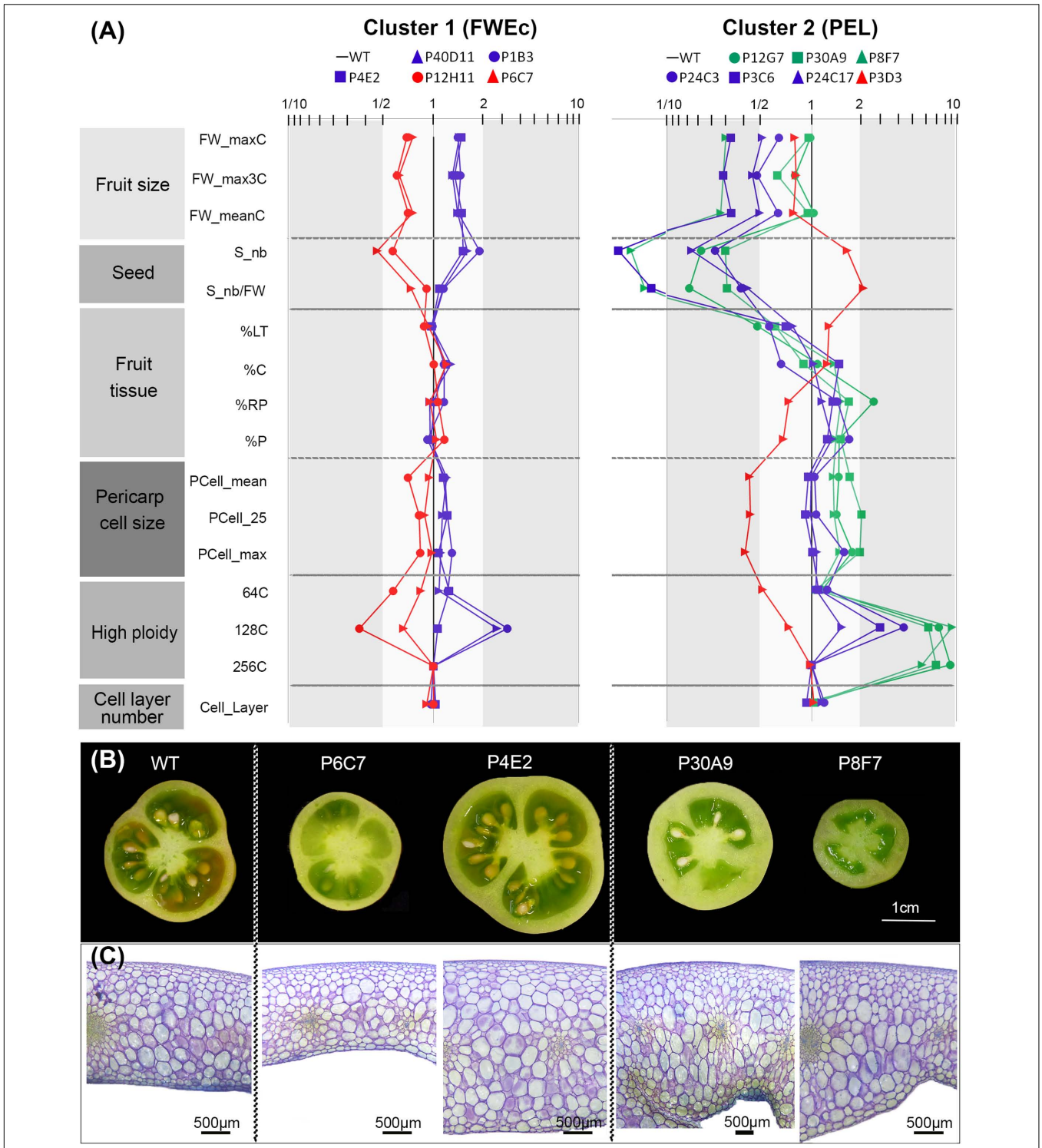

FIGURE 6 | Variation of fruit, tissue and cell-related traits in mutants from the two clusters. **(A)** Fruit trait patterning in cluster 1 associates with fruit weight (FWEc) and in cluster 2 with pericarp elongation (PEL). Value for each trait corresponds to the ratio between the mutant and the WT, plotted in logarithmic scale. The WT is set at 1 to easily identify up and down variations. The color label is used to distinguish 'low' (red), 'high' (blue), and 'extreme' (green) ploidy phenotypes. **(B)** Fresh equatorial sections from breaker stage fruits showing fruit tissue morphology of WT and representative mutants from each cluster. In cluster 1, small fruit mutant (P6C7) and large fruit (P4E2) mutants are shown. In cluster 2, normally sized (P30A9) and small (P8F7) thick-pericarp mutants are shown. **(C)** Pericarp equatorial sections from breaker fruits stained with toluidine blue showing cellular organization in WT and representative mutants in both clusters (same as in **Figure 7B**).

the proportion of 64C to 256C nuclei into "low" (P3D3, P12H11, P6C7 mutants), "high" (P4E2, P24C17, P40D11, P3C6, P1B3, and P24C4) and "extreme" (P8F7, P12G7, and P30A9) ploidy categories (**Figure 6A** and Supplementary Figure 4). The most striking feature is the large increase in 64C to 256C nuclei in the "extreme" ploidy mutants, and in particular of 128C and 256C nuclei. It is noteworthy to mention that 256C nuclei are not detected in WT and other mutant pericarp cells and that there is a 10-fold increase in 128C nuclei in these mutants compared to the WT (Supplementary Figure 4).

The Shape of Pericarp Cells Is Markedly Different Depending on the Cluster

Even though endopolyploidy is a major factor contributing to fruit tissue growth, and hence to fruit size, additional mechanisms are likely involved in the coordination of fruit growth at organ or tissue levels. As illustrated in fruit pericarp sections (**Figure 6C**), the largest cells appeared more elongated in the thick-pericarp mutants from cluster 2 than in WT or cluster 1 mutants. We therefore evaluated for these cells the *X*/*Y* ratio, where *X* and *Y* describe the cell dimensions according to the two main axes of fruit growth, along the medio-lateral axis (*X*, periclinal growth) and along the abaxial–adaxial axis (*Y*, anticlinal growth) (**Figures 2A**, **7A**). In cluster 1 mutants, the largest cells within the pericarp harbored a round shape except for one mutant (P6C7) where cells were slightly flattened (**Figure 7B**). Strikingly, in cluster 2, several thick-pericarp mutants (P24C17, P8F7, P30A9, and P12G7) showed a significant increase in the cell elongation along the *Y*-axis, which may explain the formation of lobes at the inner face of the pericarp. The thin-pericarp mutant P3D3 displayed the opposite phenotype, with highly flattened cells.

DISCUSSION

In the recent years, considerable progresses have been made regarding the determinism of the large increase in fruit weight and of fruit shape variations associated with the domestication and subsequent improvement processes in tomato (Lin et al., 2014; Blanca et al., 2015). Analysis of the natural diversity in cultivated tomato germplasm, led to the identification of nine major QTLs and the cloning of six key regulators controlling fruit weight and shape (see Tanksley, 2004; van der Knaap et al., 2014 for review). Remarkably, most QTLs described so far affect floral meristem, ovary carpel development and cell multiplication in the young fruit. Many of these QTLs participate in the same regulatory circuits (Lippman and Tanksley, 2001; Wu et al., 2015; Xu et al., 2015) that control fruit weight and shape, the two traits being not clearly separated. Many questions remain to be addressed. Is there any limit to the increase in fruit weight when the multiplication of carpels as in *lc* and *fas* (Muños et al., 2011; Xu et al., 2015) or the proximal-distal cell multiplication that deforms the fruit as in *sun* and *ovate* (Liu et al., 2002; Xiao et al., 2008) are not considered? Do the late stages of early fruit development (cell expansion stage) contribute to the variations in fruit weight and tissue morphology in tomato and, if so, are these variations controlled by one single or by several developmental modules?

Additional fruit weight and shape QTLs detected in tomato (Grandillo et al., 1999; Gonzalo and van der Knaap, 2008; Huang and van der Knaap, 2011; Rodríguez et al., 2013; Illa-Berenguer et al., 2015) should help address these questions. Many of these QTLs with lower effects are likely modifiers of the major QTLs already identified or may be involved in different fruit growth processes. This would suggest that a larger set of genes governs fruit size. In classical segregating populations used for map-based cloning, the magnitude of the effect of major loci is often overshadowing the smaller effects of minor QTLs. In addition, the reduced genetic diversity available in cultivated tomato and the low number of spontaneous mutants available may not be sufficient to uncover the various circuits regulating fruit growth and patterning (Lin et al., 2014; van der Knaap et al., 2014). Altogether, this may partly explain the low number of fruit weight/shape QTLs cloned to date (<10).

In this context, we reasoned that the new genetic and phenotypic diversity created by EMS saturated mutagenesis may overcome these limitations and help unraveling developmental modules controlling tomato fruit growth (weight and tissue morphology). EMS induces point mutations evenly distributed over the genome, a number of which may be deleterious (Greene et al., 2003). In tomato, EMS mutants already proved to be of great interest for studying various aspects of plant development involved in yield (Park et al., 2014; Xu et al., 2015), leaf development (Berger et al., 2009; Zsögön et al., 2015) or fruit cuticle (Petit et al., 2014, 2016). The mutant collection we developed in the cv. Micro-Tom (Just et al., 2013) is highly mutagenized and, considering the density and impact on protein function of the mutations (Garcia et al., 2016; Petit et al., 2016), 1700 to 3500 EMS mutants are sufficient to reach saturated mutagenesis in tomato (ca. 35 000 genes). Moreover, the genetic background of all the mutant lines from an EMS mutant population is identical, except for the induced mutations, and the phenotypes associated with loss-of-function mutations are revealed in the first mutant generations. For this reason, it is possible to investigate even mild variations across organ, tissue and cellular scales.

Even after excluding hundreds of carpel number and fruit shape mutants from the analysis, our screen led to the successful identification of robust fruit weight and tissue morphology mutants. As expected, these alterations are largely independent from early events affecting ovary and fruit patterning. The cell divisions along the abaxial–adaxial and proximal/distal axes are likely unaffected since we did not observe any variation in fruit shape or in the number of pericarp cell layers. However, increased cell divisions along the medio-lateral axis cannot be excluded, especially in the epidermis of fruits from large fruit mutants. Altogether, our results indicate that alterations in the cell expansion process and hence in cell size are primarily responsible for the variations in fruit weight and tissue morphology observed. An important finding is also the discovery that mutants grouped in two different clusters, affecting either whole fruit growth or more specifically the pericarp. The developmental processes and regulatory circuits affected in our set of selected mutants are

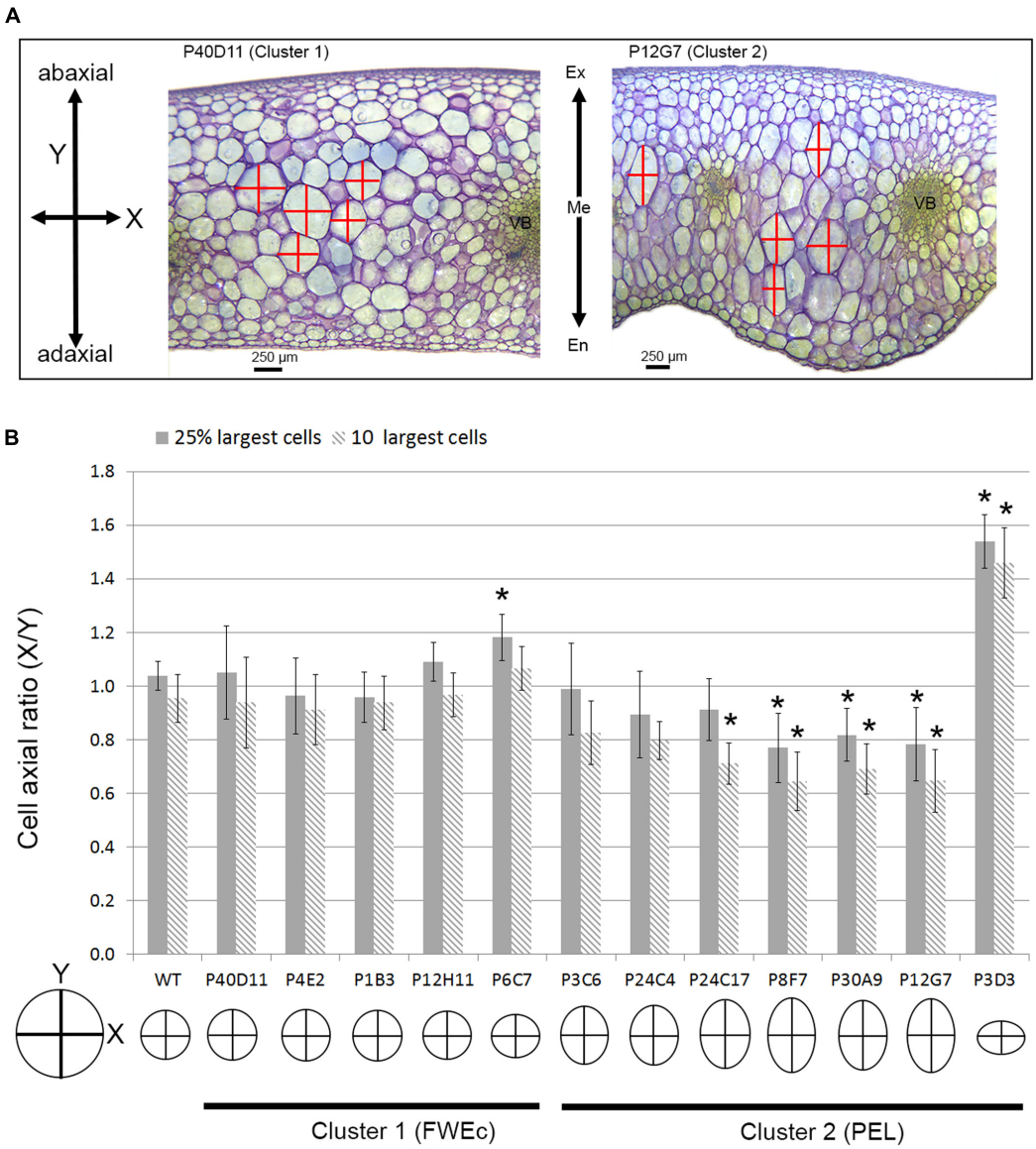

FIGURE 7 | Pericarp cell expansion in fruit weight and tissue morphology mutants. **(A)** Fruit pericarp section stained with toluidine blue for P40D11 (cluster 1) and P12G7 (cluster 2) mutants. In P12G7 mutant, the outgrowth of the pericarp toward the locular cavity of the fruit, forming lobes, is clearly visible as well as the elongated shape of the largest cells. Pericarp cell dimensions along the medio-longitudinal (*X*) and adaxial–abaxial (*Y*) axis used to measure cell shape are indicated. En, endocarp; Me, mesocarp; Ex, exocarp. **(B)** Cell axial ratio (*X*/*Y*) of the 10 and 25% largest cells inside the pericarp for FWEc mutants of cluster 1 and PEL mutants of cluster 2. Asterisks represent significant difference (*t*-test, *P*-value < 0.01) between the mutant and the WT. A representation of cell shape is given for each mutant based on the ratio values obtained for the 10 largest cells.

therefore likely different from those involved in other fruit weight and tissue morphology variants previously described in tomato (see Tanksley, 2004; van der Knaap et al., 2014 for reviews).

Developmental modules exist from genetic (gene regulatory network or GRNs) to organismal levels and therefore can be studied at nearly every scale of organization (Scarpella et al., 2010; Davila-Velderrain et al., 2014; Zhan et al., 2015). We can consider that the fruit is organized through modules expressing basic behaviors at cellular and tissue levels. For most modules, modular functions are usually carried out by a group of highly interconnected genes involved in a GRN that interact and frequently overlap with other modules (Benítez et al., 2007). In plants, the identification of modules and corresponding GRNs have been to date limited to specific cellular behaviors or developmental processes such as cell fate determination during flower development (Espinosa-Soto et al., 2004; Urbanus et al., 2010; Davila-Velderrain et al., 2014) or leaf development (Ichihashi et al., 2014; González and Inzé, 2015; Horst et al., 2015). The leaf can be represented in a two-dimensional system, thus allowing detailed and combined

TABLE 1 | Properties of fruit growth modules.

Module	Cellular events	Morphological roles	*Genes in the GRN*	Reference
CAN*	Cell identity –cell fate	Meristem identity and organization, carpel number, fruit shape	*WUSCHEL (lc) CLAVATA3 (fas) CLE9, HPAT, CLV1*	Muños et al., 2011; Xu et al., 2015
FEL*	Proximal-distal patterning, cell division	Anisotropic ovary and fruit growth (proximal-distal), fruit shape	*OVATE, SUN*	Liu et al., 2002; Xiao et al., 2008; Wu et al., 2015
FWEa*	Cell division	Placenta and columella growth-Ovary and fruit weight	*CNR (fw2.2)*	Frary et al., 2000; Cong et al., 2002
FWEb*	Cell division	Pericarp and radial pericarp growth-Fruit weight	*KLUH (fw3.2)*	Chakrabarti et al., 2013
FWEc*	Isotropic cell expansion	Coordinated tissue growth and fruit weight	*Nd**	This study
PEL*	Anisotropic cell expansion	Abaxial/adaxial pericarp elongation, pericarp thickness	*Nd**	This study

**CAN, carpel number; FEL, fruit elongation; FWE, fruit weight; PEL, pericarp elongation; GRN, gene regulatory network; Nd, not determined.*

analysis of genetic interactions, of spatial patterns and of cell type determination and arrangement in the leaf (Scarpella et al., 2010; Ichihashi et al., 2014). However, in contrast to the leaf, the fruit is a bulky organ displaying more complex cellular and tissue patterning. Therefore, the few regulatory networks described for the fruit remain largely incomplete. A starting point to identify such networks is to define the basic set of modules mobilized during fruit growth through a top-down decomposition approach. Based on previous reports, a set of tomato fruit growth modules and their role in the determination fruit weight, fruit shape and tissue morphology can be tentatively identified (**Table 1**). These are early modules controlling either floral meristem cell fate and carpel number or ovary and early fruit growth by cell multiplication (**Table 1**). They include the 'carpel number' (CAN), 'fruit elongation' (FEL) and 'fruit weight' (FWEa and FWEb) modules that may overlap. Interactions of the regulatory networks including the *CLV3-WUSCHEL* circuit and the *SUN* and *OVATE* pathways were proposed to capture most of the fruit shape variations in the cultivated tomato (Rodríguez et al., 2011; Wu et al., 2015; Xu et al., 2015). The FWEa and FWEb modules described so far involve two programs of development governed by the *CNR* and *KLUH* genes, respectively. These modules control the early cell division patterns in the different fruit tissues and are at the origin of variations in fruit weight and, likely, in tissue morphology (see van der Knaap et al., 2014 for review).

Here we identified two additional fruit growth modules, the 'fruit weight' FWEc and the 'pericarp elongation' (PEL) modules (**Table 1**), which correspond to the two clusters of mutants displaying specific fruit weight and tissue morphology characteristics (**Figures 5–7**). Both modules control pericarp cell expansion during early fruit growth, with consequences on either whole fruit (FWEc module; cluster 1 mutants) or only on pericarp tissue (PEL module; cluster 2 mutants). The FWEc module organizes and synchronizes the growth from all fruit tissues. Indeed, the tissue morphology and cell shape isotropy (growth equal in all directions) are preserved whatever the variations in cell size and fruit weight observed in cluster 1 mutants. The PEL module controls pericarp cell elongation along the adaxial–abaxial axis. The resulting cell shape anisotropy (unidirectional growth) is restricted to pericarp and provokes an increase in pericarp thickness and its deformation, as observed for several mutants of cluster 2. Thus, though they are likely interconnected to allow fruit growth and patterning during the cell expansion stage of the fruit, these new fruit growth modules appear to be autonomous, at least to some extent, as the fluctuations in one module do not entail changes in the fruit, tissue and cell characteristics controlled by the second module.

At this stage the modular functions underlying FWEc and PEL modules are unknown and a broad range of gene functions and categories can be involved in the corresponding GRNs. In the FWEc module, factors regulating endoreduplication and cell turgor pressure (Chevalier et al., 2014; Okello et al., 2015) and those involved in non-cell-autonomous signaling pathways are likely candidate. In the PEL module that displays a strong anisotropic growth of the pericarp cells, genes implicated in cell wall and microtubule loading are strong candidates (Verbelen et al., 2001; Baskin and Jensen, 2013).

CONCLUSION

Our results support the existence of two distinct developmental modules regulating fruit growth by cell expansion and affecting tomato fruit weight and tissue morphology without altering carpel number and fruit shape. The new insights gained into tomato fruit development and the wealth of data available from this study will considerably contribute to improve the current dynamic models of fruit growth (Baldazzi et al., 2012). Thanks to the recent advances in deep sequencing technologies and to the high quality tomato genomic sequence available (Tomato Genome Consortium, 2012), we recently developed a mapping-by-sequencing strategy readily allowing the identification of causal mutations in the Micro-Tom EMS mutants (Garcia et al., 2016; Petit et al., 2016). Using this strategy, the set of available mutants will therefore help deciphering the genetic network underlying the two modules and shed new light on the poorly known processes controlling fleshy fruit growth.

AUTHOR CONTRIBUTIONS

LF and CR designed the research. CM, JJ, LF, and DJ performed experiments. CM, LF, and AM. analyzed data. LF, CM, CR, CC, ML-C, and FG interpreted the data. LF and CR wrote the manuscript.

FUNDING

This research was funded by a grant from the 'Plant Biology and Breeding' division of INRA (BAP2013_46 - TOMCRO).

ACKNOWLEDGMENTS

Thanks to Jean-Philipe Mauxion for his help in mutant phenotyping, Isabelle Atienza for taking care of the plants, Catherine Cheniclet and Christopher Sauvage for helpful discussions and advices.

SUPPLEMENTARY MATERIAL

The Supplementary Material for this article can be found online at: http://journal.frontiersin.org/article/10.3389/fpls.2017.00988/full#supplementary-material

REFERENCES

Aflitos, S., Schijlen, E., de Jong, H., de Ridder, D., Smit, S., Finkers, R., et al. (2014). Exploring genetic variation in the tomato (Solanum section Lycopersicon) clade by whole-genome sequencing. *Plant J.* 80, 136–148. doi: 10.1111/tpj.12616

Baskin, T. I., and Jensen, O. E. (2013). On the role of stress anisotropy in the growth of stems. *J. Exp. Bot.* 64, 4697–4707. doi: 10.1093/jxb/ert176

Baldazzi, V., Bertin, N., de Jong, H., and Génard, M. (2012). Towards multiscale plant models: integrating cellular networks. *Trends Plant Sci.* 17, 728–736. doi: 10.1016/j.tplants.2012.06.012

Benítez, M., Espinosa-Soto, C., Padilla-Longoria, P., Díaz, J., and Alvarez-Buylla, E. R. (2007). Equivalent genetic regulatory networks in different contexts recover contrasting spatial cell patterns that resemble those in Arabidopsis root and leaf epidermis: a dynamic model. *Int. J. Dev. Biol.* 51, 139–155. doi: 10.1387/ijdb.062183mb

Benjamini, Y., and Hochberg, Y. (1995). Controlling the false discovery rate: a practical and powerful approach to multiple testing. *J. R. Stat. Soc. Ser. B Stat. Methodol.* 57, 289–300.

Berger, Y., Harpaz-Saad, S., Brand, A., Melnik, H., Sirding, N., Alvarez, J. P., et al. (2009). The NAC-domain transcription factor GOBLET specifies leaflet boundaries in compound tomato leaves. *Development* 136, 823–832. doi: 10.1242/dev.031625

Bertin, N., Causse, M., Brunel, B., Tricon, D., and Génard, M. (2009). Identification of growth processes involved in QTLs for tomato fruit size and composition. *J. Exp. Bot.* 60, 237–248. doi: 10.1093/jxb/ern281

Blanca, J., Montero-Pau, J., Sauvage, C., Bauchet, G., Illa, E., Díez, M. J., et al. (2015). Genomic variation in tomato, from wild ancestors to contemporary breeding accessions. *BMC Genomics* 16:257. doi: 10.1186/s12864-015-1444-1

Bolger, A., Scossa, F., Bolger, M. E., Lanz, C., Maumus, F., Tohge, T., et al. (2014). The genome of the stress-tolerant wild tomato species *Solanum pennellii*. *Nat. Genet.* 46, 1034–1038. doi: 10.1038/ng.3046

Bourdon, M., Pirrello, J., Cheniclet, C., Coriton, O., Bourge, M., Brown, S., et al. (2012). Evidence for karyoplasmic homeostasis during endoreduplication and a ploidy-dependent increase in gene transcription during tomato fruit growth. *Development* 139, 3817–3826. doi: 10.1242/dev.084053

Chakrabarti, M., Zhang, N., Sauvage, C., Muños, S., Blanca, J., Cañizares, J., et al. (2013). A cytochrome P450 regulates a domestication trait in cultivated tomato. *Proc. Natl. Acad. Sci. U.S.A.* 110, 17125–17130. doi: 10.1073/pnas.1307313110

Cheniclet, C., Rong, W. Y., Causse, M., Frangne, N., Bolling, L., Carde, J. P., et al. (2005). Cell expansion and endoreduplication show a large genetic variability in pericarp and contribute strongly to tomato fruit growth. *Plant Physiol.* 139, 1984–1994. doi: 10.1104/pp.105.068767

Chevalier, C., Bourdon, M., Pirrello, J., Cheniclet, C., Gévaudant, F., and Frangne, N. (2014). Endoreduplication and fruit growth in tomato: evidence in favour of the karyoplasmic ratio theory. *J. Exp. Bot.* 65, 2731–2746. doi: 10.1093/jxb/ert366

Chitwood, D. H., Klein, L. L., O'Hanlon, R., Chacko, S., Greg, M., Kitchen, C., et al. (2016). Latent developmental and evolutionary shapes embedded within the grapevine leaf. *New Phytol.* 210, 343–355. doi: 10.1111/nph.13754

Chitwood, D. H., Ranjan, A., Martinez, C. C., Headland, L. R., Thiem, T., Kumar, R., et al. (2014). A modern ampelography: a genetic basis for leaf shape and venation patterning in grape. *Plant Physiol.* 164, 259–272. doi: 10.1104/pp.113.229708

Cong, B., Liu, J., and Tanksley, S. D. (2002). Natural alleles at a tomato fruit size quantitative trait locus differ by heterochronic regulatory mutations. *Proc. Natl. Acad. Sci. U.S.A.* 99, 13606–13611. doi: 10.1073/pnas.172520999

Davila-Velderrain, J., Servin-Marquez, A., and Alvarez-Buylla, E. R. (2014). Molecular evolution constraints in the floral organ specification gene regulatory network module across 18 angiosperm genomes. *Mol. Biol. Evol.* 31, 560–573. doi: 10.1093/molbev/mst223

De Veylder, L., Larkin, J. C., and Schnittger, A. (2011). Molecular control and function of endoreplication in development and physiology. *Trends Plant Sci.* 16, 624–634. doi: 10.1016/j.tplants.2011.07.001

Doebley, J. F., Gaut, B. S., and Smith, B. D. (2006). The molecular genetics of crop domestication. *Cell* 127, 1309–1321. doi: 10.1016/j.cell.2006.12.006

Espinosa-Soto, C., Padilla-Longoria, P., and Alvarez-Buylla, E. R. (2004). A gene regulatory network model or cell-fate determination during *Arabidopsis thaliana* flower development that is robust and recovers experimental gene expression profiles. *Plant Cell* 16, 2923–2939. doi: 10.1105/tpc.104.021725

Frary, A., Nesbitt, T. C., Grandillo, S., Knaap, E., Cong, B., Liu, J., et al. (2000). fw2.2: a quantitative trait locus key to the evolution of tomato fruit size. *Science* 289, 85–88. doi: 10.1126/science.289.5476.85

Garcia, V., Bres, C., Just, D., Fernandez, L., Wong Jun Tai, F., Mauxion, J. P., et al. (2016). Rapid identification of causal mutations in tomato EMS populations via mapping-by-sequencing. *Nat. Protoc.* 11, 2401–2418. doi: 10.1038/nprot.2016.143

González, N., and Inzé, D. (2015). Molecular systems governing leaf growth: from genes to networks. *J. Exp. Bot.* 66, 1045–1054. doi: 10.1093/jxb/eru541

Gonzalo, M. J., and van der Knaap, E. (2008). A comparative analysis into the genetic bases of morphology in tomato varieties exhibiting elongated fruit shape. *Theor. Appl. Genet.* 116, 647–656. doi: 10.1007/s00122-007-0698-7

Grandillo, S., Ku, H. M., and Tanksley, S. D. (1999). Identifying loci responsible for natural variation in fruit size and shape in tomato. *Theor. Appl. Genet.* 99, 978–987. doi: 10.1007/s001220051405

Greene, E. A., Codomo, C. A., Taylor, N. E., Henikoff, J. G., Till, B. J., Reynolds, S. H., et al. (2003). Spectrum of chemically induced mutations from a large-scale reverse-genetic screen in Arabidopsis. *Genetics* 164, 731–740.

Horst, R. J., Fujita, H., Lee, J. S., Rychel, A. L., Garrick, J. M., Kawaguchi, M., et al. (2015). Molecular framework of a regulatory circuit initiating two-dimensional spatial patterning of stomatal lineage. *PLoS Genet.* 11:e1005374. doi: 10.1371/journal.pgen.1005374

Huang, Z., and van der Knaap, E. (2011). Tomato fruit weight 11.3 maps close to fasciated on the bottom of chromosome 11. *Theor. Appl. Genet.* 123, 465–474. doi: 10.1007/s00122-011-1599-3

Ichihashi, Y., Aguilar-Martínez, J. A., Farhi, M., Chitwood, D. H., Kumar, R., Millon, L. V., et al. (2014). Evolutionary developmental transcriptomics reveals a gene network module regulating interspecific diversity in plant leaf shape. *Proc. Natl. Acad. Sci. U.S.A.* 111, 2616–2621. doi: 10.1073/pnas.1402835111

Illa-Berenguer, E., Van Houten, J., Huang, Z., and van der Knaap, E. (2015). Rapid and reliable identification of tomato fruit weight and locule number

loci by QTL-seq. *Theor. Appl. Genet.* 128, 1329–1342. doi: 10.1007/s00122-015-2509-x

Just, D., Garcia, V., Fernandez, L., Bres, C., Mauxion, J. P., Petit, J., et al. (2013). Micro-tom mutants for functional analysis of target genes and discovery of new alleles in tomato. *Plant Biotechnol.* 30, 1–7. doi: 10.5511/plantbiotechnology.13.0622a

Klee, H. J., and Giovannoni, J. J. (2011). Genetics and control of tomato fruit ripening and quality attributes. *Annu. Rev. Genet.* 45, 41–59. doi: 10.1146/annurev-genet-110410-132507

Lemaire-Chamley, M., Petit, J., Garcia, V., Just, D., Baldet, P., Germain, V., et al. (2005). Changes in transcriptional profiles are associated with early fruit tissue specialization in tomato. *Plant Physiol.* 139, 750–769. doi: 10.1104/pp.105.063719

Lin, T., Zhu, G., Zhang, J., Xu, X., Yu, Q., Zheng, Z., et al. (2014). Genomic analyses provide insights into the history of tomato breeding. *Nat. Genet.* 46, 1220–1226. doi: 10.1038/ng.3117

Lippman, Z., and Tanksley, S. D. (2001). Dissecting the genetic pathway to extreme fruit size in tomato using a cross between the small-fruited wild species *Lycopersicon pimpinellifolium* and L. esculentum var. *Giant Heirloom. Genet.* 158, 413–422.

Liu, J., Van Eck, J., Cong, B., and Tanksley, S. D. (2002). A new class of regulatory genes underlying the cause of pear-shaped tomato fruit. *Proc. Natl. Acad. Sci. U.S.A.* 99, 13302–13306. doi: 10.1073/pnas.162485999

Menda, N., Semel, Y., Peled, D., Eshed, Y., and Zamir, D. (2004). In silico screening of a saturated mutation library of tomato. *Plant J.* 38, 861–872. doi: 10.1111/j.1365-313X.2004.02088.x

Monforte, A. J., Diaz, A., Caño-Delgado, A., and van der Knaap, E. (2014). The genetic basis of fruit morphology in horticultural crops: lessons from tomato and melon. *J. Exp. Bot.* 65, 4625–4637. doi: 10.1093/jxb/eru017

Muños, S., Ranc, N., Botton, E., Bérard, A., Rolland, S., Duffé, P., et al. (2011). Increase in tomato locule number is controlled by two single-nucleotide polymorphisms located near WUSCHEL. *Plant Physiol.* 156, 2244–2254. doi: 10.1104/pp.111.173997

Okello, R. C. O., Heuvelink, E. P., de Visser, P. H. B., Struik, P. C., and Marcelis, L. F. M. (2015). What drives fruit growth? *Funct. Plant Biol.* 42, 817–827. doi: 10.1071/FP15060

Paran, I., and van der Knaap, E. (2007). Genetic and molecular regulation of fruit and plant domestication traits in tomato and pepper. *J. Exp. Bot.* 58, 3841–3852. doi: 10.1093/jxb/erm257

Park, S. J., Jiang, K., Tal, L., Yichie, Y., Gar, O., Zamir, D., et al. (2014). Optimization of crop productivity in tomato using induced mutations in the florigen pathway. *Nat. Genet.* 46, 1337–1342. doi: 10.1038/ng.3131

Périn, C., Hagen, L. S., Giovinazzo, N., Besombes, D., Dogimont, C., and Pitrat, M. (2002). Genetic control of fruit shape acts prior to anthesis in melon (*Cucumis melo* L.). *Mol. Genet. Genomics* 266, 933–941. doi: 10.1007/s00438-001-0612-y

Petit, J., Bres, C., Just, D., Garcia, V., Mauxion, J. P., Marion, D., et al. (2014). Analyses of tomato fruit brightness mutants uncover both cutin-deficient and cutin-abundant mutants and a new hypomorphic allele of GDSL lipase. *Plant Physiol.* 164, 888–906. doi: 10.1104/pp.113.232645

Petit, J., Bres, C., Mauxion, J. P., Tai, F. W., Martin, L. B., Fich, E. A., et al. (2016). The Glycerol-3-Phosphate acyltransferase GPAT6 from tomato plays a central role in fruit cutin biosynthesis. *Plant Physiol.* 171, 894–913. doi: 10.1104/pp.16.00409

Pound, M. P., French, A. P., Wells, D. M., Bennett, M. J., and Pridmore, T. P. (2012). CellSeT: novel software to extract and analyze structured networks of plant cells from confocal images. *Plant Cell* 24, 1353–1361. doi: 10.1105/tpc.112.096289

Rodríguez, G. R., Kim, H. J., and van der Knaap, E. (2013). Mapping of two suppressors of OVATE (sov) loci in tomato. *Heredity* 111, 256–264. doi: 10.1038/hdy.2013.45

Rodríguez, G. R., Moyseenko, J. B., Robbins, M. D., Morejón, N. H., Francis, D. M., and van der Knaap, E. (2010). Tomato analyzer: a useful software application to collect accurate and detailed morphological and colorimetric data from two-dimensional objects. *J. Vis. Exp.* 37:1856. doi: 10.3791/1856

Rodríguez, G. R., Muños, S., Anderson, C., Sim, S. C., Michel, A., Causse, M., et al. (2011). Distribution of SUN, OVATE, LC, and FAS in the tomato germplasm and the relationship to fruit shape diversity. *Plant Physiol.* 156, 275–285. doi: 10.1104/pp.110.167577

Rothan, C., Just, D., Fernandez, L., Atienza, I., Ballias, P., and Lemaire-Chamley, M. (2016). Culture of the tomato micro-tom cultivar in greenhouse. *Methods Mol. Biol.* 1363, 57–64. doi: 10.1007/978-1-4939-3115-6_6

Saito, T., Ariizumi, T., Okabe, Y., Asamizu, E., Hiwasa-Tanase, K., Fukuda, N., et al. (2011). TOMATOMA: a novel tomato mutant database distributing Micro-Tom mutant collections. *Plant Cell Physiol.* 52, 283–296. doi: 10.1093/pcp/pcr004

Scarpella, E., Barkoulas, M., and Tsiantis, M. (2010). Control of leaf and vein development by auxin. *Cold Spring Harb. Perspect. Biol.* 2:a001511. doi: 10.1101/cshperspect.a001511

Serrani, J., Fos, M., Atares, A., and Garcia-Martinez, J. (2007). Effect of gibberellin and auxin on parthenocarpic fruit growth induction in the cv micro-tom of tomato. *J. Plant Growth Regul.* 26, 211–221. doi: 10.1007/s00344-007-9014-7

Shannon, P., Markiel, A., Ozier, O., Baliga, N. S., Wang, J. T., Ramage, D., et al. (2003). Cytoscape: a software environment for integrated models of biomolecular interaction networks. *Genome Res.* 13, 2498–2504. doi: 10.1101/gr.1239303

Shirasawa, K., Hirakawa, H., Nunome, T., Tabata, S., and Isobe, S. (2016). Genome-wide survey of artificial mutations induced by ethyl methanesulfonate and gamma rays in tomato. *Plant Biotechnol. J.* 14, 51–60. doi: 10.1111/pbi.12348

Sun, L., Rodriguez, G. R., Clevenger, J. P., Illa-Berenguer, E., Lin, J., Blakeslee, J. J., et al. (2015). Candidate gene selection and detailed morphological evaluations of fs8.1, a quantitative trait locus controlling tomato fruit shape. *J. Exp. Bot.* 66, 6471–6482. doi: 10.1093/jxb/erv361

Tanksley, S. D. (2004). The genetic, developmental, and molecular bases of fruit size and shape variation in tomato. *Plant Cell* 16, S181–S189. doi: 10.1105/tpc.018119

Tomato Genome Consortium (2012). The tomato genome sequence provides insights into fleshy fruit evolution. *Nature* 485, 635–641. doi: 10.1038/nature11119

Urbanus, S. L., Dinh, Q. D., Angenent, G. C., and Immink, R. G. (2010). Investigation of MADS domain transcription factor dynamics in the floral meristem. *Plant Signal. Behav.* 5, 1260–1262. doi: 10.4161/psb.5.10.12949

van der Knaap, E., Chakrabarti, M., Chu, Y. H., Clevenger, J. P., Illa-Berenguer, E., Huang, Z., et al. (2014). What lies beyond the eye: the molecular mechanisms regulating tomato fruit weight and shape. *Front. Plant Sci.* 5:227. doi: 10.3389/fpls.2014.00227

van der Knaap, E., Sanyal, A., Jackson, S. A., and Tanksley, S. D. (2004). High-resolution fine mapping and fluorescence in situ hybridization analysis of sun, a locus controlling tomato fruit shape, reveals a region of the tomato genome prone to DNA rearrangements. *Genetics* 168, 2127–2140. doi: 10.1534/genetics.104.031013

Verbelen, J.-P., Vissenberg, K., Kerstens, S., and Le, J. (2001). Cell expansion in the epidermis: microtubules, cellulose orientation and wall loosening enzymes. *J. Plant Physiol.* 158, 537–543. doi: 10.1078/0176-1617-00277

Wu, S., Clevenger, J. P., Sun, L., Visa, S., Kamiya, Y., Jikumaru, Y., et al. (2015). The control of tomato fruit elongation orchestrated by sun, ovate and fs8.1 in a wild relative of tomato. *Plant Sci.* 238, 95–104. doi: 10.1016/j.plantsci.2015.05.019

Xiao, H., Jiang, N., Schaffner, E., Stockinger, E. J., and van der Knaap, E. (2008). A retrotransposon-mediated gene duplication underlies morphological variation of tomato fruit. *Science* 319, 1527–1530. doi: 10.1126/science.1153040

Xu, C., Liberatore, K. L., MacAlister, C. A., Huang, Z., Chu, Y. H., Jiang, K., et al. (2015). A cascade of arabinosyltransferases controls shoot meristem size in tomato. *Nat. Genet.* 47, 784–792. doi: 10.1038/ng.3309

Zhan, J., Thakare, D., Ma, C., Lloyd, A., Nixon, N. M., Arakaki, A. M., et al. (2015). RNA sequencing of laser-capture microdissected compartments of the maize kernel identifies regulatory modules associated with endosperm cell differentiation. *Plant Cell* 27, 513–531. doi: 10.1105/tpc.114.135657

Zhang, N., Brewer, M. T., and van der Knaap, E. (2012). Fine mapping of fw3.2 controlling fruit weight in tomato. *Theor. Appl. Genet.* 125, 273–284. doi: 10.1007/s00122-012-1832-8

Zsögön, A., Negrini, A. C., Peres, L. E., Nguyen, H. T., and Ball, M. C. (2015). A mutation that eliminates bundle sheath extensions reduces leaf hydraulic conductance, stomatal conductance and assimilation rates in tomato (*Solanum lycopersicum*). *New Phytol.* 205, 618–626. doi: 10.1111/nph.13084

Conflict of Interest Statement: The authors declare that the research was conducted in the absence of any commercial or financial relationships that could be construed as a potential conflict of interest.

II. Outcomes of this study and strategic choices for the rest of my thesis

This work led to the successful identification of robust fruit weight and tissue morphology mutants, which are adequate plant materials for deciphering the genetic network and cellular mechanisms underlying tomato fruit growth. Two mutants characterized by an anisotropic growth of the pericarp without changes in the final fruit size were chosen for deeper analyses: the P3D3 mutant characterized by a thin pericarp and the P30A9 mutant characterized by a thick pericarp. The objectives of my thesis are as follows:

- Identifying the locus at the origin of the phenotypic alterations;
- Understanding the role of this locus in the regulation of tissue morphology in the tomato fruit.

The mapping-by-sequencing strategy was developed in the host team to identify causal mutations at the origin of various phenotypes of interest in the EMS mutants. This strategy lasts at least 6 months for identifying a causal mutation (Garcia *et al.*, 2016). Even if the approach proves to be efficient for the identification of several causal mutations (Petit *et al.*, 2016), it was not the case for all the mutants studied in the team. Hence, this crucial part of the work remains challenging. The identification of the causal mutation and therefore the underlying gene could reveal candidates with highly diverse molecular functions, including proteins of unknown functions. In this context, the functional characterization of the underlying gene is performed, through the development of specific assays according to the putative role of each candidate. This strategy is expected to reveal new regulators of fruit growth. Even if the opportunity to study proteins barely described is motivating and exciting, this part of the work could be challenged by the limits of tools and knowledge available in the fruit system or for the tomato model. In this context, this part of my PhD work will be developed step by step, depending on the constant emerging hypothesis.

During my PhD., I have developed both aspects for this approach :

- First, I performed the mapping-by-sequencing strategy to identify the causal mutation at the origin of the thick pericarp in the P30A9 mutant.
- Second, I performed the functional characterization of the gene responsible for the thin pericarp in P3D3 mutant.

Chapter III

–

RESULTS & DISCUSSION

Part I

Towards the identification of the mutation responsible for the thick pericarp phenotype: case of P30A9 mutant.

Results

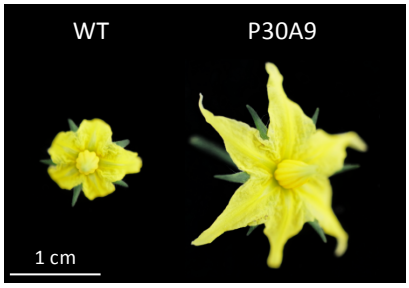

Figure 14: **Flower at anthesis in the WT Micro-Tom and P30A9 mutant.**

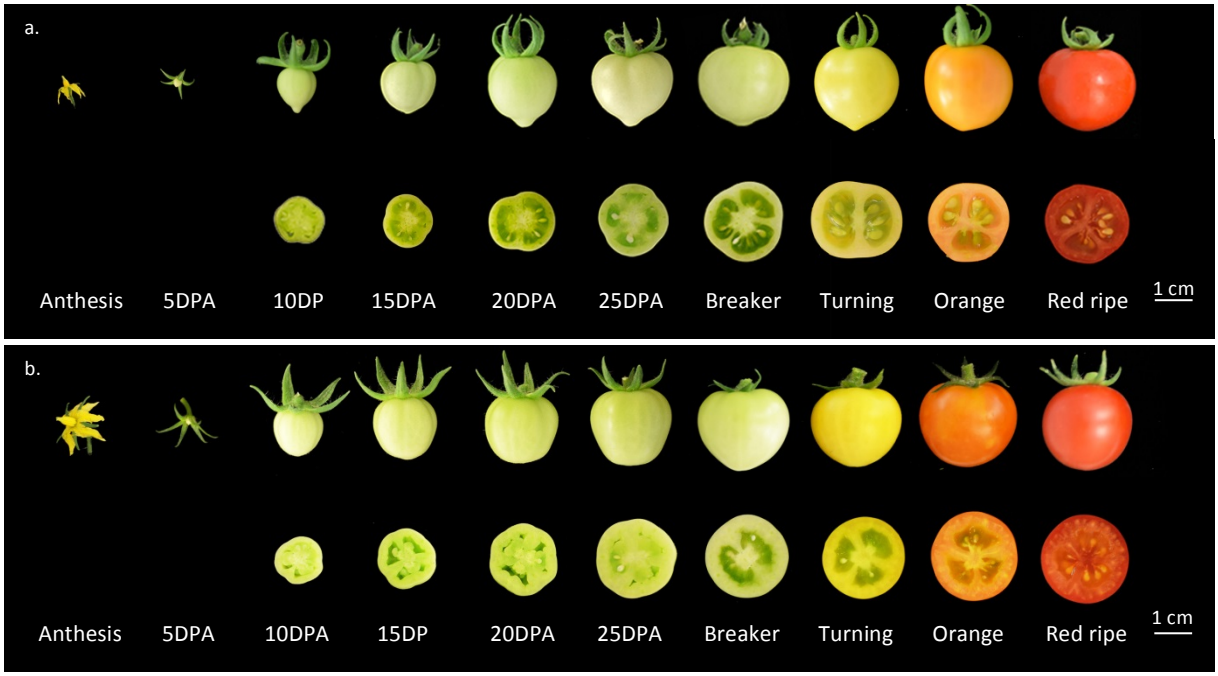

Figure 15: **Fruit development from anthesis to the end of ripening in the WT Micro-Tom and P30A9 mutant**. a. WT Micro-Tom whole fruit and equatorial section. b. P30A9 mutant whole fruit and equatorial section mutant.

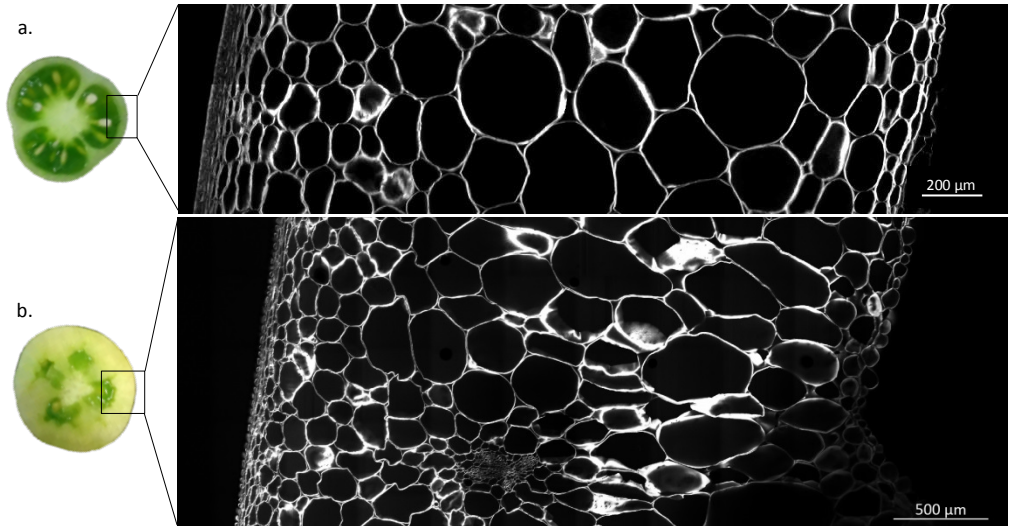

Figure 16: **Equatorial section of the pericarp**. Whole equatorial section and pericarp section. a. Pericarp section in the WT Micro-Tom. b. Pericarp section in P30A9 mutant. Cell walls are stained with calcofluor.

I. P30A9 mutant: more than a thick pericarp mutant

P30A9 mutant was selected among the EMS mutant collection, because it presented a strong increase in pericarp thickness, comparing to the WT Micro-Tom. The previous phenotypic analyses of this mutant revealed that the increase in pericarp thickness was associated with an increase in cell size and pericarp cells ploidy level, at breaker stage (Musseau *et al.*, 2017). Furthermore, the change in pericarp thickness was not associated with an increase in the final fruit size. To complete this preliminary characterization, I checked if the changes observed at breaker stage were also true all along the fruit growth. Furthermore, I looked for phenotypical modifications in other fruit tissues and plant organs.

- *Vegetative and floral development*

At the plant level, P30A9 mutant showed no alteration in plant size; however it presented slight alterations in leaves: leaves were slightly larger, flattened and unruffled and presented a slight change in color (Supplementary Figure 1). At anthesis, flowers were enlarged in P30A9 when compared to the WT with the sepal, petal and stamen size increased approximately by 4-fold (Figure 14). Surprisingly, this increase in floral organs size did not affect the ovary size (Supplementary Figure 2). Although the difference in flower size in the mutant remains a very interesting character, we did not go further into the phenotypic characterization of the flowers.

- *Fruit development*

From anthesis to the red ripe stage, fruit phenology and whole size did not seem to be altered in P30A9 mutant (Figure 15). However, looking at the fruit anatomy, fruit tissues developed quite differently comparing to the WT Micro-Tom. From 15 DPA onwards, pericarp thickness was thicker in the mutant, and this difference was even more severe at breaker stage (Figure 15). The increase in pericarp thickness was concomitant with the increase in the septum thickness and with a reduction of the locular tissue area (Figure 15). P30A9 mutant also produced less seeds per fruit (a dozen per fruit), compared to the WT (around twenty seeds per fruit) (data not showed). The pericarp morphology in P30A9 mutant suggested a centripetal growth of this tissue inwards the center of the fruit (Figure 16). Indeed, marked invaginations

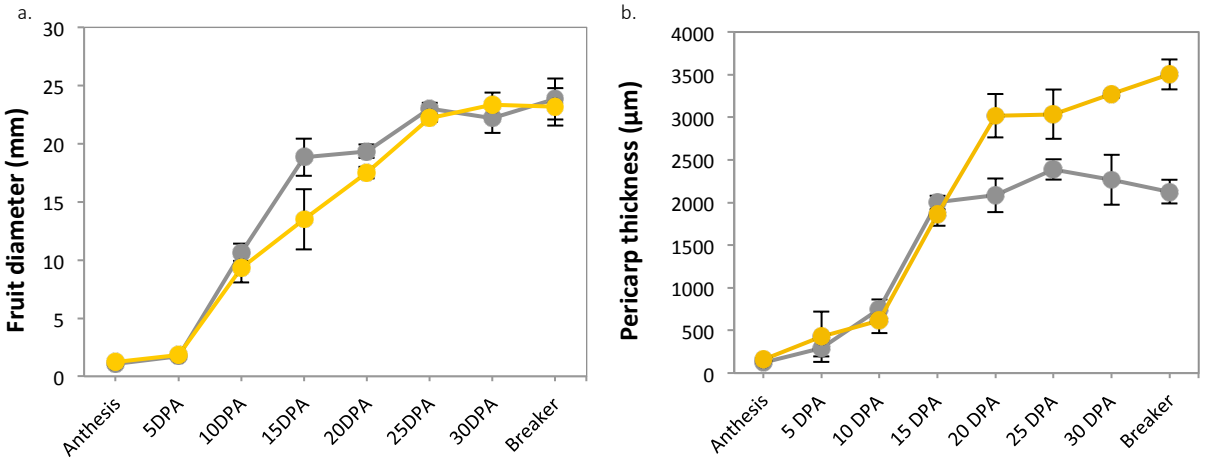

Figure 17: **Evolution of fruit growth in the WT Micro-Tom and P30A9 mutant.**
a. Kinetic of fruit diameter. b. Kinetic of pericarp thickness. (Error bar: standard deviation, n=3)

WT
P30A9

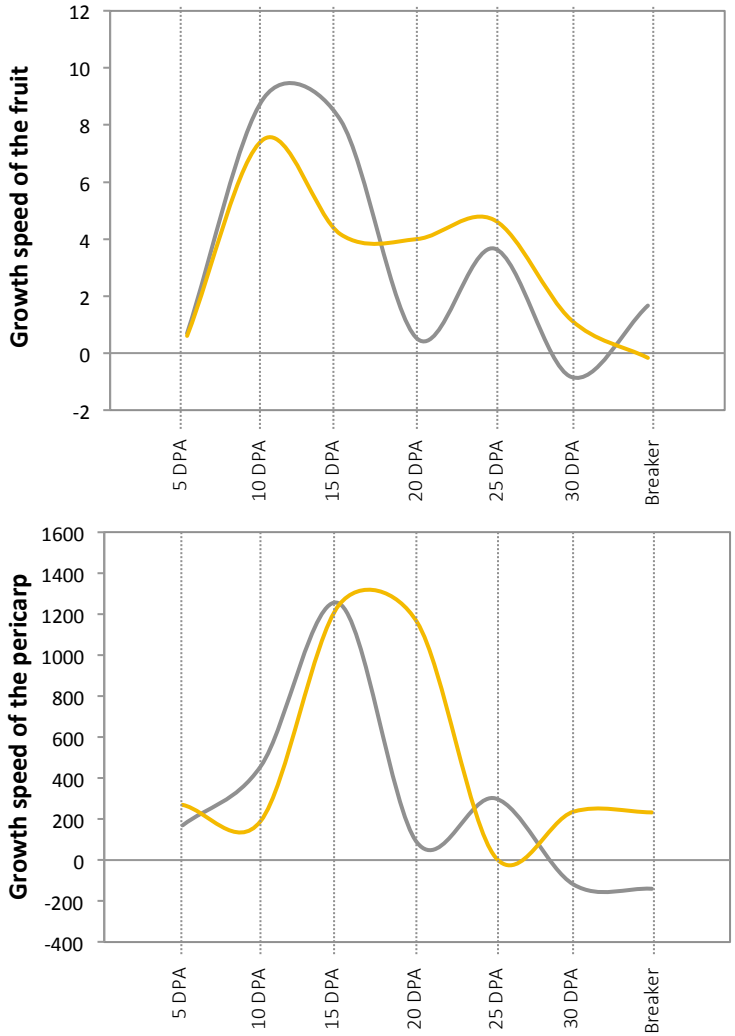

Figure 18: **Growth speed of the fruit and the pericarp tissue in WT Micro-Tom and P30A9 mutant.** (n=3)

WT
P30A9

were present at the endocarp side, suggesting that growth of the tissue was constraint at the exocarp side, allowing only a progression of the tissue towards the center of the fruit (Supplementary Figure 3). The pericarp developed to the detriment of the other central fruit tissues (locular tissue, placenta) and concomitantly with a reduction in seed number. Interestingly, P30A9 fruit anatomy looked similar to parthenocarpic fruits. Indeed, Micro-Tom WT is able to produce small parthenocarpic fruits at a low rate that also present a thick pericarp and large septums. However, in contrast to parthenocarpic fruits, P30A9 mutant was still able to produce a few seeds and to reach the expected final fruit size.

By looking in more details, we could notice that fruit growth in P30A9 was not completely equivalent to the WT all along fruit development. At early stages, fruit growth was not altered in P30A9 mutant and the fruit diameter was similar to the WT Micro-Tom (Figure 17.a.). However, at 10 DPA a slight reduction in fruit size settled in P30A9 that was more visible at 15 DPA. The difference in fruit size was partially caught up at 20 DPA to reach the WT size at 25 DPA. Thereafter, mutant fruit size remained comparable to the WT fruit size until the end of fruit growth at breaker stage. P30A9 mutant was selected for this work because of its thick pericarp, since it had a 1.5 fold thicker pericarp than WT fruits at breaker stage (Figure 17.b.). However, there was no difference in pericarp thickness between WT and P30A9 from anthesis to 10 DPA. The increase in pericarp thickness in P30A9 was only evident from 15 DPA onwards (Figure 17.b.). The fruit growth speed and the pericarp growth speed, related to the increase in fruit diameter and pericarp thickness followed a similar behavior in the WT with two pics of different intensity (Figure 18). The WT fruit growth speed was at its maximum between 10 DPA and 15 DPA for the first pic, and at 25 DPA for the second pic. The WT pericarp growth speed presented also a second pic at 25 DPA likely associated with the increase in fruit growth speed (Figure 18). Fruit growth speed curve of P30A9 fruits also presented two pics, at the same moment but with different intensities compared to the WT. The first pic of fruit growth speed was lower and shorter than the WT, while the second is higher. Moreover, the slow-down at 20 DPA was not so marked in the mutant than in the WT for which fruit growth speed is strongly reduced around 20 DPA (Figure 18). This could be explained by the pericarp growth speed, which was maintained at a high level at 20 DPA in the mutant while the pericarp growth speed in the WT was low at this moment. Indeed, the first intense pericarp growth speed in P30A9 had a comparable intensity than in WT fruits, but it seemed to be delayed to last longer in P30A9 compared to the WT. In addition, the slow-down of pericarp growth was also delayed (25 DPA in P30A9 instead of 20 DPA in the WT), followed by a reprise of growth speed at 30 DPA, which lasted until breaker, whereas the pericarp growth speed was maintained in WT fruits. These results suggested that a compensation mechanism could took place in P30A9, to counterbalance fruit growth retardation that took place between 10 and 15 DPA, by

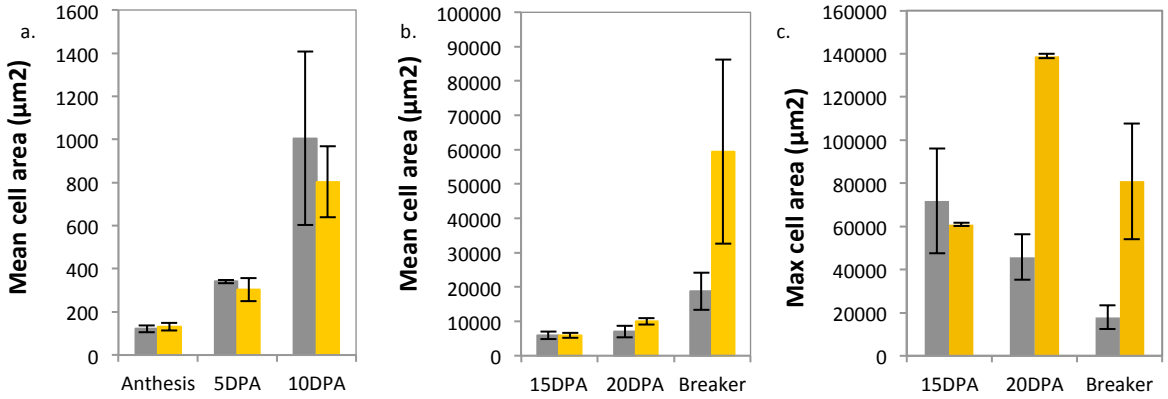

Figure 19 **Pericarp cell size during fruit growth in the WT Micro-Tom and P30A9 mutant.** a. Mean pericarp cell area during the cell division phase. b. Mean pericarp cell area during the cell expansion phase. c. Maximum cell area during the cell expansion phase. (Error bar: standard deviation, n=3)

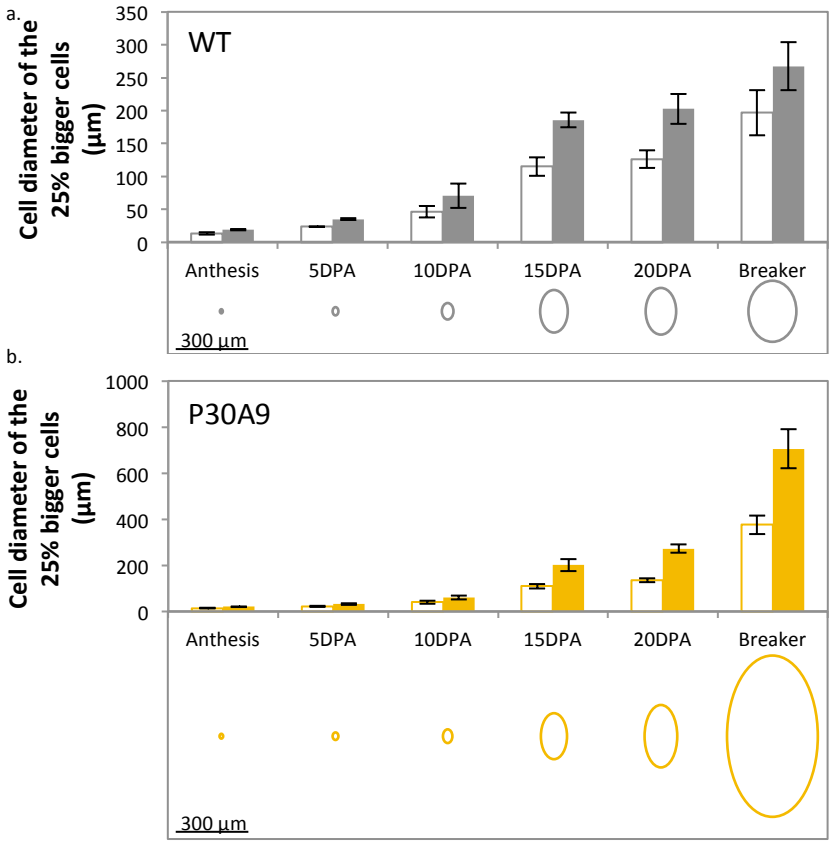

Figure 20: **Evolution of pericarp cell shape in the WT Micro-Tom and P30A9 mutant**. a. Kinetic of the minimum (white barplots) and maximum (grey barplots) cell diameters of the 25% bigger cells in the pericarp of the WT Micro-Tom. b. Kinetic of the minimum (white barplots) and maximum (yellow barplots) cell diameters of the 25% bigger cells of P30A9 mutant. For each genotype the lower panel corresponds to a schematic representation of the cell size and shape according to the upper bar diagram. (Error bar: standard deviation, n=3)

maintaining longer its pericarp growth which will allow the production of a fruit with a final size comparable to WT.

- *Pericarp characteristics*

At the cellular level, the increase in pericarp thickness in WT fruit was concomitant with an increase in pericarp mean cell area. From anthesis to 15 DPA, mean cell size remained similar between both genotypes (Figure 19.a). Differences in cell area appeared at 20 DPA and due to the heterogeneity of cell size within a pericarp tissue, were particularly obvious when looking at the maximum cell area (Figure 19.b, 19.c). This was in agreement with the increase in pericarp thickness observed at 20 DPA (Figure 17.b). At breaker stage, the difference in cell size was more important even considering all cells of the pericarp, suggesting that a greater proportion of pericarp cells had higher cell area. The mean cell area in P30A9 was three times higher than in the WT, with the largest cells inside the pericarp reaching up to 80000 μm^2 (against 20000 μm^2 at best for the WT) (Figure 19.c). If considering only the 25% largest cells inside the pericarp, to focus on the cells that account for a significant part of the pericarp growth, these observations were even more severe. Indeed, at breaker stage, the minimum diameter of those cells was two-fold higher in P30A9 mutant and the maximum cell diameter was increased by about 2.5, compared to the WT (Supplementary Figure 4).

As previously noticed in Musseau *et al.* (2017), P30A9 mutant presented an aberrant cell shape at breaker stage, with very elongated mesocarp cells. This observation was confirmed here by calculating the minimum and maximum diameter of the 25% largest pericarp cells, along fruit growth (Figure 20). Interestingly, whereas the minimum/maximum cell diameter ratio was of 1.2-1.5 in WT Micro-Tom, it was of 2 in P30A9 from 15 DPA onwards. This ratio was representative of the elongation of these large mesocarp cells in P30A9 mutant when compared to large WT cells (Figure 20).

Ploidy level was measured in pericarp cells as endoreduplication is known to be associated with cell growth in tomato pericarp (Chevalier *et al.*, 2014; Cheniclet *et al.*, 2005). Along fruit growth, the ploidy index remained comparable in WT and P30A9 mutant (Supplementary Figure 5). However, since the ploidy index is the average of all the nuclei from 2C to 256C found in the pericarp, it might not be representative of modifications for a certain type of nuclei and may not highlight subtle differences between nuclei. To circumvent this problem, we thus examined the evolution of the different ploidy classes in the pericarp of the WT and in P30A9 mutant. For nuclei with low ploidy level (2C-64C), similar

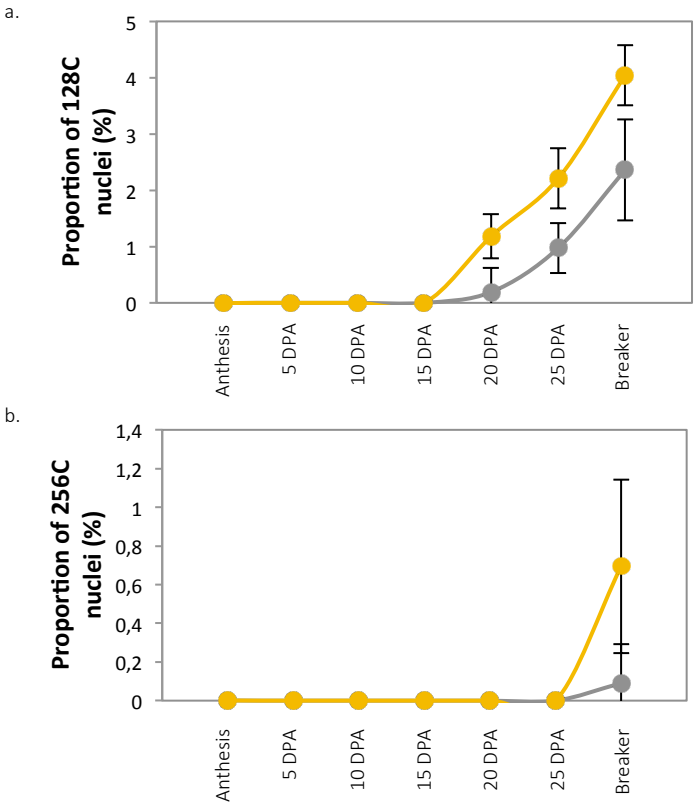

Figure 21: **Changes in ploidy level in pericarp cells during fruit growth**. a. Evolution of the 128C nuclei from anthesis to breaker stage. b. Evolution of the 256C nuclei from anthesis to breaker stage. (Error bar: standard deviation, n=3)

WT
P30A9

trends of accumulation were observed in the WT and P30A9 mutant. Interestingly, when looking at the proportion of nuclei with the highest ploidy level inside the pericarp (128C and 256C), differences between the WT and P30A9 mutant were evident. Indeed, at 20 DPA, 25 DPA and breaker stage, the P30A9 mutant pericarp cells presented highest proportion of 128C nuclei compared to the WT: 1.2 %/0.2 % of the total nuclei at 20 DPA, 2.2 %/0.9 % of the total nuclei at 25 DPA and 4.0%/2.4% of the total nuclei at breaker stage (Figure 21.a). In the same way, P30A9 mutant pericarp presented highest proportion of 256C nuclei compared to the WT. These nuclei were indeed rarely present in the WT (0.09 % of the total nuclei) and more present in the mutant (0.7 % of the total nuclei) (Figure 21.b).

To sum up, P30A9 mutant presented fruits with a normal final size, characterized by a large pericarp due to the differentiation of large elongated cells presenting high ploidy level. This rise in P30A9 pericarp tissue development was associated with a limited development of other fruit tissues like the placenta/columella and the locular tissue, and to a reduced seed number within the fruits. The characterization of P30A9 fruit growth along fruit early development revealed a transitory decrease of fruit growth between 10 and 15 DPA, followed by the occurrence of an increase in pericarp thickness, pericarp cell size, and proportion of 128C and 256C nuclei in the pericarp. Altogether, these results suggested the impairment of some fruit growth regulatory processes within P30A9 fruit and possibly the establishment of a rescue mechanism to compensate for the reduction of fruit growth. This was sustained at least in part by endoreduplication to increase significantly the pericarp cell size and orient cell expansion in the direction of the pericarp growth. Therefore, the identification of the causal mutation seemed very promising for the identification of a new regulator of fruit tissue morphology, probably in relation with endoreduplication.

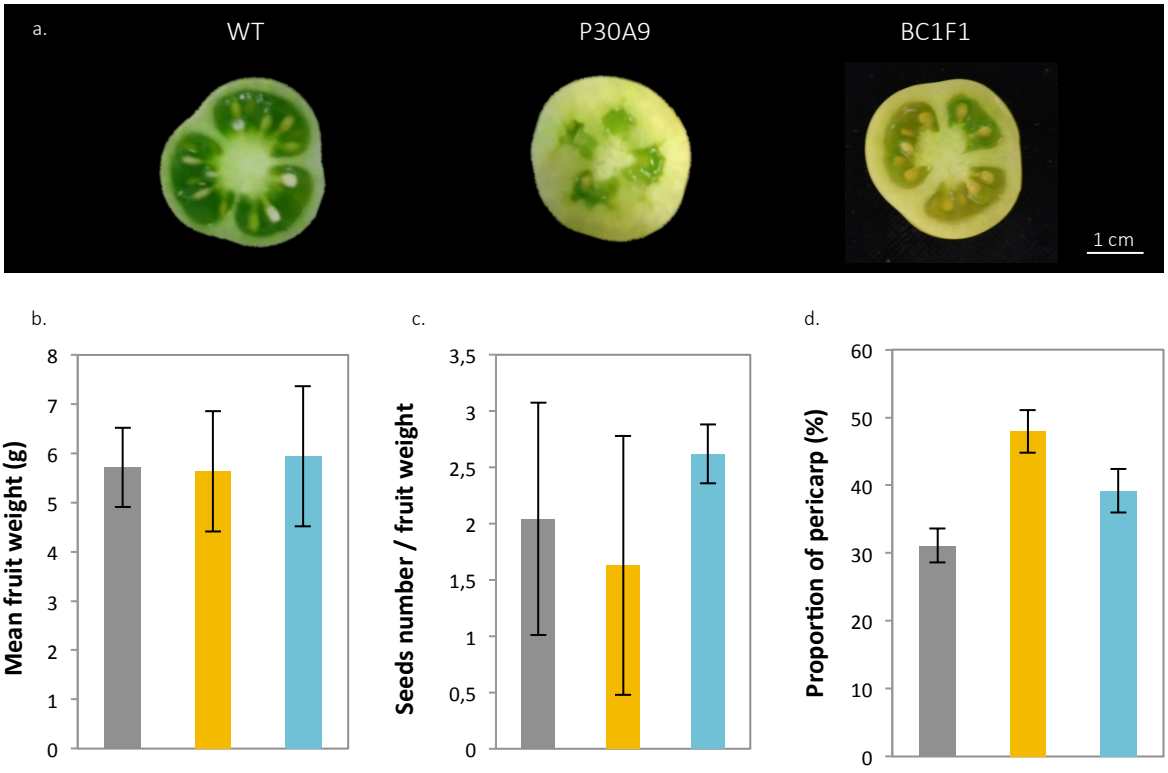

Figure 22: **Phenotypic characterization of the control individuals of the segregant population.** a. Phenotype at breaker stage. b. Mean fruit weight. c. Seed number per fruit weight. d. Pericarp thickness. (Error bar: standard deviation, 3<n<14)

II. Identification of the causal mutation using a mapping-by-sequencing strategy

The mapping-by-sequencing strategy was initiated to identify the causal mutation in the P30A9 mutant. The strategy consists to generate a segregant BC1F2 population by back-crossing the mutant with a WT Micro-Tom. BC1F2 segregant individuals are then pooled depending on their phenotype, either WT-like or mutant-like phenotype, for whole genome sequencing. The analysis of allele distributions in both pools allows the identification of the region of interest, carrying the causal mutation. The causal mutation is then identified from the other linked mutations, by recombinant analysis using the same segregant population. I had performed the mapping-by-sequencing strategy for the P30A9 mutant, including the characterization of the segregant BC1F2 population, the NGS data analysis using the pipeline already published (Garcia *et al.*, 2016) and the recombinant analysis. It took around 15 months.

II.a. Phenotypic characterization of the segregant population

- *Evaluation of the phenotype of interest: pericarp thickness*

A total of 355 F2 individuals were produced backcrossing a P30A9 mutant in M4 generation with a WT Micro-Tom line, from which 313 individuals (88%) were considered for fruit size and morphology analysis. The remaining individuals were excluded from the study, as they presented defects in their vegetative development (no germination, small plant size, developmental delay) or defects in flower or fruit production (less than six fruits per plant). In addition to the pericarp thickness (three fruits per plant), I measured for each 313 individuals, the fruit weight (six fruits per plant) and the ratio of seed number per fruit weight (three fruits per plant), at breaker stage because these parameters could influence the phenotype of interest. Multi-

locular fruits and small parthernocarpic fruits were excluded from the analysis, as these fruits could induce a bias in the analysis. 23 individuals were used as parental controls, including 14 WT Micro-Tom, 6 P30A9 mutants and 3 BC1F1 individuals, from the original backcross. As P30A9 mutant, F1 individuals presented no change in the final fruit size (Figure 22.b). However, they showed a slight increase in pericarp thickness compared to the WT Micro-Tom (Figure 22.d). This increase in pericarp thickness in F1 individuals remained below the mean value of P30A9 mutant. At this stage, this result could suggest that either the thick pericarp trait involved incomplete dominance inheritance, producing an intermediate phenotype at the heterozygous state, or that this trait was influenced by hybrid vigor that is known to increase certain characteristics (Lippman and Zamir, 2007; Krieger *et al.*, 2010).

Phenotyping was also performed taking into account possible environmental/external effects on the studied trait. Indeed, each plant was annotated according to its position in the greenhouse. Phenotyping data of the F2 individuals were analyzed using principal component analyses, as a first visualization of variability and to detect possible effects on the micro-environmental conditions and the relation between the variables. No effect of the position of the plant in the greenhouse on the observed variability was detected (data not shown).

In this study, we considered the proportion of the pericarp tissue inside the fruit (called thereafter proportion of pericarp and expressed as a percent), which is independent of fruit size variations. Indeed, it appeared the appropriate variable, in order to evaluate the pericarp thickness variation in the population and to exclude erratic interpretation to due fruit size variations.

- *Distribution of the F2 individuals according to their pericarp thickness*

Before selecting F2 individuals that will be pooled for WGS, it is necessary to look at the frequency distribution of the population. F2 individuals were widely distributed according to their pericarp thickness from 22% to 62% of pericarp inside the fruit (Figure 23). Control individuals presented a wide range of pericarp proportion variation; sometimes overlapping that makes it difficult to clearly classify values as WT-like or mutant-like. In addition, the F1 controls remained in the upper part of the WT variation that did not permit to settle between the incomplete dominance or the hybrid vigor hypotheses (Figure 23). In this context, it was very difficult to define a threshold to discriminate between the WT and mutant behaviors in this F2 population. I then considered the different possible Mendelian inheritance scenarios, involving one locus in view to establish thresholds and intent to constitute the bulks despite these limitations. The

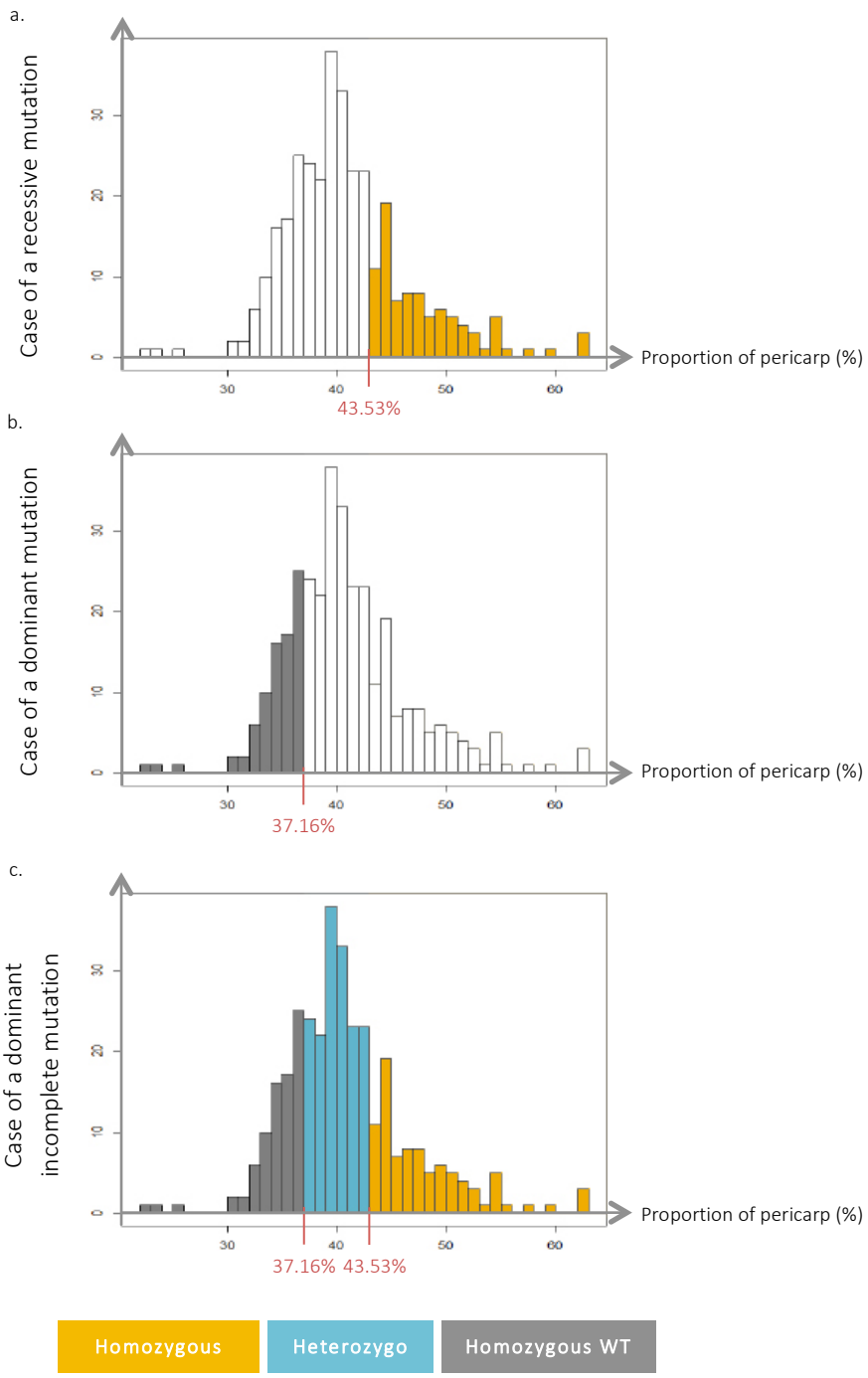

Figure 24: **Distribution of the 313 F2 individual frequencies depending on the inheritance scenarios.** a. Distribution in the case of a recessive mutation. All the individuals above the threshold at 43.53% of pericarp thickness are homozygous for the mutant allele. b. Distribution in the case of a dominant mutation. All the individuals below the threshold at 37.16% of pericarp thickness are homozygous for the WT allele. c. Distribution in the case of a dominant incomplete mutation. All the individuals above the threshold at 43.53% of pericarp thickness are homozygous for the mutant allele, all the individuals below the threshold at 37.16% of pericarp thickness are homozygous for the WT allele and all individuals between the two thresholds are heterozygous.

scenarios I presented below are theoretical and exclude possible overlapping variations that exist between the different groups of genotypes.

- In the case of a recessive mutation (Figure 24.a), 25% of individuals with the highest pericarp proportion should be homozygous for the mutation. The value of pericarp proportion should be in the same range of variation than the parental mutant controls. In this case, the threshold to discriminate mutant and WT-like phenotypes approximated to 43.53% of pericarp proportion. All individuals above this threshold should be homozygous for the mutation, while all individuals below this threshold should be heterozygous or homozygous for the WT allele. Only one P30A9 control was found below this threshold; while all WT and F1 control individuals were indeed below this threshold. This inheritance scenario remained compatible with the segregation.
- In the case of a dominant mutation (Figure 24.b), only 25% of individuals with the lowest pericarp proportion should be WT homozygous as the WT parental controls. The threshold in this case approximated to 37.16 % of pericarp proportion. All individuals below this threshold should be homozygous WT, while all individuals above this threshold should be heterozygous or homozygous for the mutant allele and present the mutant thick pericarp phenotype. P30A9 and F1 control individuals were all above this threshold, which is in agreement with this scenario. However, four WT control individuals (28%) were above it, making unlikely this inheritance scenario.
- In the case of an incomplete dominant mutation (Figure 24.c), 25% of the individuals with the highest pericarp proportion should be homozygous for the mutation, and be found above the threshold at 43.53% of pericarp thickness. 25% of the individuals with the lowest pericarp proportion should be homozygous for the WT allele and be present below the threshold at 37.16% of pericarp proportion. 50% of the remaining individuals should be heterozygous and be found between the two thresholds. These heterozygous individuals presented in this case an intermediate phenotype. F1 control individuals were found between these two thresholds and also presented an intermediate phenotype of pericarp proportion. This inheritance scenario remained also compatible.

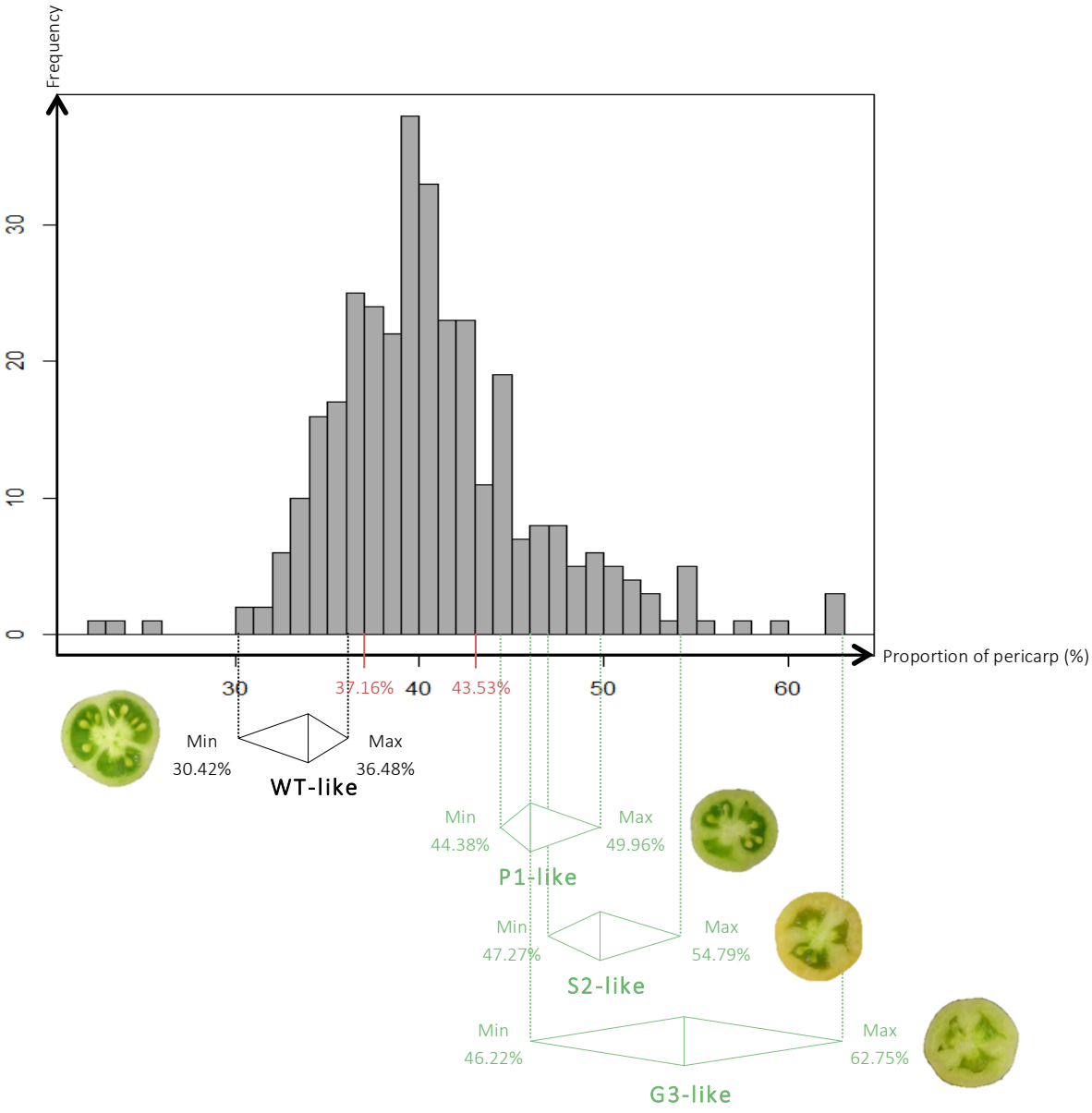

Figure 25: **Constitution of the WT-like and Mutant-like bulks depending on the pericarp proportion.** Variability in pericarp proportion in each bulk (WT-like bulk in black, mutant-like bulks in green) is represented by the diamond, below the distribution frequency graph. The middle of the diamond points the mean pericarp proportion, the left and right extremities of the diamond represent the minimum and maximum pericarp proportion, respectively.

According to the involvement of a Mendelian single locus to control pericarp thickness in this population, two inheritance scenarios remained possible: a recessive or an incomplete dominant inheritance of the mutation.

- *Constitution of the bulks for Next-Generation Sequencing*

In order to limit erratic classification of individuals in the bulks, and considering the different inheritance scenarios, it was decided to divide the mutant-like bulk into three bulks, covering the different expressivity of the mutant phenotype in the F2 population. The separation of the mutant-like bulks was made according to the proportion of the pericarp inside the fruit, but took also into account the number of seeds inside the fruit and the visual appreciation of the septum thickness and presence of pericarp invaginations (Figure 25). First, 17 F2 individuals, characterized by a thick pericarp, above the WT Micro-Tom and F1 control range, were grouped in the P1-like bulk (Figure 25). Second, 14 F2 individuals characterized by a thick pericarp and thick septums, were grouped in the S2-like bulk (Figure 25). Finally, 9 F2 individuals presenting the highest pericarp and septum thickness and a few seeds were grouped in the G3-like bulk (Figure 25). The 40 F2 individuals that maked up the WT-like bulk were chosen according to their pericarp thickness, in a range that included all the WT control individuals (Figure 25). Taken separately, individuals in each mutant-like bulk had different pattern of pericarp and septum thickness, and seed numbers (Supplementary Figure 7). Separating those individuals in three different bulks was actually the best solution. The four bulks were whole genome sequenced to identify the causal mutation.

II.b. Analysis of allelic distributions in the WT-like and mutant-like bulks

- *Genome analysis of the WT-like and P30A9-like bulks*

The analysis of DNA sequences from WGS of Micro-Tom bulks is done in routine in the group using the bioinformatics tools and pipelines described in Garcia *et al.* (2016). I did myself all the different steps of sequence analysis that allowed me familiarize with command line procedure and WGS visualization. NGS sequences from the WT-like and mutant-like bulks followed the same procedures that consist of:

Chromosome	Total variants	Absent in other WT MT	+ Absent in other mutant MT	+ Absent in M82 and in *S.Pimpinellifolium*
Chr 0	66877	3325	970	814
Chr 1	66210	3678	1754	1582
Chr 2	164353	2218	897	817
Chr 3	96006	2648	1276	1159
Chr 4	82774	2566	1342	1213
Chr 5	479322	2944	1368	1296
Chr 6	30339	1925	1007	893
Chr 7	36376	2628	1397	1253
Chr 8	23217	2589	1298	1194
Chr 9	30258	2466	1263	1181
Chr 10	19760	2637	1379	1232
Chr 11	201133	2803	1193	1102
Chr 12	55233	2854	1364	1302
All chr	1351858	35281	16508	15038

Table 2: **Number of EMS mutations in the P30A9-like bulks along the tomato chromosomes.** First column indicates the chromosomes; the second column lists the number of total variants after filtering on the read depth (10<DP<100); the third column is the number of variants obtained after removing the natural polymorphism present in Micro-Tom; the fourth column is the number of variants from column 3 but specific of P30A9 mutant and so absent in other Micro-Tom mutants; the last column is the number of variants from column 4 not represented in M82 and *S. Pimpinellifolium* accessions.

- Read mapping against the tomato reference genome,
- Calling all variants (SNPs and small INDELS) present in each bulk genome in comparison with the Heinz genome.

Variant dataset (csv files) are further processed to:

a. Identify common or specific variants between bulks,
b. Identify the presence or absence of variants in other reference genomes (such as non-mutagenized Micro-Tom genomes, other Micro-Tom mutants from the same collection, the commercial accession M82 and the wild specie *Solanum Pimpinellifolium*),
c. Calculate allelic frequencies for each variant.

This additional information allows in part (a) reducing background of false positive variants and (b) discriminating variants specific to the Micro-Tom accession (natural polymorphism) and variants specific to the studied mutant (induced polymorphism) that we further considered as EMS mutations. Indeed, sequence variations exist between different Micro-Tom lines already sequenced and the Micro-Tom lines we sequenced; they are not the same that the initial line used for the EMS treatment. Looking for variants present or absent in M82 and *Solanum Pimpinellifolium* or other accession permits to reduce a lot the number of variants, considering that variants found in the natural diversity are unlikely EMS mutations. This remains questionable but permits in a first screen to reduce the number of false positive EMS variants.

In the case of P30A9 mutant, the comparison with 8 others Micro-Tom mutants (already sequenced in the group) and 4 WT Micro-Tom allowed identifying more than 16000 mutations specific to the P30A9 mutant (Table 2), which was quite in agreement with previously sequenced Micro-Tom mutants (Petit *et al.*, 2014). This number of variants was reduced to 15000 mutations by deducing the variants also present in M82 and *Solanum Pimpinellifolium* genomes (Table 2). The distribution of these remaining variants along the 12 tomato chromosomes was constant, meaning that no infrequent introgression was present in this mutant background (Supplementary Figure 7). So, we next had to search for the causal mutation among the putative 15000 EMS mutations identified in the P30A9 bulks.

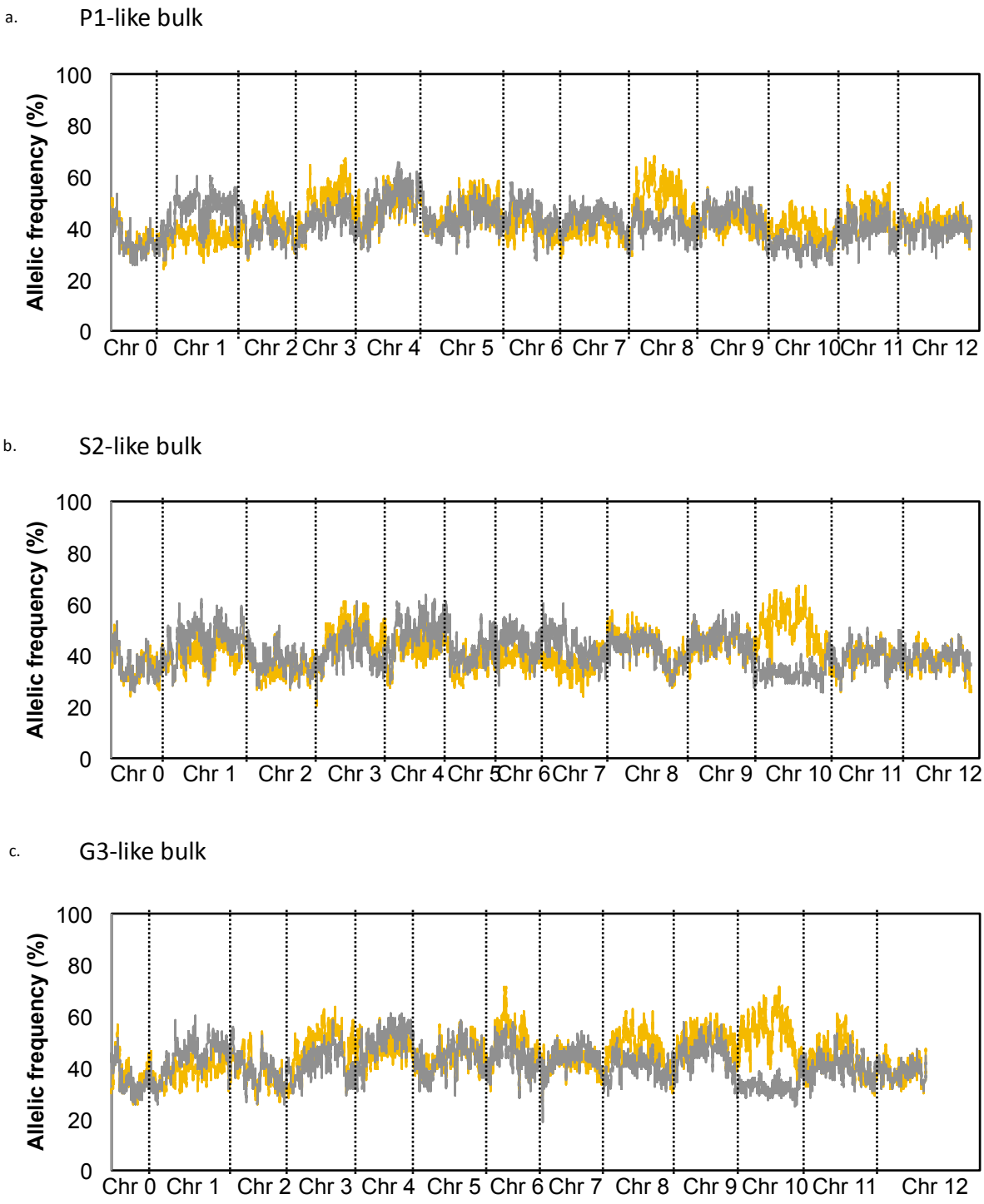

Figure 26: **Repartition of the allelic frequencies of the WT-like and Mutant-like bulks along the tomato genome.** a. Repartition of the allelic frequencies in the P1-like bulk. b. Repartition of the allelic frequencies in the S2-like bulk. c. Repartition of the allelic frequencies in the G3 like bulk.

- *Allelic frequency analysis*

Analysis of allelic frequencies of the EMS mutations, in the WT-like and mutant-like bulks allowed identifying the region linked to the character of interest, in our case the thick pericarp phenotype. Indeed, we expected that regions unlinked to the thick pericarp phenotype would segregate as 1:2:1 in each bulk, corresponding to mutation with similar allelic frequency around 0.5 in the mutant and the WT-like bulks. The chromosomal region that carries the causal mutation is expected to have a different allelic frequency in the mutant and the WT-like bulks. An higher allelic frequency of the mutation is expected in the mutant-like bulk (close to 1 for a recessive mutation and close to 0.66 for a dominant mutation) than in the WT-like bulk (close to 0.33 or 0 for a recessive or dominant mutations, respectively) (Garcia *et al.*, 2016).

Allelic frequencies of the mutations along the tomato chromosomes obtained for the three independent P30A9-like bulks are represented in comparison with the WT-like bulk in Figure 26. This representation in sliding windows plots the average of allelic frequencies for 30 successive mutations. Interestingly, different regions of interest were identified between the three mutant-like bulks. In P1-like bulk, a difference in allelic frequency between the WT-like and the mutant-like bulk was found in chromosome 8, while in S2-like bulk, a difference was noted for chromosome 10 (Figure 26.a, 26.b). Surprisingly, a difference was visible for both candidate chromosomes in the G3-like bulk, with a strong signal of association on chromosome 10 compared to the one observed on chromosome 8 (Figure 26.c). The regions associated with chromosome 10 and 8 highlighted almost all the chromosomes. This was already observed in previous studied mutants when the causal mutation was in linkage disequilibrium (LD) with the centromeric region. Indeed, the centromeric regions represent approximately 80% of the tomato genome, and in this context most of the chromosome correspond to centromeric regions (Tomato Genome Consortium, 2012). When a causal mutation is located close to the centromere, all the centromere will be in LD with the causal mutation due to the lower recombination rates observed in these regions, and will follow similar allelic frequency pattern.

The pattern of association was different on chromosome 10 and chromosome 8. For chromosome 10, as expected the allelic frequency was increased in the S2 and G3 mutant-like bulks while it was reduced in the WT-like bulk. However, for chromosome 8, only a slight increase was observed in the P1 and G3 mutant-like bulks and no reduction of the allelic frequencies was observed in the WT-like bulk. In this context, the association for this locus would be restricted to the mutant P1 phenotype, with an over-representation of the mutant allele in this bulk. In contrast, no association was visible in the WT-like bulk,

indicating that this locus segregates as 1:2:1 in these bulks. As the associated chromosomal regions appeared different in the different mutant like bulks, the constitution of three mutant-like bulks was indeed necessary to represent the wide range of the pericarp thickness variations observed in the F2 population. This observation sustained that the pericarp thickness phenotype in the P30A9 mutant is complex and/or possibly involved different locus with different impact on the phenotype. One hypothesis is that the causal mutation in chromosome 8 may cause a slight increase in pericarp thickness in the P1-like bulk, while mutation in chromosome 10 may induce a more drastic increase in pericarp thickness in the S2-like and G3-like bulks. However, chromosome 8 was also highlighted in the G3-like bulk which could means that both loci could have an additive effect on the pericarp thickness.

At least, two candidate regions were identified through this sliding window approach. However, the high recombination rate in euchromatin regions was sufficient to break LD of the adjacent mutations, as it was already the case for a previous studied mutant. In this condition, the sliding window representation was not adequate for these regions and could hide candidate mutations, by averaging the allelic frequency of the causal mutation to adjacent unlinked mutations. In this context, allelic frequency of each mutation was also analyzed separately, over recombining regions. In both cases of a possible recessive or dominant incomplete mutation, the allelic frequencies patterns would be similar. The allelic frequency ratio between the P30A9-like and the WT-like bulks should be similar around 3. Furthermore, the allelic frequency of the mutation should be found close to 1 in the mutant-like bulk. According to these parameters, the other loci to be considered are listed below (Supplementary Table 1):

- Chromosome 3 highlighted in the three mutant-like bulks,

- Chromosome 4 highlighted only in the S2-like bulk,

- Chromosome 7 also highlighted only in the S2-like bulk.

Interestingly, loci on chromosome 8 were detected with this approach only in the P1-like and S2-like bulks and not in G3-like bulk, in contrast to the sliding window approach, probably because the criteria of selection of candidate mutations are not the same through both approaches. Loci on chromosome 10 were also detected through this approach in S2-like and G3-like bulks, in agreement with the sliding window detection. To further validate the candidate regions and identify the causal mutation(s), I followed the investigation with a recombinant analysis, focused on all these candidate regions.

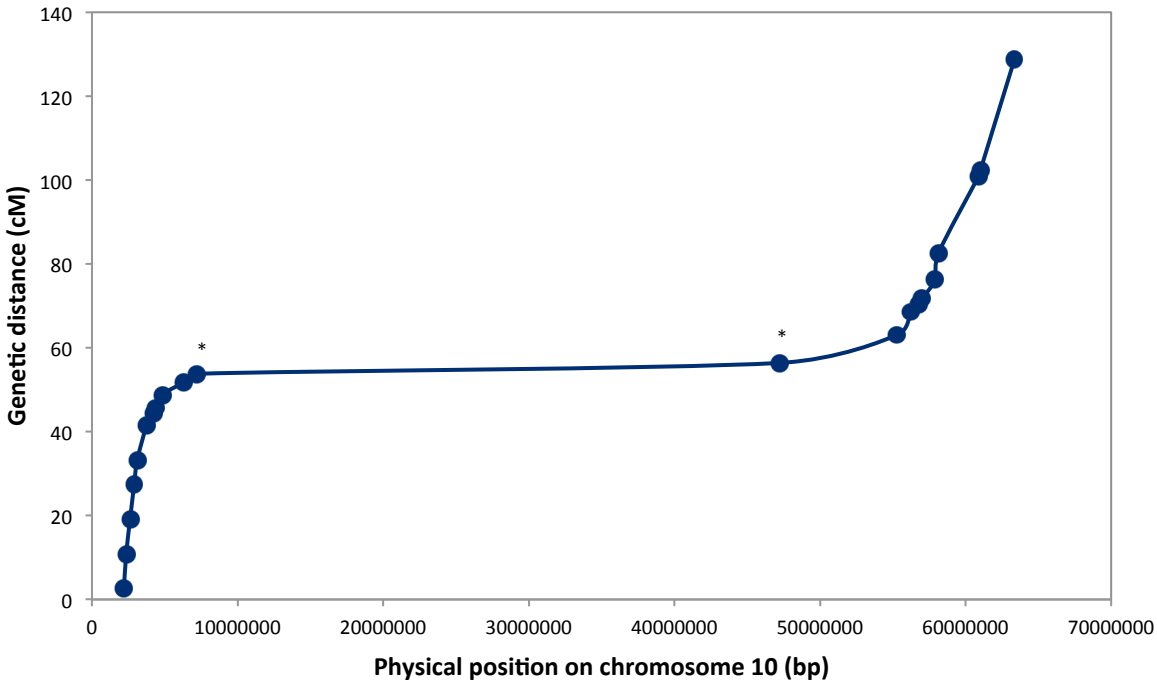

Figure 27: **Linkage map of chromosome 10.** This graphic was made using 22 markers (represented by the dots) along the chromosome 10. * indicates the centromeric region with no recombination.

II.c. Recombinant analysis of the F2 individuals for identifying the causal mutation

Candidate regions were analyzed using EMS mutations as marker for recombinant analysis in the F2 segregant population. For technical purposes, only 182 individuals of the population were used for genotyping. 80 of these individuals were present in the WT-like and P30A9-like bulks, the remaining individuals were chosen randomly. The recombinant analysis was made on 182 individuals with the objective to validate the candidate regions identified through mapping by sequencing and reduce the region of interest to precisely locate the causal mutation. This step requires a perfect association between genotype and phenotype for all the individuals analyzed. Because of the difficulty to infer an accurate phenotype for all of the individuals in relation with the points mentioned in the previous paragraphs, recombinant analysis was performed with 0%, 10%, 15% or 20% of missing individual data around the previous defined thresholds. Missing data corresponding to 10%, 15% and 20% were evaluated on the total F2 population and corresponded to 41, 60 and 75 missing individuals. The objective here was to limit possible erratic phenotype inference that would for sure limit the success to locate the causal mutation.

- *Recombinant analysis on chromosome 10*

A total of 22 markers were designed, covering the entire chromosome 10. Mapmaker software calculates the recombinant rate between two markers based on the genotyping data. The linkage map using the 22 markers on chromosome 10 displayed a maximum genetic distance of 114.2 cM, which is relatively close to the published data (approximately 110 cM for the chromosome 10, according to Tomato Genome Consortium, 2012). By comparing the known position in base pairs of the markers (physical distance) to rate of recombination in cM (genetic distance), we could easily position the centromeric region presenting low recombination rate. The centromeric region was found to be between the markers at positions 6334068 and 47227225 (Figure 27). The linkage map including the causal mutation was establish coding the P30A9 mutation in the case of a recessive mutation, as it was the most likely hypothesis (cf Chapter V Material and Methods). When considering all the individuals, the causal mutation was not grouped with the 12 markers used on chromosome 10. In this case, no further P30A9 mapping was established with this population (Table 3). The P30A9 mapping was performed using the population with 10%, 15% or 20% of missing individuals. In these cases, the causal mutation was grouped with 12 markers of chromosome 10, suggesting that excluding individuals presenting phenotypic value around the previously determined

	All individuals	±10%	±15%	±20%
Function « group »	Unlinked	**Linked**	**Linked**	**Linked**
Function « try »	-			
		0	-1.92	-3.67
2006525		-53.77	-49.05	-38.63
2193471		-26.45	-22.5	-12.49
2350019		-6.85	-5.79	0
4367406		-30.46	-25.94	-11.48
6334068		-44.92	-37.89	-17.31
7178559		-33.95	-27.81	-8.17
47227225		-28.08	-23.15	-7.65
55267208		-28.32	-22.91	-8.41
57030305		-26.72	-22.41	-8.46
58145149		-11.92	-9.31	-4.36
61017351		-8.94	-3.87	-3.2
63354209		-0.39	0	-1.29

Table 3: **Localization of P30A9 mutation on chromosome 10 using MAPMAKER.** Both « group » and « try » fucntions were used to validate a possible link and position on chromosome 10. The best score are hilighted in red.

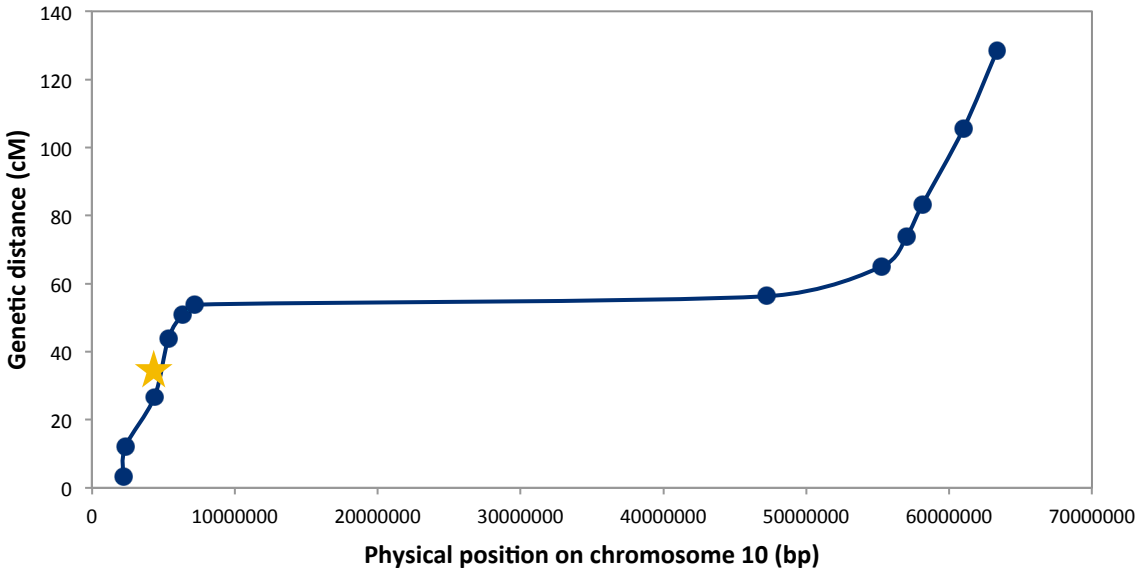

Figure 28: **Linkage map of the causal mutation on chromosome 10.** This graphic was made using the 12 markers (represented by the dots) along the chromosome 10. The star indicates the putative position of the causal mutation.

thresholds allowed grouping the causal mutation on chromosome 10. This result suggested that many mistakes in phenotype inference were probable.

The linkage map established the causal mutation either:

- At the beginning of chromosome 10, 57.2 cM far away from the first marker 2006825 (Table 3). By positioning the causal mutation there, the genetic distance of the chromosome 10 was increased to 171.4 cM, so this localization was unlikely.
- At the end of chromosome 10, 34.3 cM after the last marker 63354209 (Table 3). By positioning the causal mutation there, the genetic distance of the chromosome 10 was increased to 148.1 cM, which was also unlikey.
- Between the markers 2350019 and 4367406 (Table 3, Figure 28). By positioning the causal mutation there, the genetic distance of the chromosome 10 was increased to 119.2 cM. The causal mutation was mapped at 16.4 cM from position 2350019 and 13.7 cM from position 4367406. The interval mapping of P30A9 locus represented 20 cM, covering 2017387 bp. In view to list all the putative candidate mutations present in this region, I considered all the mutations with a 10<DP<100 and absent in the WT Micro-Tom lines, used as controls. In this condition, I did not filter the mutations present in others mutants and in the accessions M82 and *S. pimpinellifolium*, to be sure to not exclude a mutation already present in these genotypes. Among the 140 putative mutations, only seven presented an allelic frequency up to 70%, and a 1.5 fold difference in allelic frequency between the mutant-like and the WT-like bulks (Table 4). These filters allowed selecting both recessive and incomplete dominant mutations and were not too stringent because of the difficulty in phenotype inference, previously mentioned. One missense variant, 3 upstream gene variants, 2 downstream gene variants and 1 intergenic variant were identified. Upstream gene variants ranged between 473 to 4073 bp away from genes. The missense mutation was present in the Solyc10g008510 coding for a pentatricopeptide repeat-containing domain protein. The mutation induced an amino acid change from Thr to Ile at position 350 over 711 amino acids. The genes adjacent to the upstream and downstream variants are listed in Table 4.

Even if the missense mutation appeared interesting as it was in a coding gene region, at this step further phenotyping and genotyping experiments are required for improving fine mapping of the causal mutation. Additional markers should be developed on the other identified candidate chromosomes for QTL mapping and in view to test for possible interactions between loci.

Position	WT allele	Mut allele	Mut allelic frequency	WT allelic frequency	Ratio Mut/WT	Annotation	Gene Name	Distance to feature
2626539	C	T	70.21	41.67	1.69	Missense variant	Solyc10g008510.1	
2913086	C	T	73.08	46.15	1.58	Upstream gene variant	Solyc10g008860.1	4073
3115453	C	T	78.05	38.89	2.01	Upstream gene variant	Solyc10g009090.2	1413
3574424	G	C	70	38.46	1.82	Downstream gene variant	Solyc10g009470.1	3588
3615647	C	T	82.22	27.27	3.01	Intergenic region	Solyc10g009480.2-Solyc10g009490.1	
3766103	A	T	86.36	45	1.92	Upstream gene variant	Solyc10g009620.1	2680
4270535	T	A	83.87	35.29	2.38	Upstream gene variant	Solyc10g011980.2	1834

Table 4: **Mutations between the markers 2350019 and 4367406.**

- *Recombinant analysis on chromosomes 3, 4, 7 and 8*

The same work was performed on the candidate region on chromosome 3, 4, 7 and 8. Marker located on the candidate regions were genotyped and no clear association was confirmed for these four chromosomes. False candidate regions were commonly identified through mapping-by-sequencing possibly due to the undesirable selection of other traits in the bulks.

Part I

Towards the identification of the mutation responsible for the thick pericarp phenotype: case of P30A9 mutant.

Discussion and perspectives

I. Phenotypic and genetic issues in P30A9 mutant

The phenotype of interest in the F2 segregant population revealed a range of phenotypic expression of the pericarp thickness. At this stage, it is difficult to conclude if the high variation is due to:

- Incomplete penetrance knowing that this variation was already visible in the parental mutants,
- Variable phenotypic expressivity and/or additive interaction between different loci.

- *Is pericarp thickness the only phenotype of interest in P30A9 mutant?*

Thick pericarp in the initial P30A9 mutant was associated with high ploidy level and increase in pericarp cell size, together with a reduction in seed number and locular tissue growth. All these traits were also segregating in the population and were known to influence the pericarp thickness (Musseau *et al.*, 2017). The clear association of these traits in the population was not evident, so it was difficult to confirm if the traits co-segregate because they are part of the same mutant phenotype or because they influence each other's.

In the population the most extreme thick pericarp phenotypes exhibiting tissue invagination and large septums were also the ones producing relatively small fruits with few seeds. For this reason, a large part of the G3-like bulk was constituted by individuals producing small fruits with a few seeds, which is not the case of the S2 and P1 bulks. However, the candidate region associated with the S2 and G3 phenotypes is the same (CH10) that likely suggests that an additional phenotype affecting seed development is segregating in the population.

- *Is the P30A9-like phenotype present into the natural diversity of tomato?*

As previously described, P30A9 mutant was characterized by a centripetal growth of the pericarp with invaginations of the endocarp inside the fruit. This character is also found in the commercial tomato accession M82. Indeed, M82 tomato fruits do not present a smooth endocarp surface and the pericarp also forms invaginations towards the center of the fruit. M82 pericarp is also characterized by large pericarp cells, with an anisotropic expansion, and a reduce number of seeds. Similarly, small Micro-Tom

parthenocarpic fruits and G3-like fruits present similar pericarp morphology including invaginations and thick pericarp. However, the P30A9 fruits were able to grow while parthenocarpic fruits remain small fruits. So, similar P30A9 fruit characteristics are present in the tomato natural diversity. In this context, the events leading to P30A9-like fruits are not rare and probably involved basic mechanisms that are already used in other natural populations.

Considering this, we could suggest that the causal mutation in P30A9 may affect common major loci/genes already involved in the observed natural variability. The genetic determinants of tomato parthenocarpy are associated with the hormonal regulation, notably related to auxin and gibberellin, which both induce parthenocarpy on Micro-Tom (Serrani et al., 2007). Similarly, the genetic determinants at the origin of P30A9-like pericarp characteristics in natural diversity (as in M82) were not investigated. Looking for locus variations common between M82 and P30A9 mutant could be a solution for identifying the causal mutation.

- *Is the P30A9 thick pericarp a quantitative trait influenced by many genes?*

Pericarp thickness is a complex quantitative trait probably regulated by many molecular factors in the natural diversity. In the segregating population, even taking into account the fruit size and the absence of seed, it was not possible to solve the partial incoherence between genotypes and phenotypes. Mapping of the causal mutation on chromosome 10 was only possible removing individuals from the analysis, suggesting that many individuals do not follow the expected association genotype/phenotype for chromosome 10. Of course it could be due to an erratic phenotypic classification of these individuals. We may also wonder if another mutation(s), or natural polymorphism segregate(s) in the population and influence(s) the pericarp thickness in an additive or independent way. The P1-like bulk that grouped individuals with thicker pericarp was not associated with the candidate region on chromosome 10. A signal is evident by the allelic frequency analysis on chromosome 8 but only in the individuals exhibiting a thick pericarp phenotype. This case was already observed in other Micro-Tom mutants. Different regions can exhibit association patterns only with one bulk, possibly in relation with the phenotyping. Indeed, in some case the phenotype of interest could be obvious in certain physiological contexts that correspond to specific allelic combinations. These alleles could be in this context over-represented in the mutant bulks even if they are not causal. In this context, the association between chromosome 8 and the P1 phenotype is not so evident. At this stage, we cannot exclude the possible involvement of another locus responsible

for the P1 phenotype. Next steps would be to test for interactions between loci, in view to see if the variation for the pericarp thickness in the P30A9 population is better explained.

- *Which is the underlying locus of the causal mutation(s) on chromosome 10?*

Different candidate regions were identified on chromosome 10. One was found between the markers 2350019 and 4367406, which corresponds to a region of approximately 20 cM, covering 2017387 bp. Most of the candidate mutations, presenting an allelic frequency up to 70% and a difference in allelic frequency between the WT-like and the mutant-like bulks up to a ratio of 1.5, had a "modifier" impact. This means that the mutation is a non-coding variant or a variant affecting non-coding regions, where the impact prediction is difficult. It concerns variants found in regulatory regions, that is to say upstream and downstream a gene, in intron or intergenic regions. In the case of P30A9 mutant, one missense mutation is present in the Solyc10g008510 and other candidate mutations are found between 515 and 4628 bp, upstream, downstream or between two genes. Nevertheless, these candidate mutations remain interesting.

Indeed, the *Locule Number* (*LC*) locus, which is involved in the control of the number of carpel in tomato fruit, was fine mapped in an intergenic region of 1608 bp located between a putative ortholog of *WUSCHEL* and a WD40 motif containing protein. Further association mapping led to the identification of two single nucleotide polymorphisms located 1080 bp downstream of the putative tomato ortholog of *WUS* (Muños et al., 2011).

II. Towards a happy ending for P30A9 mutant

As pericarp thickness in P30A9 mutant revealed to be a complex trait, further phenotypic characterization is required in the segregant population. The objective would be to decompose these traits in different related characters and identify traits that correlate together. Indeed, morphological characterization of the pericarp thickness variation, as its size, is not sufficient to illustrate all the variation at the cellular scale. Subtle variations as in the ploidy level, especially the proportion of 128C and 256C nuclei at breaker stage could be a useful indicator to discriminate the variations in pericarp thickness. In the same way, cell size and cell shape could be other parameters to be considered even if their characterization at a population scale is more time consuming. The increase in flower size is also an interesting trait that could be used to correlate with the pericarp thickness, invaginations, nucleus ploidy etc. All this deeper characterization would help to discriminate the different putative pericarp thickness phenotypes and improve association studies.

F3 individuals could be an adequate material to investigate these other traits already in regards to their genotypes at chromosome 10. Even if my work on P30A9 mutant ends here, I am convinced that with further efforts in defining the P30A9 phenotype, we could understand its inheritance mechanism and identify the underlying gene(s). This mutant is anyway an adequate material to decipher cellular mechanisms involved in tissue morphology variations in relation with endoreduplication.

Part I

Towards the identification of the mutation responsible for the thick pericarp phenotype: case of P30A9 mutant.

Supplemental data

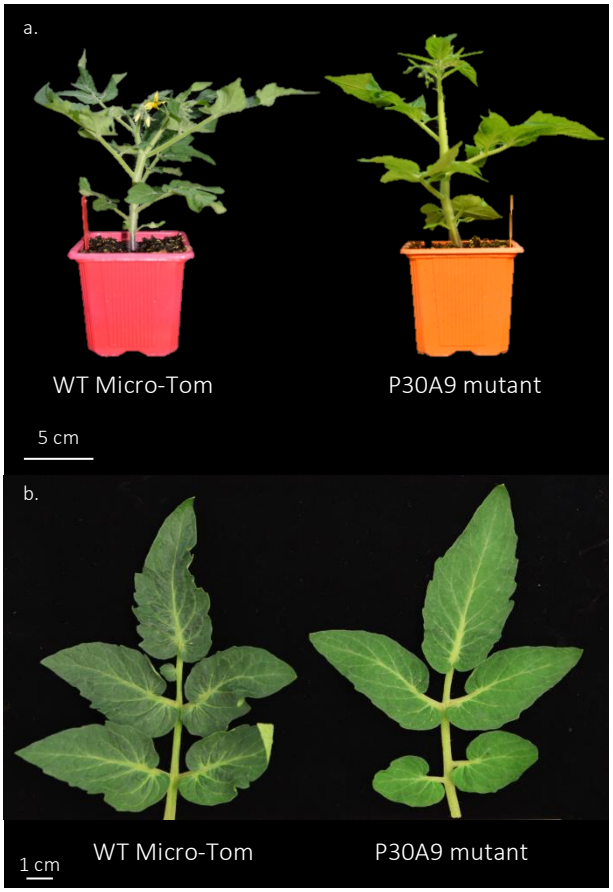

Supplementary Figure 1: **Vegetative development of P30A9 mutant.** a. Whole WT and P30A9 plants. b. Leaves of WT and P30A9 plants.

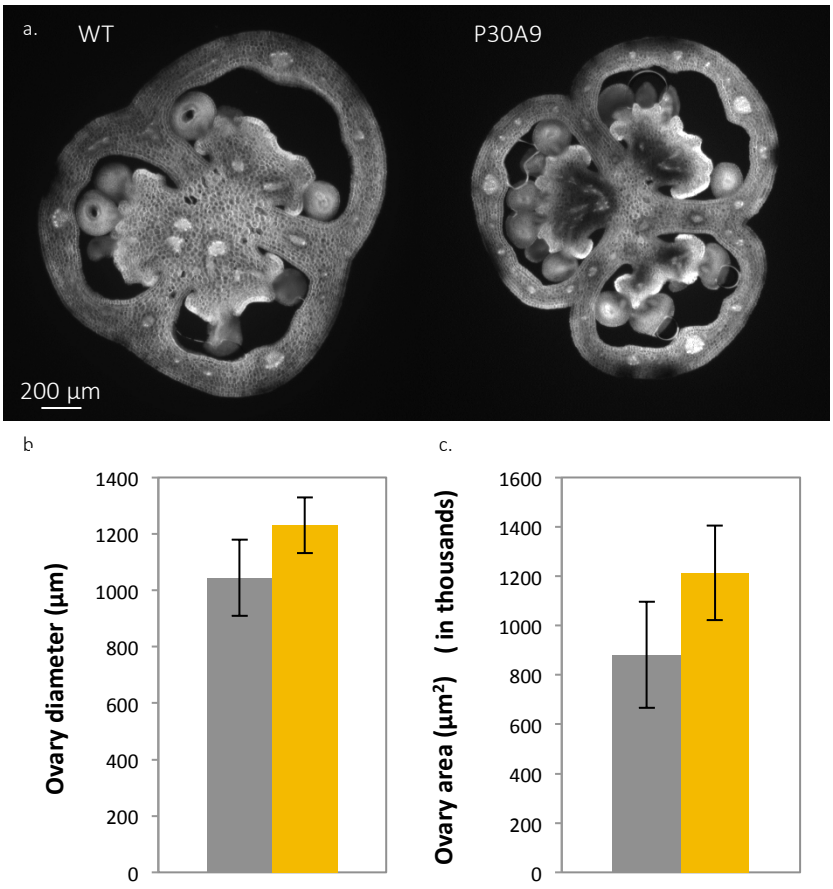

Supplementary Figure 2: **Ovary characteristics at anthesis.** a. WT and P30A9 mutant ovary in transversal sections. b. Ovary diameter in WT Micro-Tom and P30A9 mutant. c. Ovary area in WT Micro-Tom and P30A9 mutant. (Error bar: standard deviation, n=3)

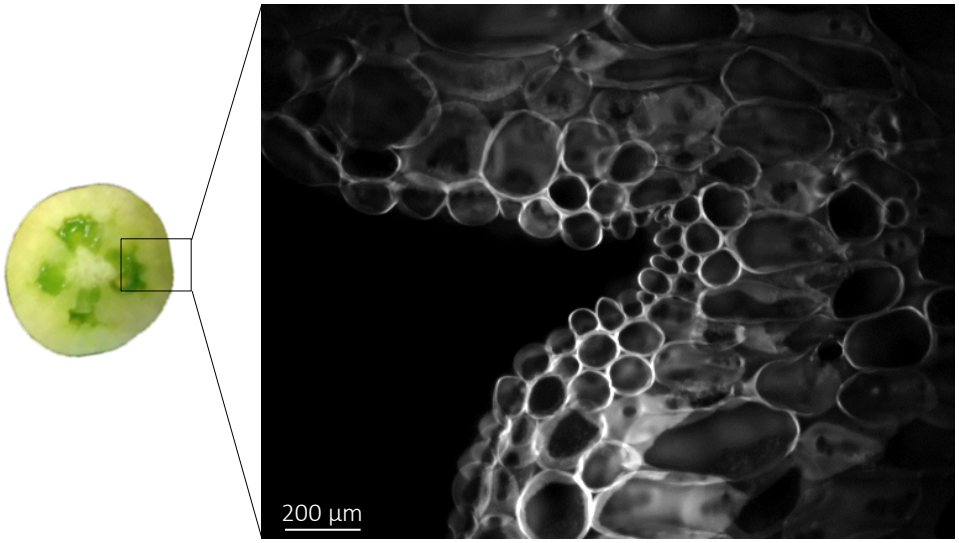

Supplementary Figure 3: **Zoom on the endocarpe invagination in P30A9 mutant at breaker stage.** Cell walls are stained with calcofluor.

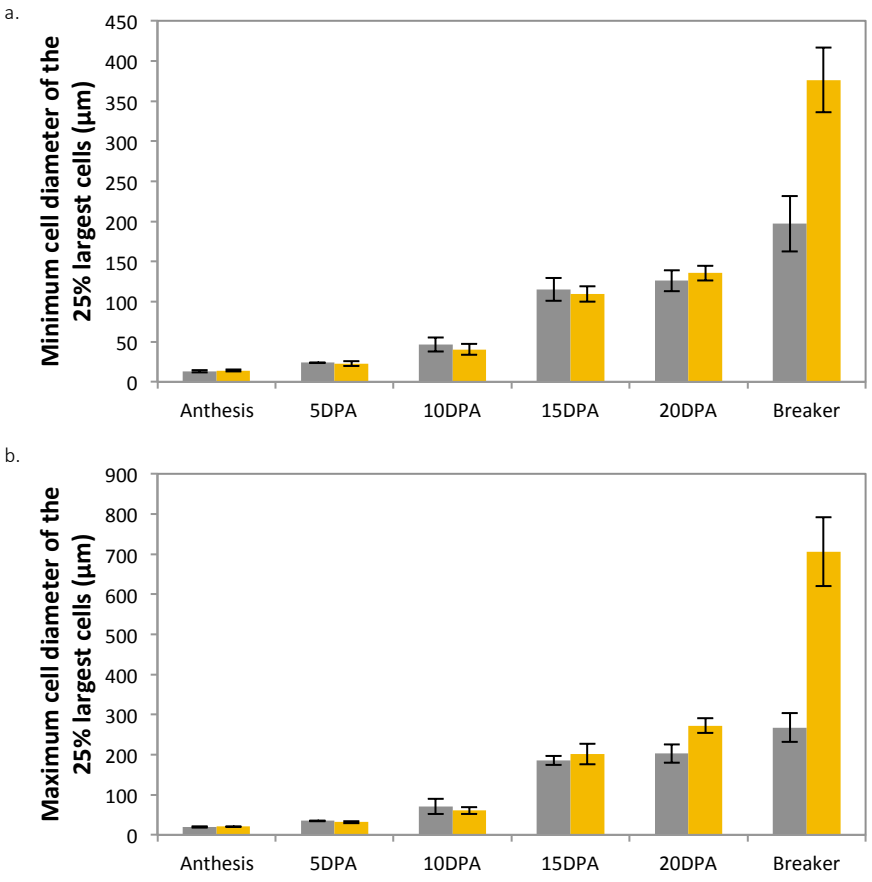

Supplementary Figure 4: **Cell diameter of the 25% larger pericarp cells in WT and P30A9 fruits**. a. Kinetic of the minimum cell diameter of the 25% largest cells. b. Kinetic of the maximum cell diameter of the 25% largest cells. (Error bar: standard deviation, n=3)

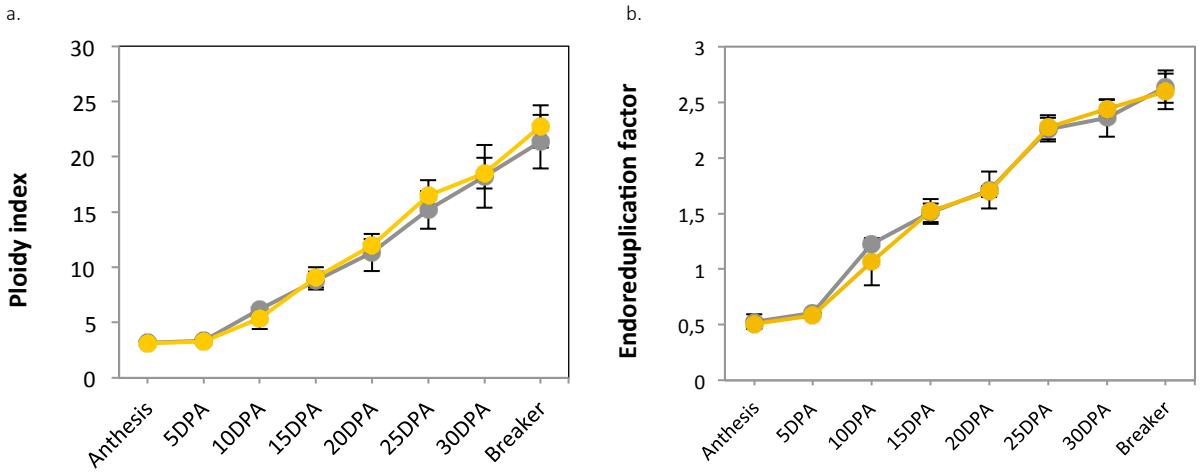

Supplementary Figure 5: **Ploidy index and endoreduplication factor in the pericarp cells of WT and P30A9 fruits.** a. Ploidy index from anthesis to breaker stage. b. Endoreduplication factor from anthesis to breaker stage. (Error bar: standard deviation, n=3)

WT
P30A9

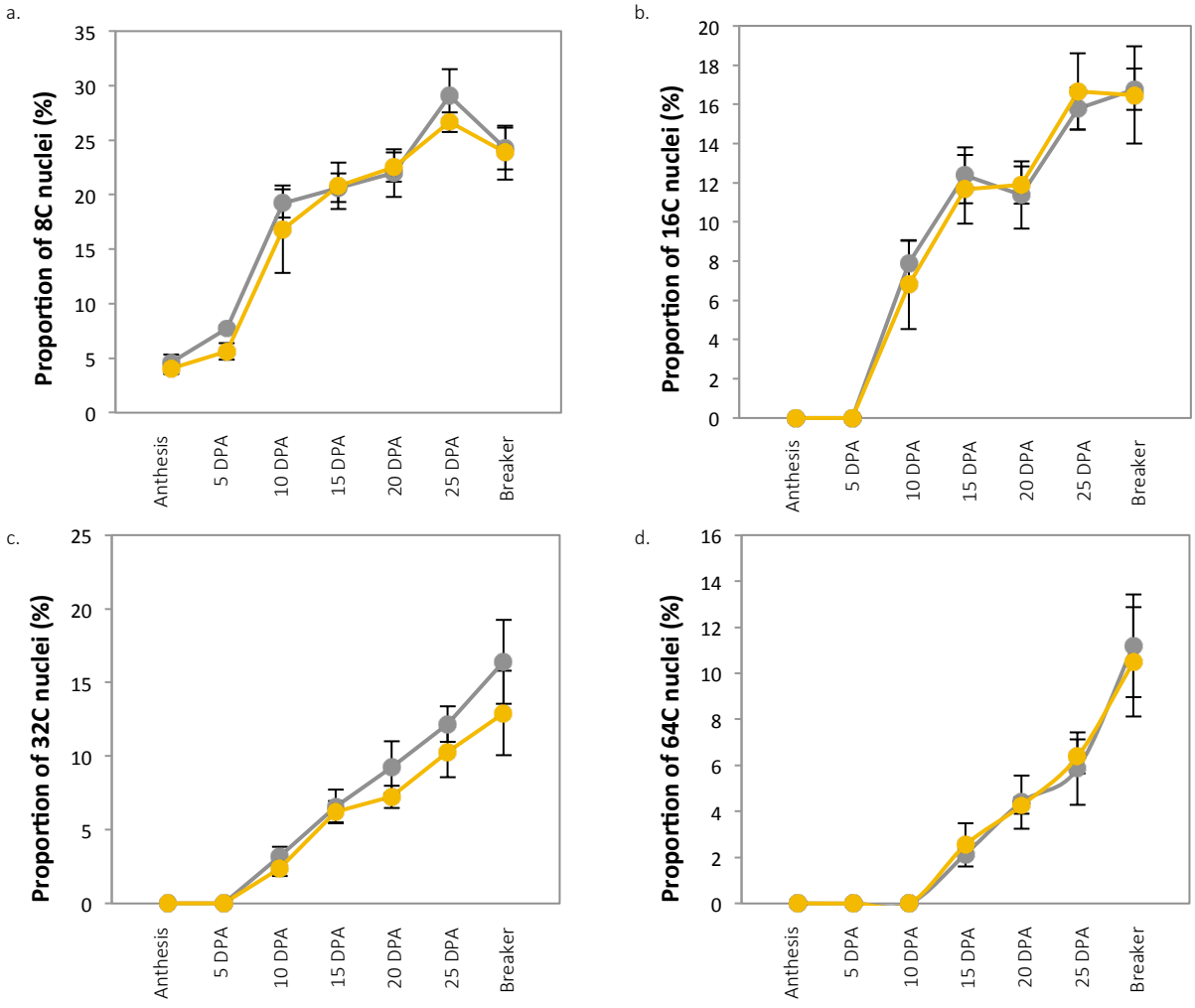

Supplementary Figure 6: **Ploidy level in the WT and P30A9 pericarp.** a. Proportion of 8C nuclei from anthesis to breaker stage. b. Proportion of 16C nuclei from anthesis to breaker stage. c. Proportion of 32C nuclei from anthesis to breaker stage. d. Proportion of 64C nuclei from anthesis to breaker stage. (Error bar: standard deviation, n=3)

WT
P30A9

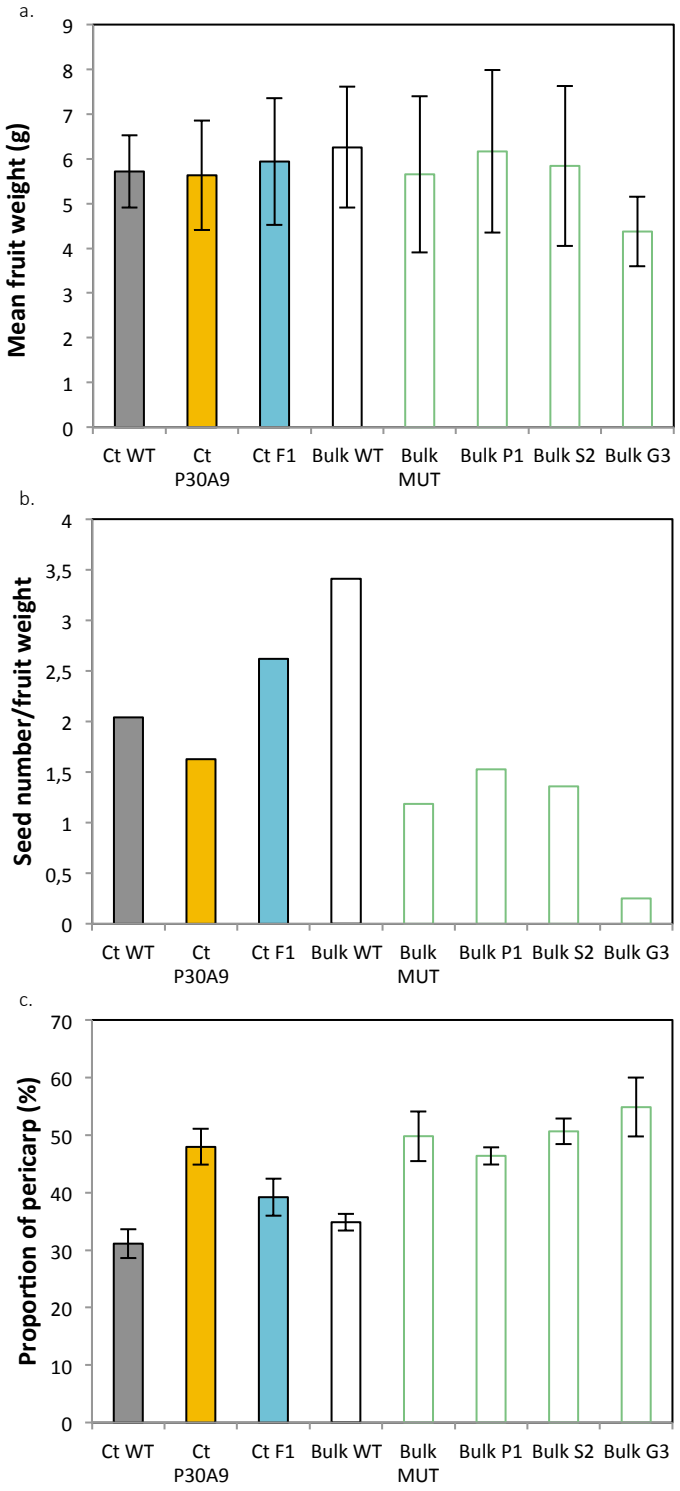

Supplementary Figure 7: **Phenotypic characterization of the WT-like and mutant-like bulks comparing to the parental controls**. a. Mean fruit size. b. Seed number per gram of fruit. c. Proportion of pericarp inside the fruit. Bulk MUT represents the combination of the three Mutant-like bulks (Error bar: standard deviation).

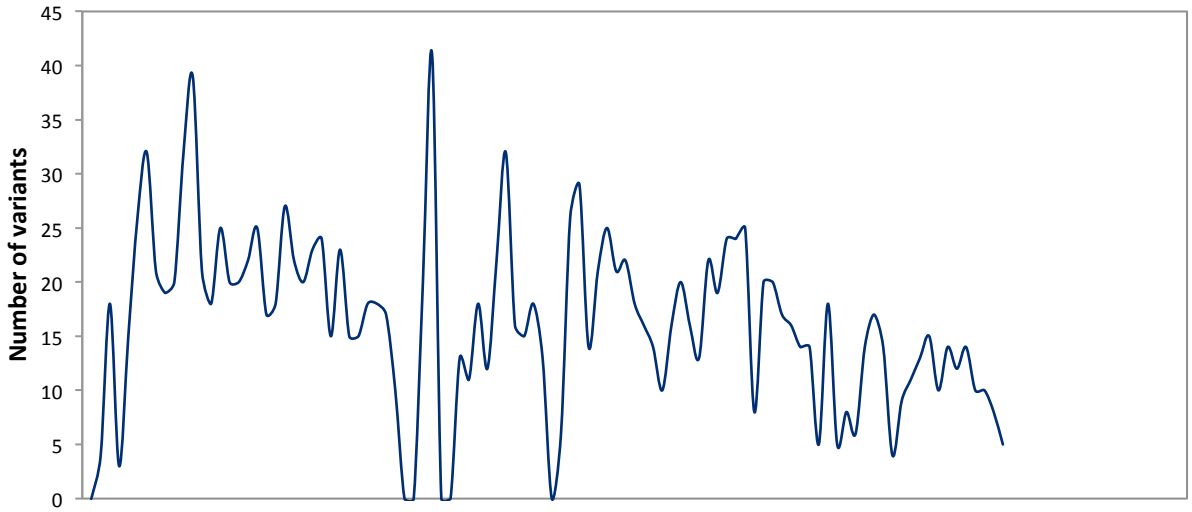

Supplementary Figure 8: **Distribution of EMS mutations along the chromosome 1.** Number of EMS mutations is represented in sliding windows of 30 mutations.

	P1-like bulk	S2-like bulk	G3-like bulk
ch00	2	5	2
ch01	3	5	4
ch02	4	4	3
ch03	12	12	13
ch04	4	11	0
ch05	5	7	1
ch06	2	4	6
ch07	4	11	6
ch08	12	10	8
ch09	6	2	3
ch10	5	45	79
ch11	7	8	5
ch12	5	4	5

Supplementary Table 1: **Looking for causal mutation in recombining regions.** The number of putative causal mutations on each chromosome was defined by considering an allelic frequency of the mutation superior or equal at 0.85 and a minimum factor of 2.5 between the WT-like and the mutant-like allelic frequencies.

Part II

Functional characterization of the Guanylate Binding Protein: case of P3D3 mutant.

Results

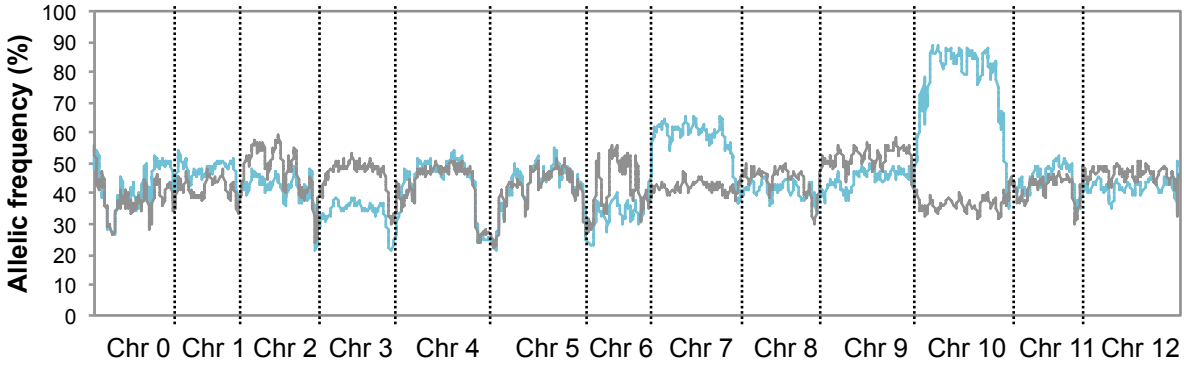

Figure 29: **Repartition of the allelic frequencies of the WT-like and mutant-like bulks along the tomato genome.**

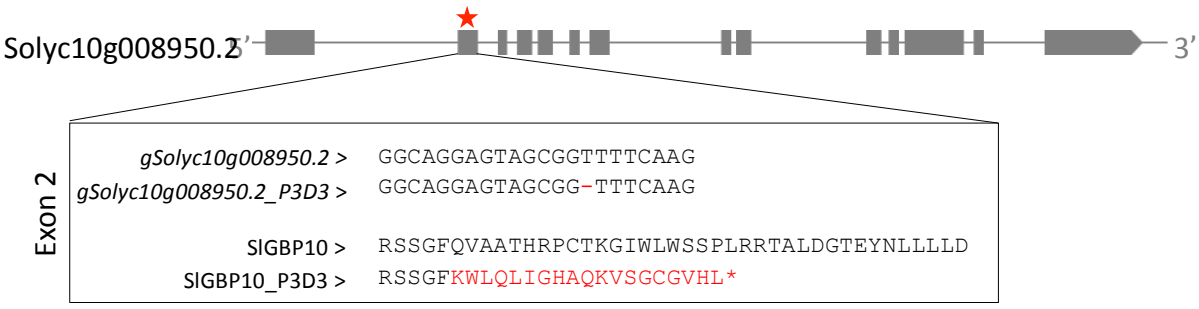

Figure 30: **Location of the EMS causal mutation and its effect on the protein sequence, in P3D3 mutant**. Grey boxes represent exons. The red star represents the location of the EMS mutation. * means the presence of a premature stop codon.

I. Identification of the mutation at the origin of the thin pericarp phenotype

I.a. The causal mutation is at the locus of the Guanylate binding protein

The P3D3 mutant is a thin pericarp mutant part of cluster II, which is characterized by an anisotropic cell expansion (Musseau *et al.*, 2017). In contrast to P30A9, pericarp cells are smaller and flattened, and the cellular organization inside the pericarp looks completely anarchic at breaker stage. In parallel to my work on P30A9, the identification of the mutation causing the P3D3 phenotype was performed in the team. The same mapping-by-sequencing strategy was completed and revealed a strong difference in the allelic frequency between the WT-like and the mutant-like bulks on chromosome 10 (Figure 29). The following recombinant analysis allowed identifies precisely the causal mutation corresponding to a deletion of a thymine in the second exon of the Guanylate Binding Protein gene (Solyc10g008950.2) (Figure 30). This deletion causes the presence of a premature stop codon in the amino acid sequence, resulting in a shortened coding region (99 amino acids over 1071 of the total protein (Figure 30).

I.b. Validation of the locus using genome editing

Because P3D3 mutant corresponds to a genetic background with many EMS mutations, the validation of the identified locus was the next essential step. For this purpose, mutations were induced on Exon 1 of the Solyc10g008950.2, using CRISPR-Cas9 editing technology. An allelic series was generated using the same guide resulting in different mutations: deletions and several one-base insertions (Figure 31). The one-base insertion (thymine, adenine and guanine) caused a premature stop codon early in exon 1 (Figure

Figure 31: **Location of the CRISPR mutations and their effects on the protein**. Grey boxes represent the exons. The red star represents the location of the mutations. * means the presence of a premature stop codon.

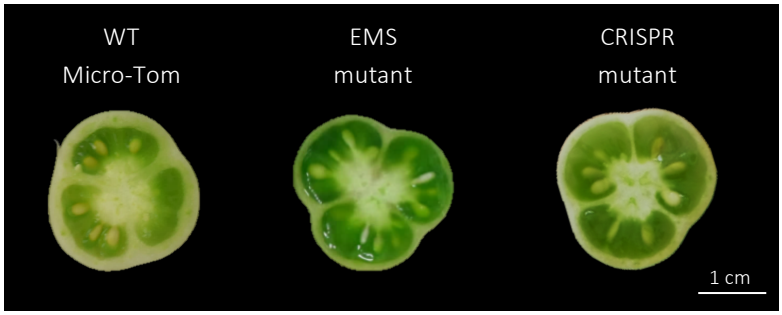

Figure 32: **Equatorial fruit sections at breaker stage.**

31), while the one-base (cytosine) or the ten-bases deletions caused a frameshift with the production of a stop codon further in exon 2 (Figure 31). All mutations were thought to be knock-out mutations (KO) causing any resulting proteins to be abnormally shortened. Homozygous CRISPR-Cas9 mutant lines phenocopied the thin pericarp phenotype observed in the P3D3 mutant which confirmed that the causal mutation was in the Guanylate Binding Protein locus (Figure 32). We next wanted to verify if the thin pericarp phenotype was specific to the Micro-Tom background or if this phenotype could be transferred to other genetic backgrounds. Thus, we transferred the EMS mutation at the locus of the Guanylate Binding Protein locus to the M82 industrial variety, by crossing the P3D3 mutant with M82. M82 produces large fruits with thick pericarp. The F2 individuals that were homozygous mutated for the GBP did not exhibit specific reduction in pericarp thickness in relation with the GBP mutation (Supplementary Figure 9). The thin pericarp phenotype was then supposed to be expressed in the Micro-Tom because of this particular genetic background known to be already mutated for fruit hormonal and growth pathways (Carvalho *et al.*, 2011). However, homozygous *gbp* F2 individuals presented the same strong cellular disorganization than P3D3 mutant, with a reduction in cell size and modified pericarp cell shape (Supplementary Figure 9). The cellular disorganization of P3D3 mutant could be transferred to another genetic background. So, I further focused my study on the cellular alterations inside the pericarp as a consequence of the disruption of the Guanylate Binding Protein than on the pericarp thickness phenotype that seems to be restricted to the Micro-Tom background.

The objective of this part of my thesis work was to initiate the functional characterization of the GBP in plants, especially in the tomato fruit. For this purpose, I worked either with the EMS mutant thereafter called the P3D3 mutant or either with the CRISPR KO lines. Two CRISPR lines were studied in parallel as they did not produce the same mutated protein. The CRISPR line called CR4 and CR8 with different transgene insertional events and different mutation events were used (Figure 31). As GBP homologs in plants had not received much attention, in the following text I simply termed the GBP homologs according to their chromosome localization and not according to the number of the corresponding homologs in other species as conventionally. The studied tomato GBP is thereafter called SlGBP10, as it corresponds to the GBP on chromosome 10 of *Solanum lycopersicum* and the *Slgbp10* mutants refer either to P3D3 mutant or CR4 and CR8 CRISPR KO lines.

II. From the identification of the causal mutation to the functional characterization of the underlying gene

- *Short overview of the GBPs function*

Guanylate-Binding Proteins are large GTP binding proteins, part of the Dynamin protein superfamily with conserved GTP binding domains and which arise from a common ancestor. However GBPs related-proteins (GBPs and atlastins) might fall a part from the rest of the dynamin-related proteins because the GTPase domain is the only significant region of sequence conservation (Praefcke and Mcmahon, 2004). Dynamins are composed of a N-terminal GTPase domain, whose activation causes an intramolecular conformational change, a conserved middle domain, which mediates the molecular interaction between dynamins during self-assembly, and a C-terminal GTPase effector domain (GED), which stimulates the GTPase activity (Konopka and Schleede, 2006; Fujimoto & Tsutsumi, 2014). Plants have homologs to most Dynamins and Dynamin-related proteins found in animals (such as the *Arabidopsis thaliana* DRP1 and DRP2) (Konopka and Schleede, 2006). Dynamins have been shown to play significant role in regulating actin assembly and organization for endosomal/vesicular trafficking and throughout the cell cycle (Konopka and Schleede, 2006; Samaj *et al.*, 2004).

GBPs are not found in *Drosophila melanogaster* or *Caenorhabditis elegans*, but are present in human and plants. Unlike dynamins, GBPs can hydrolyze GTP not only to GDP, but also to GMP. Human GBPs have been showed to interact *in vivo* with the actin cytoskeleton and are expressed in response to interferon stress for actin remodeling (Ostler *et al.*, 2014; Vestal and Jeyaratnam, 2011). The human GBP1 has also been described as an inhibitor of the nuclear delivery of virions by disrupting the formation of actin filaments (Zou *et al.*, 2017) and as a regulator of T cell activation (Forster *et al.*, 2017). Therefore, Guanylate-Binding Proteins are described to have important functions in many cellular processes in humans. However, the role and function of GBPs in plants have never been described so far.

- *GBP homologs*

Two complete GBP genes are found in the tomato genome: *SlGBP10* on chromosome 10 (*Solyc10g008950.2*) which is mutated in *Slgbp10* mutants and another one on chromosome 2

a.

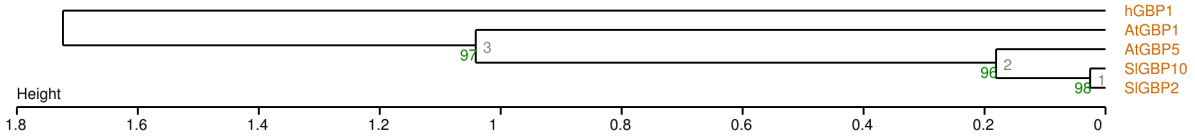

b.

Genome	GBP	Protein size (AA)	Sequence homology (%) / Query coverage (%)			
			SlGBP10	SlGBP2	AtGBP5	AtGBP1
Solyc10g008950.2	**SlGBP10**	1071	-	82 / 100	64 / 98	35 / 99
Solyc02g077600.2	**SlGBP2**	1076		-	63 / 95	33 / 89
At5g46070	**AtGBP5**	1082			-	33 / 75
At1g03830	**AtGBP1**	1013				-

Figure 33: **Amino acid sequence homology between the different GBPs.** a. Phylogenetic tree of the human GBP1 (hGBP1) and the plant GBPs. *Arabidopsis* AtGBP5 is the closest homologous protein of the tomato SlGBP10. b. Table of the corresponding amino acid sequence homology between the *Arabidopsis* and tomato GBPs.

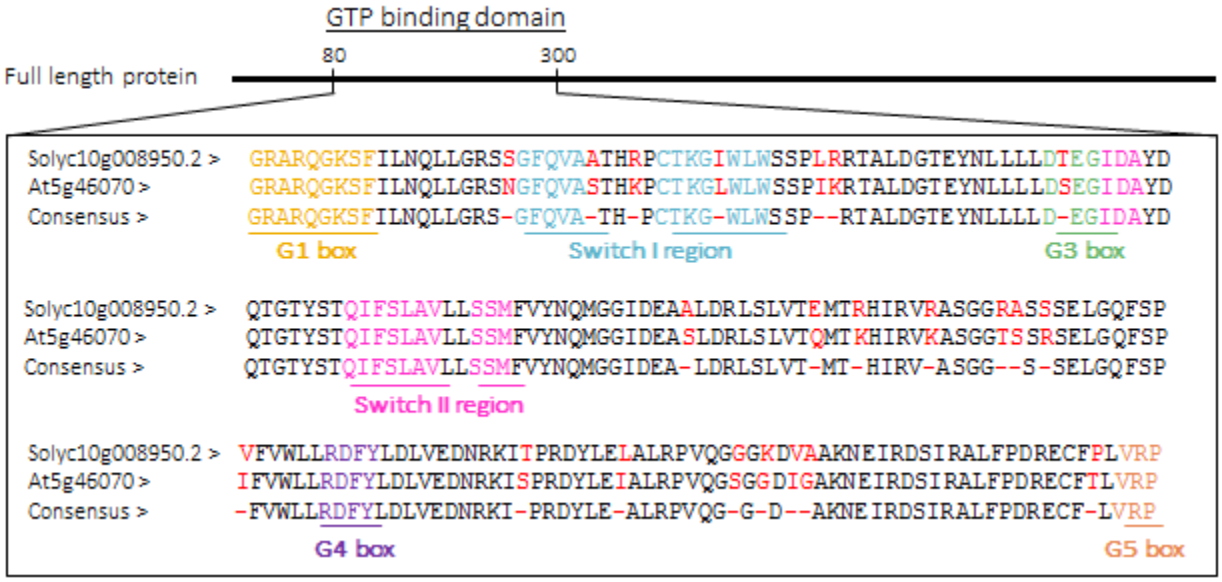

Figure 34: **Sequence alignment of the GTP binding domains of the tomato SlGBP10 and *Arabidopsis* AtGBP5.** Conserved « dynamin-like » GTP binding domains are highlighted with different colors. Differences in amino acid sequences are highlighted in red.

(*Solyc02g077600.2*), called *SlGBP2* (Figure 33). At the amino acid level, both tomato proteins share 82% of homology on 100% of query coverage (Figure 33.b, Supplementary Figure 10). They also share common GTP binding motifs that are conserved in the Dynamin superfamily and are necessary for their GTPase function (Supplementary Figure 10). In the *Arabidopsis thaliana* plant model, two GBPs are annotated, one on chromosome 1 (*At1g03830*) and one on chromosome 5 (*At5g46070*), respectively called *AtGBP1* and *AtGBP5* (Figure 33). In contrast to the tomato SlGBPs, *Arabidopsis* AtGBPs share less homology and it is obvious in the GTPase domain (Supplementary Figure 11), with only 33% of homology on 75% of sequence coverage (Figure 33.b). The best homolog of SlGBP10 in *Arabidopsis thaliana* corresponds to AtGBP5. Both proteins share 64% of homology on 98% of query coverage, with a very high percentage of homology in the GTPase domain (Figure 33.b, Figure 34).

- *Expression pattern of GBPs in tomato and Arabidopsis thaliana*

Both tomato *SlGBP10* and *SlGBP2* are lowly expressed in leaves and flowers, but higher expressed in roots, stem and fruits (Supplementary Figure 12, 13). Gene expression in fruit did not exhibit any specific pattern in relation with the tissue or the fruit stage (Supplementary Figure 12,13). *SlGBP2* homolog presents a similar pattern, but it is expressed at lower levels than *SlGBP10* (Supplementary Figure 13). In *Arabidopsis thaliana*, *AtGBP5* and *AtGBP1* are mostly expressed in dividing tissues or organs, such as the apical meristem, the flower buds, the seed and young siliques (Supplementary Figure 14, 15).

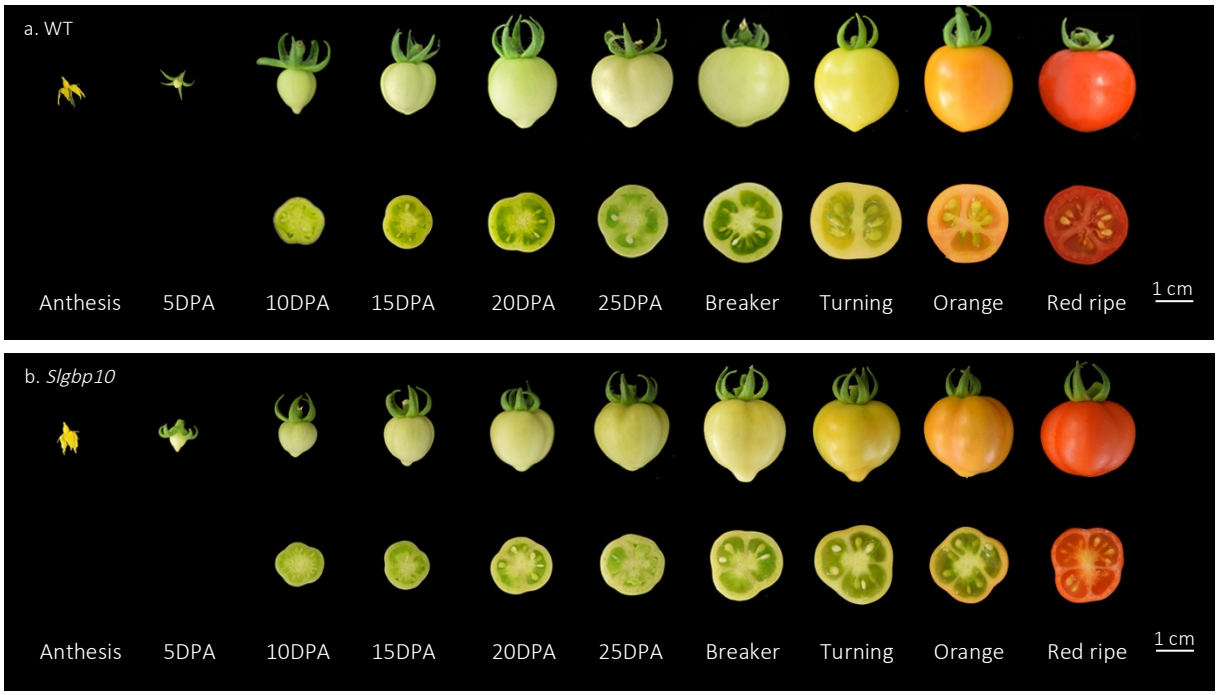

Figure 35: **Fruit development from anthesis to the end of ripening.** a. WT Micro-Tom whole fruit development and its equatorial section. b. *Slgbp10* mutant whole fruit development and its equatorial section.

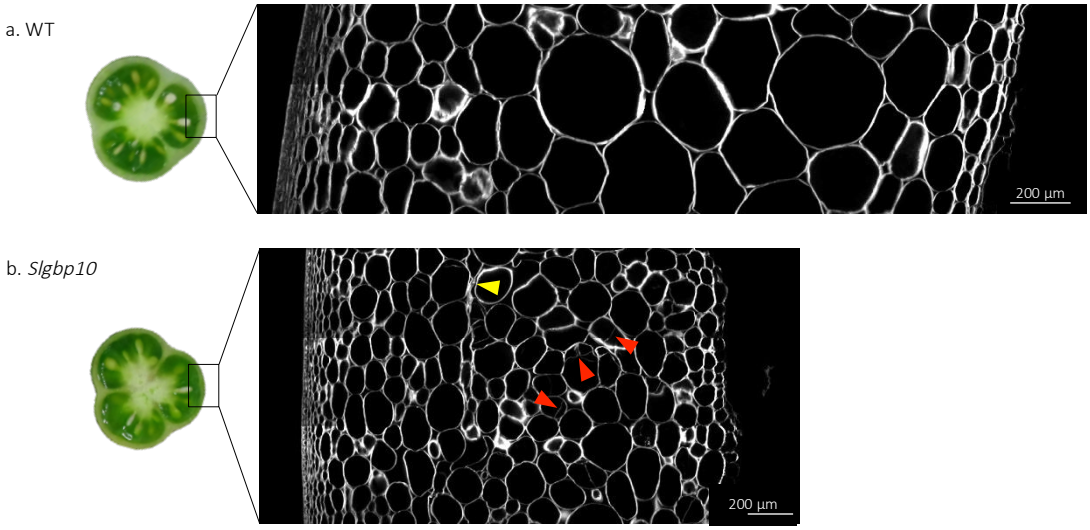

Figure 36: **Equatorial section of the pericarp at breaker stage.** a. Pericarp section in the WT Micro-Tom. b. Pericarp section in P3D3 mutant. Equatorial portion of pericarp were stained with calcofluor. Red arrow-heads highlight the additional cell walls, the yellow arrow-head highlight a stack of cell walls.

III. The thin pericarp phenotype: the tip of the iceberg

III.a. Phenotypic alterations in Slgbp10 mutants are mainly affecting the fruit

P3D3 mutant was first selected and characterized for its alterations on fruit tissue morphology, with a strong reduction in pericarp thickness associated with a reduction in cell size and cell ploidy level, without changes in the final fruit size (Musseau *et al.*, 2017). The previous phenotypic analysis of this mutant was focused on the fruit, mainly the pericarp tissue and at breaker stage. In view to know (i) if the disruption of the GBP induces other modifications than the ones observed in the fruit and (ii) when the alterations takes place in the fruit, I performed a deeper phenotypic characterization of the *Slgbp10* mutants.

- *Vegetative development*

At the whole plant level, *Slgbp10* mutant showed no obvious alterations in the vegetative development (Supplementary Figure 16). However, the mutant presented strong alterations in root development, with a delay in the initiation of lateral roots and limitation of their growth (Supplementary Figure 17). However these alterations did not impair the development of the plant. Alterations of root development were not further characterized to focus my study on the fruit.

- *Fruit development*

At the fruit level, no obvious differences in fruit size were observed, but a strong reduction in pericarp thickness was noticeable from 20 DPA, to the end of ripening (Figure 35). On the contrary, mutant fruits developed more locular tissue and seeds than in the WT Micro-Tom (Musseau *et al.*, 2017). One could imagine that either the locular tissue might develop more in order to compensate for the reduction in pericarp thickness and reach the final fruit size or that the outgrowth of the locular tissue generates a force such as to limit the late expansion of the pericarp.The classic evolution of fruit color during maturation was also impaired in *Slgbp10* mutants. From 20DPA, brown spots appeared inside and at the

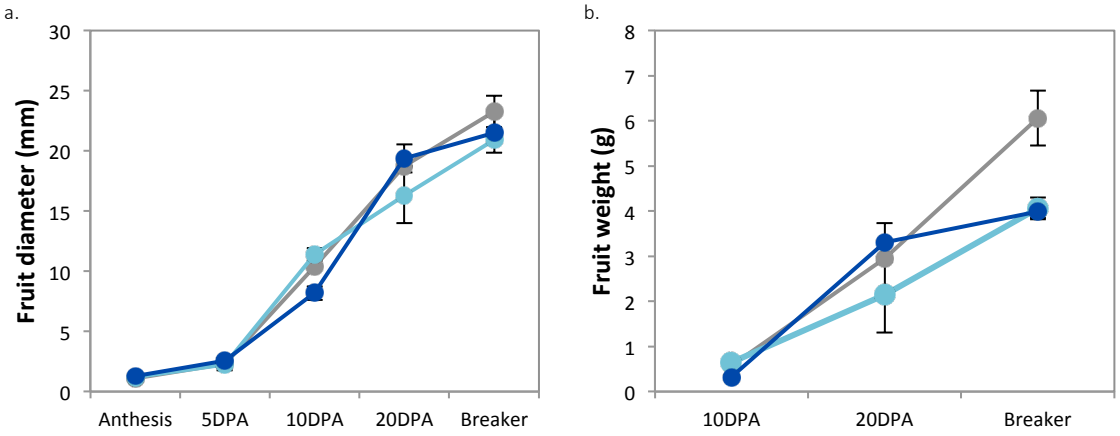

Figure 37: **Evolution of fruit size during fruit growth.** a. Kinetic of fruit diameter from anthesis to breaker stage. b. Kinetic of fruit weight during cell expansion. (Error bar: standard deviation, n=3)

WT
CR4
CR8

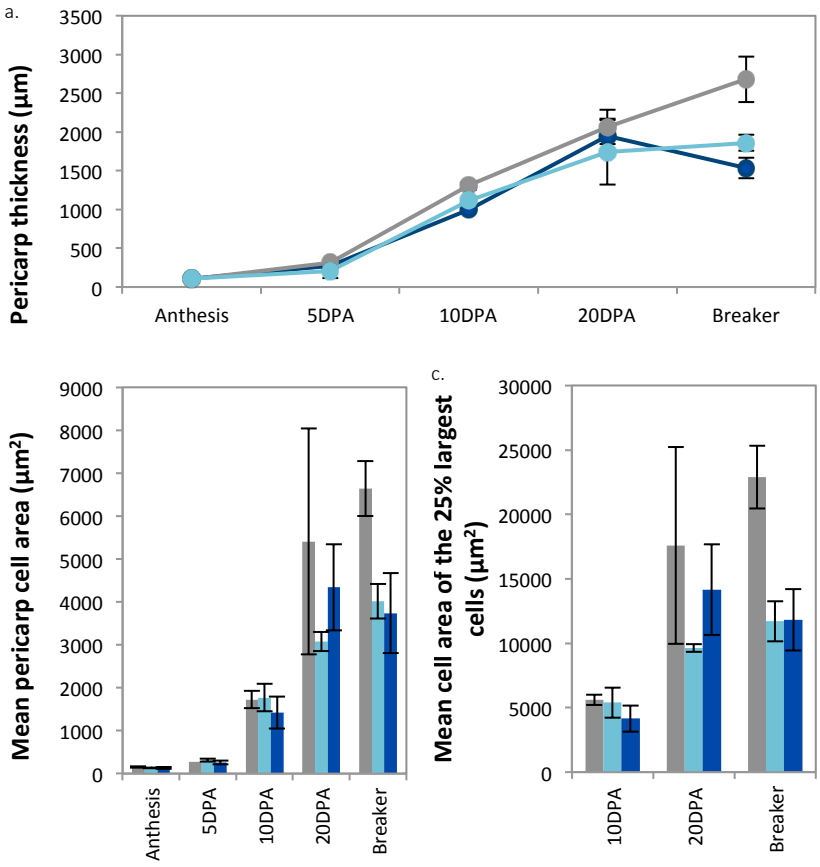

Figure 38: **Characterization of the pericarp.** a. Kinetic of pericarp thickness. b. Evolution of the mean pericarp cell size. c. Evolution of the maximum pericarp cell size during cell expansion. (Error bar: standard deviation, n=3)

WT
CR4
CR8

surface of the pericarp, giving darker green color to the whole fruit at mature stage when the fruit normally turns white. The brown stain was even more evident around breaker stage, when yellow color takes place. Turning and orange stages looked also darker than the WT Micro-Tom. These brown stains were never reported in other Micro-Tom mutants.

III.b. Primary and secondary metabolite compositions are altered in P3D3 mutant

In relation with the brown spots observed inside and at the surface of the pericarp, I looked for metabolic changes in the pericarp between the CR4 and CR8 mutant lines and the WT Micro-Tom, at different stages of fruit development. Interestingly, both primary and secondary metabolites showed a different pattern according to the fruit developmental stage and the genotypes (Supplementary Figure 18). The metabolic patterns at 15 DPA, 20DPA and 25 DPA in the WT were also close to the ones at 15DPA and 20 DPA of the mutant and only the metabolic pattern at Red Ripe stage was clearly different (Supplementary Figure 18). This great difference at Red Ripe stage was meaningful with all the metabolic modifications that take place during ripening. Indeed, over the fruit development, the differences between metabolic content of green and ripe fruits were more pronounced than comparing two green fruits at different stages. The primary metabolic patterns at 15 DPA and 20 DPA between the WT and the *Slgbp10* mutants were close. In contrast, at 25 DPA and Red Ripe stages, *Slgbp10* mutants strongly differed from the WT (Supplementary Figure 18). Interestingly, metabolic pattern at 25 DPA in the mutants appeared completely a part from the rest, while the metabolic pattern tended to get similar to the WT pattern, at Red Ripe stage. Primary and secondary metabolisms followed similar patterns, with a strong change at 25 DPA in the *Slgbp10* mutants (Supplementary Figure 18.b).

So, *Slgbp10* mutants presented an unusual metabolism already at 25 DPA before the Breaker stage corresponding to the entry into ripening processes. Metabolic differences were always noted at the end of ripening, but appeared less important than the ones observed at 25 DPA. The singular metabolic behavior at 25 DPA was concomitant with the apparition of the brown spots observed inside and at the surface of the pericarp of P3D3 mutant. Further metabolism studies are required to identify the metabolites at the origin of these changes.

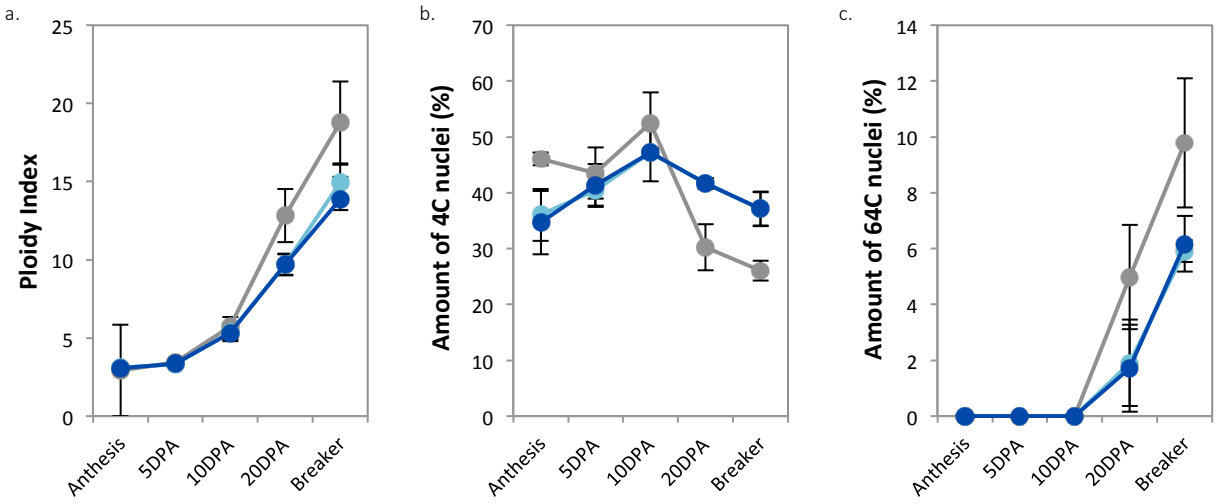

Figure 39: **Evolution of ploidy level along fruit growth.** a. Ploidy index. b. Amount of 4C nuclei. c. Amount of 64C nuclei. (Error bar: standard deviation, n>3)

III.c. Slgbp10 mutants are characterized by a strong cellular disorganization that appears during late fruit growth

In the WT Micro-Tom, the pericarp tissue presented a gradient of cell size with the larger round cells in the inner mesocarp inside the pericarp, at breaker stage (Figure 36.a). As previously mentioned, P3D3 mutant presents a reduction in pericarp thickness with aberrant pericarp cell size and shape (Figure 36.b) (Musseau *et al.*, 2017). Pericarp tissue seemed to crush against the epicarp and cellular organization, including cell size and shape, is not conserved. As a result, the different cell layers could not be discriminated easily and stacks of cell wall created large breaks inside the pericarp. These alterations were evident at breaker stage (Figure 36.b).

In order to know if the cellular alterations in P3D3 mutant are also found at earlier fruit stages, I realized a kinetic analysis of fruit growth including pericarp sections from anthesis to breaker stage. At the fruit level, no strong difference in fruit diameter were noticed, in contrast to the final fruit weight a breaker stage which was reduced in the CRISPR mutants (Figure 37). This reduction was associated with a reduction in pericarp thickness, which is noticeable at breaker stage (Figure 38.a). The major differences in pericarp thickness were found at breaker stage, with a 1.5 fold reductions (Figure 38.a). At the cell level, modifications were noted already at 20 DPA with small cell size, which was obvious at breaker stage with again a 1.5 fold reduction in the mutants (Figure 38.b). At breaker stage, *Slgbp10* mutants could not reach large cell size comparable to the WT, with the 25% of the largest cells reaching an average of 12000 μm^2, instead of 23000 μm^2 in the WT Micro-Tom (Figure 38.c). So the decrease in pericarp thickness that initiated at 20 DPA and increased at breaker stage was correlated with a decrease in pericarp cell area because of the inability to reach the largest cell sizes.

As endoreduplication is mainly related to cell growth inside the pericarp, I also measured the ploidy level inside the pericarp. Compared to the WT, the *Slgbp10* mutants showed a decrease in ploidy index from 20DPA (Figure 39.a). This was due to a higher proportion of small nuclei (4C nuclei) (Figure 39.b) and a lower proportion of highly polyploid nuclei (64C) (Figure 39.c) (Supplementary Figure 19). Changes in nuclei proportion took place after 10 DPA to be significantly different at 20 DPA and even more drastic at breaker stage. Parameters analyzed in the mutant followed late sequential alterations from (1) modification in the ploidy level of the pericarp cells after 10 DPA, with an impact noted on the cell size in the same time step, (2) to consequences visible at the tissue level only at breaker stage.

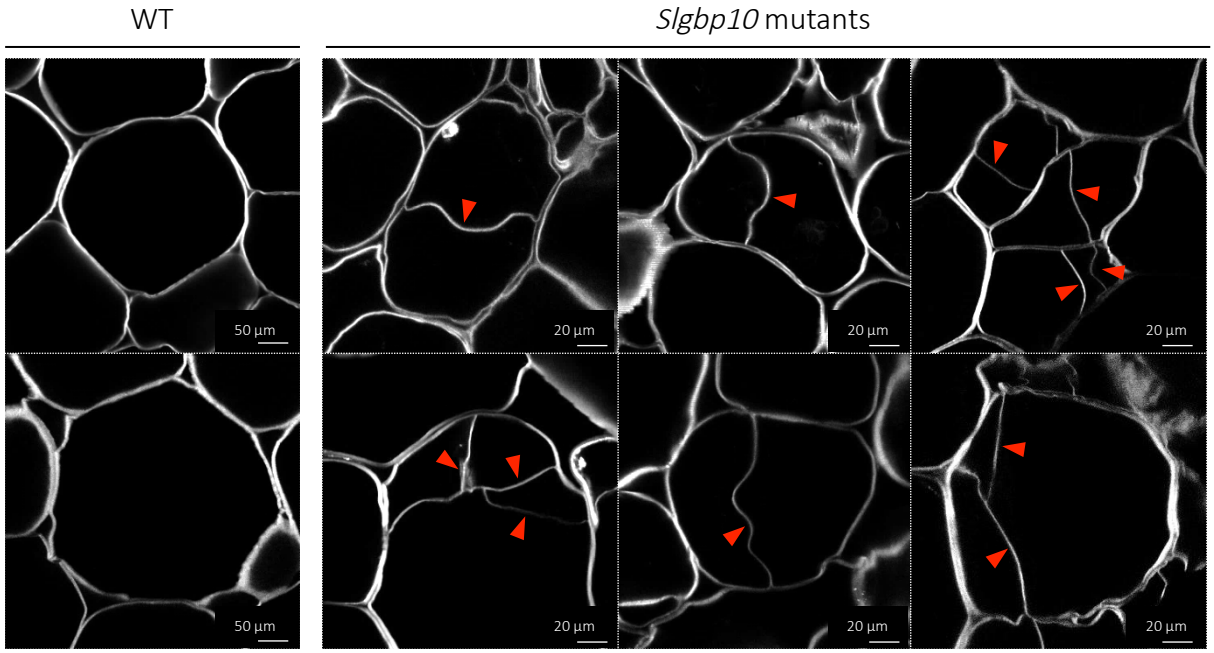

Figure 40: **Cellular alterations inside the pericarp in the *Slgbp10* mutants at breaker stage.** Cell walls are stained with calcofluor. Red arrow-heads highlight the additional cell walls.

III.d. Cell division is altered in Slgbp10 mutants

Interestingly, *Slgbp10* mutants presented additional cell walls and abnormal cell division pattern inside the pericarp at breaker stage, when there is normally no more cell division (Figure 40). Therefore, the additional cell walls seemed to be formed inside many small and large cells in the inner mesocarp. This new cell walls were curvy and not centered with respect to the initial cell as commonly observed during the formation of a new cell plate during cytokinesis. Some cells presented extreme cell division pattern with two or three internal cell walls dividing the cell in 3 to 4 unequal parts (Figure 40). This additional cell wall could be related to an ectopic production of cell walls or due deposition after cell division. The observation of the nucleus in large cells remained difficult using a confocal because cells are so large that labelling and observation over a stack is limited. However, in small cells and in many occasions for large cells I was able to distinguish a nucleus in the different parts of the cell (Supplementary Figure 21). In this context, it is likely the deposition of cell walls occurred following new cell division events. In contrast to normal cell division the new cell walls remained curved as immature cell plate, and the new cell walls did not separate the new independent daughter cells, as cell walls remained clearly associated to the parental one. These aberrant cell division patterns were patchy inside the tissue. This phenotype was very strong at breaker stage and appeared very rarely, earlier during fruit growth (Supplementary Figure 20).

In relation with this striking phenotype, previous transcriptomic analysis on the P3D3 mutant revealed that the expression of genes involved in cell division was affected at 10 DPA. Transcriptomic analysis was performed at early fruit stage with the aim to point the early genomic events related with the late alterations. The altered regions inside the pericarp (mainly mesocarp tissue between two vascular tissues) were dissected using laser microdissection for further RNA sequencing. RNA seq analysis revealed in addition to genes involved in cell division, many genes involved in cell organization and cell wall loading and metabolism (Supplementary Table 3). Altogether, these results suggested that disruption of SlGBP10 altered cell division and related mechanisms during tomato fruit growth.

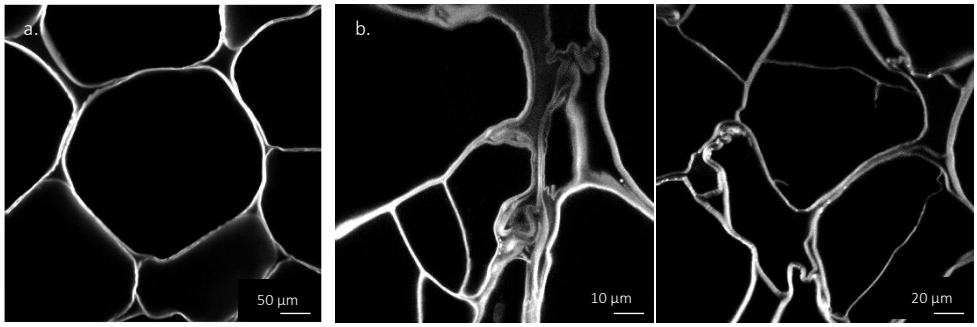

Figure 41: **Cell wall deposition alteration at breaker stage.** a. in WT Micro-Tom. b. in *Slgbp10* mutants. Cell walls are stained with calcofluor.

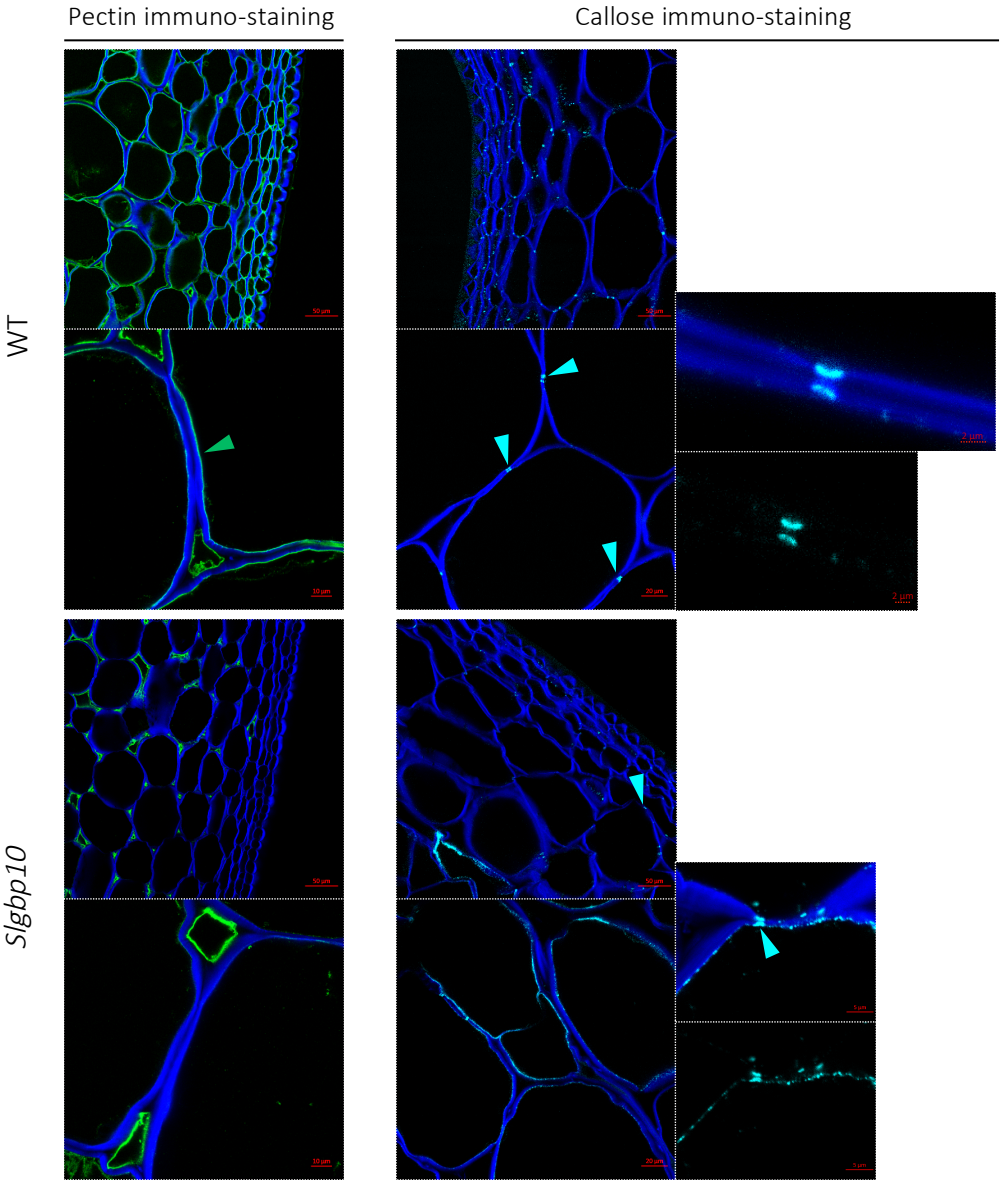

Figure 42: **Pectin and callose deposition patterns in the *Slgbp10* mutants, at breaker stage.** Dark blue is calcofluor, green is pectin, clear blue is callose. The green arrow-head highlights the layer of pectin deposition in the inner face of the cellulosic layer. Clear blue arrow-heads highlight plasmodesmata.

III.e. Slgbp10 mutants show defects in cell adhesion and cell communication

In addition to cell division alterations, *Slgbp10* mutants presented stack of cell wall deposition (Figure 41). At this point it was very difficult to conclude if these stacks are ectopic accumulation of cell wall or cells that were flattened upon mechanical constraints (Figure 41). This cell wall accumulation was located at the position of transition between the sub-epidermal cell layers (E1-E3) and the mesocarp cell layers (M'-M), as described in Renaudin *et al.*, 2017. This accumulation was at the origin of periclinal lines of breaks inside the mesocarp where cells appeared not cohesive anymore. This phenotype was very strong at breaker stage and not observed earlier during fruit growth (Supplementary Figure 20).

Further characterization of the cell wall was performed in the team looking for pectin and callose deposition pattern as they are involved in cell adhesion and cell communication processes. Immunostaining of the tomato pericarp with an antibody against partially unmethyl-esterified pectins (JIM5 anti-homogalacturonan) revealed a difference in pectin deposition pattern between the WT and the mutant at breaker stage. In the WT, low methyl-esterified pectins were found in intercellular junctions together with the inner side of the cellulose layer (Figure 42). In the *Slgbp10* mutants, low methyl-esterified pectins were still found in intercellular junctions but not in the inner position of the cell wall (Figure 42). Moreover, along pericarp section, few labelling was present in the outermost cell layers in the mutant. Demethyl-esterification of homogalacturonans increased during normal tomato fruit development (Steele *et al.*, 1997), meaning that *Slgbp10* mutants were unable to correctly set up cell wall modification along fruit growth.

Immunostaining of callose (anti-1,3 β-glucan) in the tomato pericarp also revealed a difference in callose deposition pattern. In the WT, callose deposition is mainly located around plasmodesmata (Figure 42). In the *Slgbp10* mutants, there was still callose deposition at the plasmodesmata, but labelling was less intense meaning either fewer plasmodesmata or smaller callose deposition around plasmodesmata (Figure 42). In addition, *Slgbp10* mutant presented an ectopic callose deposition in breaks and for some cells in the inner side of the cellulose layer (Figure 42). As callose regulates cell-to-cell communication via plasmodesmata, these results suggested possible alterations in cell communication in the tomato pericarp (Otero *et al.*, 2016). The difference in pectin and callose deposition observed, when SlGBP10 was disrupted in the *Slgbp10* mutants should contributes to the global mutant phenotype involving. In

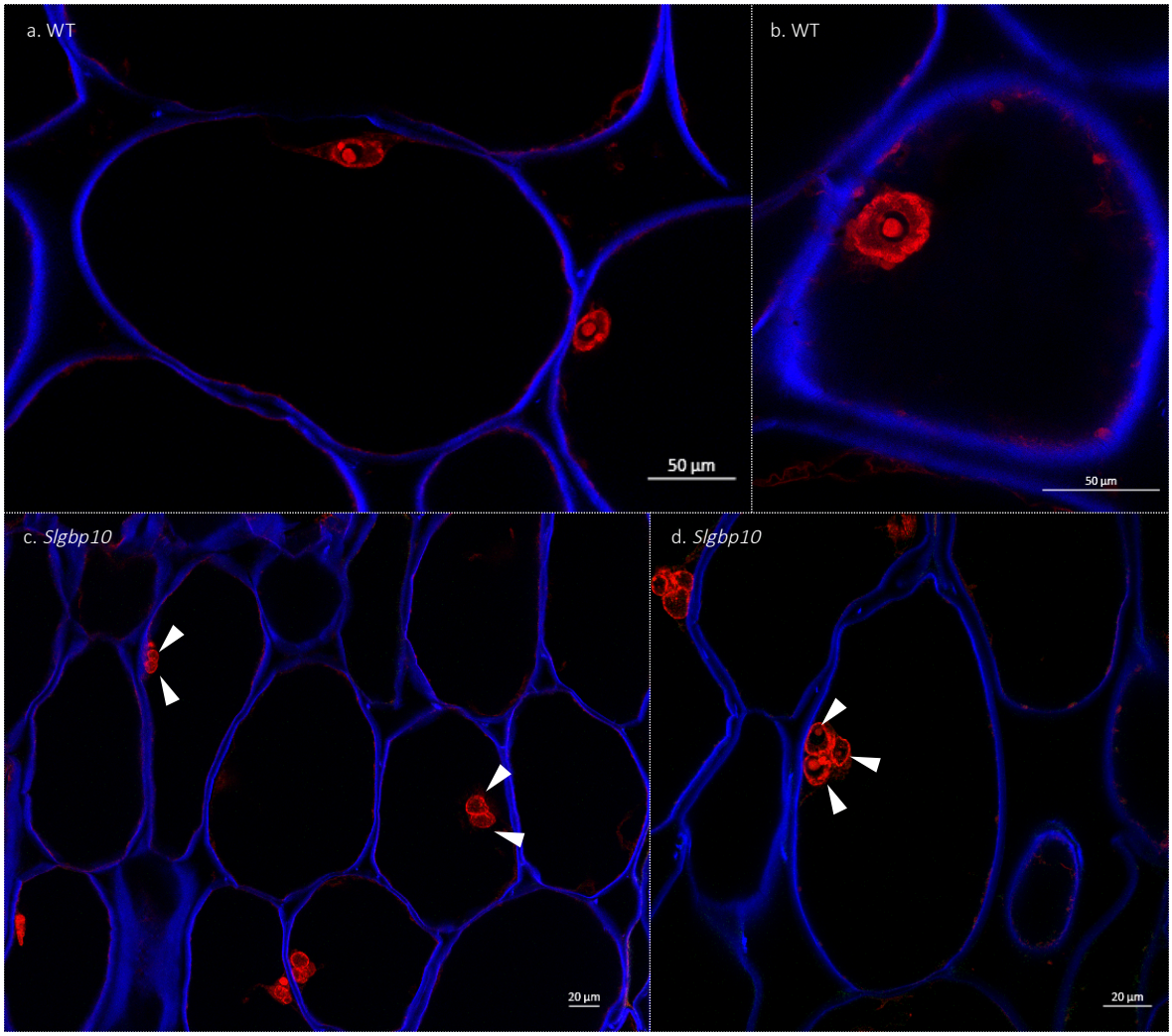

Figure 43: **Morphology of pericarp nuclei**. a.b WT pericarp cells and nuclei. c.d. Pericarp cells and nuclei in *Slgbp10* mutant. Cell walls are stained with calcofluor (blue), nuclei are stained with propidium iodide (red). Arrow-heads indicate the lobes.

addition, or as a consequence to the cell division alterations, cell adhesion and cell communication defects contributed to the whole pericarp disorganization observed in the *Slgbp10* mutants.

III.f. Alteration of nucleus morphology in the pericarp cells of the Slgbp10 mutants

Since nucleus is central in cell division, analysis of nucleus through microscopic observations was initiated. This work was performed in the team while I was writing my PhD manuscript, and I present here the first results we have obtained. At breaker stage, the reduction in pericarp cell size, aberrant pericarp cell shape, anarchic cell plate formation and defects in cell adhesion were concomitant with alterations in the nucleus morphology. Starting from 25 DPA, nuclei from the inner mesocarp became multi-lobed nuclei (Figure 43). WT nuclei were round to oval, presenting small invaginations of the nuclear envelope and a large unique nucleolus (Figure 43). In contrast, nuclei of *Slgbp10* cells presented multi-lobed and many nucleoli (Figure 43). Nuclei presenting until 8 lobes were observed (Supplementary Figure 22). At this step of the analysis, we cannot confirm if the lobes are independent or fused. The presence of multiple nucleoli in these multi-lobed nuclei suggest either that the fusion of nucleolus is impaired modifying subsequently the overall morphology of the nucleus or that each lobes correspond to a single nucleus (Supplementary Figure 23). Interestingly, small epicarp cells and cells from the sub-epidermal layer that are mainly composed of 2C or 4C cells, presented normal nucleus morphology (Supplementary Figure 24). Indeed, only the large cells present in the mesocarp that undergo endoreduplication were associated with this alteration in nucleus morphology.

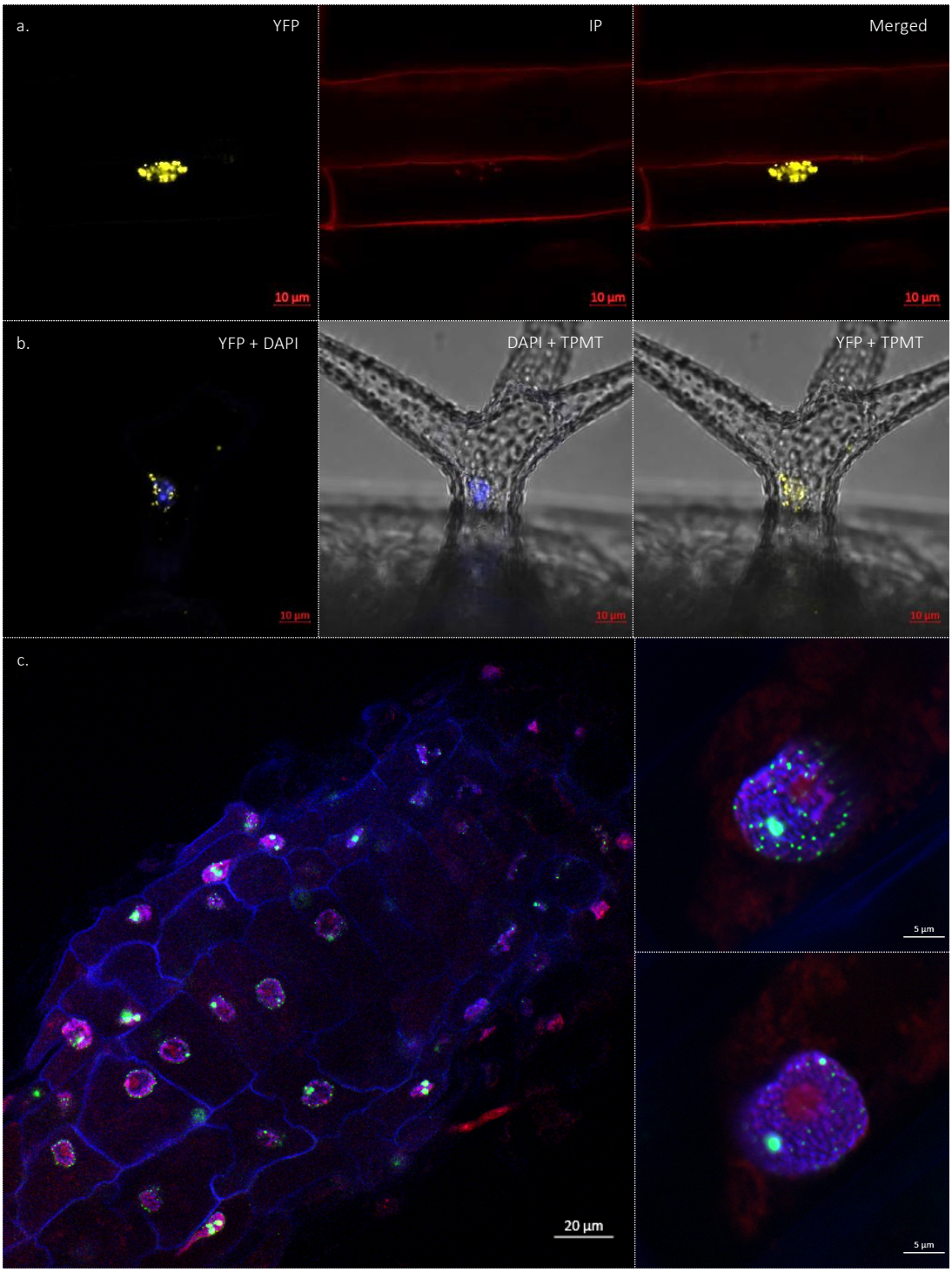

Figure 44: **Subcellular localization of SlGBP10.** SlGBP10 expressed under a constitutive p35S promoter and fused in Nterm with YFP. a. Localization in the *Arabidopsis* root elongation zone. b. Localization in the *Arabidopsis* leaf trichomes. c. Localization in the tomato root epidermal cells and corresponding increase resolution of nuclei (images correpond to the projection over all the stack images). Red is propidium iodide and blue is DAPI, green or yellow is YFP.

IV. Study of the tomato Guanylate Binding Protein SlGBP10

IV.a. Localization of the tomato SlGBP10.

- *Subcellular localization of SlGBP10 in different plant organs*

Tomato SlGBP10 was cloned into a Gateway expression vector, under the 35S promotor and at the N-terminal part with the YFP fluorescent protein for subcellular localization analysis. We first tested the construction using transient transformation of tobacco leaves. In this tissue, tomato SlGBP10 localized at the nucleus (Supplementary Figure 25). At this point, it was very difficult to claim that the localization was at the nuclear envelope or in the inner or outer face of the nucleus. The localization signal was not diffuse or linear, but rather punctuated, according to little dots (Supplementary Figure 25). This localization signal was similar to localization of known proteins locate at the nuclear pores, such as the Nup proteins (Dubois *et al.*, 2012).

In order to confirm and precise this nuclear localization, we next transformed stably tomato Micro-Tom and *Arabidopsis thaliana*, using the same vector. Again, SlGBP10 in *Arabidopsis* roots was found at the nucleus and the labelling was also punctuated (Figure 44.a). However, SlGBP10 in *Arabidopsis* roots was more located inside the nucleus in comparison with the localization mainly at the periphery in tobacco leaves (Figure 44.b) (Supplementary Figure 27). We found the same localization pattern in *Arabidopsis* pavement cells (Supplementary Figure 26). In *Arabidopsis* leaf trichomes, some fluorescent dots seemed outside of the nucleus (Figure 44.b). However localization imaging required to be improved for a better resolution and DAPI labelling. In tomato roots, SlGBP10 was still present at the nucleus and also visualized as dots. In this specie, different sizes of dots were observed, with one to three large dots found inside the nucleus, while small dots were either found at the nucleus periphery or elsewhere inside the nucleus depending on the observed nucleus (Figure 44.c). Staining with DAPI and propidium iodide revealed that SlGBP10 never co-localized within the nucleolus. All these variations in the SlGBP10 localization suggested that its fine localization might be cell-type and/or specie dependent.

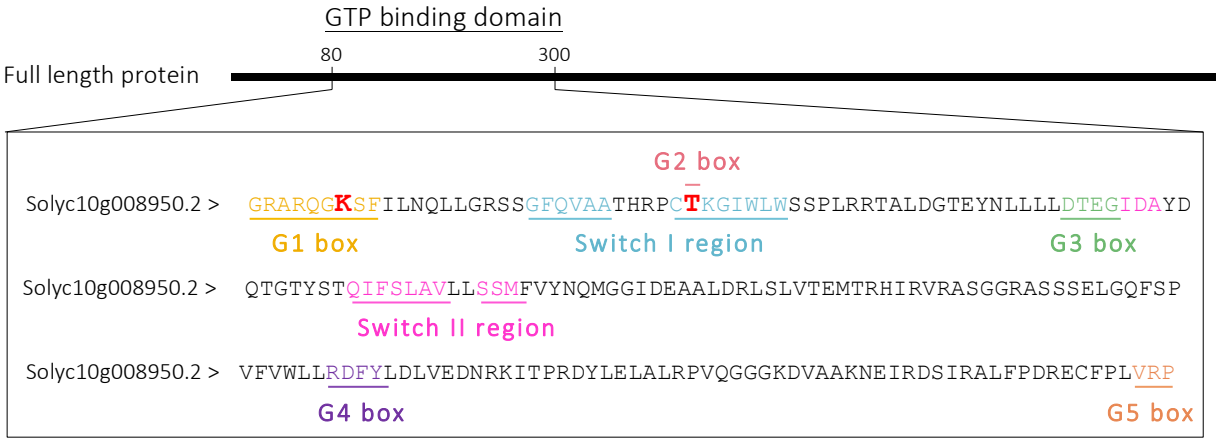

Figure 45: **GTP binding motifs mutated in SlGBP10.** GTP « dynamin-like » binding domains are highlighted in different colors. The larger uppercase red K inside the G1 box corresponds to the amino acid that is mutated in *Slgbp10_K85A.* The larger uppercase red T inside the G2 box corresponds to the amino acid that is mutated in *Slgbp10_T109A.*

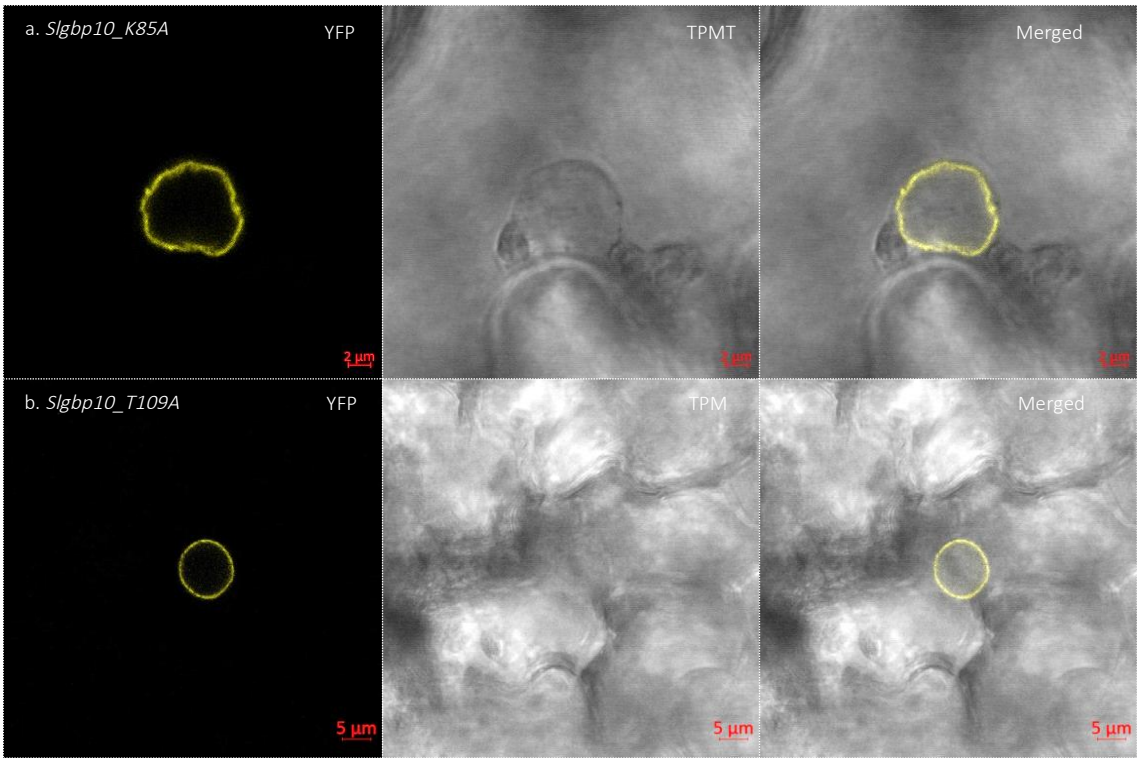

Figure 46: **Localization of the mutated *SlGBP10_K85A* and *SlGBP10_T109A* in tobacco leaves.** a. Localization of *Slgbp10_K85A.* b. Localization of *Slgbp10_T109A* Yellow is YFP.

Further co-localization with different markers of the nuclear envelope and other nuclear structures should improve our understanding of SlGBP10 localization. It is also well admitted that proteins expression under the p35S constitutive promotor could induce biases of localization with protein accumulation in other cell compartments than the real ones. Indeed, localization was shown to be in some cases due to the accumulation of the proteins expressed under constitutive promoters (Lisenbee *et al.*, 2003). Even if no localization is observed into the nucleolus, we should keep in mind the limits of this localization.

- *Is SlGBP10 localization associated to its GTPase function?*

As briefly previously mentioned, the guanylate binding protein is a large GTP binding protein, which has the particularity to hydrolyze GTP to both GDP and GMP. Previous results showed that this GBP is localized in the nucleus. We wondered whether its nuclear localization was related to its GTPase function. We intented to reproduce the work from King *et al*. (2004), who mutated the GTPase domains of the human dynamin-like GTPase MxB, causing a delocalization of the protein, using the tomato SlGBP10. Alike SlGBP10, the MxB protein is localized at the nucleus, more precisely at the cytoplasmic face of the nuclear pores. By changing one amino acid in the GTP binding domain or in the GTPase activity domain, these authors were able to produce dominant negative mutants that respectively cannot bind GTP, or can bind GTP but do not hydrolyze GTP. They showed that abolishing the GTP binding almost completely prevented MxB targeting to the nuclear envelope whereas the loss of GTPase activity blocked the protein at the nuclear envelope. They concluded that the localization of the MxB dynamin-like protein is closely related to its function (King *et al.*, 2004).

The focused study on the GTP binding motifs in the tomato protein allowed find the equivalent amino acids to be mutated. The key motifs for the GTP binding and GTPase activity, that are common to all the dynamin proteins are as follow (according to Praefcke & Mcmahon, 2004) : the G1 motif that coordinates the phosphate, the G2 motif involved in catalysis, the G3 motif that forms a hydrogen bond with the γ-phosphate of GTP and the G4 motif involved in base and ribose coordination (Figure 45). Switch 1 and Switch 2 regions are the loops that move (switch) on GTP hydrolysis. These switch regions have different conformations in the GTP-bound compared to the GDP-bound state (Praefcke and Mcmahon, 2004). For amino acid correspondence, we choose to substitute the lysine 85 which is present in the G1 box, with an alanine in order to create a dominant negative mutant that cannot bind GTP (Figure 45). This mutated protein will be called *Slgbp10_K85A*. We also chose to substitute the threonine in position 109 in the G2

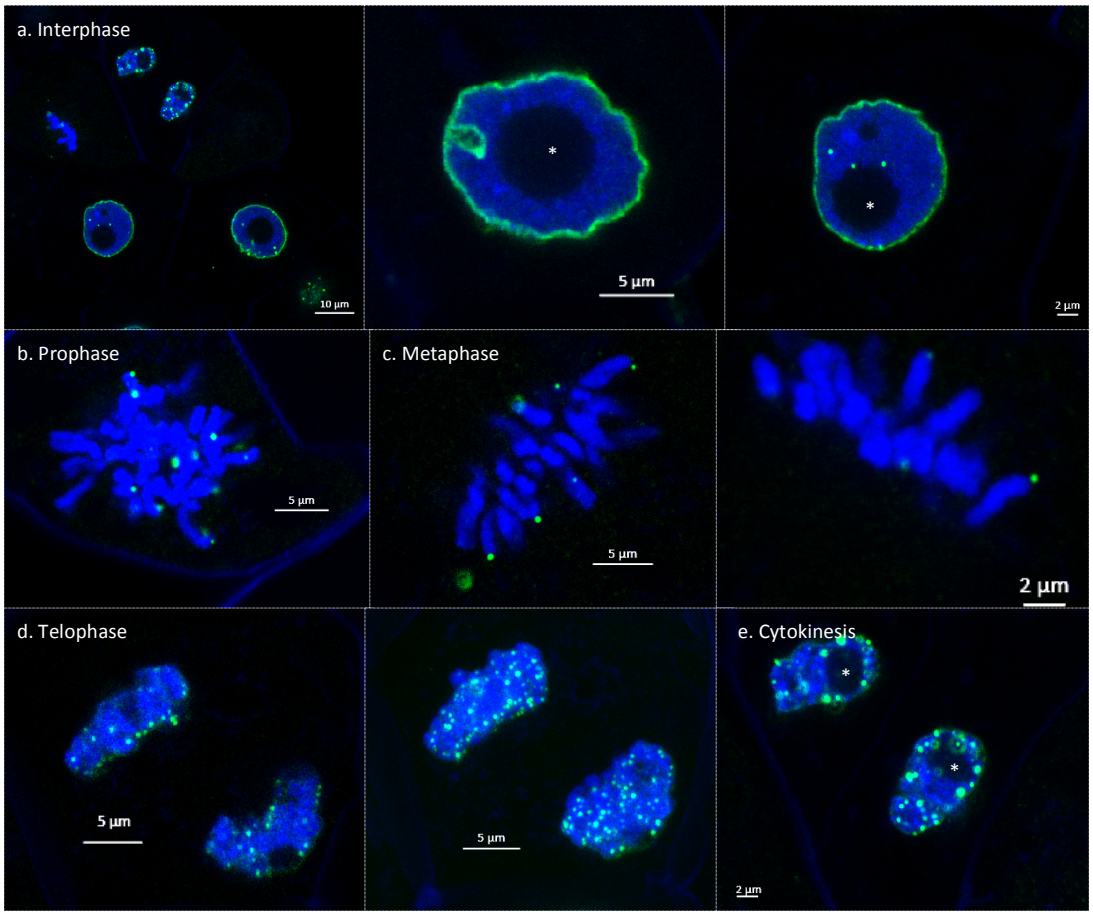

Figure 47: **Subcellular localization of SlGBP10 during BY2 cell division.** SlGBP10 expressed under a constitutive p35S promotor and fused in Nterm with YFP a. Localization in interphase nuclei. b. Localization in a prophase nucleus. c. Localization in metaphase nuclei. d. Localization in telophase nuclei. e. Localization during cytokinesis (image correponds to the projection over all the stack images). Blue is DAPI, green is YFP. * highlight the nucleolus.

motif, with an alanine, in order to create a dominant negative mutant enable to hydrolyze the GTP (Figure 45). This mutated protein will be called *Slgbp10_T109A*.

Transient expression in tobacco leaves confirms that the construction was efficient and revealed a slight difference in localization between SlGBP10 and the mutated proteins (Figure 46). Both mutated protein versions were still located in the nucleus, close to the nuclear envelope, but appeared more linear for *Slgbp10_K85A* and *Slgbp10_T109A* comparing to the punctuated signal obtained for SlGBP10 (Figure 46).

IV.b. Localization and function of SlGBP10 during cell division

As SlGBP10 seemed to be a nuclear protein, we wanted to see if the localization of the protein might change during cell division. For this purpose, we transformed BY-2 tobacco cells, as a model for cell division studies (Geelen and Inze, 2001) with the same constructions comprising SlGBP10 or the mutated versions, under the p35S promotor and fused in its N-terminal part to YFP. For this work, I realized all the transformations of the BY-2 cells and initiated the observations that were further optimized by the team to localize the proteins during the mitosis.

- *Subcellular localization of SlGBP10 during cell division*

In BY-2 cells, as in other organs previously studied, SlGBP10 was localized mainly at the nuclear envelope in interphase nuclei. The signal of localization looked linear at the periphery of the nucleus (Figure 47.a). However, this localization signal was more or less intense depending on the observed nucleus, until very few labeling was distinguished just before the entrance into the preprophase. In addition, some interphase nuclei presented also a localization inside or at the periphery of the nucleus, co-localizing with DAPI labeling and revealed as dots. In each case, localization was excluded from the nucleolus region (Figure 47). Interestingly, localization of SlGBP10 changed depending on the cell cycle progression. During early preprophase, when DNA begins to condensate, the linear signal of SlGBP10 disappeared and only a few little dots were visible close to the nucleus periphery (Figure 47.b). From prophase, when the envelope is completely degraded and DNA condensate to metaphase, SlGBP10 co-localized with DNA as little dots. Most of dots seemed to be located to the extremity of the condensed chromosomes (Figure

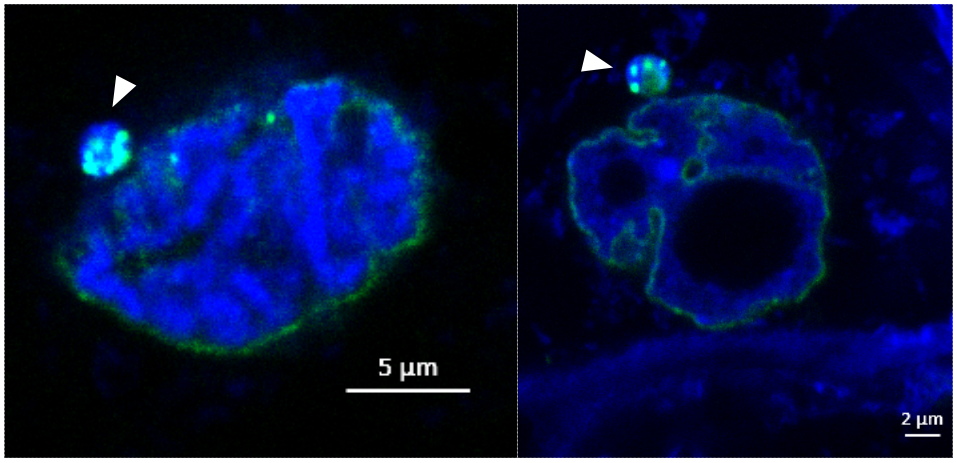

Figure 48: **Specific localization of SlGBP10 outside BY2 cell nucleus.** SlGBP10 expressed under a constitutive p35S promotor and fused in Nterm with YFP. Blue is DAPI, green is YFP. Arrow-heads highlight the micro nulceus-like structure.

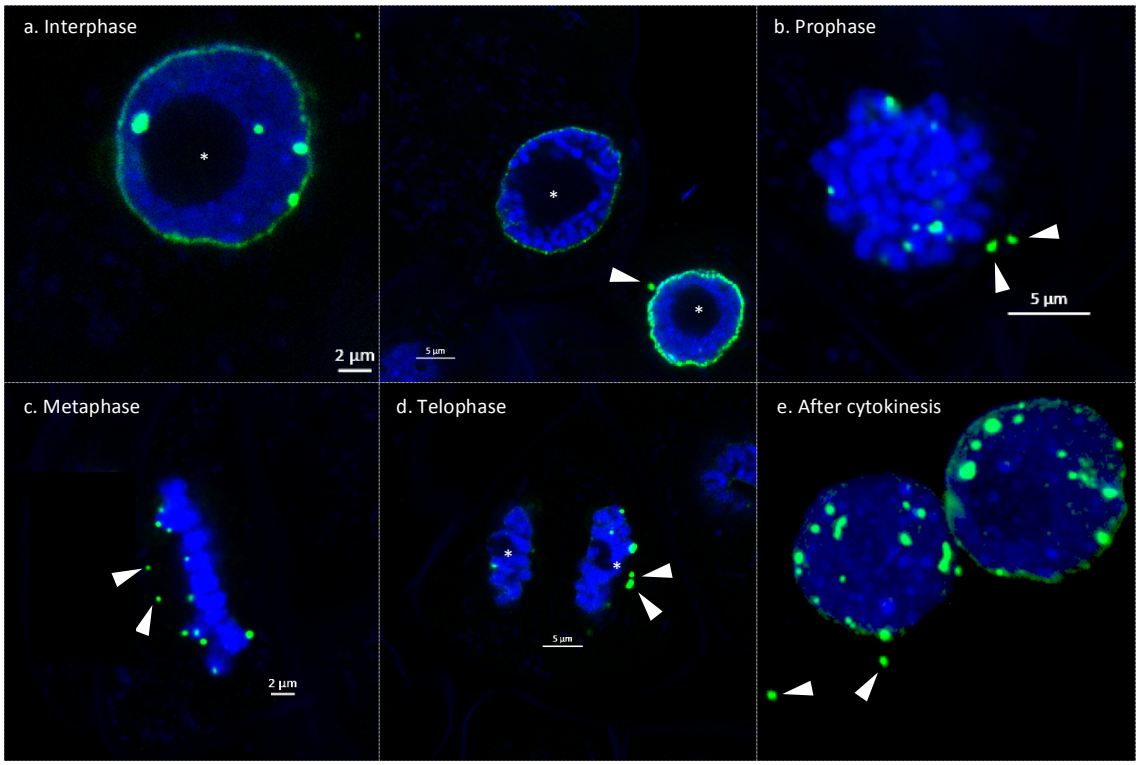

Figure 49: **Subcellular localization of *Slgbp10_A85* during BY2 cell division.** *Slgbp10_A85* expressed under a constitutive p35S promotor and fused in Nterm with YFP. a. Localization in interphase nuclei. b. Localization in a prophase nucleus. c. Localization in a metaphase nucleus. d. Localization in a telophase nucleus. e. Localization after cytokinesis. Blue is DAPI, green is YFP. * highlight the nucleolus. Arrow-heads indicate the fluorescent dots outside the nucleus.

47.c). The number of dots was variable according to the observed nucleus. During cytokinesis, when the new nuclear envelopes are formed around the dividing nuclei, fluorescent dots corresponding to SlGBP10 localization increased including the appearance of larger dots (Figure 47.e). A thin linear signal encircling the nucleus was again subtly visible at this stage. To summarize, the SlGBP10 localization seemed very specific during mitosis, co-localizing with DNA and exhibiting an increase of accumulation over the progress into mitosis steps. As protein accumulation increased a lot at the end of mitosis, we could hypothesize that SlGBP10 might have a role in decondensation processes of the chromatin.

In a few observations, we were able to detect another interesting localization for the SlGBP10. The fluorescent dots generally found inside or at the periphery of the nucleus were grouped outside the nucleus in a likely independent structure (Figure 48). This structure labeled with DAPI, is supposed to be composed of DNA. Interestingly, while the majority of the intense fluorescent dots were found in this structure adjacent to the nucleus, a remaining slight linear signal of SlGBP10 was still found at the periphery of the nucleus.

Interestingly, when overexpressed in tobacco BY-2 cells, SlGBP10 seemed to disrupt cell division (Supplementary Figure 28). Transformed cells, with the vector containing SlGBP10, did not show the same aspect as the WT culture. The transformed 7 day-old culture was still transparent and aggregates of cells were clearly eye-visible. This culture needed twice as long time to reach the WT cellular aspect (data not shown). Furthermore, while WT BY-2 cells were well separated and formed small chains, BY-2 cells overexpressing SlGBP10 did not form chains and remained together as large aggregates (Supplementary Figure 28). Hence, the overexpression of SlGBP10 seemed to delay cell division and to impair normal differentiation of the cells.

- *Subcellular localization of mutated SlGBP10 during cell division*

BY-2 cells were also transformed with the mutated SlGBP10 versions in order to see if the GTPase activity is required for correct protein localization. Differences in the *Slgbp10_K85A* localization could be observed during each step of mitosis, with dot signals of localization found outside of the nucleus (Figure 49). In addition, *Slgbp10_K85A* dots seemed larger than the ones observed for the functional protein. This observation suggested that the mutation in the GTPase binding domain might alter the proper localization of SlGBP10. In contrast to the SlGBP10 culture, the *Slgbp10_K85A* culture seemed to grow normally, the

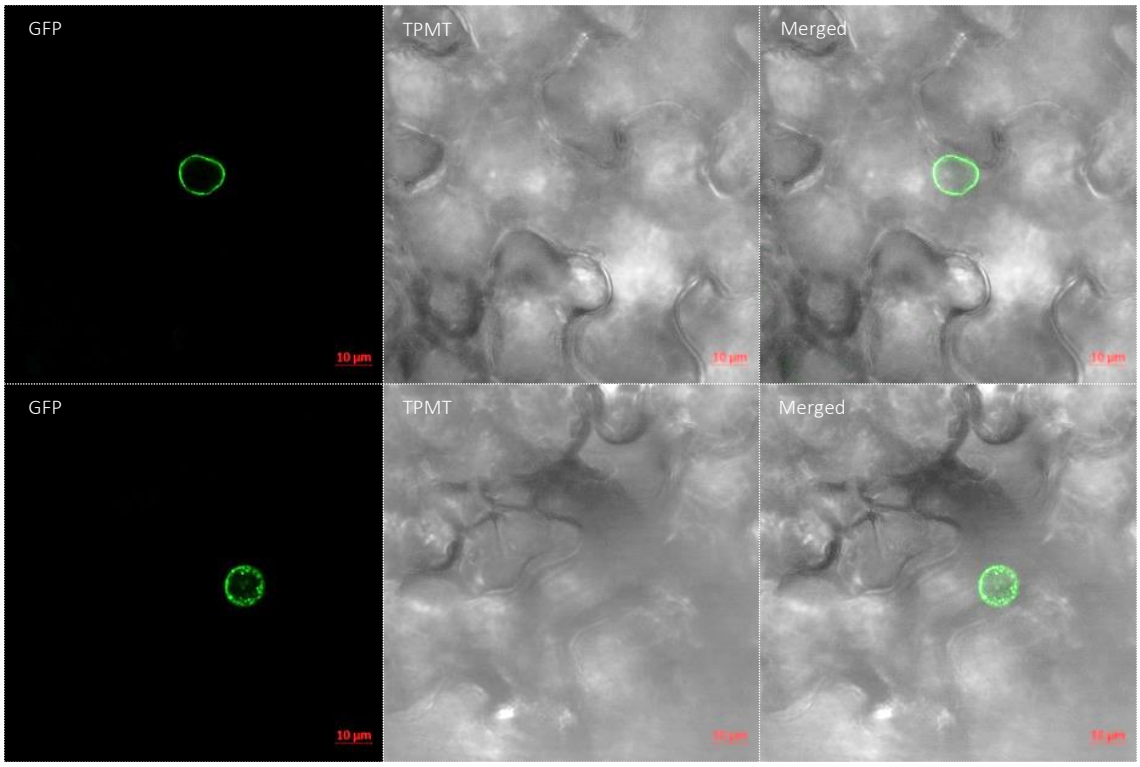

Figure 50: **Subcellular localization of AtGBP5 in tobacco leaves.** AtGBP5 expressed under the native promoter and fused in Cterm with GFP. Green is GFP.

BY-2 cells did not form aggregates. However, the shape and size of the cells seemed to be altered (Supplementary Figure 29). Further cellular characterizations are required to understand better the effects of the *Slgbp10_K85A* mutation on tobacco cells, and especially during cell division. The characterization of the BY-2 culture overexpressing the *Slgbp10_T109A* is still in progress.

IV.c. Subcellular localization of Arabidopsis AtGBP5 homolog

In order to go deeper into the functional characterization of the GBP in plants, we also looked for the subcellular localization of the *Arabidopsis thaliana* closest AtGBP5 homolog. The protein was cloned in this case under its native promoter called pAT5, and fused in its C-terminal part to GFP. The objective of this study was to compare localization of both homologs that were under different promoters in view to get rid of the possible mis-localization caused by the use of the constitutive p35S promoter. Of course in parallel to this study, the conservation of function between both homologs should also be investigated through *Arabidopsis* mutant complementation.

In transient expression on tobacco leaves, the *Arabidopsis* AtGBP5 seemed to be similarly localized at the nucleus alike the tomato *SlGBP10* gene. The protein was also found close to the nuclear envelope and formed those little dots (Figure 50). In order to have a better subcellular localization of the protein, we stably transformed *Arabidopsis thaliana* Columbia accession and BY-2 cells, with the same construction. The upcoming results looked promising, as the localization of both SlGBP10 and AtGBP5 looked similar in tobacco leaves.

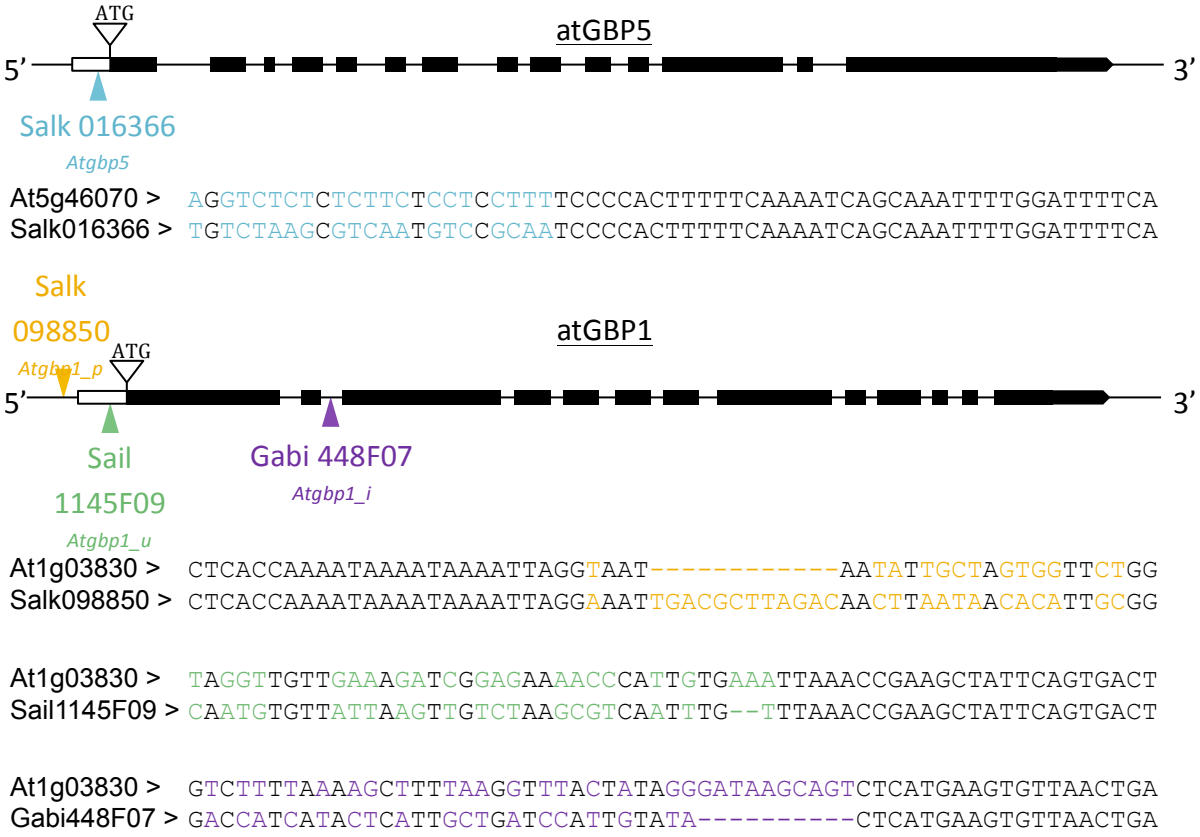

Figure: **T-DNA insertions in the *Arabidopsis* T-DNA mutants.** Black boxes represent the exons. White boxes represent the 5'UTR regions. Arrow-heads represent the insertion sites of the T-DNAs.

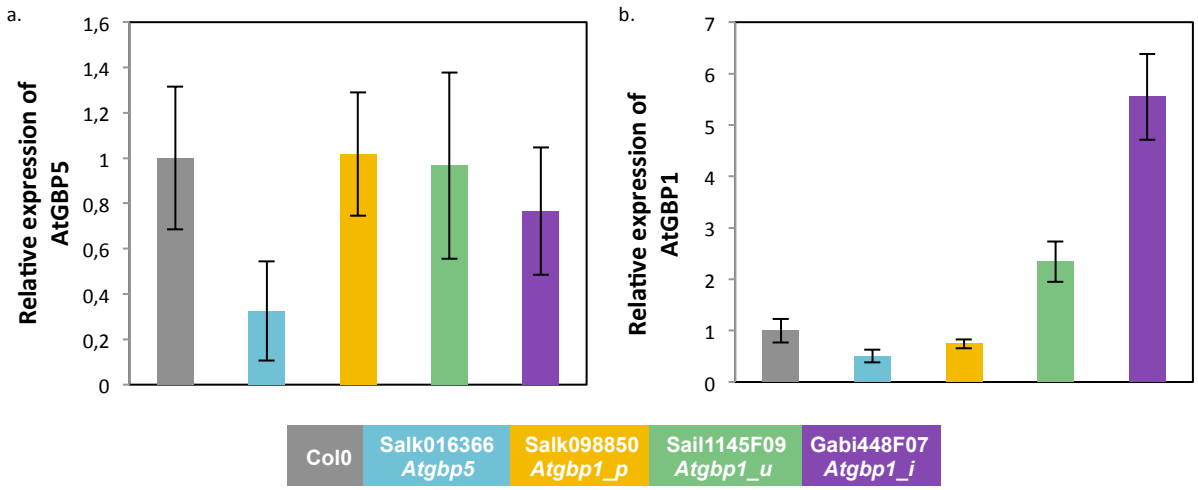

Figure: **Relative expression level of AtGBP5 and AtGBP1 in the T-DNA mutants**. a. Relative expression level of AtGBP5. b. Relative expression level of AtGBP1. RNAs were extracted from 7 days-old plantlets. (Error bar: standard deviation, n=3)

V. Looking for tissue disorganization in *Arabidopsis* T-DNA mutants

V.a. Selection and validation of Arabidopsis T-DNA mutants

In order to understand the function of GBPs in *Arabidopsis thaliana*, we first chose to work with available T-DNA mutants. We looked for interesting T-DNA mutants in the locus of both *AtGBP5* and *AtGBP1*. Surprisingly, a few T-DNA mutants were available for both genes and no T-DNAs were inserted in the coding region. Indeed, all the available T-DNA mutants were annotated with a T-DNA insertion in regulatory regions (promotor, 5'UTR and 3'UTR regions, introns). We finally ordered five T-DNA mutants: two mutants on *AtGBP5* called Salk016366 (*Atgbp5*) and Salk078670 and three mutants on *AtGBP1* called Salk098850 (*Atgbp1_p)*, Sail1145F09 (*Atgbp1_u*) and Gabi448F07 (*Atgbp1_i*) (Figure 51).

I first verified for the T-DNA insertion localization and the effects of this insertion in the gene expression level (Figure 52). For Salk078670, no insertion could be identified in the received seed stock. Salk016366 (*Atgbp5)* T-DNA was inserted in the 5'UTR region of *AtGBP5* (Figure 51) and caused a three-fold time reduction of the corresponding gene expression level (Figure 52). Interestingly, Salk016366 (*Atgbp5)* mutant was also characterized by a two-fold time reduction of *AtGBP1* expression level (Figure 52) suggesting possible control of *AtGBP1* expression through AtGBP5. Salk098850 T-DNA was inserted in the promotor of *AtGBP1* (Figure 51), causing a two-fold time reduction of the corresponding gene expression level (Figure 52). Sail1145F09 and Gabi448F07 T-DNA mutants were characterized by a T-DNA insertion in the 5'UTR and in the second intron of *AtGBP1*, respectively (Figure 51). Both T-DNA insertions caused an increase in the relative expression of *AtGBP1* (Figure 52). The 5'UTR and the second intron of *AtGBP1* could include regulatory motives involved in the negative control of its expression that could explain an increase in expression, when these sequence regions were disrupted. None of the T-DNA mutants for *AtGBP1* exhibited significant change in *AtGBP5* expression level (Figure 52). At that point of the study, all T-DNA mutants seemed to represent an interesting source of plant material in order to study the function of *Arabidopsis* GBPs.

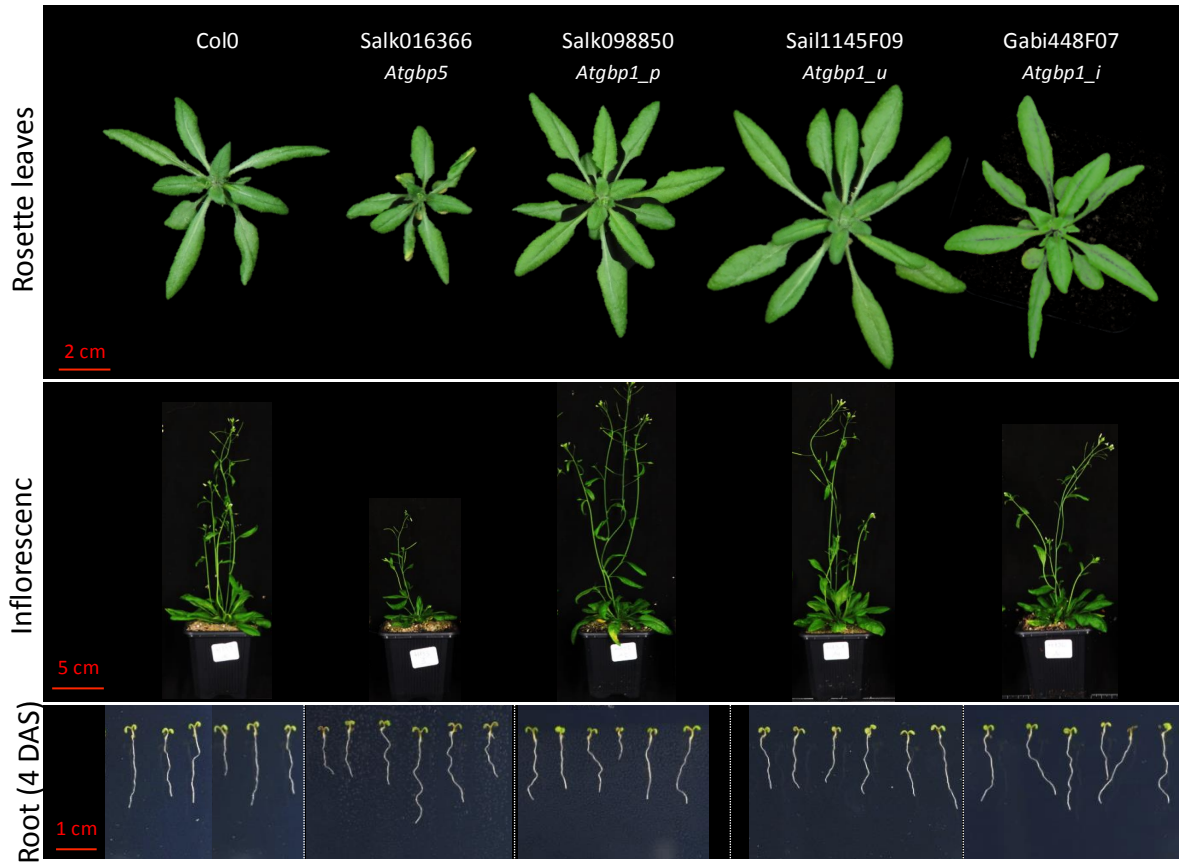

Figure 53: **Rosette, inflorescence and root phenotypic characterization of the *Arabidopsis* T-DNA mutants.**

V.b. Phenotyping of the Arabidopsis T-DNA mutants

I first looked for alterations in vegetative development between Col-0 and the T-DNA mutants (Figure 53). Salk016366 (*Atgbp5)* showed almost a significant two-fold time reduction in the maximum diameter of the rosette, and also a reduction in inflorescence length, even not significant due to the variability of the Col-0 (Supplementary Figure 30). Surprisingly, all the *Atgbp1* mutants displayed around three-fold increase in rosette maximum diameter, whatever the change in *AtGBP1* gene expression (Figure 52). In this context, it is supposed that the increase in rosette diameter was not related to *AtGBP1* expression level. No difference in the inflorescence growth was observed compared to Col-0 for the three *Atgbp1* mutants. Root development did not seem to be altered in all the studies T-DNA mutants. Indeed, 4 day-old plantlets showed comparable roots to Col-0 (Figure 53). This observation was confirmed in 10 day-old plantlets. Our next investigations focused on Salk016366 (*Atgbp5)* T-DNA mutant, which presented most of the phenotypic differences.

As Salk016366 (*Atgbp5)* was characterized by growth defects, I checked for tissue disorganization or aberrant cell division patterns in different organs in this mutant, hoping to identify comparable cellular alterations as observed in the pericarp of the *Slgbp10* mutants. I first studied the cellular organization in the root tip and in the embryo, in which cell division patterning is highly organized and well-described in the *Arabidopsis thaliana* model (Supplementary Figure 31). At different stage of root development, no strong cellular alterations were noticed: cell size and shape together with the cell layer number were similar in Col-0 and the mutant roots (Supplementary Figure 31.a). Cell divisions during embryo development were also not impacted by the reduction of At*GBP5* expression level in the *Atgbp5* mutant (Supplementary Figure 31.b). As rosette leaves size was reduced in the mutant, we next looked for cellular disorganization in the leaf pavement cells. Again no strong alterations in pavement cell size and shape were noted in *Atgbp5* T-DNA mutant (Supplementary Figure 31.c). No evident growth phenotype was identified, but we should keep in mind that the T-DNA mutant was not a KO mutant but a known-down mutant. Indeed, the reduction in gene expression could be insufficient to provoke cellular alterations as we expected.

However, when looking at pavement cells, I noticed a strange trichome shape in *Atgbp5* mutant (Supplementary Figure 31.e). Indeed, all the leaf trichomes in the mutant presented an aberrant size and shape (Supplementary Figure 31.f). Under scanning electron microscopy, we could easily notice that all

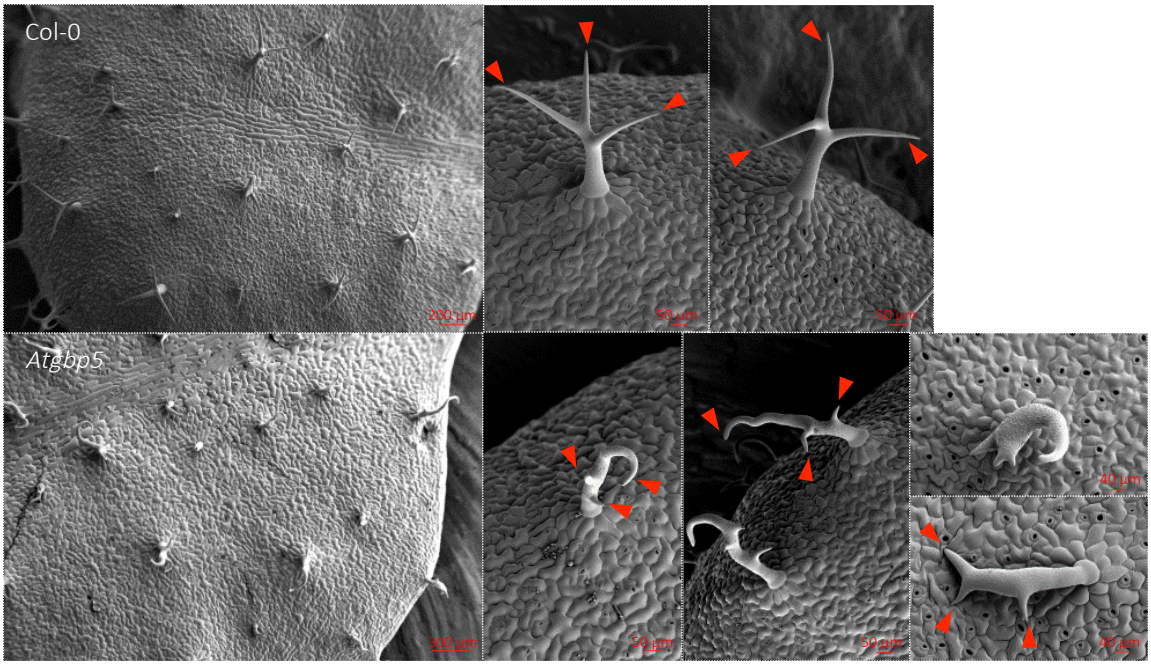

Figure 54: **Difference in trichome shape between Col-0 and *Atgbp5* T-DNA mutant.** Red arrow-heads indicate trichome branches.

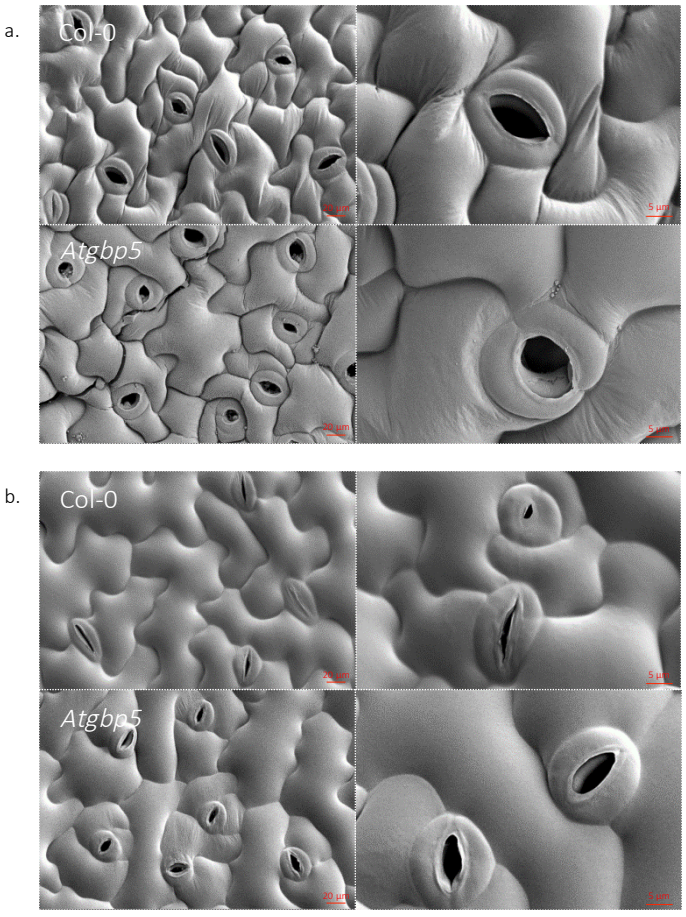

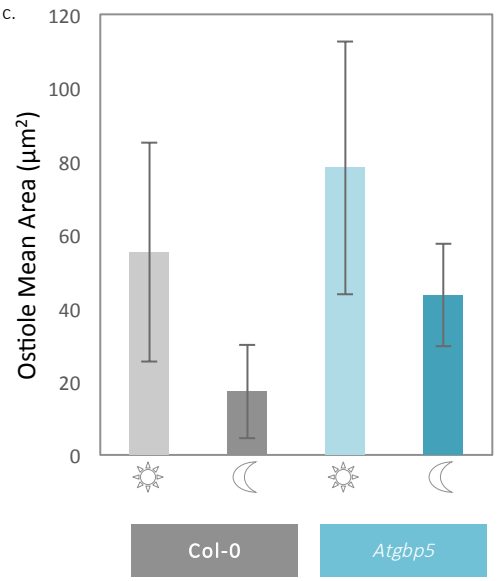

Figure 55: **Difference in stomatal movement in different light-dark treatment between Col-0 and *Atgbp5 T-DNA* mutant.** a. Stomatal opening under light. b. Stomatal closure after 12h in dark. c. Ostiole mean area under light (represented with a sun), or in dark (represented with a crescent moon). (Error bar: standard deviation, n=3)

trichomes were altered with different morphology (Figure 54). The abnormal trichomes maintained the same number of branches but were completely twisted. This twisted trichome phenotype was actually very well described in the literature called "distorted" trichomes (El-Assal *et al.*, 2004; Mathur *et al.*, 2003; Saedler *et al.*, 2004; Schwab *et al.*, 2003), and in the following section, I will describe a little bit deeper this phenotype.

V.c. Atgbp5 T-DNA mutant presents a "distorted" phenotype

In *Arabidopsis thaliana*, eight mutants (*alien, crooked, distorted1, distorted2, gnarled, klunker, spirrig,* and *wurm*) are characterized by a common randomly mis-hapened phenotype of leaf epidermal trichomes, that are called "distorted" (Hülskamp *et al.*, 1994). "*Distorted*" genes encode subunits of two different complexes that directly regulate the actin cytoskeleton: the actin-related protein (ARP)2/3 complex that nucleates actin filaments and the WAVE complex that regulates the activity of ARP2/3 (Zimmermann *et al.*, 2004). Distorted mutants present also others correlated alterations, such as defects in etiolated hypocotyl growth in the dark (Zimmermann *et al.*, 2004; Mathur *et al.*, 2003) and defects in stomatal closure in the dark (Isner *et al.*, 2017).

Therefore, we were wondering whether the *Atgbp5* mutant presented also these two phenotypes. In the dark, the elongated hypocotyl from Col-0 accession and hypocotyl cells were cohesive with the neighboring cells and regular (Supplementary Figure 32). In *Atgbp5* mutants, hypocotyl epidermal cells were twisted and not always cohesive with curling ends creating breaks in this cell layer (Supplementary Figure 32). Furthermore, *Atgbp5* stomata closure showed reduced sensitivity to darkness (Figure 55). After 12 hours in the dark, stomata of Col-0 were almost completely closed, with a three-fold reduction of the ostiole area (Figure 55.c). However, stomata of *Atgbp5* T-DNA mutant remained opened, with only a 1.5 fold reduction of the ostiole area (Figure 55.b). Alterations on hypocotyl growth and stomatal closure in the dark were not as strong as in *wrm, dis1,* or *opal5* mutants (Zimmermann *et al.*, 2004; Mathur *et al.*, 2003; Isner *et al.*, 2017). This could also be due to the fact that the *Atgbp5* mutant was not a KO mutant. Altogether, phenotyping of *Atgbp5* confirmed that this mutant displayed the "distorted" phenotypes.

V.d. Is Atgp5 locus responsible for the distorted phenotype?

As T-DNA mutants could present other insertional T-DNAs, a validation of the implication of the GBP5 locus in the distorted phenotype was required. For this purpose, different populations in segregation were produced to analyze the association between the mutation at the *AtGBP5* locus and the distorted phenotype. Indeed, if the *AtGBP5* is responsible for the phenotype, we expected that all individuals homozygous for the mutation will present the distorted phenotype while WT and heterozygous individuals were expected to have normal trichomes (in the simplest case of a recessive mutation).

The following populations were produced:

1) Crossing the Salk016366 (*Atgbp5*) with Salk098850 (*Atgbp1_p*) T-DNA mutants,
2) Crossing the Salk016366 (*Atgbp5*) with Sail1145F09 (*Atgbp1_*) T-DNA mutants,

in order to obtain a *Atgbp1/Atgbp5* double mutant for further phenotypic characterization.

3) Crossing the Salk016366 (*Atgbp5*) with a microtubule reporter line (Microtubule-Binding Domain (MBD) was fused to the fluorescent protein RFP), in order to visualize the microtubule cytoskeleton in the *Atgbp5* background.
4) Crossing the Salk016366 (*Atgbp5*) with an actin reporter line (Actin-Binding Domain 2 (ABD2) was fused to the fluorescent protein RFP), in order to visualize the actin cytoskeleton in the *Atgbp5* background .

Results of the segregation are presented in Table 5.a.

First from the initial seed stock, 100% of the individuals presenting the “distorted” phenotype were homozygous mutant for the T-DNA insertion on *AtGBP5*. Similarly, 100% of the individuals presenting the “distorted” phenotype were homozygous mutant for the T-DNA in the different F2 segregations. However not all the *Atgbp5* homozygous individuals harbored the “distorted” phenotype (Table 5.a). This result likely suggested that mutation at the *AtGBP5* locus was not sufficient to induce the distorted phenotype but necessary, suggesting that a second mutated locus might be implicated in the “distorted” phenotype, in combination with the mutated AtGBP5. Indeed, as all the distorted phenotypes were homozygous *Atgbp5*, the mutation at this locus was probably recessive. In theory, 1/16 (6%) or 3/16 (18.75%) of individuals were expected to exhibit the distorted phenotype in the case of a second recessive or

a.

F2 population	Total individuals	Homozygous *Atgbp5*	"distorted" phenotype	% on total Homozygous *Atgbp5*
Salk016366 x Salk098850	92	34 (36%)	10 (11%)	29,41
Salk016366 x Sail1145F09	92	31 (34%)	9 (10%)	29,03
Salk016366 x RFP-MBD	55	17 (31%)	4 (7%)	23,53
Salk016366 x ABD2-GFP	52	12 (23%)	6 (12%)	50,00

b.

Population	Parental F2 phenotype *Atgbp1/Atgbp5*	Total F3 individuals	"distorted" phenotype
a	«Distorted » phenotype	50	50 (100%)
b	«Distorted » phenotype	50	50 (100%)
c	WT phenotype	48	9 (19%)
d	WT phenotype	48	9 (19%)
e	WT phenotype	49	11 (23%)
f	WT phenotype	50	0 (0%)

Table 5: **Results of the association studies and crossings**. a. Association studies of the distorted phenotype on 4 independent populations. b. Association study of the distorted phenotype in F3 generation.

dominant mutation, respectively. As the distorted phenotype ranged between 7% to 12% over the total population, and 23% to 50% over the homozygous *Atgbp5* mutants, the second mutation was probably recessive. However, as the populations remained small, I analyzed six F3 segregations from F2 double *Atgbp1/Atgbp5* mutants, presenting or not the "distorted" phenotype, in order to confirm the recessivity of the second mutation. All the F3 individuals were by consequences homozygous for the mutated allele of AtGBP5. Segregations are presented in Table 5.b.

- In population a and b, 100% of the F3 displayed a "distorted" phenotype. The initial F2 individuals were probably homozygous for the second causal locus and all F3 individuals should be homozygous too.
- In population c, d and e, from 18 to 23% of the F3 individuals had a "distorted" phenotype. The initial F2 individuals were probably heterozygous for the second causal locus that segregated in the F3 affecting approximately ¼ of individuals as observed for recessive mutation.
- In population f, none of the F3 individuals showed a "distorted" phenotype. The initial F2 individual was probably WT homozygous for the second locus.

To summarize, in the initial seed stock, all "distorted" individuals were mutated for both *AtGBP5* and the unknown locus. The distorted phenotype appeared to be provoked by the combination of two homozygous mutations, including one affecting the *AtGBP5* locus. The identification of the second mutated locus might be an interesting candidate in order to understand the putative role of AtGBP5 in actin remodeling during trichome development. However, because the association studies are dependent on the population size, in order to definitively confirm the involvement of AtGBP5 in the "distorted" phenotype, complementation assay of the *Atgbp5* mutant were initiated. The mutant was transformed with the tomato *SlGBP10* gene and *Arabidopsis AtGBP5* using the previous construction. Plants transformed with the tomato *SlGBP10* gene were not complemented as trichomes remained distorted (data not showed). In this context, we can suppose that the SlGBP10 protein had not the same function as its *Arabidopsis* homolog for trichome development. Only the final complementation with the *Arabidopsis* gene which is under progress will definitely validate the role of the AtGBP5 in this phenotype.

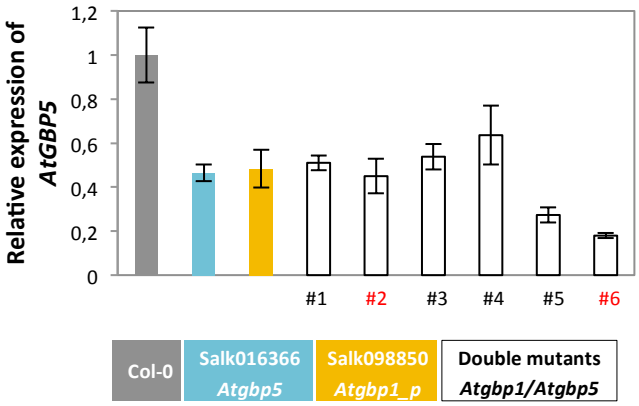

Figure 56: **Relative expression level of *AtGBP5* in the *Atgbp5/Atgbp1_p* double mutants.** RNAs were extracted from young rosette leaves. Double mutants displaying a "distorted" phenotype are highlighted in red. (Error bar: standard deviation, n=3)

V.e. Growth alterations are not accentuated in the double mutant Atgbp1/Atgbp5

By crossing the Salk016366 (*Atgbp5)* with Salk098850 (*Atgbp1_p)* T-DNA mutants, I generated a double mutant for *Atgbp1/Atgbp5* with the aim to see if simultaneous mutation in the homologous genes could accentuate growth phenotypic alterations.

Among the six homozygous double mutants generated in the F2 population, all of them presented a reduction in expression level of *AtGBP5* (Figure 56). As the expression of *AtGBP1* in Salk098850 (*Atgbp1_p)* parental mutant was no drastically reduced, the expression of *AtGBP1* in the double mutants was not tested. Four F2 double mutants had an expression similar to that of the parental mutant control (Figure 56). Two double mutants presented a distorted phenotype, however no relation between *AtGBP5* expression level and the "distorted" phenotype (individual number 2 and 6) was obvious. In this context, difference in *AtGBP5* expression in mutant backgrounds was not essential for the distorted phenotype. None of the six double mutants either with or without the distorted phenotype was notably impaired in their development (data not shown).

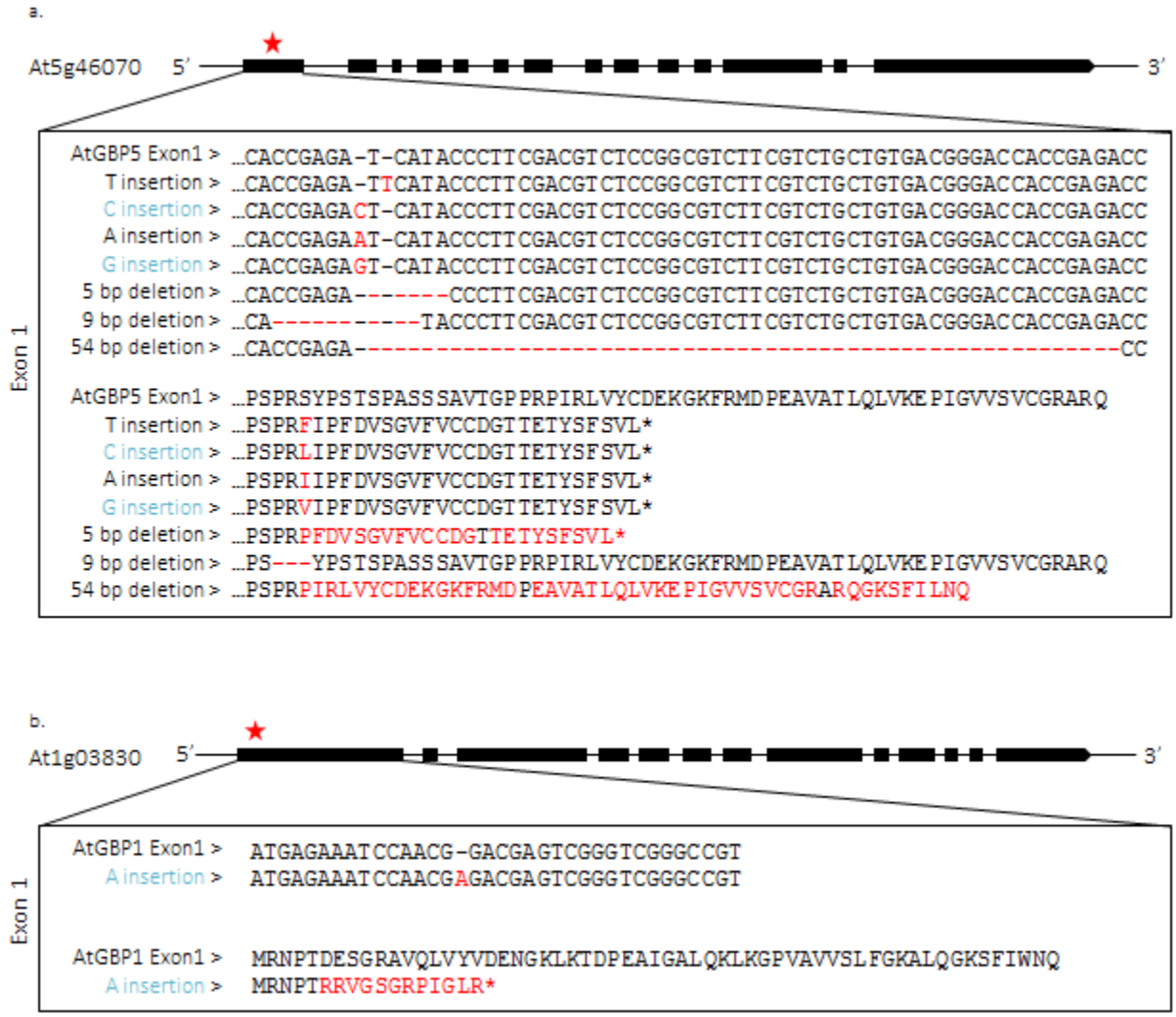

Figure 57: **AtGBP5 and AtGBP1 genomic sequences and predicted amino acid sequence for the *Arabidopsis* CRISPR mutants**. a. Genomic sequence and amino acid sequence of the CRISPR At*gbp5* mutant. b. Genomic sequence and amino acid sequence of the CRISPR At*gbp1* mutant. Black boxes represent the exon. The red star represents the location of the mutation. * mean a stop codons.

VI. Looking for tissue disorganization in *Arabidopsis* KO mutants

As the selected T-DNA mutants were not KO mutants, I generated KO mutants for both AtGBP5 and AtGBP1, using CRISPR Cas9 editing technology. Two generations after the transformation with vectors containing the Cas9 enzyme, I obtained an allelic series of mutations in both genes (Figure 57). For *AtGBP5*, I could generate seven different mutated alleles in exon 1 (one base insertion or several base deletions) (Figure 57.a). Mutations of one base insertion or the 5 base deletion induced a premature stop codon early in Exon1 (Figure 57.a). Mutations corresponding to 9 base and 54 base deletions did not induce a premature codon stop in exon 1, meaning that the protein even modified in its sequence of exon1 could be produced (Figure 57.a). For *AtGBP1*, I could generate only one mutated allele on exon1 with one A insertion. At the protein level, this insertion induced a premature stop codon in exon 1 (Figure 57.b). For further characterization, I only used CRISPR mutants that presented mutated alleles at the homozygous state in the T2 generation:

- One mutant characterized by an insertion of a C in Exon 1 of *AtGBP5*, called *Atgbp5_cr1* mutant,
- One mutant characterized by an insertion of a G in Exon 1 of *AtGBP5*, called *Atgbp5_cr2* mutant,
- One mutant characterized by an insertion of a A in Exon 1 of *AtGBP1*, called *Atgbp1_cr1* mutant.

As expected, the CRISPR mutants of *Atgbp5* both displayed two or three-fold reduction in *AtGBP5* expression level (Supplementary Figure 33), maintaining a residual expression as observed for the CRISPR tomato mutants (data not shown). This residual expression is probably the turnover of mRNA before degradation (Keeling *et al.*, 2004). Surprisingly, in the *Atgbp5* mutants an increase in *AtGBP1* expression level was noted, while in the Salk016366 (*Atgbp5*) T-DNA mutant, it was slightly repressed (Supplementary Figure 33). Possible off-target effects were checked on the homologous gene in the different CRISPR mutants and could not explain this increase of expression. So, the feedback of AtGBP5 on *AtGBP1* expression was not so clear and should be due to the different genetic backgrounds between T-DNA and CRISPR mutants. For the CRISPR *Atgbp1* mutant, the level of expression of *AtGBP1* was increased, as it was

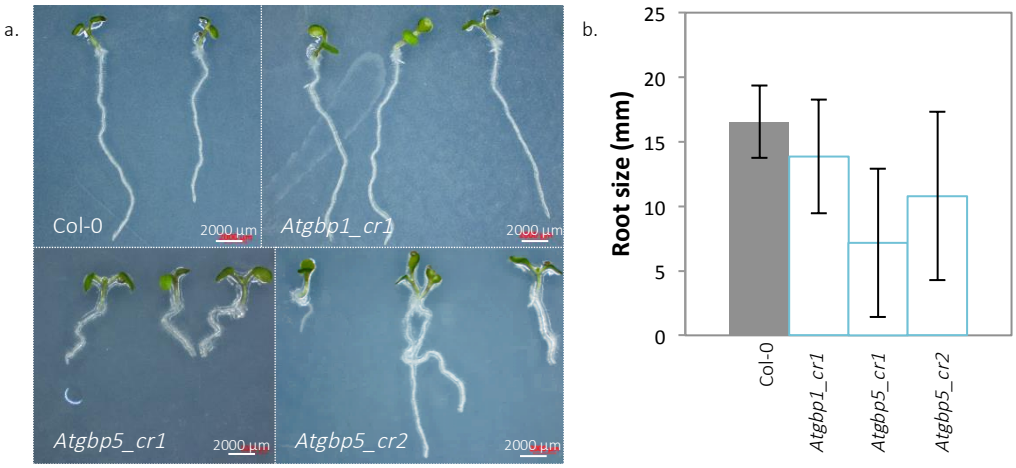

Figure 58: **Root development of 5 days-old seedlings** a. Phenotype of the roots in the CRISPR mutants compared to Col. b. Root size of the CRISPR mutants compared to Col.

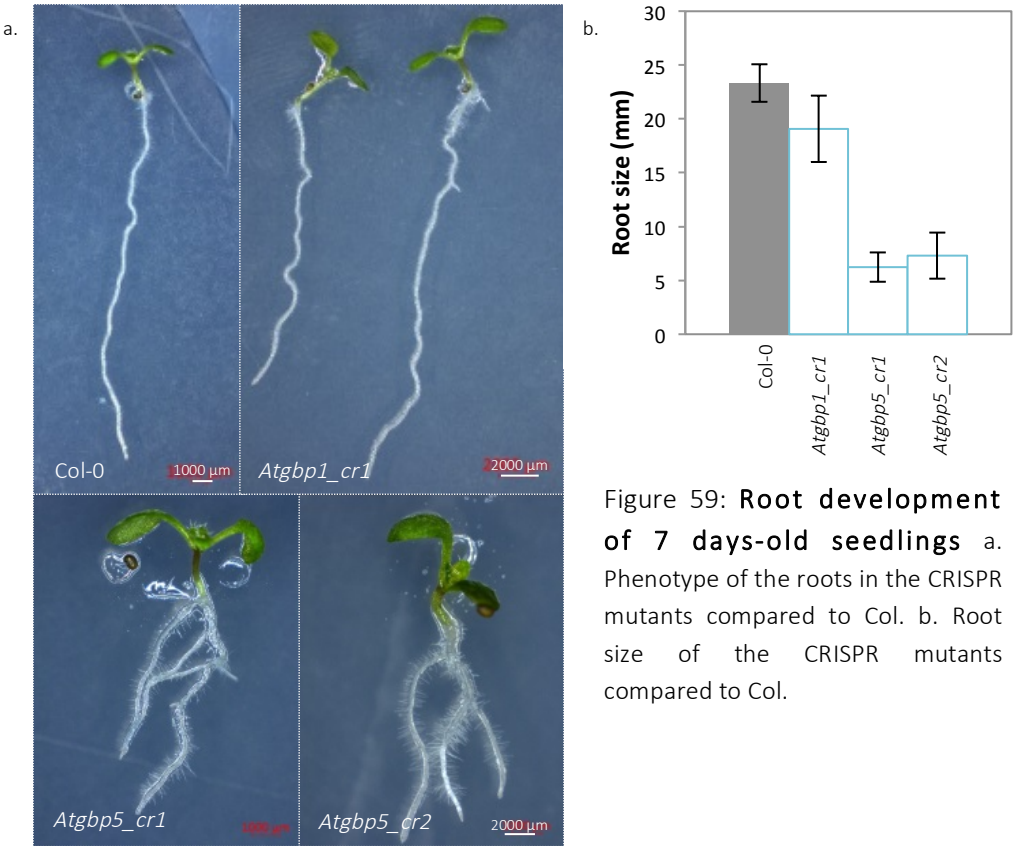

Figure 59: **Root development of 7 days-old seedlings** a. Phenotype of the roots in the CRISPR mutants compared to Col. b. Root size of the CRISPR mutants compared to Col.

already the case of two of the *Atgbp1* T-DNA mutants. It was also difficult to explain this gene expression increase in CRISPR KO backgrounds. Indeed, we supposed that the increase of expression in the T-DNA mutants was probably due to alteration of negative regulatory motives, present in the 5'UTR region and first intron. In the *Atgbp1* mutant, no significant difference of *AtGBP5* expression was noted as previously observed for T-DNA mutants.

The vegetative development of the CRISPR mutants was similar to Col-0, with no striking modification in rosette and leaf sizes (Supplementary Figure 34). All the CRISPR lines presented normal trichome size and shape (Supplementary Figure 34). A remarkable phenotypic alteration was observed for root development. Indeed, from 5 DAS, *Atgbp5_cr1* and *Atgbp5_cr2* mutants showed a reduction in primary root size (Figure 58), with an increase in root hair outgrowth. At 7 DAS, the difference in primary root size was stronger, with a three-fold time reduction between *Atgbp5* mutants and Col-0 (Figure 59). In addition, both *AtGBP5* mutants developed important adventive roots, which did not develop in the Col-0 at the same stage (Figure 59.a). Interestingly, this altered root phenotype was not observed in the Salk016366 (*Atgb5*) T-DNA mutant, suggesting that the reduction in *AtGBP5* expression level was not sufficient to induce this phenotype. No alteration was observed for *Atgbp1_cr1* mutant at 5DAS, while a slight reduction in the primary root length was observed at 7 DAS, but the root pattern was similar to Col-0, with the initiation of lateral roots (Figure 59.a). Considering the unexpected increase in *AtGBP1* expression level in this mutant, which was similar to Sail1145F09 (*Atgbp1_u*) and Gabi448F07 (*Atgbp1_i*) T-DNA mutants, the absence of phenotypic alterations seemed logical and in this context, it was difficult to evaluate for gene function redundancy.

Part II

Functional characterization of the Guanylate Binding Protein: case of P3D3 mutant.

Discussion

I. Is the Guanylate Binding Protein a negative regulator of cell division, involved in the maintenance of endoreduplication in tomato pericarp?

The role and function of GBPs in plants have never been described so far. The study of the tomato *Slgbp10* KO mutants is a unique opportunity to start the functional characterization of GBPs in plants. Indeed, the impairment of the Guanylate Binding Protein function in tomato induced strong defects in the cellular organization inside the pericarp, which appear from 20 DPA. The alterations affect cell size and cell shape, together with alterations in cell wall and nuclear ploidy and morphology. None of these cellular alterations are found before 20 DPA, suggesting that the role of SlGBP10 is crucial during latefruit growth, probably during the cell expansion phase.

Some alterations, such as stack of cell walls creating lines of breaks inside the pericarp, together with some extreme flattened cells, suggest possible centrifugal constraints inside the tissue. Indeed, a force seems to push and crush the mesocarp cells towards the exocarp, the fruit cuticle probably imposing a rigid structure. This centrifugal force may be caused either by the extension of the locular tissue that is more imporant in this mutant or by the apparition of new cells inside the mesocarp. Indeed, the unexpected formation of additional cell walls and new nucleated small cells after 20 DPA likely suggests new events of division. In addition, spectacular observations of very large cells, probably polyploidy cells, presenting one to four new thin cellulosic cell walls which divide the cell asymmetrically, also suggest new events of division. In these large cells, it was possible to identify a nucleus in each newly formed "daughter cells". Moreover, the major part of the mesocarp cells (M and M' cell layers) present a change in nuclear morphology. These cells should either be multinucleated or have multi-lobed nuclei. In the case of multinucleated cells, we currently do not know whether the newly formed nuclei contain the same DNA content. Interestingly, the E1 to E3 exocarp cells exhibit normal nuclear morphology. In these exocarp cell layers, cells display a low-polyploid level if any (Bourdon *et al.*, 2012): these observations likely suggest that polynuclear cells or poly-lobed nuclei only happen when cells are in a polyploid state. I will further discuss, what is known about the poly-lobed nuclei or polynuclear cells and the possible division of polyploid cells, in view to better understand the *Slgbp10* mutant alterations and to advance in the understanding of the role of the GBP in tomato.

- *Occurrence of polynuclear cells and poly-lobed nuclei among eukaryotes*

Poly-lobed nuclei are commonly found in human immune cells, such as the granulocytes which are usually lobed into three segments. They are also called polymorphonuclear leukocytes or polymorphonuclear neutrophils depending on the varying shapes of the nucleus. As the number of lobes increased in case of leukemia, liver disease, cancer etc… (Chan *et al.*, 2010), it suggests that the change in nuclear morphology in this case constitutes a phenotype associated with abnormal development. As another example, human megakaryocytes are large bone marrow cells responsible for the production of blood thrombocytes (platelets), which are necessary for normal blood clotting. Megakaryocytes undergo endomitosis upon maturation: metaphase or anaphase can occur but the sister chromatids never fully separate, and cytokinesis never happens, resulting in globulated nuclear structure (Nagata *et al.*, 1997; Vitrat *et al.*, 1998). However, to my knowledge no or/few examples of plant poly-lobed nuclei have been described so far in plant cells.

Multinucleated cells or polynuclear cells can occur under physiological conditions by the fusion of the plasma membranes of cells thus forming syncytia. Syncytium is a normal cell structure for many fungi in which nuclei behave independently despite sharing a common cytoplasm (Roberts and Gladfelter, 2015). Animal cells can also form syncytium. As an example, the large skeletal muscle fibers are formed by the fusion of thousands of individual muscle cells. The syncytium of cardiac muscle is also well described and allows the rapid coordinated contraction of muscles along their entire length. Binucleate cells are commonly found in cancer cells, probably arising from chromosome non disjunction (Shi and King, 2005). In plants, the tapetum cells, found within the anther between the sporangenous tissue and the anther wall, normally have more than one nucleus per cell. The multinucleated tapetal syncytium is formed in the anther locule by fusion of tapetal protoplasts. The unusually large nuclear constitution of the tapetum helps it in providing nutrients and regulatory molecules to the forming pollen grains (Zhang and Yang, 2014). Plant parasitic nematodes induce several multinucleated giant cells or the formation of multinucleated syncytium (de Almeida Engler and Gheysen, 2013). In case of the formation of multinucleated syncytium, cell wall dissolution is followed by the fusion of adjacent cells, while in the case of the formation of giant cells, synchronous waves of mitotic activity uncoupled from cytokinesis give rise to large multinucleated cells (de Almeida Engler and Gheysen, 2013; Vieira and de Almeida Engler, 2017). Both strategies impinge on the deregulation of the cell cycle, involving a major role for endopolyploidy (Vieira *et al.*, 2012). Multinucleated cells can be induced in plants by treatment with γ-Hexachlorocyclohexane, which induced multipolar anaphases. During the multipolar mitosis chromatids

are distributed into unbalanced groups, followed by the inhibition of cytokinesis in these multipolar cells. This treatment results in the formation of multinucleated cells containing unbalanced nuclei (Hervas, 1987; Hervas, 1976). So, multinucleated cells or poly-lobed nuclei are currently found in eukaryote during normal and/or pathologic development, including in plants.

- *Occurrence of divisions after polyploidization in human, animal and plant*

Polyploid cells are mainly defined as non-dividing cells, because the evidence in linking a polyploid state to mitosis is lacking due to the absence of natural polyploid mitotic cycles. In humans, polyploidy often occurs in specific tissues as part of terminal differentiation in highly differentiated tissue, such as liver parenchyma, heart muscle, placenta and in bone marrow. Polyploidy also is found in many tumors, and the enhanced chromosomal instability suggests that such polyploid cells contribute to tumor aneuploidy (abnormal number of chromosomes in a cell) (Storchova and Pellman, 2004). During normal development, human polyploid megakaryocytes have been shown to divide again (Leysi-Derilou *et al.*, 2010). Megakaryocyte differentiation and maturation involved polyploidization (until 16N) through endomitosis, due to aborted cytokinesis and prematurely ending of mitosis (Leysi-Derilou *et al.*, 2010). However, part of these polyploid megakaryocytes can fully complete mitosis following nuclear division, completion of cytokinesis and cell abscission, in *in vitro* cell culture. Division of polyploid megakaryocytes occurs symmetrically and asymmetrically and division of tetraploids to more than two daughter cells also occurs, giving birth to three well defined nuclear lobes of similar size, contained into the same cell (tri-lobular megakaryocytes). Interestingly, the mitotic potential was found to vary as a function of ploidy level: the frequency of cell division amongst polyploid megakaryocytes is inversely correlated to their ploidy level (Leysi-Derilou *et al.*, 2010).

In animal cells, two types of polyploid cells resulting from endomitosis, were found to divide. Polyploid *Drosophila* cells undergo normal mitotic cycles as part of a remodeling process that forms the adult rectal papillae and during the adult ileum development in the mosquito *Culex pipiens* (Fox *et al.*, 2010). Indeed, polyploid *Drosophila* rectal cells re-enter into the mitotic cell cycle despite having previously undergone at least two cycles of endopolyploidy, during larval development. This observation was also found in polyploid mosquito ileal cells which re-enter into the normal mitotic cycle. Thus, polyploidization during development is not an irreversible step, as had been widely believed. Furthermore, Fox *et al.* (2010) proved that the general characteristics of polyploid mitotic cycles, including cell cycle gene expression and

function, appear to be normal, such as cyclin E and A. They proposed that the rarity of polyploid mitotic cycles during development might be because of the significant cost imposed by this strategy by decreasing genomic stability.

In the plant kingdom, cell division after endopolyploidization event was only described in response to an external stress. In *Allium* roots, it was observed that a treatment with indole-acetic acid may induce division of polyploid cells (Chouinard, 1951). The same observation was noticed, in tobacco in response to wounding stimuli. However, this response seems to be restricted to nuclei below 16C ploidy level, as above 16C cells do not respond to wounding stimuli (Geitler, 1948). In apricot fruit, both wounding and auxin treatments cause an enlargement of parenchyma cells, through endomitosis but no induction of mitosis in cells with up to 64C ploidy level (Bradley, 1954; Bradley and Crane, 1955). Resumption into division process for polyploid cells was also described for plant cells, however it seems limited to low and intermediate ploidy levels. Division of polyploid plant cells can also occurs *in vitro* by transferring cells to a medium containing auxin and cytokinin (Valente *et al.*, 1998). The induced divisions are amitotic, meaning that cytoplasm and parental chromosomes are randomly distributed in daughter cells.

To conclude, a few examples of polyploid cells, undergoing endoreduplication or endomitosis, are able to divide again are present in human, animal and plant, depending on the cell type fate or under stress conditions.

- *Putative function of the GBP in tomato pericarp*

During normal fruit growth, a gradient in ploidy levels is set up from the exocarp to the endocarp, with the larger polyploid cells (up to 256C), at the center of the mesocarp. This faculty in tomato to produce highly polyploid mesocarp cells is thought to stimulate cell expansion and therefore to boost fruit growth (Chevalier *et al.*, 2014). The transition between the mitotic cell cycle towards the endoreduplication cycle has been largely studied and regulators controlling the entry into endoreduplication have been already described. However no study on the control of the end of endoreduplication has been reported to our knowledge. The extreme phenotype observed in the *Slgbp10* mutants opens many questions: Is this endoreduplication or endomitosis in the *Slgbp10* mutants? FISH analysis could answer to this

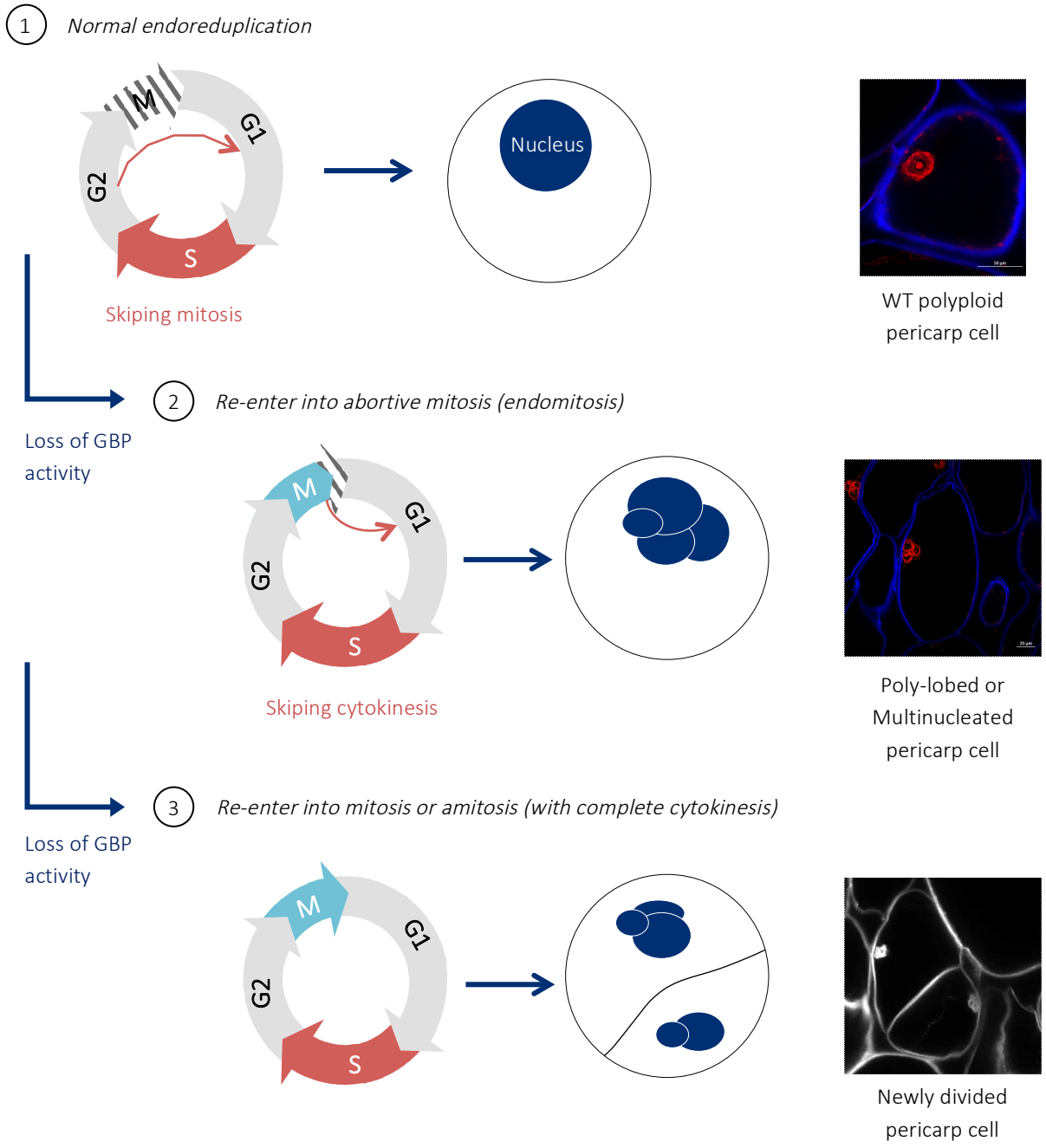

Figure 60: **Proposed models resulting in poly-lobed nuclei or multinucleated pericarp cells in *Slgbp10* mutant.**

question (Bourdon *et al.*, 2012). Is there a signal or control specifying the end of endoreduplication? What happens in a cell, after the end of endoreduplication? Is a highly polyploid cell able to divide again? Is a highly polyploid cell able to re-enter into mitosis or amitosis? Is a polyploid cell able to finish cytokinesis? In this last case, how are polytene chromosomes segregating during polyploid nucleus division? These questions arise from the pericarp alterations observed in the *Slgbp10* mutants. Indeed, polyploid pericarp cells seem able to divide again and in some case, seem able to reach late steps of mitosis (or amitosis) with the formation of new cell walls. After 20 DPA, close to 25 DPA according to the metabolic profiles, something happens in the mutant pericarp cells. We can suppose that this moment corresponds to the possible end of endoreduplication. Once endoreduplication is finished, we can suppose that all the cell division machinery is present and available to support new division. We also imagine that division of a polyploid cell is costly in term of energy and complex, in term of division of the cellular components. The large vacuole, typical of the fleshy tissue cells, should be a mechanical constraint for the formation of a new cell plate in a perfect median position. So, it is easy to think that cytokinesis in polyploidy cells results in aberrant cell wall positioning to incomplete cytokinesis. In addition, for the endoreduplicated cells, the number of chromosomes arranged in polytenes, should also complicate the different mitosis steps and leads to incomplete and aberrant nucleus divisions. No information is available in literature about the mechanisms of division involving polytene chromatids. We only can hypothesize that the GBP is involved in the negative control of division after endoreduplication and/or that GBP repress a premature exit in the endoreduplication process promoting to restart division (through mitosis or amitosis) (Figure 60)

.

II. Is the Guanylate Binding Protein involved in the control of cell division process?

In plants, the Guanylate Binding Protein seems to be a nuclear protein. When overexpressed in BY-2 cells, GBP limits normal cell division. Indeed, these cells divide more slowly and remain in large aggregates, making them unable to reach a normal differentiated aspect of BY-2 cells. This impact on BY-2 cells also supports a role of the GBP in the control of cell division.

Interestingly, Dr Daniel Van Damme (VIB – Ghent; personal communication) reported the interaction between AURORA 3 and AtGBP5 in Arabidopsis in *in vivo* Tap-tag experiments. AURORA3 is a β-Aurora kinase, acting as a serine/threonine kinase, involved in the kinetochore–microtubule attachment. Three Aurora kinases are present in *Arabidopsis* that are subdivided into the α-Aurora (Aurora 1 and 2) and β-Aurora (Aurora 3) sub-groups. All AtAurora proteins are highly expressed in actively dividing cells (roots and flower tissues), with an expression peak at the onset of mitosis and a decrease in expression at the end of mitosis (Demidov *et al.*, 2005). The *Arabidopsis* α-Aurora proteins are involved in establishing bipolar spindles, chromatin/histone modifications, and cell division orientation (Weimer *et al.*, 2016). Both *Arabidopsis* α-Aurora kinases show dynamic localization throughout mitosis because they associate with prophase spindle microtubules and kinetochore spindle microtubules during metaphase and anaphase, and with the growing cell plate during cytokinesis (Demidov *et al.*, 2005). A role for the α-Aurora in microtubule stability was suggested (Weimer *et al.*, 2016). The β-Aurora kinase AtAurora 3 is found as dots around the nucleolus of interphase nuclei, which are thought to be chromocenters and at centromeres during metaphase, which suggest that it likely plays a role in chromosome separation (Demidov *et al.*, 2005; Weimer *et al.*, 2016). Other roles for Aurora B have been described in relation with telomere activity. In Yeast, Aurora B has been shown to be involved in telomere dispersion and disjunction during fission yeast mitosis (Reyes *et al.*, 2015). In mouse, Aurora B interacts with telomeres and is a regulator of their structural integrity (Chan *et al.*, 2017; Mallm & Rippe, 2015).

All the three *Arabidopsis* AtAurora kinases can phosphorylate histone H3 at serine 10 (Demidov *et al.*, 2005; Kawabe *et al.*, 2005). Histone H3 is one of the five main histone proteins involved in the structure of chromatin in eukaryotic cells in relation with the nucleosomes. Interestingly, the overexpression of AtAurora 3 in BY-2 cells leads to unusual cell division patterns with abnormal division orientations and

spindle formation defects (Kawabe *et al.*, 2005). A treatment of BY-2 cells with an Aurora kinase inhibitor hesperadin, suppresses the phosphorylation of histone H3 and induces an aberrant chromosome segregation, such as frequent formation of lagging chromosomes and micronuclei (Kurihara *et al.*, 2006). The observations of BY-2 aggregates could be explained in part by possible alterations of cell division orientations in cells overexpressing the SlGBP10. Furthermore, the localization of SlGBP10 during BY-2 cell division follows in a certain way the localization of what is known on Aurora protein localization. Indeed, the β-Aurora kinase AtAurora 3 is found at the chromocenters of interphase nuclei, which is similar to the localization of SlGBP10 in tomato and *Arabidopsis* roots. During mitosis, from prophase to telophase, SlGBP10 is clearly associated with DNA. It is however difficult to confirm a position at the centromere or telomeres with the present data. However, the localization looks like the one obtained for the yeast Aurora B, close to telomeres with an increasing localization signal along mitosis process (Reyes *et al.*, 2015). Further investigations are needed to precise the localization of SlGBP10 during cell division and confirm a possible telomeric position.

The inhibition of Aurora kinases in BY-2 cells induces aberrant kinetochore-microtubule attachment, resulting in lagging chromosomes and the formation of micronuclei in daughter cells caused by the delay and failure of sister chromatid separation (Kurihara *et al.*, 2006; Kurihara *et al.*, 2008). The overexpression of SlGBP10 in BY-2 cells revealed an intriguing localization of SlGBP10 outside the nucleus in a likely independent structure, labeled with DAPI. This structure may be a micronucleus, resulting from the failure of sister chromatid separation due to the overexpression of SlGBP10 in BY-2 cells. Furthermore, *Arabidopsis* RNAi mutants for the three Aurora kinases show strong defects in the development of the primary root meristems and the apparition of adventitious roots (Petrovská *et al.*, 2012). Again, these alterations are similar to the ones obtained in the *Atgbp5* KO mutants. The tomato GBP10 mutants also present defect in root development, which remain to be precisely characterized. Altogether, this suggests that AtGBP5 and Aurora kinases may be involved in the same regulatory pathway.

The interaction between AtGBP5 with AtAurora 3 is a very nice indication to further understand in the role of GBPs in plants. To confirm this result, we currently test the *in vitro* interaction of the two tomato Aurora homologs with the tomato SlGBP10. The ongoing result will offer interesting advances in the understanding of the role of the plant GBPs in cell division control.

III. Perspectives of the study

In order to confirm or reject our current hypotheses, several experiments are currently being considered:

- Further precise localizations of SlGBP10 and AtGBP5 are required to better understand their possible involvement in cell division processes. The co-localization with telomeric regions during cell division in BY-2 cells and the localization with chromocenter in interphase nuclei should be investigated with specific markers.

- The cellular characterization of the *Atgbp5* KO mutants, especially in polyploid cells is under progress. For this purpose, as *Arabidopsis* cells do not undergo high level of polyploidy, crossings of the *Atgbp5* KO mutants with mutants displaying high level of endoreduplication is foreseen. The objective here is to check if poly-lobed nucleus or multinucleated cell phenotypes could be observed in other endoreduplicated systems such as the trichomes. In addition the CRISPR mutants and tagged-AtGBP5 reported lines will be crossed with the *Arabidopsis* AtAurora mutants and/or Aurora reporter lines in order to study possible modifications in protein localization patterns. This could give information on the involvement of the two proteins in similar pathways.

- Finally, the identification of the second mutated locus, responsible for the “distorted” phenotype in Salk016366 (*Atgbp5*) T-DNA mutant should be considered in order to understand the role of *AtGBP5* in actin cytoskeleton modification.

Part II

Functional characterization of the Guanylate Binding Protein: case of P3D3 mutant.

Supplemental data

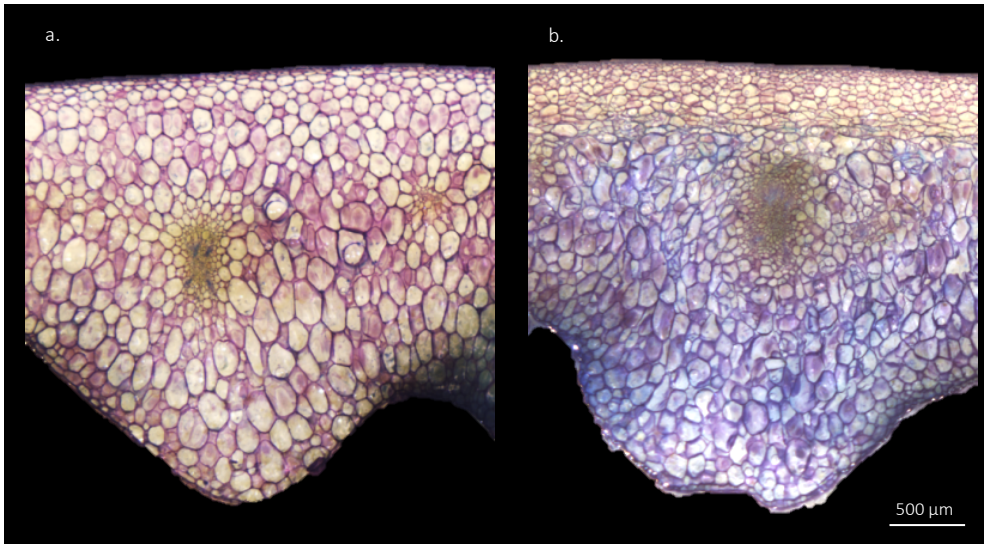

Supplementary Figure 9: **Transfer of the GBP mutation into M82 background.** a. Pericarp section of an homozygous WT GBP/GBP individual. b. Pericarp section of a homozygous mutant *gbp/gbp* individual. Pericarp portions at the equatorial part of the fruit were stained with toluidine blue.

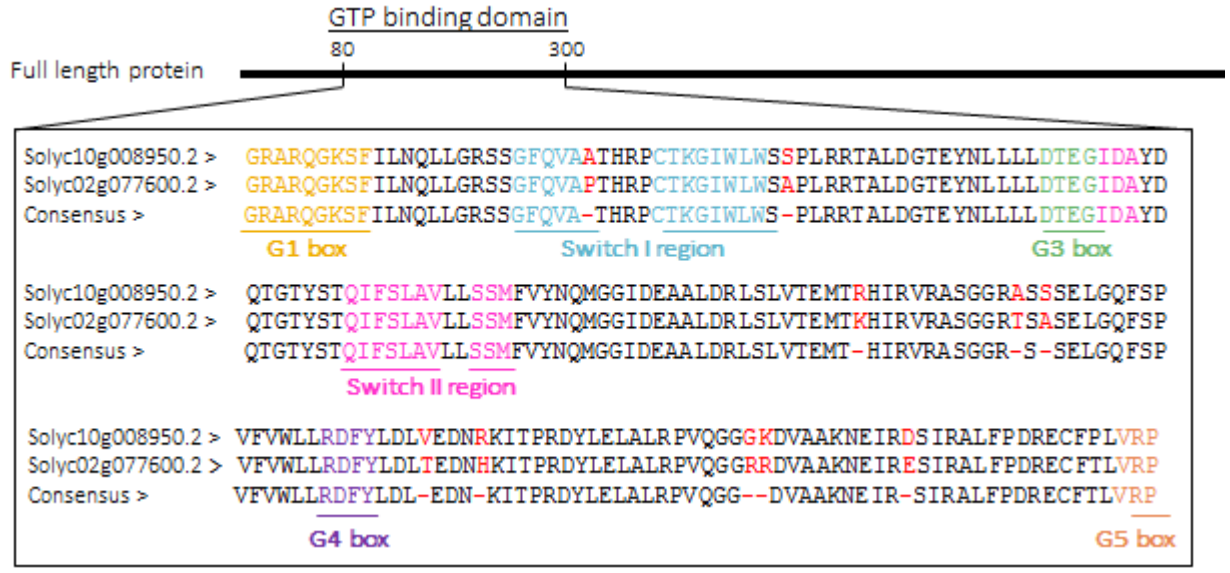

Supplementary Figure 10: **Amino acid sequence alignment of the two tomato SlGBPs.** Conserved GTP binding domains are highlighted with different colors. Differences in amino acid sequences are highlighted in red.

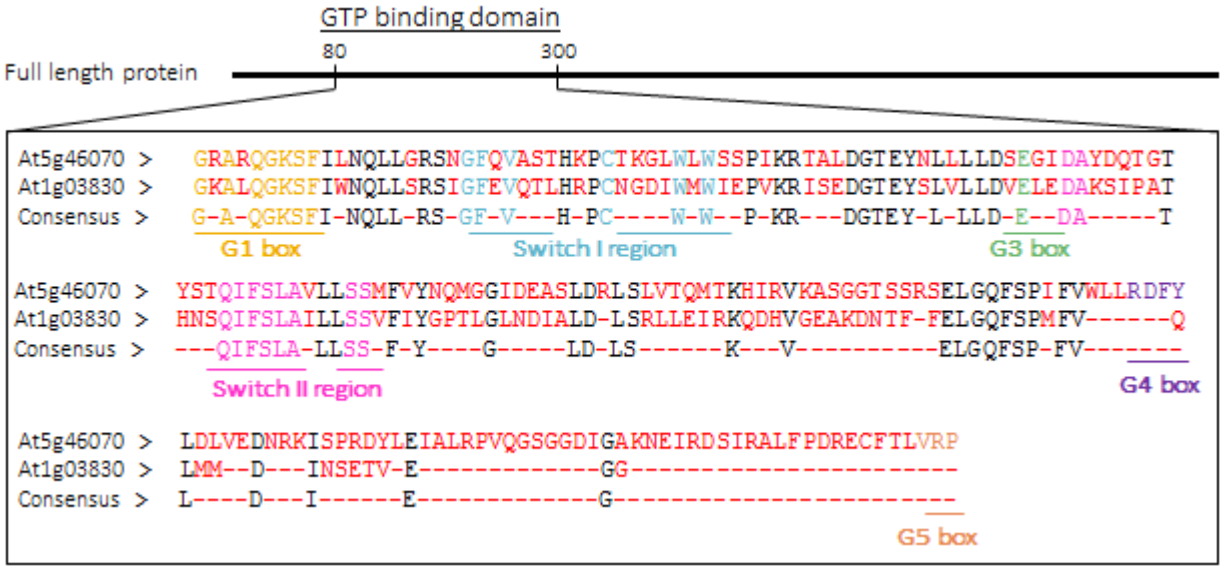

Supplementary Figure 11: **Amino acid sequence alignment of the two Arabidopsis AtGBPs.** Conserved GTP binding domains are highlighted with different colors. Differences in amino acid sequences are highlighted in red.

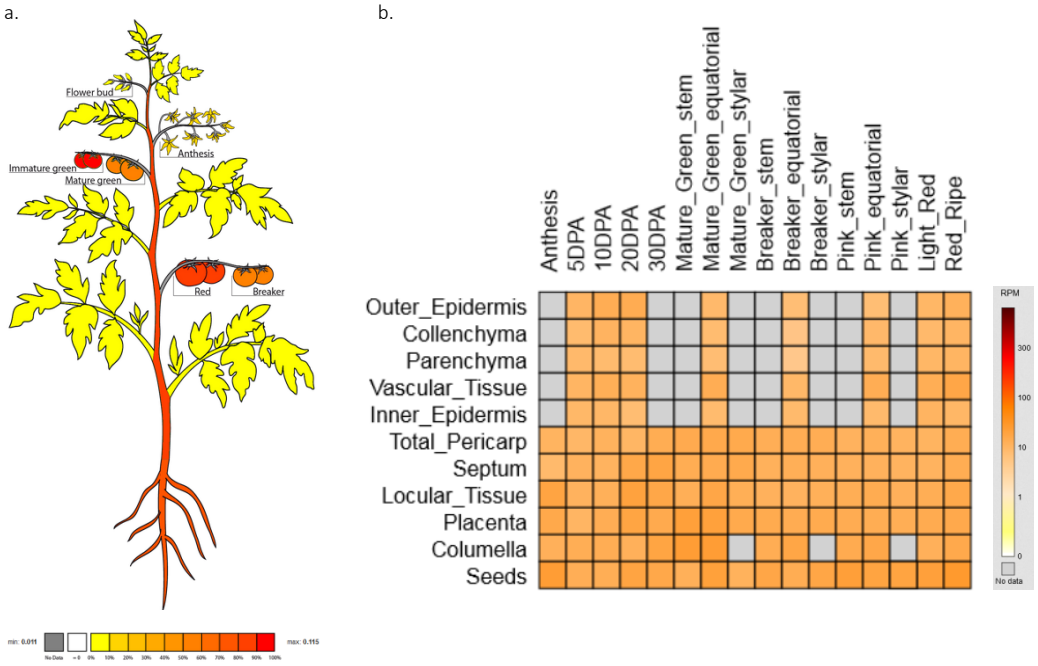

Supplementary Figure 12: **Expression pattern of *SlGBP10*.** a. Expression pattern in the whole plant. b. Expression pattern inside the fruit. According to the Sol Genomics.

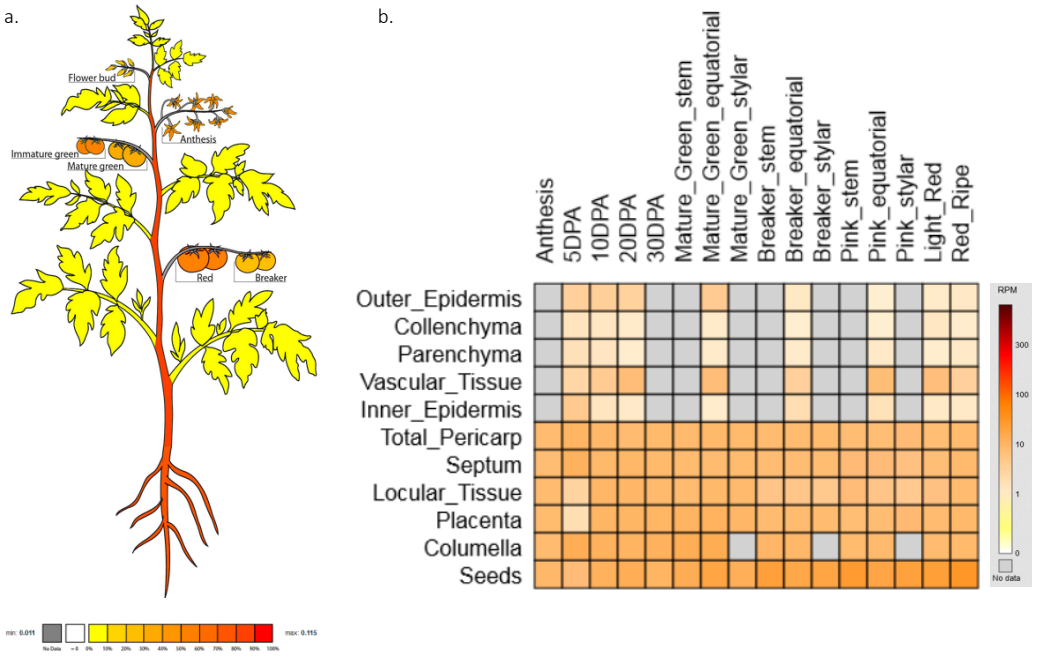

Supplementary Figure 13: **Expression pattern of *SlGBP2*.** a. Expression pattern in the whole plant. b. Expression pattern inside the fruit. According to the Sol Genomics.

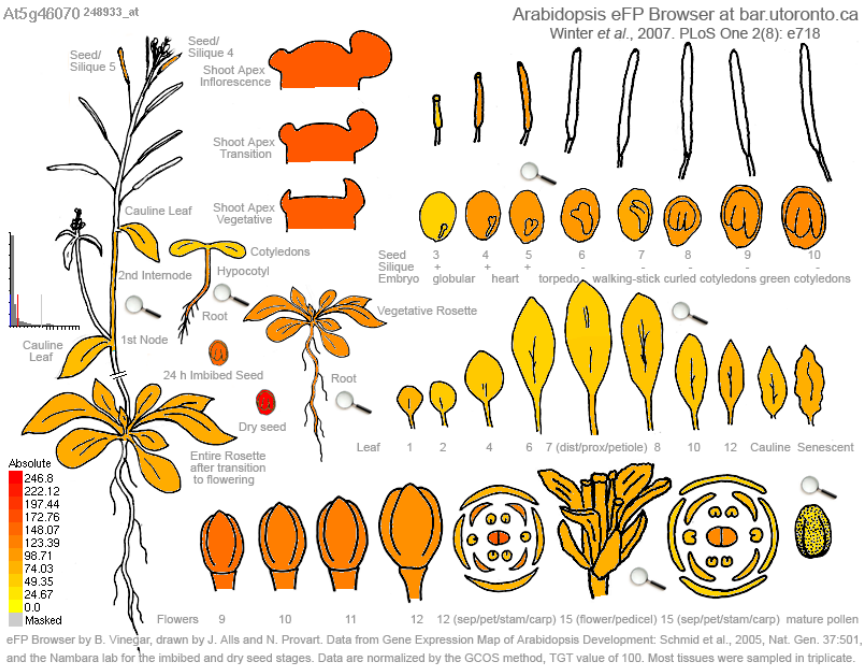

Supplementary Figure 14: **Expression pattern of *AtGBP5* in Arabidopsis thaliana plant and organ.** According to the eFP Browser.

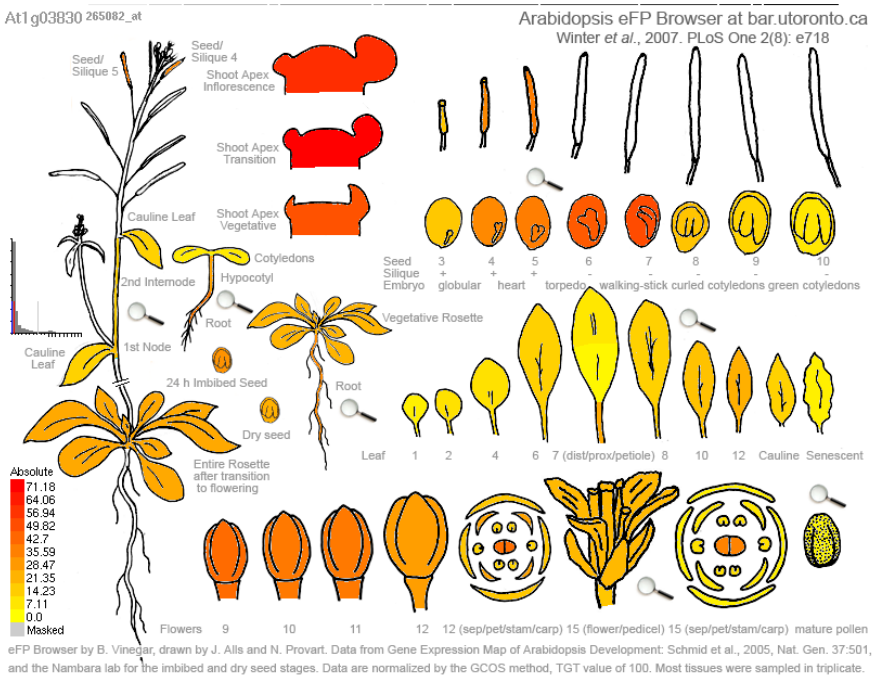

Supplementary Figure 15: **Expression pattern of *AtGBP1* in Arabidopsis thaliana plant and organ.** According to the eFP Browser.

Supplementary Figure 16: **Vegetative development of P3D3 mutant.** a. P3D3 mutant shows no change in the final plant size b. and leaf size.

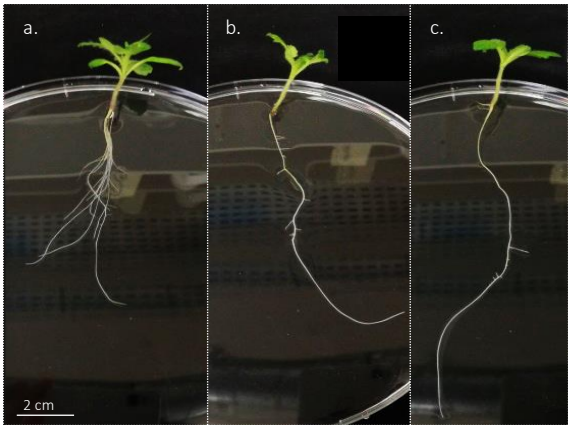

Supplementary Figure 17: **Tomato root development** a. WT Micro-Tom b. CR4 CRISPR mutant c. CR8 CRISPR mutant

a.

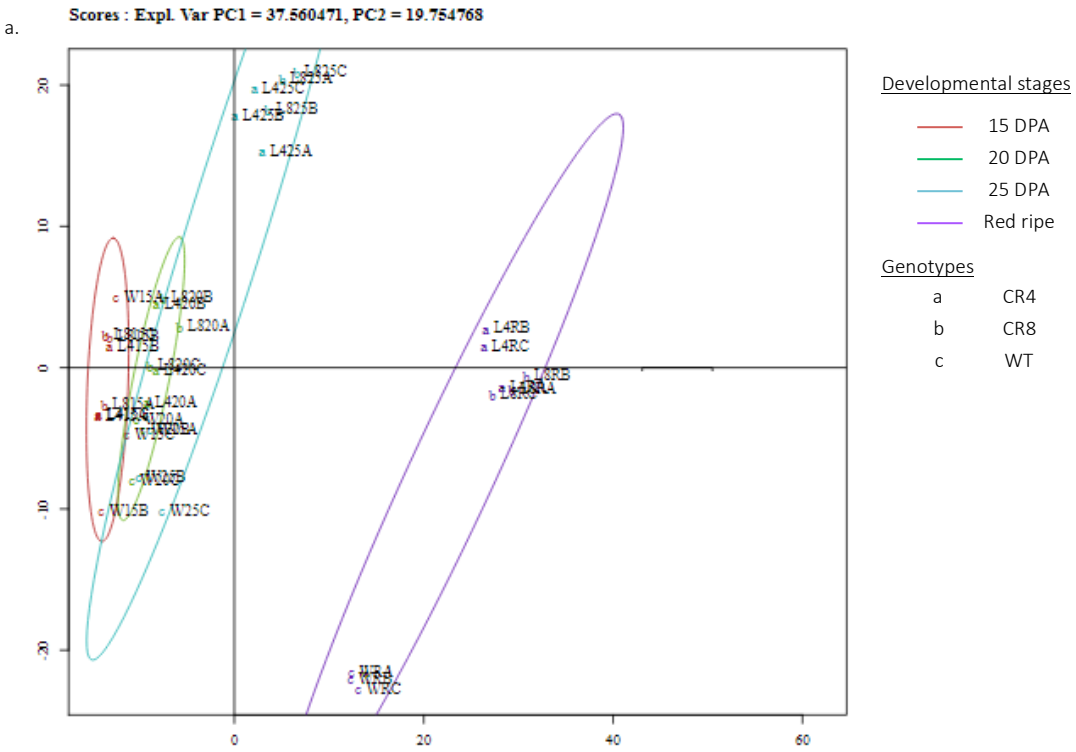

b.

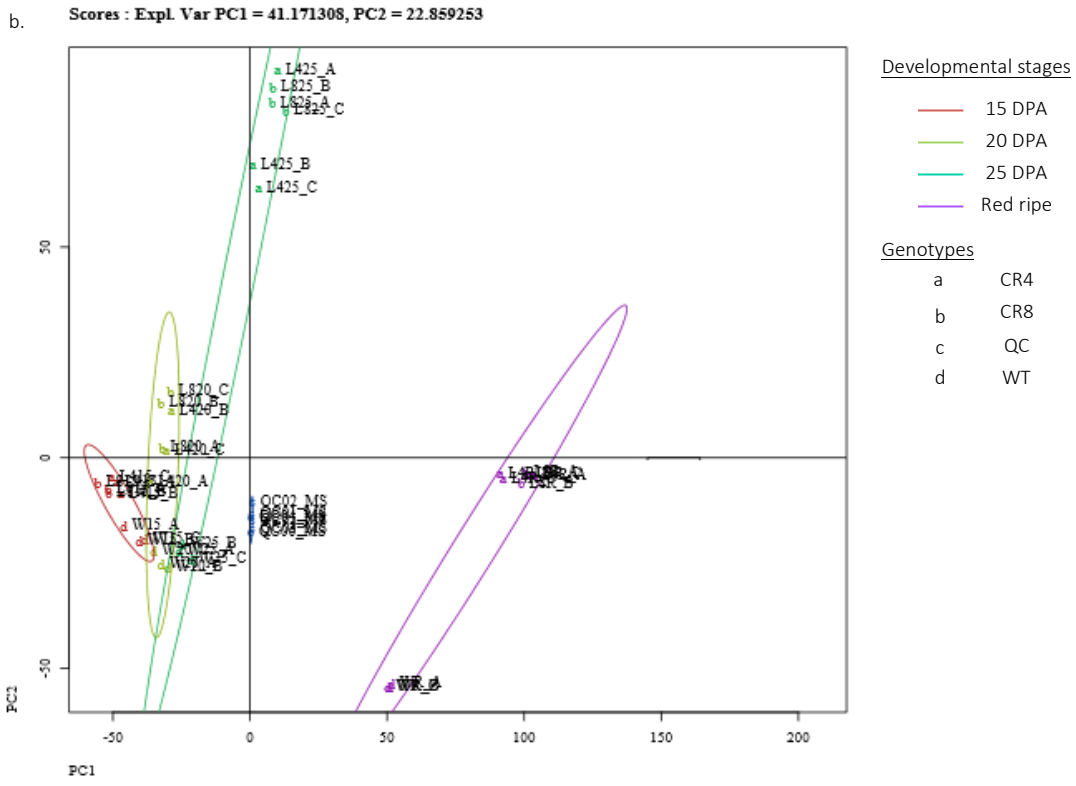

Supplemntary Figure 18: **Metabolite variations along fruit development between the *Slgbp10* KO mutants and the WT Micro-Tom.** a. PCA of primary metabolites. b. PCA of secondary metabolites. A QC sample was produced by pooling 50 µL of each sample extract.

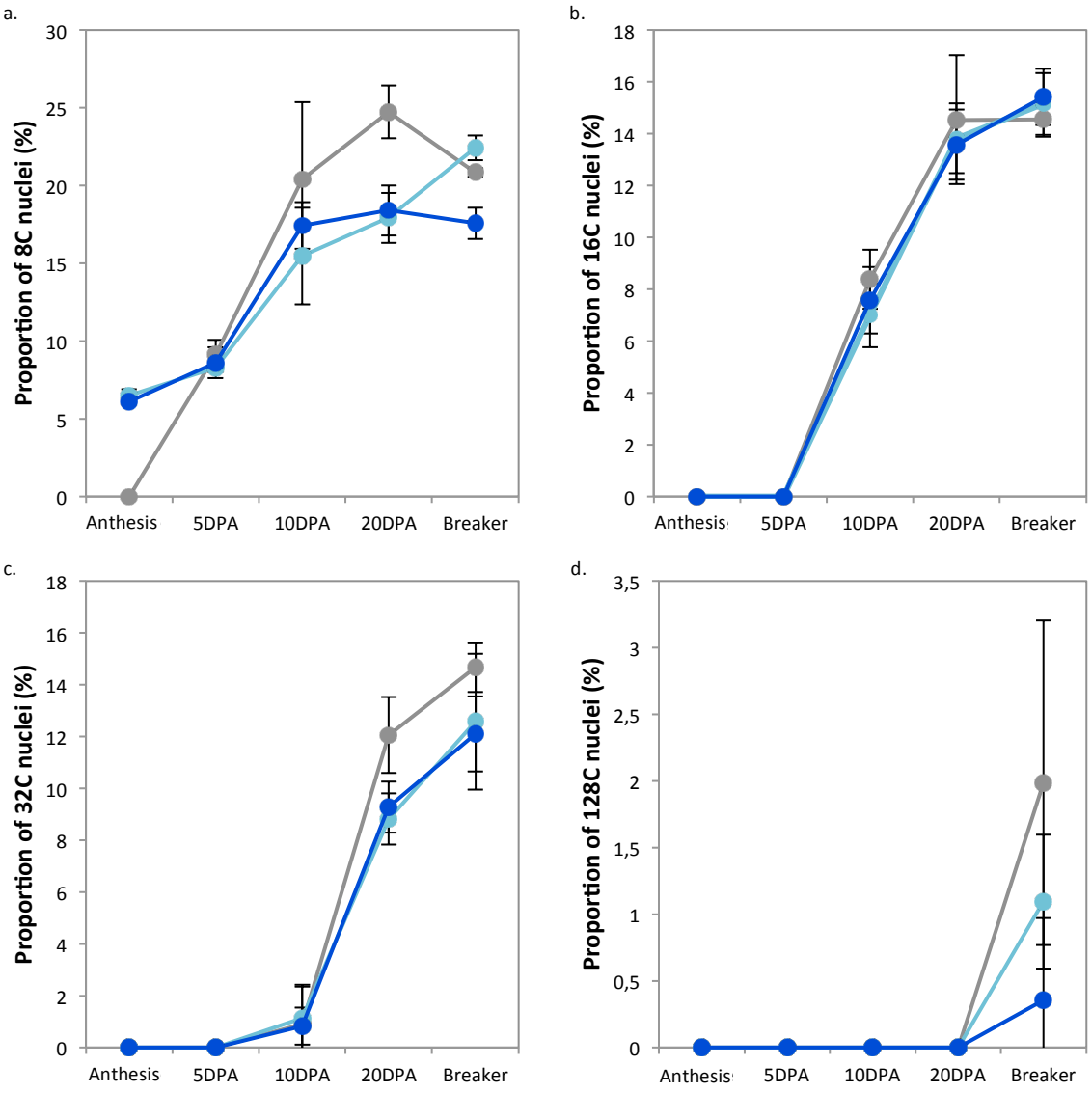

Supplementary Figure 19: **Evolution of the accumulation of nuclei according to their ploidy level.** a. Evolution of 8C nuclei. b. Evolution of 16C nuclei. c. Evolution of 32C nuclei. d. Evolution of 128C nuclei. (Error bar: standard deviation, n=3)

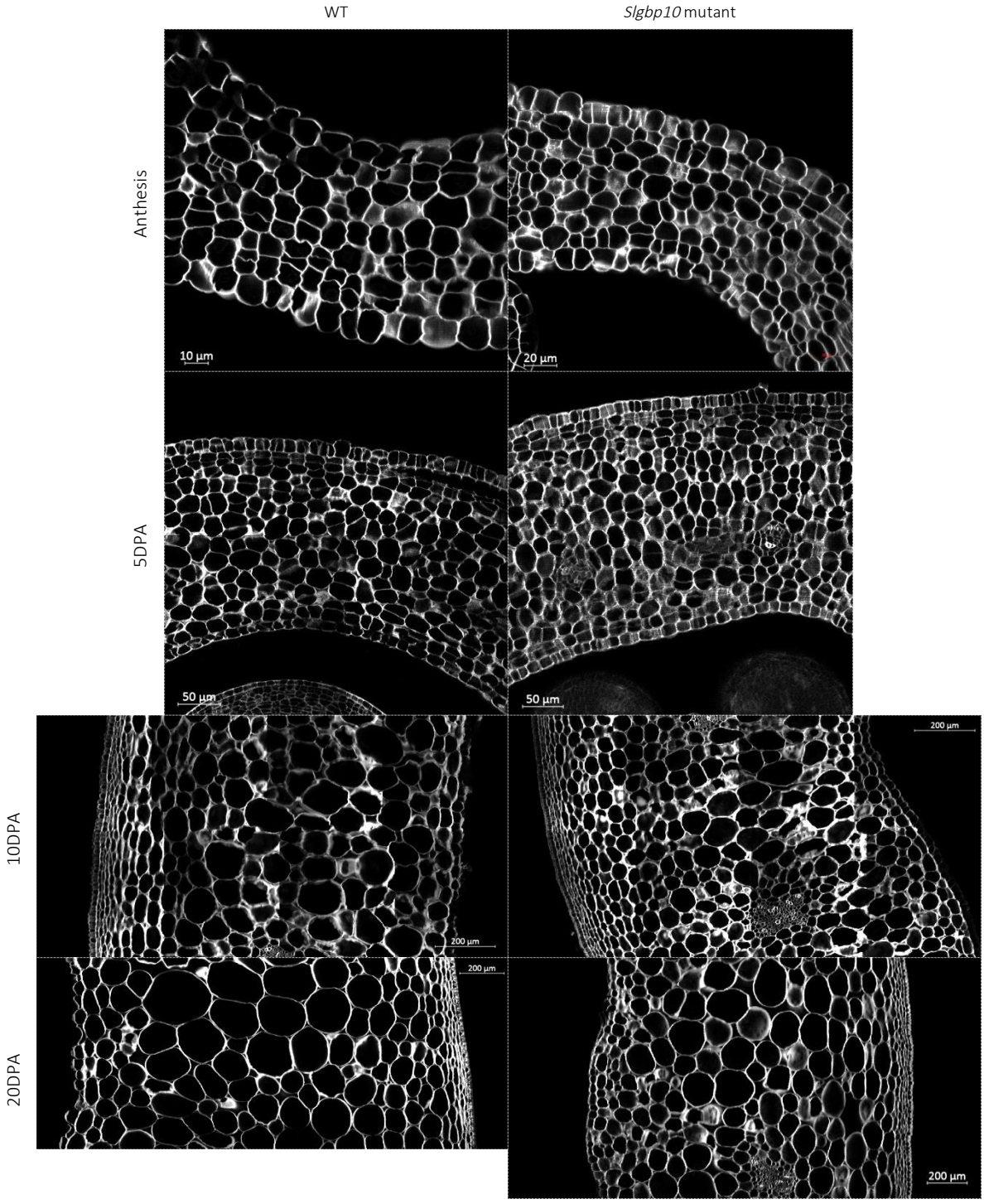

Supplementary Figure 20: **Equatorial section of the pericarp from anthesis to 20 DPA, of the WT Micro-Tom and *Slgbp10* mutant.** Equatorial portion of pericarp were stained with calcofluor.

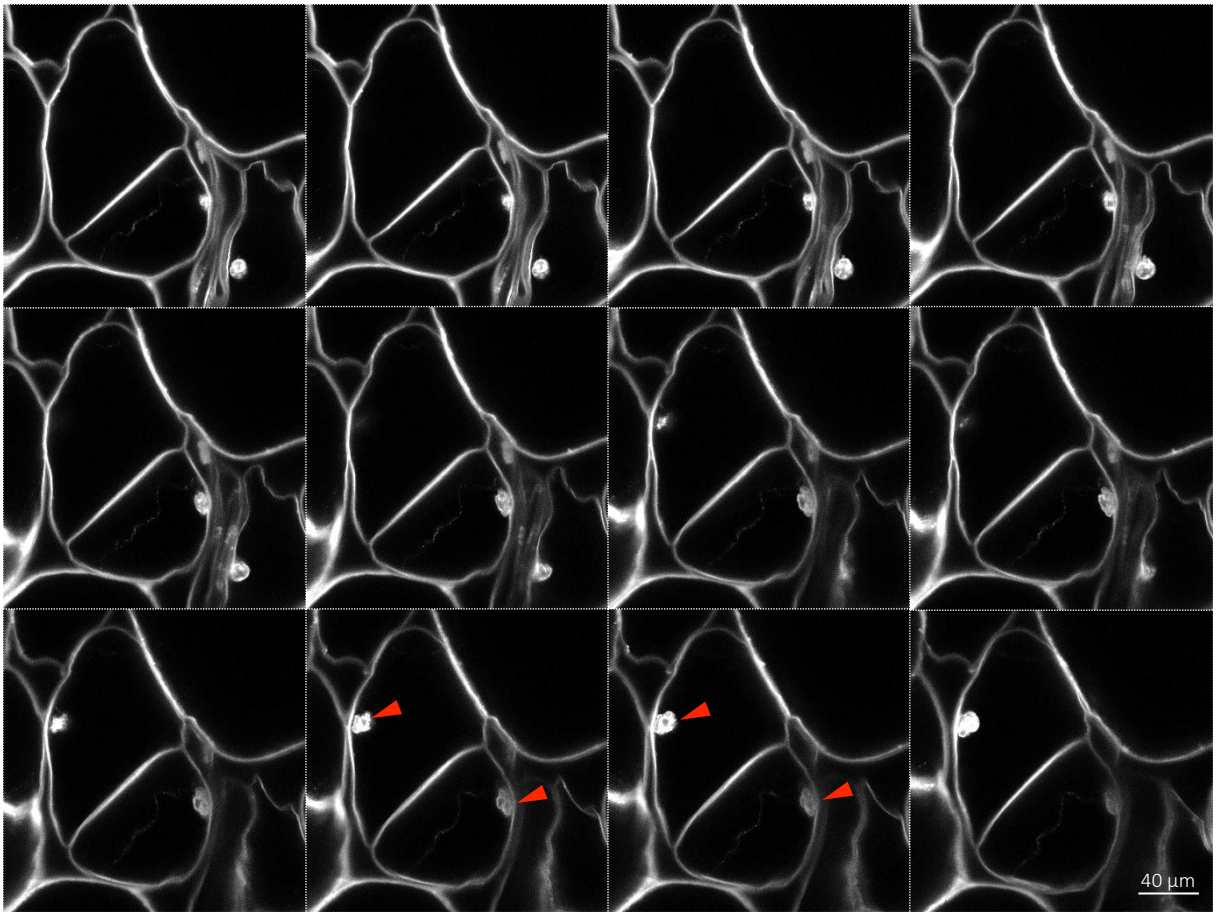

Supplementary Figure 21: **Abnormal cell division pattern inside the pericarp in the *Slgbp10* mutants, at breaker stage.** Cell walls are stained with calcofluor, nuclei are stained with DAPI. Red arrow-heads highlight the nucleus.

Solyc ID	Protein name	General fonction	Expression
Solyc03g113000.2	Chromosome structural maintenance protein-like - RINT-1/TIP-1	cell division	Down-regulated x 2
Solyc07g026620.2	Tubulin-folding cofactor E family protein	cell division	Down-regulated x 10
Solyc03g006640.2	Cyclin-like F-box family protein	cell division	Down-regulated x 10
Solyc03g096100.1	Yippee zinc-binding-like protein	cell division	Down-regulated x 80
Solyc03g096260.1	Yippee zinc-binding-like protein	cell division	Down-regulated x 100
Solyc10g055600.1	S-phase kinase-associated protein 1A	cell division	Down-regulated x 100
Solyc03g096140.1	Yippee-like protein	cell division	Down-regulated x 100
Solyc01g096170.2	Serine/threonine protein kinase	cell division	Up-regulated x 100
Solyc01g098160.2	Cell division protein kinase 12 -CDK12	cell division	Up-regulated x 2
Solyc04g079840.2	LIM domain-binding protein	cell division	Up-regulated x 2
Solyc04g078870.2	Serine/threonine-protein kinase 38	cell division	Up-regulated x 3
Solyc04g008680.2	Cell division cycle and apoptosis regulator protein 1	cell division	Up-regulated x 3
Solyc03g044160.1	Pto-like/ Serine/threonine kinase protein	cell division	Up-regulated x 5
Solyc03g032190.2	Cyclin B2	cell division	Up-regulated x 15
Solyc10g006350.2	Microtubule-associated protein TORTIFOLIA1	cell organisation	Up-regulated x 2
Solyc07g007030.1	Transmembrane 9 superfamily protein member 2 - TM9SF	cell organisation	Up-regulated x 2
Solyc05g052200.2	Protein kinase -IPR011989 Armadillo-like helical	cell organisation	Up-regulated x 3
Solyc12g005050.1	HAUS augmin-like complex subunit 4	cell organisation	Up-regulated x 3
Solyc04g008660.2	ADP-ribosylation factor GTPase-activating protein	cell organisation	Up-regulated x 3
Solyc02g079360.1	Octicosapeptide/Phox/Bem1p domain-containing protein	cell organisation	Up-regulated x 3
Solyc01g091380.2	Microtubule-associated protein MAP65-1a	cell organisation	Up-regulated x 5
Solyc02g088690.2	UDP-glucose 6-dehydrogenase	cell wall	Up-regulated x 2
Solyc01g091200.2	NAD dependent epimerase/dehydratase family protein	cell wall	Up-regulated x 2
Solyc12g055930.1	UDP-glucose 4-epimerase	cell wall	Up-regulated x 3
Solyc07g054310.1	Gty37 protein	cell wall	Down-regulated x 100

Supplementary Table 3: List of miss-regulated genes involved in cell division, cell organisation and cell wall in the *Slgbp10* mutants at 10 DPA.

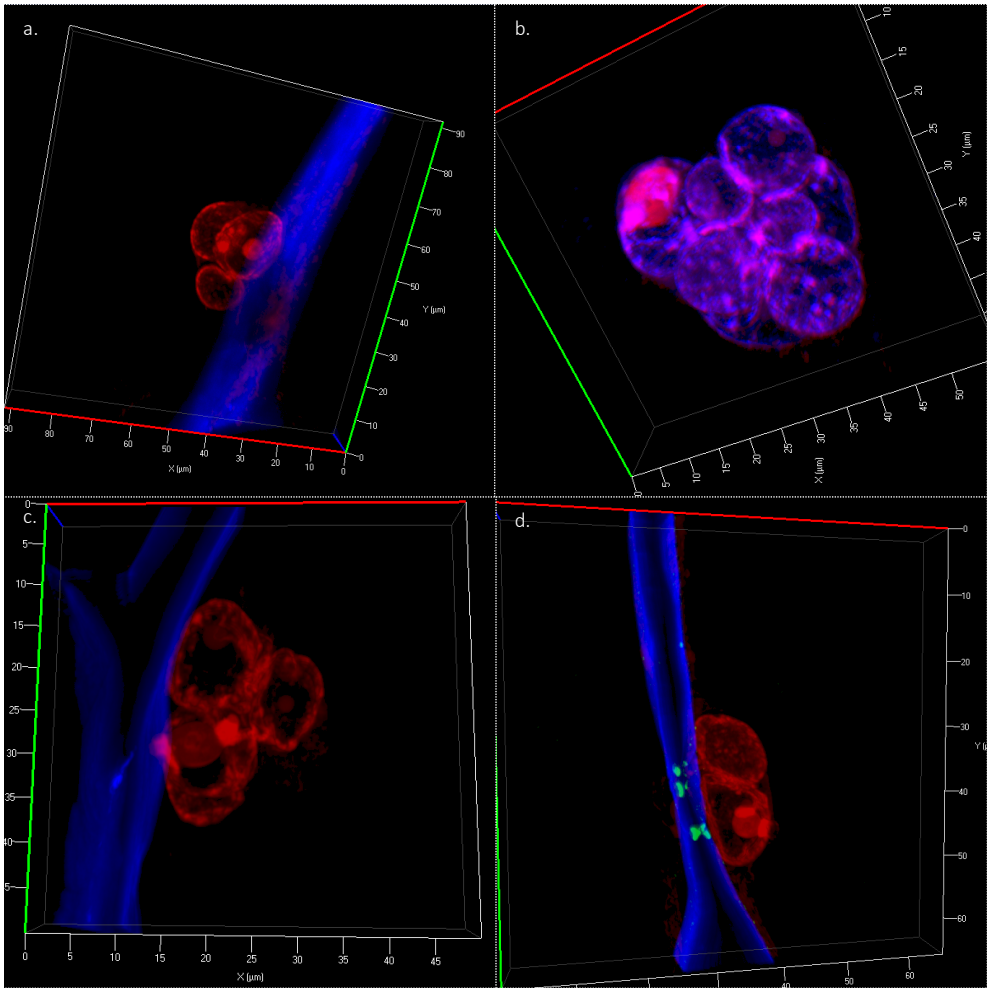

Supplementary Figure 22: **Nuclei 3D images of the *Slgbp10* mutant.** In a.c.d., cell walls are stained with calcofluor (blue), nuclei are stained with propidium iodide (red). In b. Nucleus is stained with propidium iodide (red) and DAPI (blue).

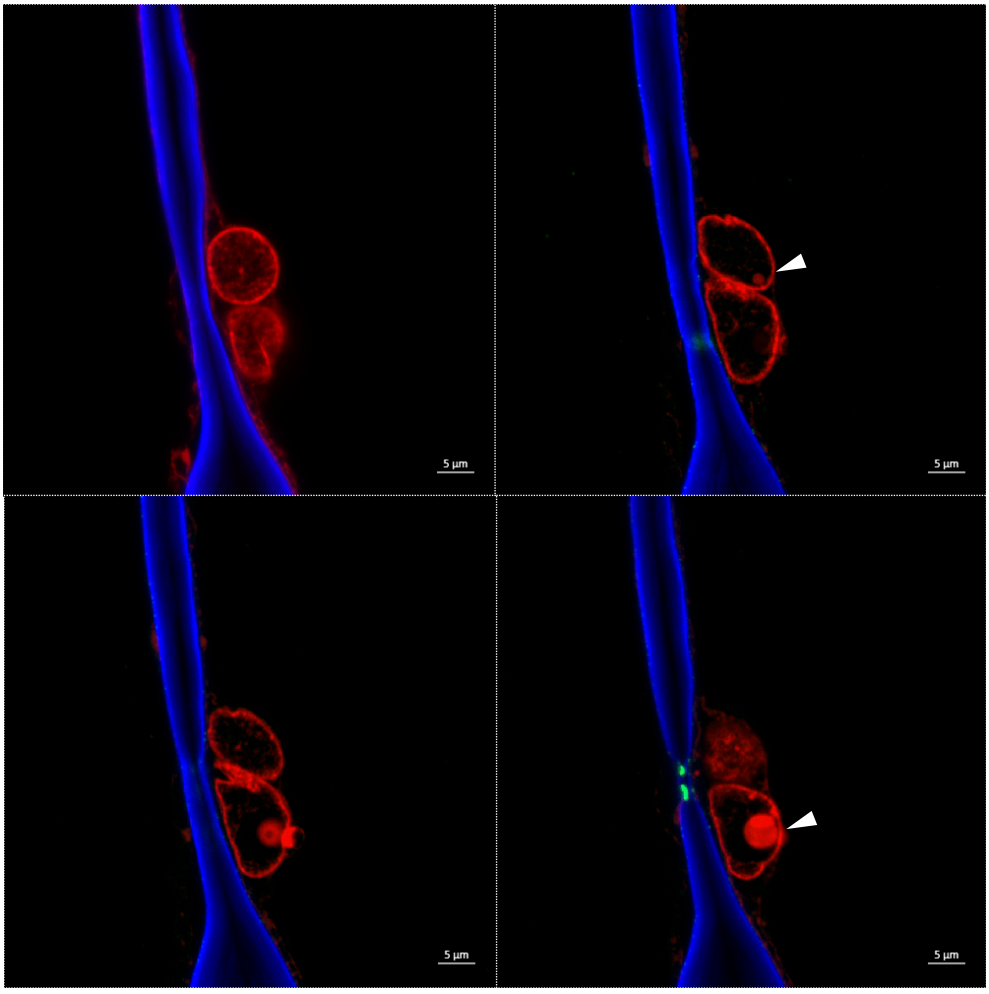

Supplementary Figure 23: **Different position in an altered *Slgbp10* mutant nucleus.** Cell walls are stained with calcofluor (blue), the nucleus is stained with propidium iodide (red). White arrow-heads indicate the nucleoli.

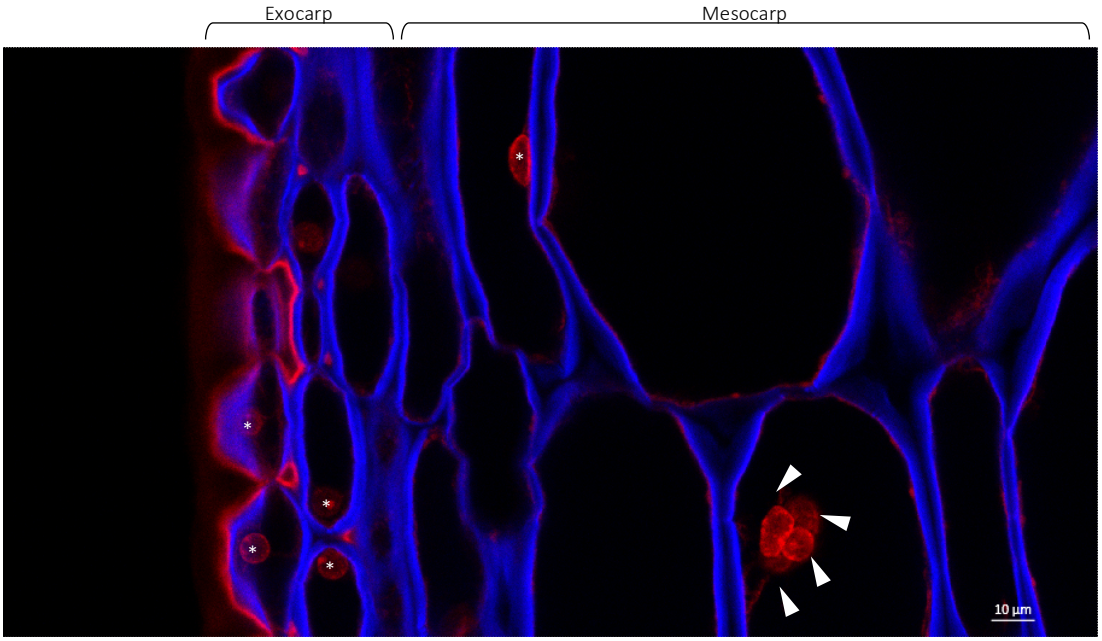

Supplementary Figure 24: **Nucleus morphology according to their position inside the pericarp of *Slgbp10* mutants.** Cell walls are stained with calcofluor (blue), nuclei are stained with propidium iodide (red). * indicates a single nucleus. Arrow-heads indicate the nucleus lobes.

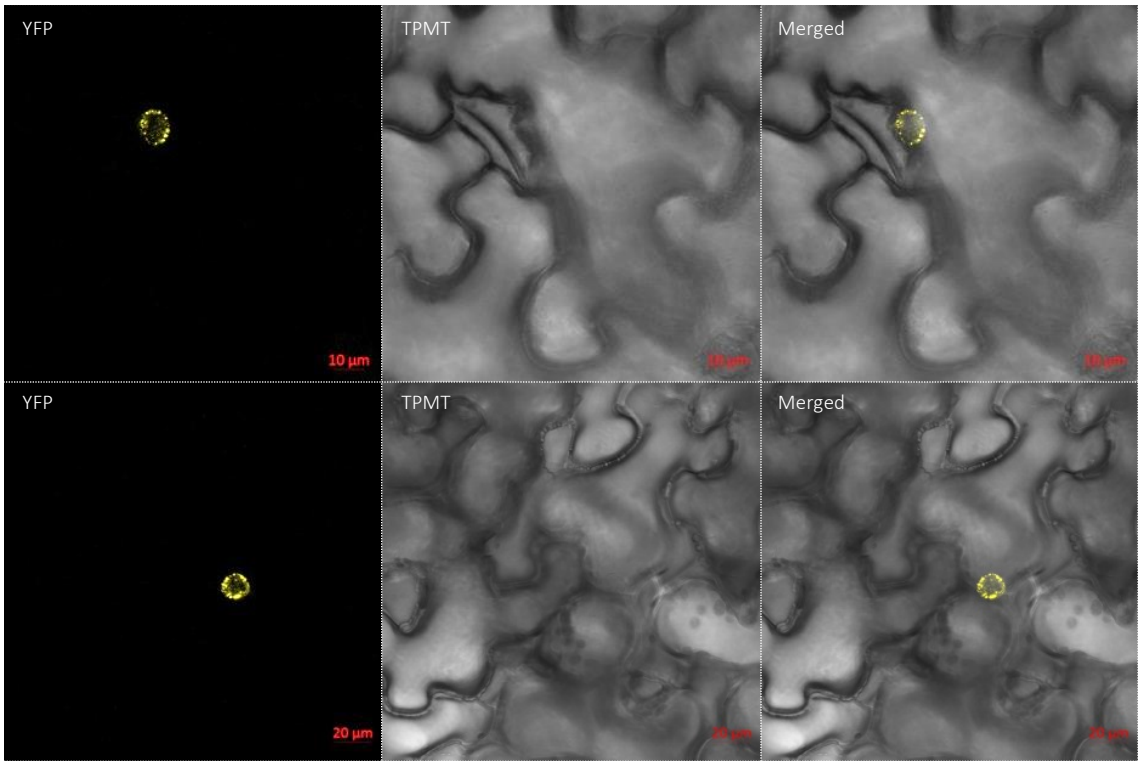

Supplementary Figure 25: **Subcellular localization of SlGBP10 in tobacco leaves.** SlGBP10 expressed under a constitutive p35S promotor and fused in Nterm with YFP. Yellow is YFP.

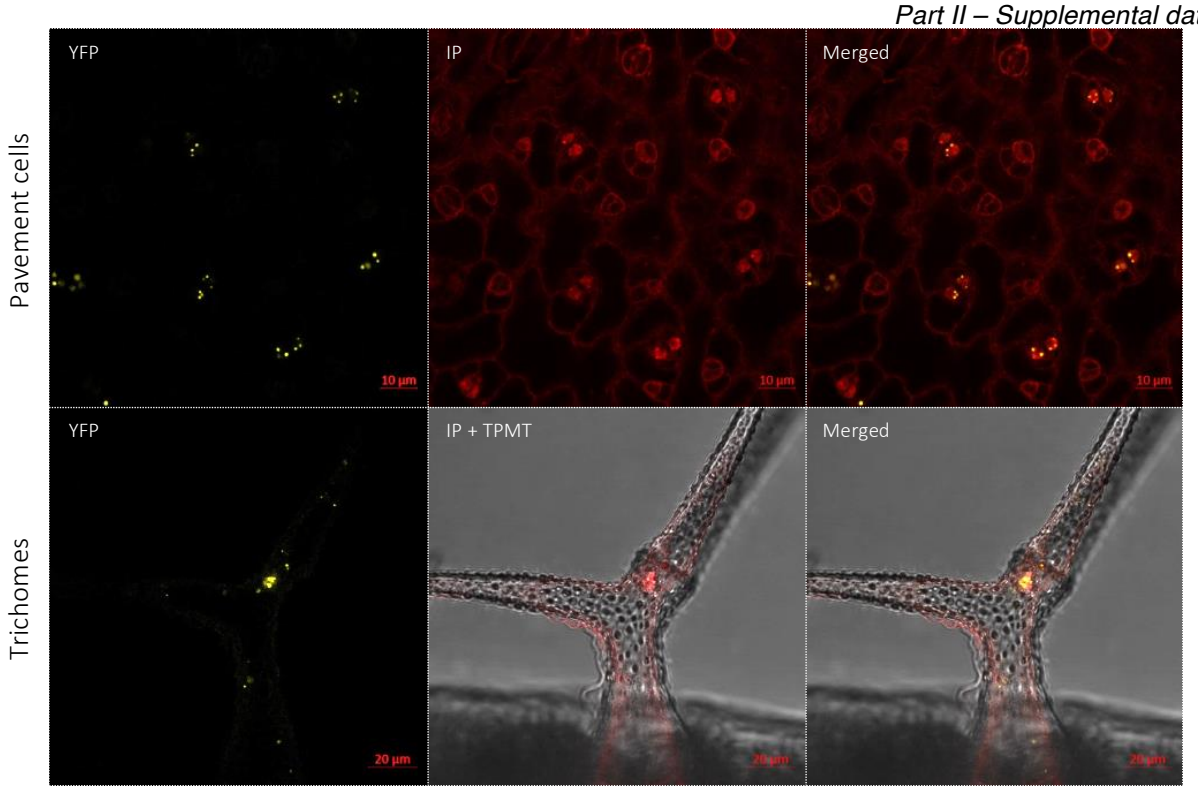

Supplementary Figure 26: **Subcellular localization of SlGBP10 in *Arabidopsis thaliana* leaves.** SlGBP10 expressed under a constitutive p35S promotor and fused in Nterm with YFP. Stainings were performed on fresh tissues. Propidium iodide (red) was used to stain membranes. Yellow is YFP.

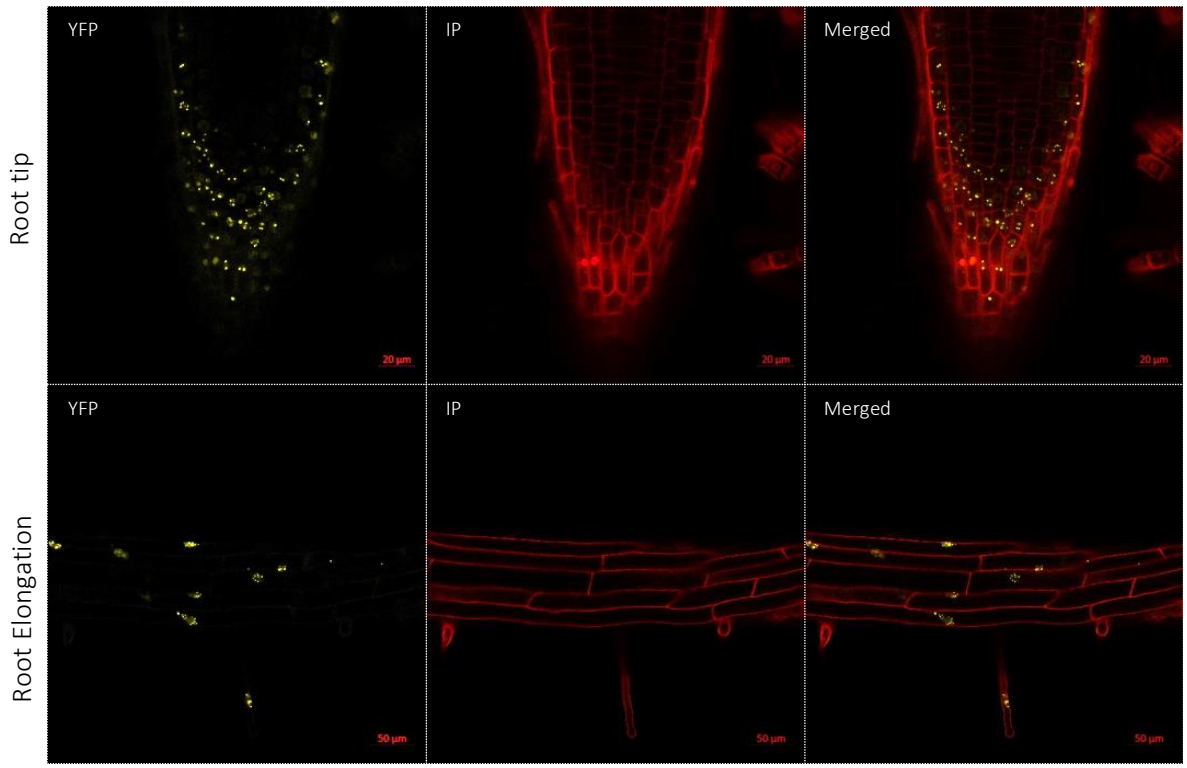

Supplementary Figure 27: **Subcellular localization of SlGBP10 in *Arabidopsis thaliana* root.** SlGBP10 expressed under a constitutive p35S promotor and fused in Nterm with YFP. Stainings were performed on fresh tissues. Propidium iodide (red) was used to stain membranes. Yellow is YFP.

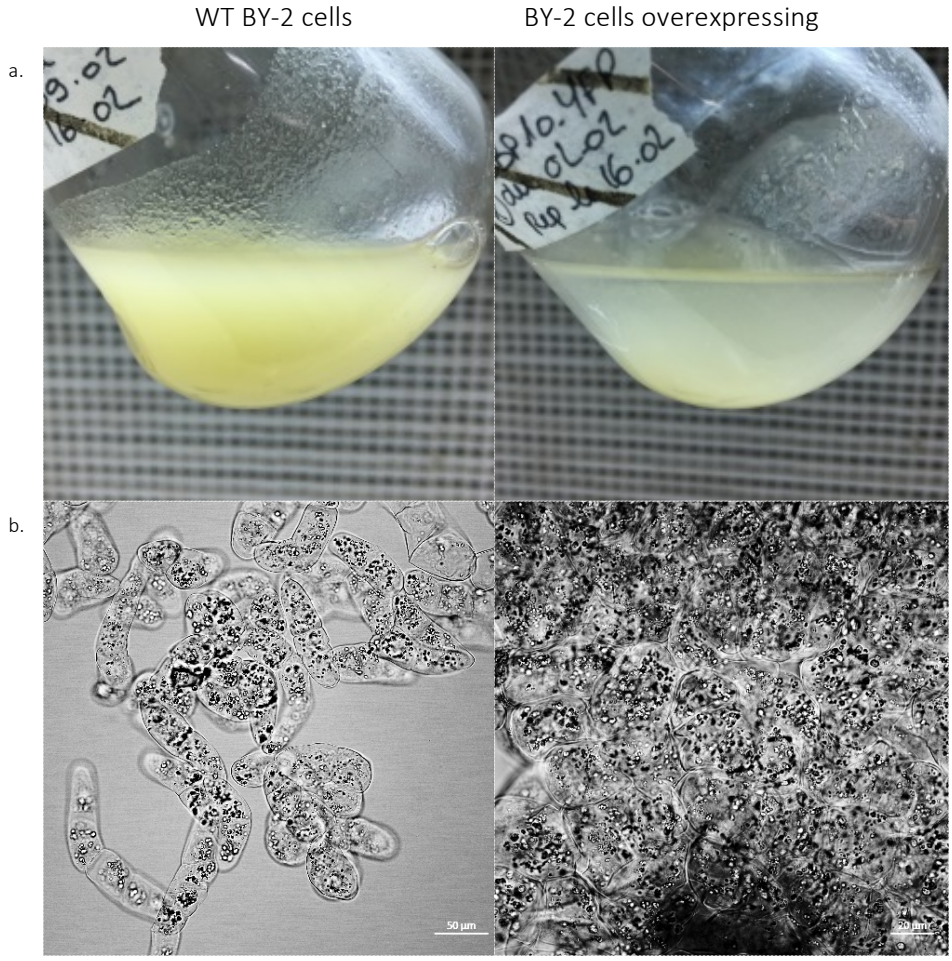

Supplementary Figure 28: **BY-2 cells culture, overexpressing SlGBP10**. a. 7-days old BY-2 cell cultures. b. Aspects of 3 days-old BY cells, observed under transmitted light.

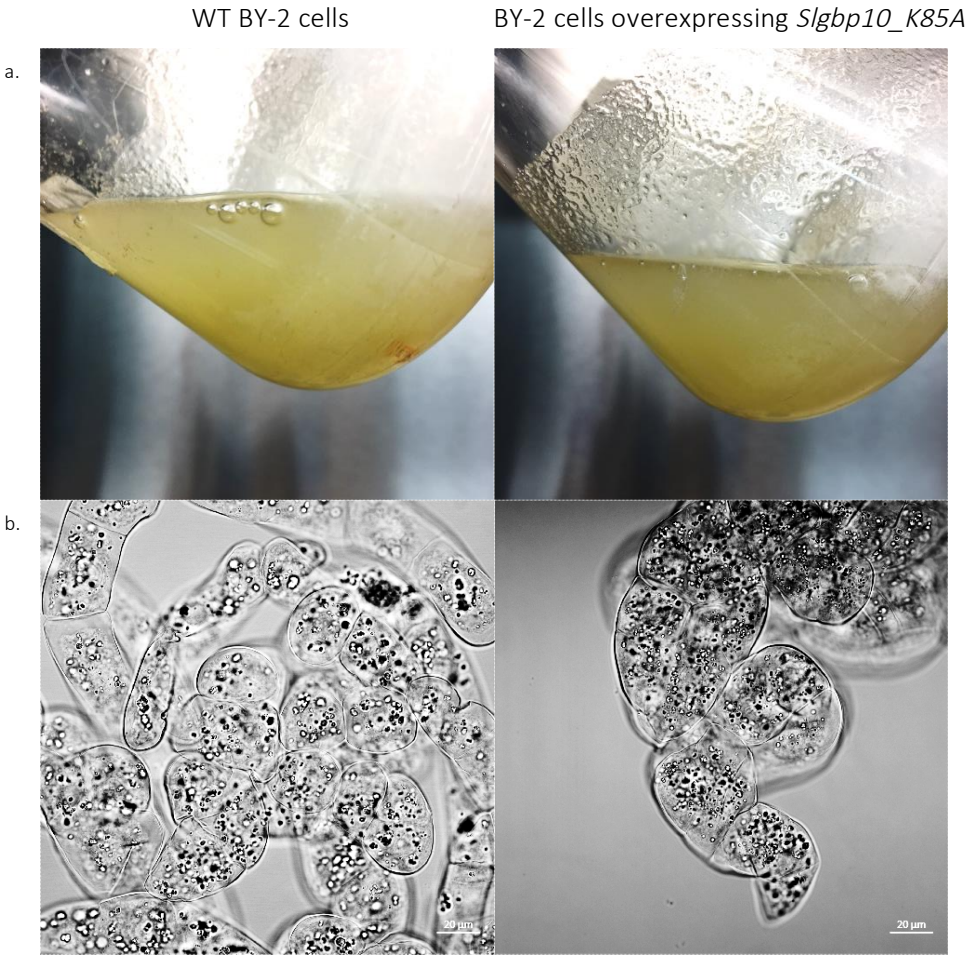

Supplementary Figure 29: **BY-2 cells culture overpressing *Slgbp10_K85A***. a. 7-days old BY-2 cells cultures. b. Aspects of 3 days-old BY cells, observed under transmitted light.

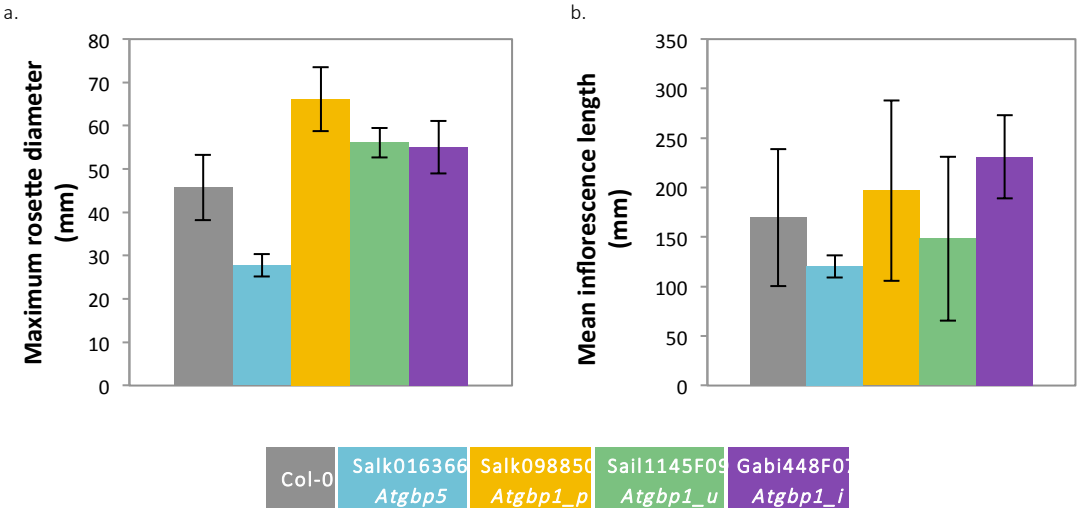

Supplementary Figure 30: **Rosette and inflorescence size in the *Arabidopsis* T-DNA mutants.** a. Rosette diameter. b. Inflorescence length . (Error bar: standard deviation, n=3)

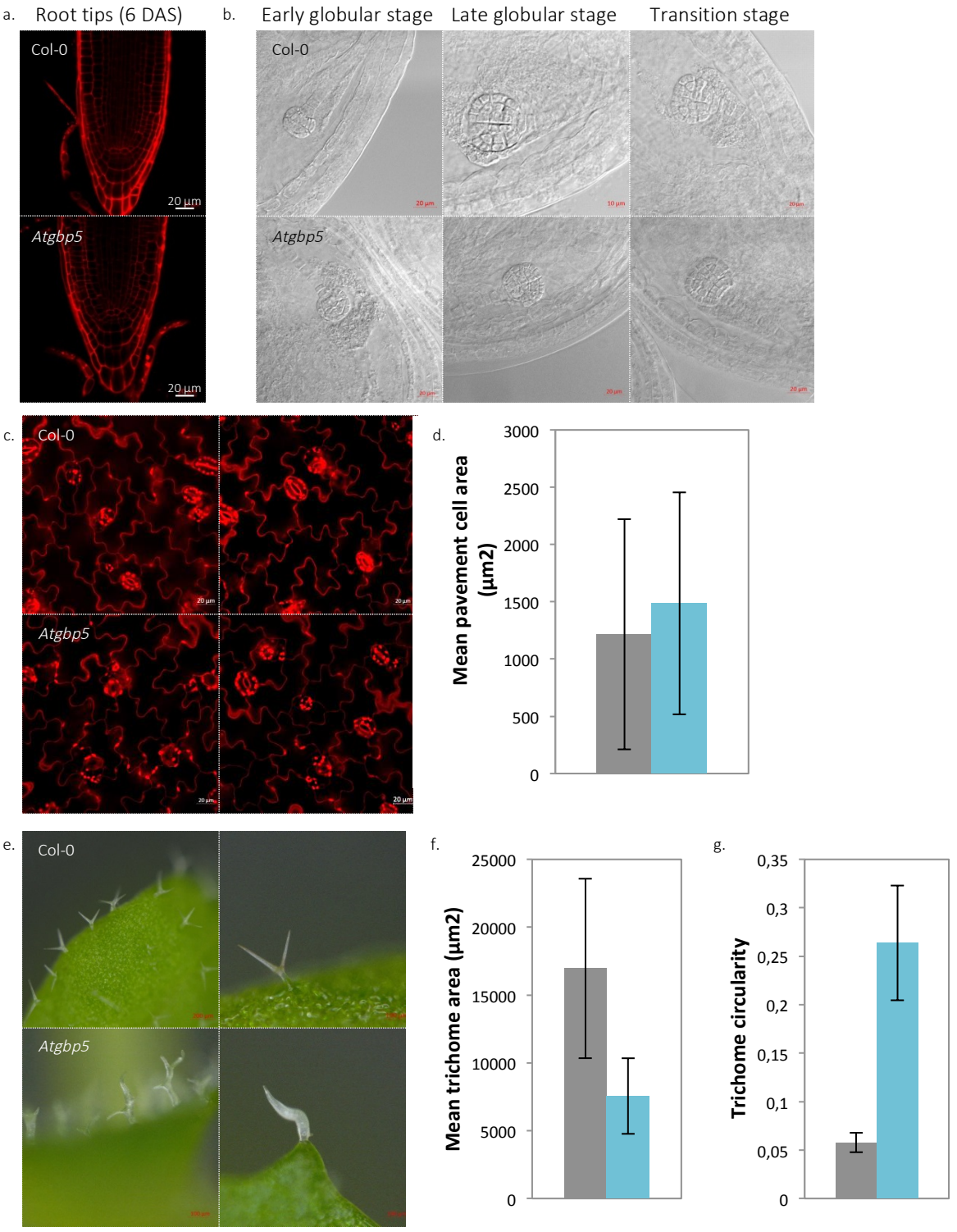

Supplementary Figure 31: **Looking for cell division alterations in *Atgbp5* T-DNA mutant.** a. Six days-old root tips stained with propidium iodide (PI). b. Embryo development. c. Cotyledon pavement cells stained with PI. d. Mean pavement cell area. e. Leaf trichome shape. f. Leaf trichome area. g. Leaf trichome circularity. (Error bar: standard deviation, n=3)

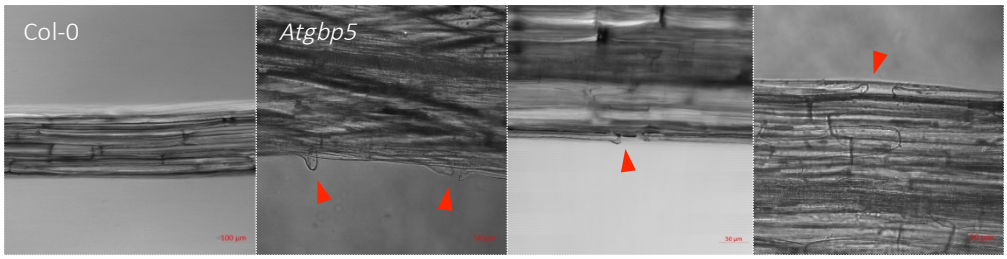

Supplementary Figure 32: **Elongated hypocotyl in Col-0 and *Atgbp5 T-DNA* mutant**. Red arrow-heads indicate non cohesive cells.

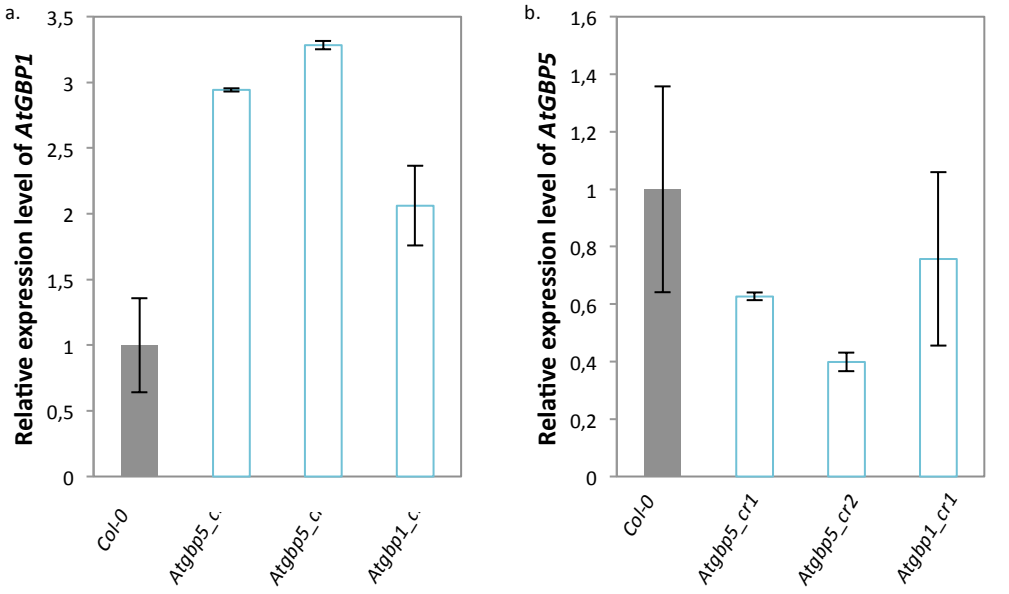

Supplementary Figure 33: **Relative expression level of *AtGBP1* and *AtGBP5* in the CRISPR mutants.** a. Relative expression level of *AtGBP1*. b. Relative expression level of *AtGBP5*. (Error bar: standard deviation, n=3)

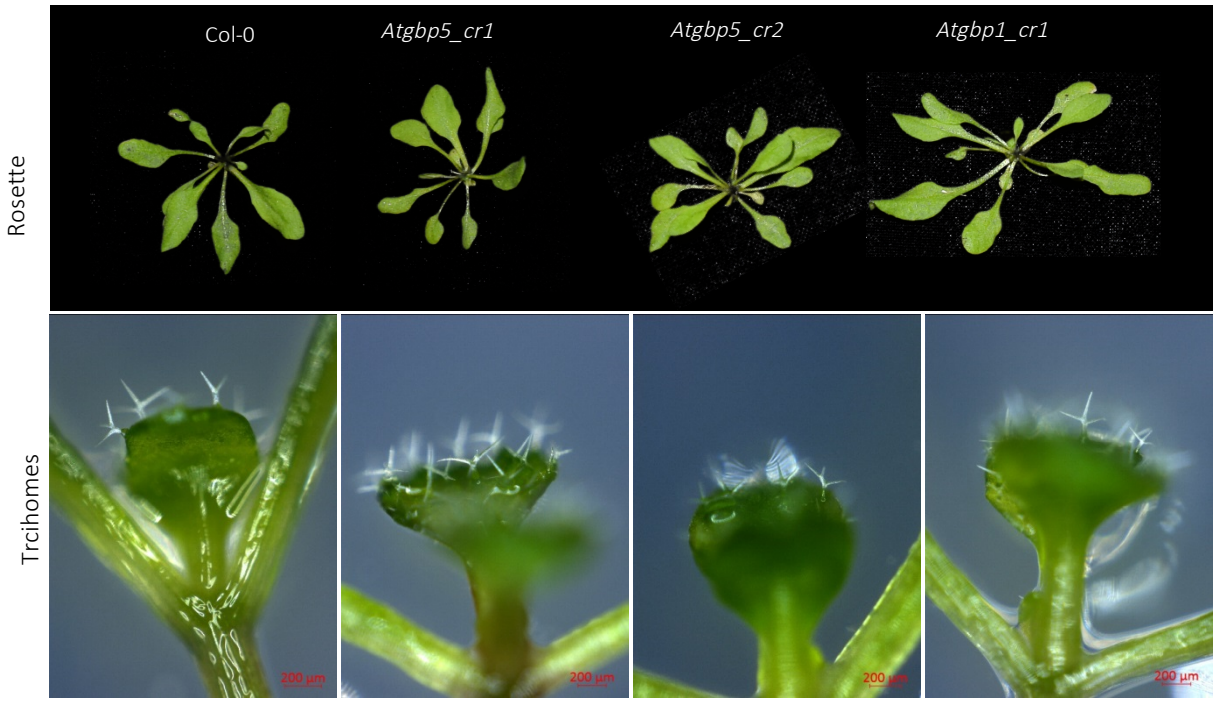

Supplementary Figure 34: **Rosette size and trichome aspect in the *Arabidopsis* CRISPR mutants**

Chapter IV

–

CONCLUSIONS & PERSPECTIVES

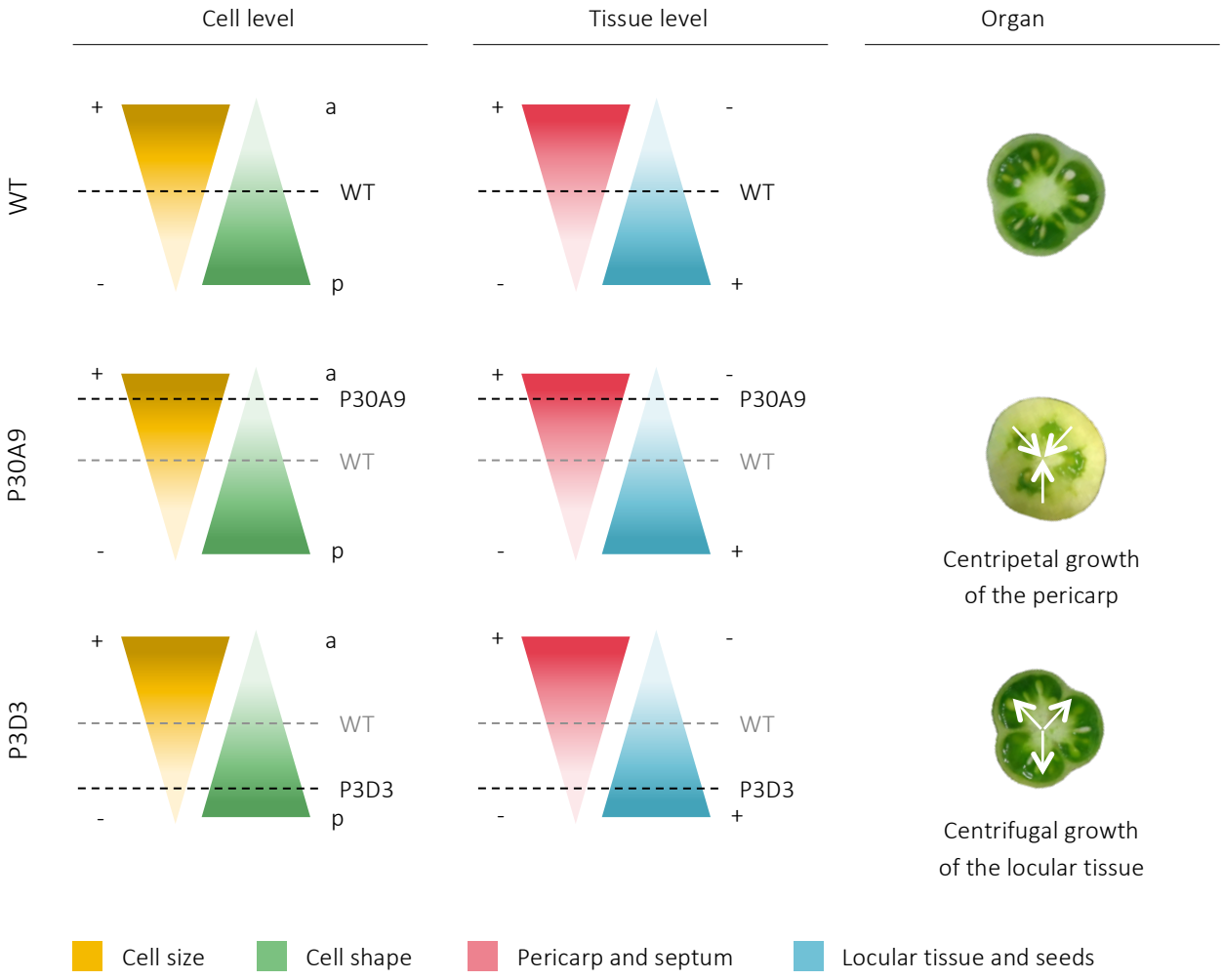

Figure 61: **Proposed model of the compensatory mechanisms at the cell, tissue and organ level.** Each phenotypic characteristic is represented by a triangle. a, means anticlinal expansion, p, means periclinal expansion.

I. Is fruit tissue morphology governing by a final fruit size control?

During this study, we have seen that the use of induced variability in Micro-Tom background allowed selecting phenotypes of interest for the understanding of tissue morphology control in tomato fruit. The multi-scale phenotypic characterization of P30A9 and P3D3 mutants along fruit growth highlighted molecular and cellular alterations, associated with changes in pericarp tissue morphology. However in these mutants, the pericarp alterations did not induce fruit size modification, but were associated with changes in locular tissue and seed development (Figure 61). These results suggest that it may exist an organ size control, allowing compensation mechanisms between fruit tissue in order to reach the expected final fruit size. This notion was therefore described by Sugimoto-Shirasu & Roberts (2003), who proposed that plant cell size may be determined at the organ level through a total organ-size checkpoint that balances cell proliferation and cell growth. This conceptual understanding of growth was first explained in animal models, in which experimental data suggested that organ size might be regulated by a "total mass checkpoint" mechanism which functions to link the regulation of cell size and cell proliferation (Potter and Xu, 2001). Plants would also set up mechanisms to keep organ size constant. This is indeed the case in plants, in which a decrease in cell proliferation is compensated by an increase in cell size. As an example, the *Arabidopsis* mutant *swp* exhibits a dwarf phenotype that can be attributed to a reduced cell number (Autran *et al.*, 2002). In leaves, this dwarf phenotype is partially compensated by an increase in cell size, which is correlated with higher endoreduplication. In contrast, petals of the *Arabidopsis swp* mutant, that do not undergo endoreduplication, are not able to compensate. This suggests that endoreduplication is a compensatory mechanism that operates to maintain leaf size at least in this mutant (Autran *et al.*, 2002).

By taking the example of P30A9 mutant, the enhancement of endoreduplication were associated with large and elongated mesocarp cells and centripetal growth of the pericarp, in order to guarantee the expected final fruit size. Indeed, in this mutant, locular tissues and seeds were reduced, suggesting an early limitation of growth. At the organ scale, this leads to the integration of the information and set up of compensatory mechanisms inducing pericarp and septum upgrowth (Figure 61). In contrast to petal, the locular tissue also is able to undergo endoreduplication. However, this tissue remained limited, suggesting that the compensatory mechanisms are fine regulated between the different tissues through their

communication, to ensure their coordinated growth. In the fruit system, the cuticle, closely related to the outmost epidermal cell layers may also have an important role in the ability of fruit growth. Indeed, the epidermis may impose mechanical constraints to the centrifugal growth of the inner fruit tissue, including the pericarp (Savaldi-Goldstein *et al.*, 2007; Bargel and Neinhuis, 2005).

The mutation of the Guanylate Binding Protein in P3D3 mutant induced various cellular disorders, associated with a reduction in final pericarp cell size and pericarp thickness. This mutant presented more seeds together with a more important progression of the locular tissue, probably in order to compensate lower endoreduplication in the pericarp. We suppose that because of the centrifugal growth of the locular tissue and of the constraint imposed by the epidermis, the pericarp has no more space, to sustain the growth recovery associated with the late restart of division in the pericarp. As a result, the pericarp is flattened (Figure 61). In this context, as for the P30A9 fruit growth, the epidermis may play the role of a mechanical constraint that prevents fruit growth to beyond the expected final fruit size (WT Micro-Tom fruit size in this case).

So, locular tissue and seeds seem to display an opposite growth pattern compared to that of the pericarp and septum, in these mutants. This suggests that variations in fruit tissue morphology involved probably compensatory mechanisms between pericarp and locular tissue in view to reach the normal final fruit size. The fruit tissue morphology variations also seem to be associated with variation in seed number. However, seed number is determined very early during fruit growth, suggesting that the compensatory mechanisms are at least in part determined early. This may imply a tight molecular and cellular coordination between fruit tissues.

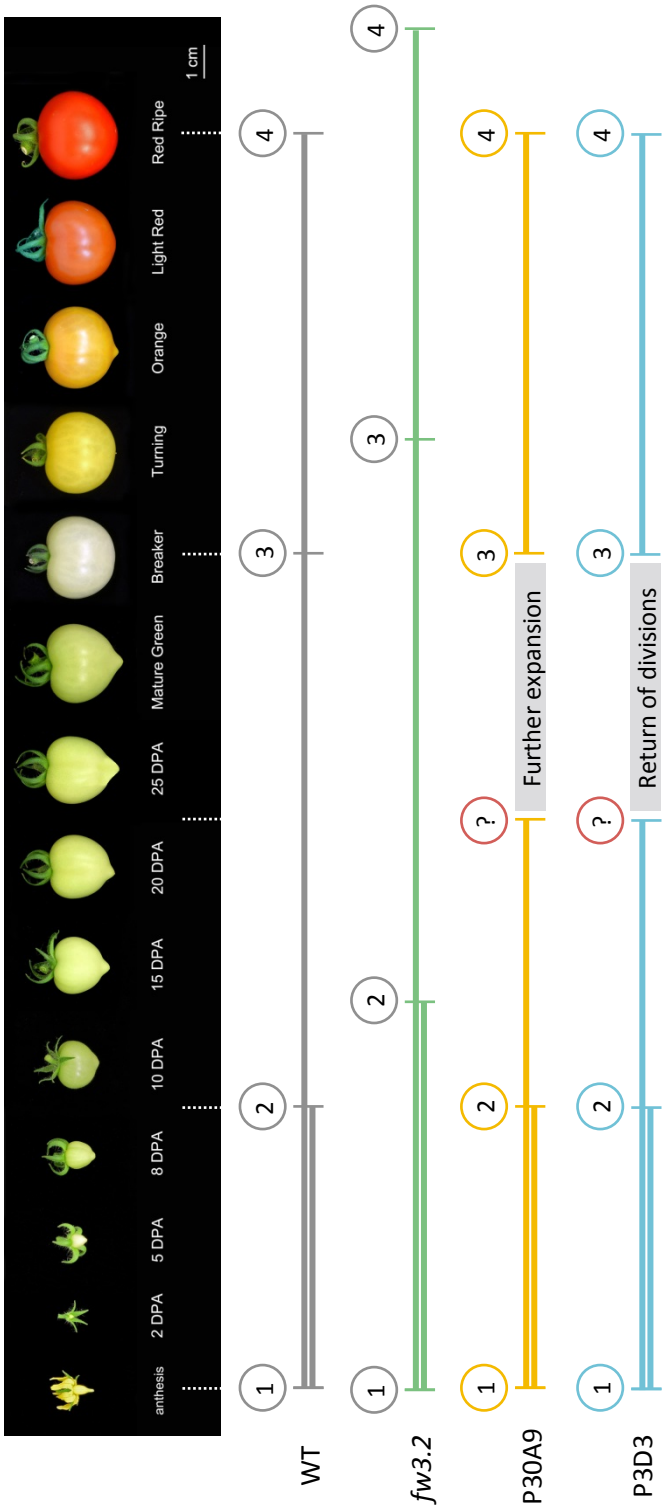

Figure 62: **Proposed model of the growth timing controls in P30A9 and P3D3 mutants.** The growth timing controls are represented by the circles. 1. Beginning of cell division and cell expansion. 2. End of cell division. This timing is expected to occur between 8 and 10 DPA in Micro-Tom, but was not measured in the mutants. 3. End of cell expansion and beginning of ripening. 4. End of ripening. ?. Unknown late control.

II. Is pericarp tissue morphology set up at late stage of fruit growth?

One interesting aspect of this study is the observation of late molecular (ploidy level) and cellular alterations of the pericarp tissue. In both P30A9 and P3D3 mutants, alterations were only visible from 20 DPA. No changes in pericarp cell ploidy level, size or shape were observed at the beginning of fruit growth. These results suggest a late set up of cellular mechanisms inside the pericarp, during the cell expansion phase.

During normal growth (in WT Micro-Tom), the expected cell size was almost reached before breaker stage around 20 DPA, for most of the cells, as growth rate was reduced after 20 DPA. Once a cell has reached its final size, the cell may enter into a developmental process not associated with further rounds of endoreduplication and volume expansion, before ripening. As for both studied mutants, modifications were visible after 20DPA at the tissue level; it suggests that tissue morphology is setting up at late stage of fruit growth. Indeed, an additional expansion period, through additional extend of endoreduplication, allowed the pericarp cells to reach very high ploidy levels, associated to large and elongated cells in the thick pericarp mutant. Similarly, an early exit from endoreduplication, with the switch into endomitosis and/or (a)mitosis induces tissue morphology change in the thin pericarp mutant. Late unknown controls are supposed to have an important role in regulating the extent of growth and so tissue morphology. These controls may be associated to early or late exit in endoreduplication (Figure 62).

Interestingly, these alterations during the cell expansion phase did not seem to impair the beginning of fruit ripening. For example, the pericarp of the mature fruit carrying the large fruit allele *fw3.2* showed extra cell divisions, leading to enlarged fruit and a concomitant delay in ripening. The delay in ripening was likely the result of an extension of the cell division stage (M. Chakrabarti *et al.*, 2013) (Figure 62). In the case of P30A9 and P3D3 mutants, the control of the beginning of ripening remains intact.

These observations offer novelty in the conceptual understanding of the fruit growth control. It is commonly established that most of the determinants governing fruit growth were established early during flower and first period of fruit development (Fernandez *et al.*, 2007; Frary *et al.*, 2000; Van der Knaap *et al.*, 2014). This study proposes that a control of late events determine also fruit growth through fruit morphology variations and highlights new insights about the genetic, cellular and molecular regulations of the cell expansion phase. Late decision during cell expansion may be determinant in order to reach the expected final fruit size. Thus, late cellular events may allow modify the tissue morphology before the beginning of ripening.

Chapter V

–

MATERIALS & METHODS

I. Biological materials

I.a. Plant materials and growth conditions

- *Micro-Tom culture*

Micro-Tom plants were grown in greenhouse in controlled conditions as described in Rothan *et al.* (2016). Flowers were regularly vibrated to ensure optimal self-pollination and thus fruit development. In order to take into account the fruit phenotypic plasticity in changing environmental conditions (mainly due to seasonal variations), the WT Micro-Tom was cultivated side-by-side with the mutant lines and used as a reference. In addition, for all the lines, the first flower from each inflorescence was removed to take into account the high incidence of abnormal fruits produced by this flower in Micro-Tom. Therefore, fruit load on the plant was reduced to six fruits per inflorescence. Micro-Tom were also cultivated *in vitro* under sterile conditions, on a Murashige and Skoog medium (Murashige and Skoog, 1962) diluted two times (MS ½), in photoperiod conditions of 16 hours of day / 8 hours of night and maintained at 22°C. Seeds were previously decontaminated with sodium hypochlorite 4.5% (v/v) and 0.05% (v/v) of Tween 20, for 15 minutes and then three times washed with sterile water.

- *Arabidopsis thaliana culture*

The WT *Arabidopsis thaliana accession* used in this study is Columbia-0 (Col-0). *Arabidopsis thaliana* plants were first grown *in vitro* under sterile conditions on a Murashige and Skoog medium (Murashige and Skoog, 1962) diluted two times (MS ½). Seeds were decontaminated in sodium hypochlorite 5% (v/v) during 5 min and rinsed at least three times with sterile water. After cold treatment at 4°C for at least 24 hours in the dark, seeds were placed in a growth chamber at 22°C with a 16 hours light /8 hours darkness cycle. After 10 days of growth, the plantlets were transferred to adapted soil in the greenhouse. Plants were maintained under mini-greenhouse for at least four days in order to allow acclimatization. In the greenhouse, plants were watered once a week at 24°C during day and 18°C during night with 75% of hygrometry. When the siliques began to dry, watering was stopped.

- *Tobacco culture*

Tobacco plants were grown in the greenhouse, watered by drip 4 times a day during 2 min, at 24°C during day and 18°C during night with 75% of hygrometry.

I.b. Tobacco BY-2 cell culture

The tobacco BY-2 (*Nicotiana tabacum* L. cv. Bright Yellow-2) suspension cells were maintained by transferring 2 mL of 7 days-old suspension in 50 mL of an adapted Murashige and Skoog medium, according to Porceddu *et al.* (2001) (MS basalt salt mixture supplemented with 30 g/L of sucrose, 0,2 g/L of KH_2PO_4, 50 mg/L of myo-inositol, 250 µL of thiamine at 10mg/mL and 20 µL of 2,4-D at 10 mg/mL – pH 5,8). Cells were cultured at 25 °C and 130 rpm shacking in the dark. BY-2 cells were also maintained as callus, petri dishes containing the adapted MS medium with 1% agarose. A part of the callus is transferred to a fresh medium one in a month.

I.c. Bacteria and growth conditions

Escherichia coli strain (E. coli) TOP10 (Invitrogen) or DH5α were used for cloning and propagation of the different plasmids. *Agrobacterium tumefaciens* strain (GV3101 or PMP90) were used as a vector of transformation to generate transgenic plants. The set of strains of *E. coli* were cultured at 37°C and that of *Agrobacterium tumefaciens* were grown at 28°C. All bacterial strains were grown in LB medium (Bactotryptone 1% (w/v); yeast extract 0.5% (w/v); NaCl 1% (w/v)) with or without antibiotics. The nature and concentration of the antibiotic used are determined by the resistance gene carried by the plasmid of interest (Table 8).

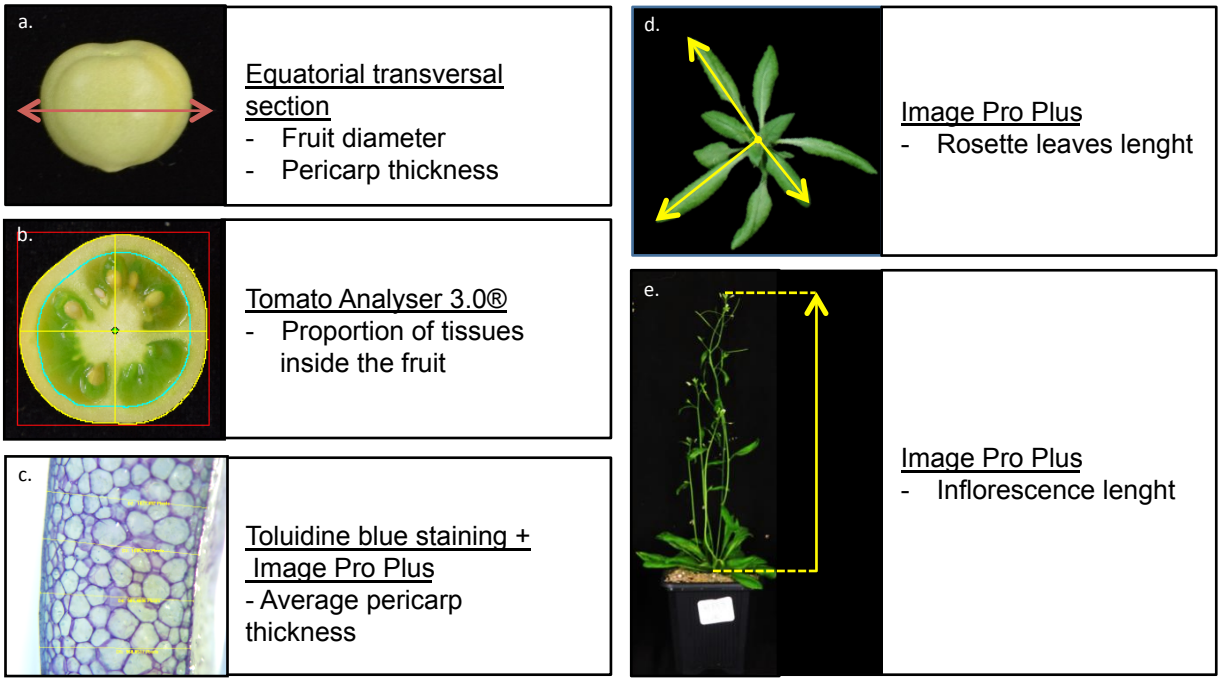

Figure 63: **Plant characterizations at the organ level**. a. Fruit diameter and pericarp thickness are measured on an equatorial transversal section. b. The proportion of each tissue inside the fruit is measured using Tomato Analyser software. c. Pericarp thickness is measured on pericarp section stained with toluidine blue. d. Rosette size is estimated by measuring three rosette leaves from the center of the rosette to the extremity of the leaf. e. Inflorescence length is measured from the bottom of the rosette to the top of the longest inflorescence.

II. Phenotypic characterizations

II.a. Tomato fruit characterization

- *At the organ level*

Tomato fruit characterization at the organ level includes measurements of fruit size and pericarp thickness that were performed at different stage of fruit growth, from anthesis to breaker stage. The average size of fruit from each plant was determined by weighing 6 fruits per plants, or measuring the fruit diameter at the equatorial fruit plan of 3 fruits (Figure 63.a). Pericarp thickness was estimating by analyzing pictures of equatorial transverse sections with the Tomato Analyzer 3.0® software (Brewer *et al.*, 2006) or after toluidine blue staining using the Image Pro® software (Figure 63.b).

- *At the cell level*

Pericarp cellular measurements were performed on equatorial sections, from pericarps a different stage of fruit growth. Pericarp sections were fixed with FAA (Formaldehyde Acetic Acid) and then cut using a vibrating blade microtome (Microm 650V®). A section from 30 µm to 150 µm, depending of the fruit stage, was further stained with calcofluor 0,01%. Calcofluor is a fluorescent dye, which specifically bounds with plant cell walls and emits a fluorescent signal under UV lamp excitation. Stained sections were observed under an epifluorescence microscope (Zeiss Axiophot®) or a confocal microscope (Zeiss LSM880®). Image analyses (excluding vascular tissues) were performed using 2 softwares: Cell SeT® (Pound *et al.*, 2012) for cell segmentation and Image Pro Plus® to automatically integrate segmented images in view to obtain various cell measurements (cell number, cell area, cell diameter and cell roundness) (Figure 64.a).

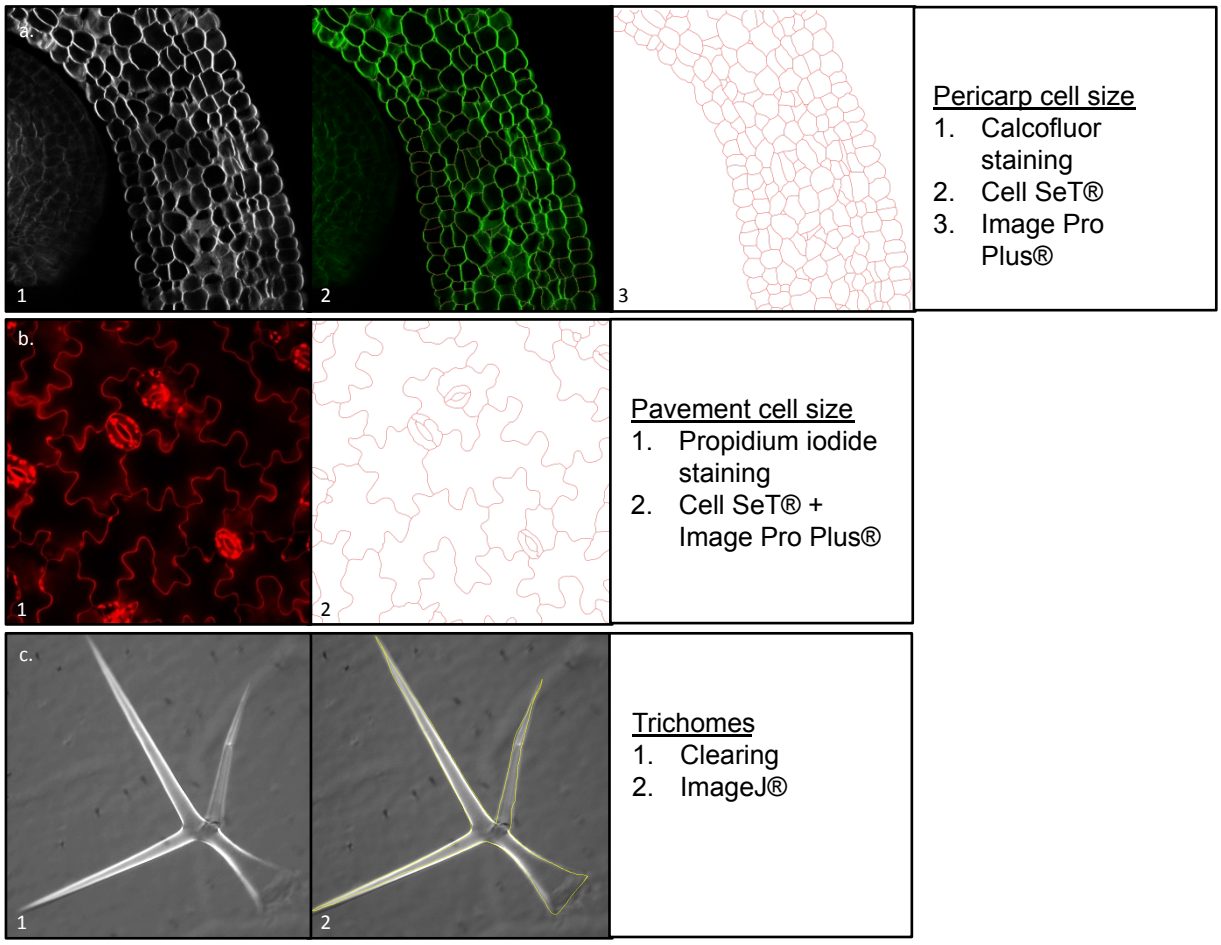

Figure 64: **Plant characterizations at the cell level**. a. Pericarp cells area was measured on a portion of pericarp stained with calcofluor. Cells where then redraw using Cell Set software and measurement were obtained using Image Pro Plus. b. *Arabidopsis* pavement cells size were measured on cotyledons stained with propidium iodide, with the help of Cell Set and Image Pro Plus software. c. Trichomes size were measured on leaves cleared with a solution of chloral hydrate and then using ImageJ.

II.b. Arabidopsis thaliana characterization

- At the organ level

Arabidopsis thaliana characterization at the organ level includes measurements of rosette leaves and inflorescence size that were performed at different stage of development (Figure 63.e). Each plant was compared with a Col-0 accession that had been sown at the same date and who grew up under the same conditions. This served as a control for each measured parameters. Pictures are analyzed using Image Pro Plus® software.

- *At the cell level*

For root and trichomes characterization, *Arabidopsis* plantlets were imaged under the macroscope Axiozoom® (Zeiss) or the binocular (Olympus SZX16®). For embryo characterization, siliques were dissected under the binocular (Olympus SZX16®) and ovules were transferred on a slide. Clearing was made with a solution of chloral hydrate, directly under the coverslip. Embryos were observed under the microscope Axiophot (Zeiss®). Pavement cell and trichomes area were determined by drawing the outline of the cell using Cell SeT® (Pound *et al.*, 2012) or ImageJ software, respectively (Figure 64.b, 64.c).

II.c. Interpretation of the phenotypic differences between genotypes

Considering the small number of observations (n=3), as well as the wide range of variability in the majority of the variables measured, the p-values given by the a non-parametric test (Wilcoxon test) were often superior at 0,05%, resulting in no-significant differences. In this context, the interpretation of the phenotypic differences observed between genotypes was based on the interpretation of trends.

III. Manipulation and analysis of nucleic acids

III.a. Nucleic acids extraction

- *DNA extraction*

For genotyping of segregant populations, genomic DNA extractions were performed on collection microtubes (racked, 10x96) (Qiagen), on around 50 mg of tomato leaves or 2 leaves of *Arabidopsis* rosette. For routine genotyping, the genomic DNA extraction of tomato or *Arabidopsis thaliana* was done from young leaves using of DNAzol solution (Sigma) and following the protocol recommended by the manufacturer.

Plasmid DNA was extracted from 5 mL or 50 mL of stationary phase culture growth, using respectively PureYield™ Plasmid Miniprep System (Promega) or Wizard® Plus Midipreps DNA Purification System (Promega), according to the protocol described by the provider. Depending on the system used, the plasmid DNA was eluted in 50 µL or 500 µL of sterile mQ water and quantified by measurement of absorbance at 260 nm via a spectrophotometer.

- *RNA extraction*

RNA extractions were extracted from fruit pericarp or *Arabidopsis* plantlets. Samples were cold grounded manually using a pestle, or mecanically using a Dangoumau® grinder, in liquid nitrogen. Between 50 to 120 mg of fresh tissue was used for RNA extraction, following the TRIzol® Reagent protocol recommended by the manufacturer (http://tools.lifetechnologies.com/content/sfs/manuals/trizol_reagent.pdf). Sodium acetate and DNase treatments (Ambion® RNA TURBO DNA-freeTM protocol) were then performed on RNA samples, in order to reduce polysaccharide content and to avoid DNA contamination, respectively. RNA quality is controlled by electrophoresis on agarose gel. In order to control the presence of contaminations by DNA, a PCR was performed on RNA samples with primers targeting a gene sequence. The absence of amplification makes it possible to consider the contamination as negligible and having no

impact for expression analyses. Reverse transcription reaction of 1 µg of RNA was achieved using the i-Script™ Bio-Rad protocol (http://www.bio-rad.com/webroot/web/pdf/lsr/literature/10020178.pdf).

III.b. Polymerase Chain Reaction (PCR)

Routine PCR reactions were performed with GoTaq® DNA Polymerase (Promega), according to the conditions recommended by the supplier from gDNA, cDNA or DNA purified plasmid. In the case of amplifications for cloning experiments, the PCRs were carried out with the PrimeStarMax kit (Takara) to minimize the risk of sequence errors. PCRs were performed on the C1000 Thermal Cycler® (Biorad).

III.c. Genotyping using KASPAR technology

Recombinant analysis of the F2 segregant population was performed using the KASPAR technology. KASP™ genotyping assays are based on competitive allele-specific PCR and enable bi-allelic scoring of single nucleotide polymorphisms (SNPs). The KASP Assay mix consists of two competitive, allele-specific forward primers and one common reverse primer. Each forward primer incorporates an additional tail sequence that corresponds with a universal FRET (Fluorescence Resonant Energy Transfer) cassette: one labelled with FAM™ dye and the other with HEX™ dye. Bi-allelic discrimination is achieved through the competitive binding of the two allele-specific forward primers (Table 6). If the genotype at a given SNP is homozygous, only one of the two possible fluorescent signals will be generated. If the genotype is heterozygous, a mixed fluorescent signal will be generated.

Kaspar mix was performed following the protocol recommended by the manufacturer. Plates were read on the Light Cycler 480 II® (Roche) and results were then manually exported to an Excel table for analysis.

Position	Allele WT	Allele Mut	Oligo Name	Sequence 5' to 3'
55267208	T	A	c10-55267208F1	gaaggtgaccaagttcatgctTGTCAAGAGATCACCGTAATGGATGT
			c10-55267208F2	gaaggtcggagtcaacggattTCAAGAGATCACCGTAATGGATGA
			c10-55267208R	GCAAGGAATTTCGCAACAAGAGTTG
56249927	C	T	c10-56249927F1	gaaggtgaccaagttcatgctTCAAAGGTTGATGCGCGTATATTAC
			c10-56249927F2	gaaggtcggagtcaacggattTCAAAGGTTGATGCGCGTATATTAT
			c10-56249927R	CTCGTTTTCTTATGCCTACAGAAGA
56772564	G	A	c10-56772564F	CCTTGTAACCTCCACTGTAAAACACC
			c10-56772564R1	gaaggtgaccaagttcatgctGGCTGAAGGTATTTTGGATAAGCG
			c10-56772564R2	gaaggtcggagtcaacggattTGGCTGAAGGTATTTTGGATAAGCA
57030305	C	T	c10-57030305F1	TTTTGTCATTCTTTAACACCCTAC
			c10-57030305F2	TTTTGTCATTCTTTAACACCCTAT
			c10-57030305R	CACCAATTGTTAAGCACTGGACGTG
57893426	C	T	c10-57893426F1	gaaggtgaccaagttcatgctTCAATGGGTTATAAACACTTCAC
			c10-57893426F2	gaaggtcggagtcaacggattTCAATGGGTTATAAACACTTCAT
			c10-57893426R	TTCAATGATGCCAAAAGAGGGAAGA
58145149	T	A	c10-58145149F1	gaaggtgaccaagttcatgctTGATTTCTAGCAGGTTTTATGTATCT
			c10-58145149F2	gaaggtcggagtcaacggattTGATTTCTAGCAGGTTTTATGTATCA
			c10-58145149R	TCATGTCAAACGGGTGTTACATGAT
60893671	G	A	c10-60893671F1	gaaggtgaccaagttcatgctACCAGGTATTAATACGGGTTGTG
			c10-60893671F2	gaaggtcggagtcaacggattACCAGGTATTAATACGGGTTGTA
			c10-60893671R	AAAGAAATACTTATCACTTTATCAGAACGA
61017351	T	A	c10-61017351F	TGACCAATATTTTTCATGACATGTAAACC
			c10-61017351R1	gaaggtgaccaagttcatgctTAGCAATGCATCTTCCGACATGA
			c10-61017351R2	gaaggtcggagtcaacggattTAGCAATGCATCTTCCGACATGT
63354209	A	T	c10-63354209F1	TGCATGTACATCCAGAAGCAACA
			c10-63354209F2	TGCATGTACATCCAGAAGCAACT
			c10-63354209R	GCAGCTGCAATGTAAAAGCTTATTCA

Table 6: **List of KASPAR primers on chromosome 10, designed for the recombinant analysis of P30A9 mutant** (Part 2) Bases write in minuscule letters correspond to the sequence of the FRET tails (gaaggtgaccaagttcatgct: FAM™ dye, gaaggtcggagtcaacggatt: HEX™ dye).

Targeted gene	Primer	Sequence (5' to 3')
AtGBP1	AT1-1qF	ACGGGGCATTCGAAATACAC
	AT1-1qR	AAACGGTGCGTTCATAGAGC
	AT1-2qF	CTGAGTTGGTCGGGTTAAAG
	AT1-2qR	TCCAAGAACGAGAAACTTGACC
AtGBP5	AT5-1qF	CTTAGAGGACAAGACTCTGTAC
	AT5-1qR	TCGGTTTACTTTCTGCAGTACC
	AT5-2qF	GATCACGGTCCTACTGATGAAG
	AT5-2qR	ATGTCCACAATCGTACTTGGTC
Actin	qAct2-F	GGCTTAAAAAGCTGGGGTTT
	qAct2-R	CGAAAACAAAAAGGGAAA
EF1	qEF1-F	GTGAAGAAGGGTGCCAAATG
	qEF1-R	GCTCAAACGCCATCAAAGTT

Table 7: **List of qPCR primers**

III.d. Real-Time PCR

Real-time PCRs were performed in order to evaluate the transcripts accumulation of candidate genes in the different experiments (Table 7). The PCR amplification was realized in the presence of SYBR Green, a fluorescent intercalating agent of DNA, which can detect the presence of double-stranded nucleic acids in the reaction mix at each PCR cycle. The real-time recording of the emitted fluorescence allows visualizing the exponential phase of the PCR reaction, in which the signal is proportional to the amount of target present in the initial sample.

The RT-PCRs were realized using Kit GoTaq Master Mix® (Promega) according to the supplier's recommended conditions, and qPCR reactions were performed on the thermocycler CFX96 Biorad™. The primers were designed to amplify the 3'UTR region, which were specific of the gene targeted (Table 7). For each gene studied and to evaluate the efficacy of the reaction, a dilution range was made from the corresponding purified qPCR product. Samples in this range were subject to the same qPCR conditions. Expression normalization was performed from reference genes chosen for their relatively constant expression levels. Technical triplicates were made on each sample.

III.e. RNAseq analysis

Laser microdissection and RNA sequencing were performed at Cornell university in Collaboration with Joycelin Rose's lab as described in Martin *et al.* (2016). This transcriptomic study was performed using 10DPA pericarp on both the WT Micro-Tom and the P3D3 mutant. Samples were prepared in biological triplicates (3 different fruits/genotype), dissecting inner mesocarp cells and excluding vascular bundles.

Plasmid	Vector type	Promotor	Bacterial resistance gene	Plants resistance gene	Tag	Size (bp)	Used in this study for
pDONR201	Gateway vector	-	Kanamycin	-	-	4470	Entry vector
pDONR207	Gateway vector	-	Gentamycin	-	-	4470	Entry vector
pGWB460	Gateway vector	35S	Spectinomycin	Kanamycin	TagRFP Cter	12399	Overexpression / Localization
pGWB461	Gateway vector	35S	Spectinomycin	Kanamycin	TagRFP Nter	12398	Overexpression / Localization
pK7WGY2	Gateway vector	35S	Spectinomycin	Kanamycin	eYFP Nter	11876	Overexpression / Localization
pK7YWG2	Gateway vector	35S	Spectinomycin	Kanamycin	eYFP Cter	11880	Overexpression / Localization
pDGB3Ω1	Goldenbraid vector	pAT5g46070	Spectinomycin	Kanamycin	GFP Nter	14804	Expression/ Localization
pEn-Chimera	Gateway vector - sgRNA coding vector	-	Ampicillin	-	-	3738	CRISPR/Cas9
pDe-CAS9	Gateway vector - Cas9 expression vector	PcUbi	Spectinomycin	Kanamycin	-	15758	CRISPR/Ca9

Table 8: **List of vectors used in this study**

Primers	Cloning	Tageted gene	Sequence (5' to 3')
attB1-GBP10-FOR	Gateway	SlGBP10	GGGGACAAGTTTGTACAAAAAAGCAGGCTACATGAGGAGGCTATTCGGTAG
attB2-GBP10-REV	Gateway	SlGBP10	GGGGACCACTTTGTACAAGAAAGCTGGGTCCTATGATTTCTGGAGGACGC
attB2-GBP10-NS-REV	Gateway	SlGBP10	GGGGACCACTTTGTACAAGAAAGCTGGGTCTGATTTCTGGAGGACGC
GBP10_F	CRISPR/Cas9	SlGBP10	ATTGCAAGTGCCTCTGGATCGATC
GBP10_R	CRISPR/Cas9	SlGBP10	AAACGATCGATCCAGAGGCACTTG
GBP5_guide283_F	CRISPR/Cas9	AtGBP5 Exon 5	ATTGGACGTCGAAGGGTATGATCT
GBP5_guide283_R	CRISPR/Cas9	AtGBP5 Exon 5	AAACAGATCATACCCTTCGACGTC
GBP5_guide18_F	CRISPR/Cas9	AtGBP5 Exon 5	ATTGGCAATTTCTAAATAGTCACG
GBP5_guide18_R	CRISPR/Cas9	AtGBP5 Exon 5	AAACCGTGACTATTTAGAAATTGC
GBP1_guide330_F	CRISPR/Cas9	AtGBP1 Exon 1	ATTGGCCCGACCCGACTCGTCCGT
GBP1_guide330_R	CRISPR/Cas9	AtGBP1 Exon 1	AAACACGGACGAGTCGGGTCGGGC

Table 9: **List of primers used for cloning experiments**

IV. Molecular cloning

IV.a. Gateway cloning

Gateway vectors (Invitrogen) were used in this study (Table 8) because it allows efficient transfer of DNA fragments between plasmids, using a proprietary set of recombination sequences.

The sequence of interest that was further inserted into the destination vector was obtained from *Arabidopsis thaliana* or tomato cDNA by PCR amplification using the DNA polymerase High fidelity PrimeStarMax (Takara). Primers used for the amplification contain attB recombination sites that will be used for recombination into an entry vector (Table 9). Cloning the purified attB-PCR fragment, into the pDONR™ 201 or pDONR™ 207 entry vectors was achieved by the BP reaction (Invitrogen). The transformed bacteria were selected on LB medium in the presence of corresponding antibiotic (Table 10). Sequencing of the plasmid allowed verify if the sequence of interest was well inserted into the entry vector.

Then, its transfer into a destination vector was performed by the LR reaction. The presence of the sequence of interest in the plasmid carried by the selected bacteria was evaluated by PCR. Then the sequence of the inserted fragment was determined by sequencing. Expression vectors pK7YWG2, pK7WGY2, pGWB460 and pGWB461 were used for transient transformation in tobacco leaves and in stable transformations in tomato, *Arabidopsis thaliana* and BY-2 suspension cells (Table 8). These vectors allowed the overexpression of the sequence of interest and its subcellular localization, thanks to the fused tag.

IV.b. Cloning of customs CRISPRs

For generation of CRISPR KO lines, constructs and cloning procedures have been made according to Fauser *et al.* (2014). Protospacers had been designed using CRISPR-P (http://crispr.hzau.edu.cn/CRISPR2/) and CRISPOR (http://crispor.tefor.net/) websites that automatically highlight the PAM sequences (NGG) in the gene of interest and estimate possible off-targets. Criteria for protospacers definition were:

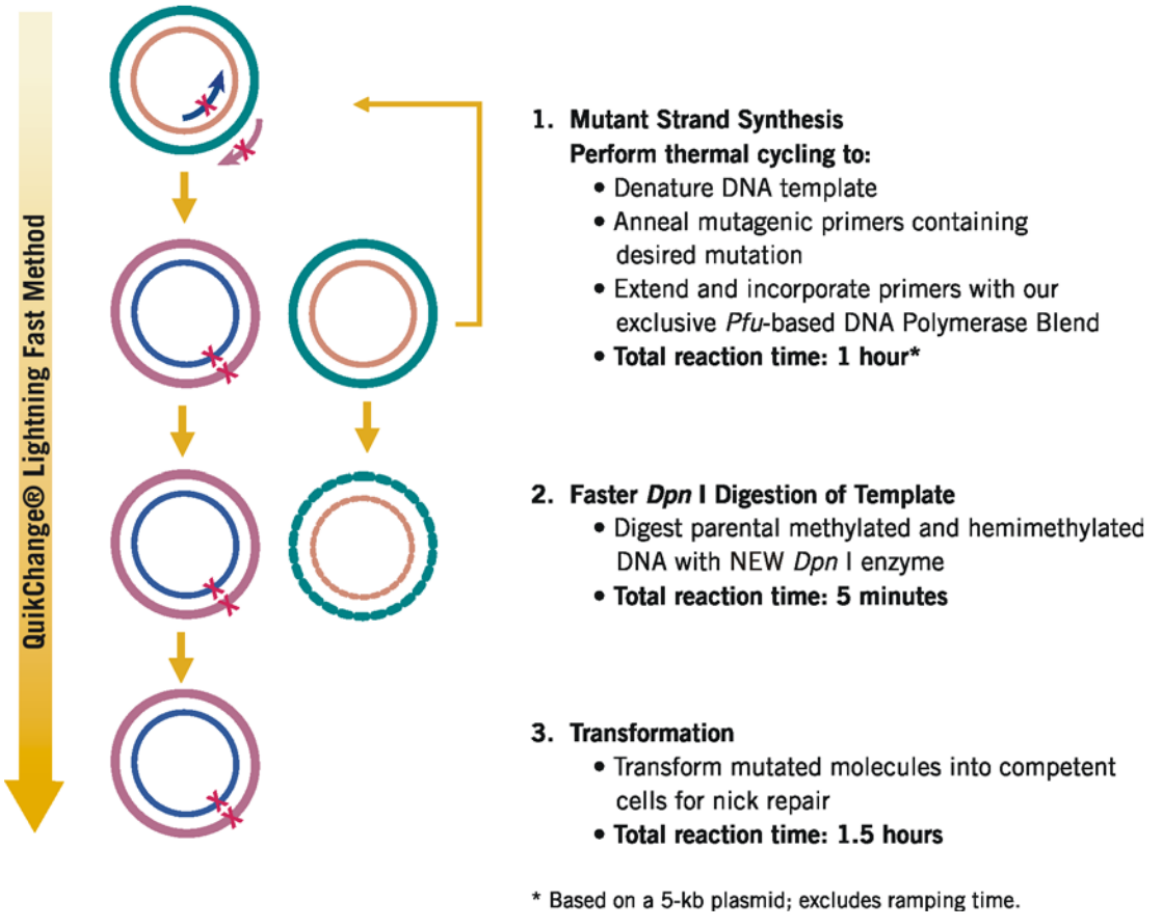

Figure 65: **Overview of the QuikChange Lightning site-directed mutagenesis method.** From Agilent Technologies website.

- Start of the sequence with a G, which is best for eukaryotes species,
- The binding site, in my case in preference on exon,
- A reduced number of possible off-targets.

Four bases ATTG or ACCC were added at the 5' end of the protospacer for forward and reverse primers definition, respectively (Table 9) which create the digestion and ligation sites.

The first step of the protocol consists in the oligo-annealing, for the generation for a double strand protospacer, at 5 min at 95°C and 20 min at room temperature. Next, the entry vector pEn-Chimera was digested with BbsI (NEB) restriction enzyme for one hour at 37°C. After purification, the digested pEn-chimera was therefore ligated to the annealed-protospacer, using T4 ligase (NEB), for one hour at room temperature. This final plasmid was used for *E.coli* transformation. 24 hours later, positive colonies were then transferred into liquid culture for plasmid extraction.

The second part of the protocol consists in the recombination of the pEn-Chimera in the Cas9 expression vector pDe-Cas9. The recombination was made by the LR clonase II (Invitrogen) for two hours at room temperature. Plasmid was then used for *E.coli* transformation. Positive colonies were transferred into liquid culture for plasmid extraction. Correct insertion of the protospacers in the plasmid was verified by sequencing.

IV.c. Cloning of mutated slGBP10

Mutation on the SlGBP10 sequence was performed using the QuickChange Lightning Site-Directed Mutagenesis Kit, which allows the quick, efficient and accurate mutagenesis of plasmid of up to 14kb (Figure 65). The protocol uses a high fidelity enzyme, a *Pfu*-based polymerase blend and a *Dpn* I enzyme. Each step of the experiments was conducted according to the supplier recommendations. The pDONR201:GBP10 was used.

IV.d. E.coli transformation

E.coli transformation was performed by electroporation using Micropulser™ (BioRad). 40 µL of electro-competent bacteria were thawed on ice and added to 1 µL of the LR or BP reaction, the ligation

reaction or a plasmid. The mixture, placed in an electroporation cell (slot 1 mm), was subjected to an electrical impulse of 1800 Volts and about 5 milliseconds. The bacteria were then incubated in 1 mL of LB medium, under 200 rpm shaking, for 45 min at 37 ° C. A fraction of the culture was spread over solid LB medium, supplemented with the appropriate antibiotics, for selection (Table 10).

Antibiotic	Concentration for bacterial culture	Concentration for tomato selection	Concentration for *Arabidopsis* selection	Concentration for BY2 cells selection
Kanamycin	50 µg/mL	150 µg/mL	50 µg/mL	250 µg/mL
Gentamycin	20 µg/mL	-	-	-
Ampicillin	100 µg/mL	-	-	-
Spectinomycin	100 µg/mL	20 mg/mL	-	-
Rifampicin	25 µg/mL	-	-	
Timentin (ticarcillin-clavulanate)	-	250 mg/L and 75 mg/L	-	100 µg/mL

Table 10: List of antibiotics used for bacteria and plants selection

V. Transient and stable plant transformations

V.a. Agrobacterium transformation

Plasmids were introduced into *Agrobacterium tumefaciens* strain GV3101 or PMP90 by electroporation using a Micropulser^{TM} (BioRad) generating an electrical pulse of 2.5 kV and about 5 ms. Bacteria were then incubated in 1 mL of LB medium, with shaking (200 rpm), for 1 hour at 28 °C. A fraction of the culture was spread on solid LB medium supplemented with rifampicin (25 µg/mL) as well as the appropriate antibiotics for selection (Table 10). Bacteria were incubating for 48 hours at 28 °C. One bacterial colony was then cultured in liquid LB medium containing the same antibiotics, at 28°C with shaking (200 rpm). At least 12 hours later, when it reached an OD_{600nm} between 0.8-1, the bacterial suspension was ready to be used for plants transformation.

V.b. Transient transformation of tobacco leaves

Transient transformation of tobacco leaves was performed by agroinflitration. The cultures of *A. tumefaciens* were centrifugald at 5000g during 10 min and the supernatant was removed. The pellet was then washed two times with mQ H_2O. The bacterial solution was transferred in a 2 mL syringe. A wound was produced on the underside of the leaf, using a cone. A small pressure on the syringe was sufficient to allow the agroinflitration. 48 hours later, a portion of the leaf was cut (above the point of infiltration) and put between a slide and a coverslip for observation under the confocal microscope LSM 880 (Zeiss).

V.c. Stable transformation of tomato

The tomato transformation was carried out from fragments of cotyledons per agro-infection as described in Cortina & Culiáñez-Macià (2004). Around 50 to 100 Micro-Tom seeds were sown, taken on ½ MS medium, grown in growing chamber at 25°C during 7-8 days, cut into 3 explants and then cultured on KCMS Petri dishes for 24 hours, in the dark at 25°C. The explants were then deep for 30 min in an MS solution containing the bacteria *A. tumefaciens* transformed with the plasmid of interest. After removal of excess culture bacterial on a sterile absorbent paper, the explants were co-cultured on KCMS solid medium for 48h in the dark at 25°C. The explants were then rinsed three times with water supplemented with 0.05% Tween 20 (v/v) and cultured on 2Z medium (MS medium supplemented with 1 mL/L of Nitsch vitamins 1.2 mg/mL of zeatin ribosid) with 250 mg/L of Timentin (ticarcillin-clavulanate) and antibiotics used for transformant selection (100mg/L of kanamycin in the case of Gateway vectors) until callus formation. The seedlings forming from calli were transplanted into jars containing rooting medium (supplemented with the antibiotics for transformant selection and ticarcillin-clavulanate 75 mg/L) until their acclimatization in greenhouse. The integration of the transgene and its expression were then monitored by PCR and RT-sPCR to verify the integration of the transgene and its expression before transfer rooted plants to a greenhouse.

V.d. Stable transformation of Arabidopsis thaliana

Arabidopsis thaliana transformation was made by dipping flowers according to the following adapted protocol (Clough and Bent, 1998). The cultures of *A. tumefaciens* were centrifugald at 5000 g during 10 min and the supernatant was removed. The bacterial pellets were then taken up in a transformation solution (glucose 5% (w/v) Silwett L77 0.05% (v/v)). Flowers were then dipped in this solution every two days until the stop of new flowers production. Plants were then left in the greenhouse, until the seeds were obtained.

After processing, the seeds were harvested and decontaminated before being sown on MS ½ medium supplemented with the appropriate antibiotic (Table 10). The resistant seedlings were analyzed by PCR for checking the insertion of the transgene into the plant genome. For plants transformed with expression

vectors containing a fluorescent tag, the expression of the transgene can be verified under the macroscope Axiozoom (Zeiss).

V.e. Stable transformation of BY-2 cells

Five days before transformation, 1 mL of 7 days-old BY-2 cells were transferred to 25 mL of a fresh MS medium, adapted for BY-2 cells. One day before the transformation, a clone of *Agrobacterium tumefaciens*, transformed with the construct of interest, was transferred to 5 mL of liquid LB medium with corresponding antibiotics. The next day, when the *Agrobacterium tumefaciens* had reached an OD_{600nm} of 1.5, the bacterial solution was centrifugald three min at 300 rpm, the supernatant was removed and then replaced with MS medium, supplemented with 1.8 % glucose (pH 5.3), to obtain an OD_{600nm} of 1. 25 mL of BY-2 cells were used and centrifugald during five min at 700 rpm. The supernatant was removed and pellet was resuspended with 25 mL of MS medium with 1.8 % glucose (pH 5.3). This was repeated twice. BY-2 cells were then treated with 12.5 µL of acetosyringone (100 mM). In a culture plate of 6 wells, 4 mL of BY-2 cells were transferred to each well, and an increasing gradient of the *A. tumefaciens* culture was added (0 µL, 10 µL, 20 µL, 50 µL, 100 µL and 200 µL). Plates were placed at 24°C, in the dark.

48 hours later, the contents of each well was transferred to a 12 mL tube and centrifugald five min at 700 rpm. The supernatant was removed and replaced by 10 mL of fresh MS medium, adapted for BY-2 cells. This step was repeated four times. During the last rinse, the pellet was resuspended in MS medium, adapted for BY-2 cells (pH 5.8), supplemented with the timentin (ticarcillin-clavulanate) and kanamycin. BY-2 cells rinsed and treated with antibiotics were transferred to a petri dish containing, solid MS medium and the same antibiotics. Petri dishes were maintained at 24°C in the dark, during at least three weeks.

After three weeks, small cell clusters appeared at the MS medium surface and were transferred to fresh solid MS medium, with kanamycin. When the small cell clusters become callus (around two weeks after transplanting), a part of the callus was taken, the cells were dissociated by grinding them slightly with a scalpel and transferred to liquid MS medium. In order to test if the transformation actually works, BY-2 cells on liquid culture can be used for genotyping and testing the presence of the transgene. BY-2 transformed with plasmid containing a fluorescent tag can also be tested under the confocal microscope.

VI. Cellular and subcellular analysis under the microscope

After appropriate staining, all organ or cells were imaged under confocal microscope LSM880® (Zeiss).

- *Of Arabidopsis organs*

For root and etiolated hypocotyl characterization, *Arabidopsis* plantlets were directly transferred under slide and coverslip, with the desired staining (Propidium iodide or DAPI - 4,6-diamidino-2-phenylindole). For pavement cells characterization, cotyledons were taken and placed in a syringe containing water, and back and forth were made in order to allow the vacuum. Resulting flat cotyledons were then stained with propidium iodide.

- *Of tomato fruit*

For immuno-localization of callose, equatorial portions of tomato pericarp were fixed with FAA (EtOH 70% 18:20, formaldehyde 37% 1:20, acetic acid 1:20, conserved at 4°C) at then blocked with milk and 5% PBS 1X for 30 min at room temperature. The pericarp was putted in contact with the antibody anti-callose 1-3 β-glucan (Biosupplies) diluted 1/250 in milk and 5% PBS 1X, at 4°C, followed by three washing 5 min in PBS 1X under constant shacking. The pericarp tissue was then transferred with the second anti-body Goat anti mouse IgG FITC (Sigma Aldrich) diluted 1/100 in milk and 5% PBS 1X, during 1.5 hour at room temperature, under shacking. This was followed by three times washing 5 min in PBS 1X under constant shacking.

Cell walls were stained with Calcofluor white stain (Sigma Aldrich) for 1 min and three times washed during 5 min in PBS 1X, under shacking.

For nuclei staining, equatorial portions of tomato pericarp were fixed with FAA (EtOH 70% 18:20, formaldehyde 37% 1:20, acetic acid 1:20, conserved at 4°C). Nuclei were stained with DAPI (diluted 1/10 on PBS 1X for one min) and 3 times washed on PBS 1X during 5 min, or/and propidium iodide for 2 min.

- *Of BY-2 cells*

BY-2 cells were either put directly under slide and cover-slip or fixed on PFA 4% (on PBS 1X) during 10 min at room temperature, and three times washed on PBS 1X during 5 min. A treatment with triton 0,1% PBS 1X (15 min at room temperature) for allowing the penetration of the DAPI. After the DAPI staining cells were again three times washed on PBS 1X. Between each step of the staining procedure, BY-2 cells were smoothly centrifugald at 4000 rpm during 2 min, for allowing removal of the supernatant.

VII. Scanning electron microscopy

Scanning electron microscopy have been performed on a GeminiSEM 300_FESEM® (Zeiss), coupled with the module CRYO-SEM PP3010T® (Quorum Technologies) for the plant tissue freezing and transfer.

Young *Arabidopsis* rosette leaves were taken and glued on a specific support using a mix of teck and colloidal graphite. This gluing is need for maintaining the tissue during the cryo-fixation. The samples were then frozen in "pasty" nitrogen, and transferred to the preparation chamber, maintained at -140 °C. Transition from -140°C to -95 °C allows sublimation, followed by platinum metallization during 30 seconds at 10 µA. The samples were then transferred from the preparation chamber to the microscope chamber, cooled to -140 °C. The observations were made in high vacuum mode (3kv).

VIII. Ploidy level analyses

Cell ploidy was determined by flow cytometry (CyFlow® Space) on pericarp tissue of the equatorial zone and at different developmental stages. Tissue was cut in extraction buffer (solution form Partec®) and solution was filtered (50 µm), to separate the waste. Nuclei were stained with the fluorescent stain DAPI, which was a able to intercalate into the double strain DNA, with high affinity to A-T rich regions. The fluorescence intensity for each nucleus wais proportional to DNA content and subsequently to its ploidy level. Finally, data from the flow cytometer were integrated using Excel®, to eliminate background noise and estimate the percent of each nucleus (calculated by dividing the number of nuclei by the nuclei total count), the ploidy index (PI = (%4C x 4) + (…) + (%256C x 256) / 100) and the endoreduplication factor (EF = (%4C x 1) + (…) + (%256C x 7) / 100).

IX. Metabolism analyses: RMN and LC-MS

Metabolic analyses were performed on the metabolome plateform of the CGFB in Bordeaux. Acquisition and statistical analyses were performed by Catherine Deborde and Stephane Merillon. Extraction was performed on pericarp tissue of three different genotypes: the WT Micro-Tom (which served as a control), the CRISPR mutant *Slgbp10_CR4* and *Slgbp10_CR8,* and four stages of development: 15 DPA, 20 DPA, 25 DPA and red ripe stages. Three fruits from different plants were pooled, and three biological replicates were made for each condition. Pericarps were frozen, finely ground in cold using a grinder (Dangoumau), the resulting powders were then freeze-dried.

- *RMN*

40 ± 1 mg of powders were put in 2 ml polypropylene microtube with conical bottom with skirt (2.0 ml SC Micro Tube protein LB from Sarstedt), for manual extraction with 750 µl of MeOD and vortex for 1 min at maximum speed. Then, 750 µl of buffer solution at pH 6 was added (phosphate buffer KD_2/K_2D PO_4 90 mM, 11 mM EDTA-d12) and vortex for 1 min at maximum speed. Then a series of three ultrasonic baths for 10 min followed with vortex for 1 min at maximum speed were used for maximum extraction efficiency. Samples were centrifugald at 13,000 rpm at 4°C for 10 min, for macromolecular compound precipitation. 900 µl of supernatant were collected and dispense into a 2 mL vial compatible with pH adjustment step (pH of 6.00 ± 0.02 with NaOD 1 M and/or DCl 1 M solution by means of BTpH titration robot, Bruker, Karlsruhe, Germany). In parallel to the extraction of the samples, a blank and a solution of glucose are used as control of the extraction. 800 µl of each sample is finally transferred on a 5-mm NMR tube (5 mm 507-pp-7 Wilmad) and 8 µl of TMSP solution is added to the sample extract.

H-NMR spectra were recorded at 500.162 MHz on a Bruker Avance III spectrometer (Bruker, Wissembourg, France), equipped with an autosampler (BACS-120) that was used at room temperature, and using an inverse ATMA BBI 5 mm z-gradient probe flushed with nitrogen gas, at 300 K. A single-pulse sequence with presaturation (zgpr) was used. In order to get the same constant temperature of the sample set run, a delay (90 s) for temperature homogenization of the sample in the magnet was used. To optimize NMR conditions, automated tuning and matching, locking, shimming (topshim) and 90° hard pulse calibration (pulsecal) were carried out for each sample, the same dedicated receiver gain was used

for all samples. Thirty-two scans of 128k data points each were acquired with single-pulse sequence with presaturation (zgpr), a 90 ° pulse angle, a 6000 Hz spectral width, a 9.35 s acquisition time and a 10.64 s recycle delay.

Apodisation (LB 0.3Hz), zero-filling (X2) and Fourier transformation of Free Induction Decay, phasing, chemical shift calibration and baseline correction of spectra, peak realignment, non-uniform bucketing and signal-over-noise ratio determination were carried out with the NMRProcFlow web tool ((Jacob *et al.*, 2017) www.nmrprocflow. org)). Each spectral region of interest or bucket was determined manually with either the intelligent bucketing (De Meyer *et al.* 2008) or variable size bucketing modules of NMRProcFlow. Each bucket is designated according to their central chemical shift value, in ppm, of the spectral region. This resulted into 600 normalized (constant sum normalization) variables or buckets with S/N >3.

Statistical analyses were performed with BioStatFlow web application (v.2.8, www.biostatflow.org). Regarding the global variance, a principal component analysis (PCA) was applied to the data matrix resulting from the bucketing step after scaling (Z-score).

- *LC-MS*

20 ± 0,5 mg of freeze-dried tomato fruit samples were extracted with 1 mL of methanol/water (70/30, v/v) with 0.1% (v:v) formic acid spiked and 10 mM methyl vanillate as an internal control to check if injection was performed correctly by the autosampler. The extraction was performed for 15 min in an ultrasonic bath at 0°C. Extracts were centrifugald at 14460 g for 5 min (Centrifugal model 1-14, Sigma) then the supernatants were filtered through 0.22 µm PVDF filters (Merck Millipore, Germany) and collected in HPLC vials. Blank extracts were performed using the same procedure yet without sample powder. A QC sample was produced by pooling 50 µL of each sample extract. The resulting methanolic extracts were analysed by LC-MS. The LC system was an Ultimate 3000 model (ThermoScientific, Germany) and the mass spectrometer a LTQ-Orbitrap Elite (ThermoScientific, Germany)

The separation was performed with a reverse phase column (C18-Gemini 2.0 x 150 mm, 3 µm, 110Å, Phenomenex, CA, USA) at a flow rate of 350 µL/min. Column was kept at a constant temperature of 30 °C. Mobile phases were 0.1% (v/v) in ultrapure water (A) and acetonitrile (B). The elution gradient was the following: initial condition, 3% B; 0-0.5min, 3% B; 0.5-1, 3-10% B; 1-9 min, 10-50% B; 9-13 min, 50-100% B; 13-14 min, 100% B; 14-14.5 min, 100-3% B; 14.5-18 min, 3% B. The injection volume was 5 µL. Mass

spectrometer was equipped with an HESI source operated in positive mode. The source parameters were the following: spray voltage, 3.2 kV; capillary temperature, 300° C; Sheath gas flow rate 60 a.u.; auxiliary gas flow rate, 20 a.u.; sweep gas flow rate, 10 a.u.; heater temperature, 300° C. The mass range was m/z 150-1500. The resolving power was 240 000. The sample injection order was randomized. QC sample was injected between each 10 samples to correct for mass spectrometer signal drift, if necessary.

Proprietary raw data were converted in mzXML format and processed with an in-house script using XCMS package v3.2.0 (Smith *et al.*, 2006). This resulted in a dataset of variables defined by their m/z and their retention time (MxTy). Variables detected in blank extraction were filtered out. No drift was detected after QC analysis and intensity drift correction was not applied. Finally, intensity was normalized according to the sample powder mass.

X. Genomic analysis: towards the identification of causal mutations

- *Overview of the bioinformatics workflow used for the NGS-mapping analysis*

The analysis was performed according to (Garcia *et al.*, 2016).

After Next Generation Sequencing, the output files were independently mapped against the 2.50 version of the Heinz reference genome. After mapping, variant detection was performed using Samtools. Thus, variant.vcf files were produced for each bulk. The WT and mutant corresponding VCF files were compared to find common and non-common variants based on their position, and to estimate their allelic frequencies in the WT-like and mutant-like bulks. Among the "common variants", the variants displaying a read depth (DP) comprises between 10 and 100 were selected.

In order to remove variants corresponding to natural polymorphisms, variants were filtered depending on their presence in different un-mutagenized Micro-Tom lines and Micro-Tom EMS mutants already sequenced in the team, and in M82 and *S. pimpinelifollim* accessions.

Allelic frequency analysis allowed finding candidate regions associated with the phenotype of interest. Regions were then validated using a couple of primers included in these regions as KASPAR markers, to genotype a subset of the population. In this way, the association identified in the bulk is quickly confirmed or not using a more comprehensive sampling. If the association is maintaining, then a recombinant analysis is performed on the corresponding chromosome or candidate region, in view to locate the causal mutation.

- *Linkage mapping of major loci*

MAPMAKER/Exp3.0 was used to establish mapping of major loci. Indeed, although the pericarp thickness is a complex quantitative trait, we expected that the trait of interest in the corresponding EMS population behaved as a qualitative trait due to one (or few) EMS mutations. Genotyping of individuals was performed using KASPAR markers defined on the EMS mutations identified through WGS data (cf section III.c). Markers were defined along the chromosome and linkage between related genotypes at markers

and pericarp thickness phenotypes of a sub-population (182 individuals) was analysed using Mapmaker/EXP3.0 software (Lincoln *et al.*, 1993). Map distances in centi Morgans (cM) were calculated from recombination frequencies by using Kosambi's mapping function (per default), and using the maximum distance and a likelihood of odd (LOD) thresholds set at 50 cM and 3.0 per default, respectively. Analysis was made according to the manual recommendations. Genotypic inference at the causal mutation was arbitrary done for each individual according to 1- the corresponding phenotypic data and fixed thresholds explained in results section 2- the involvement of a recessive or dominant mutation.

First, the linkage of the causal mutation was tested using the 'group' command with the remaining marker sequence. If the causal mutation is grouped with the remaining markers, then its most likely position in the sequence was determined using the 'try' command. Finally, the 'map' command was used to locate the causal mutation and obtained distances between neighbouring marker, by fixing the order of marker sequence including the causal mutation.

BIBLIOGRAPHY

Almeida Engler, J. de and Gheysen, G. (2013) Nematode-Induced Endoreduplication in Plant Host Cells: Why and How? *Molecular Plant-Microbe Interactions*, **26**, 17–24.

Armour, W.J., Barton, D.A., Law, A.M.K. and Overall, R.L. (2015) Differential Growth in Periclinal and Anticlinal Walls during Lobe Formation in Arabidopsis Cotyledon Pavement Cells. *The Plant cell*, **27**, 2484–500.

Autran, D., Jonak, C., Belcram, K., Beemster, G.T.S., Kronenberger, J., Grandjean, O., Inzé, D. and Traas, J. (2002) Cell numbers and leaf development in Arabidopsis: a functional analysis of the STRUWWELPETER gene. *The EMBO journal*, **21**, 6036–49.

Azzi, L., Deluche, C., Gévaudant, F., Frangne, N., Delmas, F., Hernould, M. and Chevalier, C. (2015) Fruit growth-related genes in tomato. *Journal of Experimental Botany*, **66**, 1075–7086.

Baloban, M., Vanstraelen, M., Tarayre, S., Reuzeau, C., Cultrone, A., Mergaert, P. and Kondorosi, E. (2013) Complementary and dose-dependent action of AtCCS52A isoforms in endoreduplication and plant size control. *New Phytologist*, **198**, 1049–1059.

Bargel, H. and Neinhuis, C. (2005) Tomato (Lycopersicon esculentum Mill.) fruit growth and ripening as related to the biomechanical properties of fruit skin and isolated cuticle. *Journal of Experimental Botany*, **56**, 1049–1060.

Barow, M. (2006) Endopolyploidy in seed plants. *BioEssays : news and reviews in molecular, cellular and developmental biology*, **28**, 271–81.

Barrero, L.S., Cong, B., Wu, F. and Tanksley, S.D. (2006) Developmental characterization of the fasciated locus and mapping of Arabidopsis candidate genes involved in the control of floral meristem size and carpel number in tomato. *Genome*, **49**, 991–1006.

Baskin, T.I. (2001) On the alignment of cellulose microfibrils by cortical microtubules: A review and a model. *Protoplasma*, **215**, 150–171.

Beauvoit, B.P., Colombie, S., Monier, A., *et al.* (2014) Model-Assisted Analysis of Sugar Metabolism throughout Tomato Fruit Development Reveals Enzyme and Carrier Properties in Relation to Vacuole Expansion. *The Plant Cell*, **26**, 3224–3242.

Bisbis, B., Delmas, F., Joubès, J., Sicard, A., Hernould, M., Inzé, D., Mouras, A. and Chevalier, C. (2006) Cyclin-dependent Kinase (CDK) Inhibitors Regulate the CDK-Cyclin Complex Activities in Endoreduplicating Cells of Developing Tomato Fruit. *Journal of Biological Chemistry*, **281**, 7374–7383.

Boniotti, M.B. and Gutierrez, C. (2001) A cell-cycle-regulated kinase activity phosphorylates plant retinoblastoma protein and contains, in Arabidopsis, a CDKA/cyclin D complex. *The Plant Journal*, **28**, 341–350.

Boss, P.K., Bastow, R.M., Mylne, J.S. and Dean, C. (2004) Multiple pathways in the decision to flower: enabling, promoting, and resetting. *The Plant cell*, **16 Suppl**, S18-31.

Boudolf, V., Barrôco, R., Engler, J. de A., Verkest, A., Beeckman, T., Naudts, M., Inzé, D. and Veylder, L. De (2004) B1-type cyclin-dependent kinases are essential for the formation of stomatal complexes in Arabidopsis thaliana. *The Plant cell*, **16**, 945–55.

Boudolf, V., Lammens, T., Boruc, J., *et al.* (2009) CDKB1;1 forms a functional complex with CYCA2;3 to suppress endocycle onset. *Plant physiology*, **150**, 1482–93.

Bourdon, M., Frangne, N., Mathieu-rivet, E., Nafati, M., Cheniclet, C., Renaudin, J. and Chevalier, C. (2010) Endoreduplication and Growth of Fleshy Fruits. *Progress in Botany,* **71**, 101-132

Bourdon, M., Pirrello, J., Cheniclet, C., *et al.* (2012) Evidence for karyoplasmic homeostasis during endoreduplication and a ploidy-dependent increase in gene transcription during tomato fruit growth. *Development*, **139**, 3817–26.

Boss, P., Bastow, R., Mylne, J. and Dean, C. (2004) Multiple Pathways in the Decision to Flower: Enabling, Promoting, and Resetting, *The Plant cell*, **16 Suppl**, S18-31

Bradley, M. V. (1954) Cell and nuclear size in relation to polysomaty and the nuclear cycle, *American journal of botany*, **41**, 398-402

Bradley, M. V. and Crane, J.C. (1955) The effect of 2,4,5-trichlorophenocyacetic acid on cell and nuclear size and endopolyploidy in parenchymar of apricot fruits. *American journal of botany*, **42**,273-281

Brewer, M.T., Lang, L., Fujimura, K., Dujmovic, N., Gray, S. and Knaap, E. van der (2006) Development of a controlled vocabulary and software application to analyze fruit shape variation in tomato and other plant species. *Plant physiology*, **141**, 15–25.

Breyne, P., Dreesen, R., Vandepoele, K., *et al.* (2002) Transcriptome analysis during cell division in plants. *Proceedings of the National Academy of Sciences of the United States of America*, **99**, 14825–30.

Bürstenbinder, K., Savchenko, T., Müller, J., Adamson, A.W., Stamm, G., Kwong, R., Zipp, B.J., Dinesh, D.C. and Abel, S. (2013) Arabidopsis calmodulin-binding protein IQ67-domain 1 localizes to microtubules and interacts with kinesin light chain-related protein-1. *The Journal of biological chemistry*, **288**, 1871–82.

Buschmann, H., Fabri, C.O., Hauptmann, M., Hutzler, P., Laux, T., Lloyd, C.W. and Schäffner, A.R. (2004) Helical growth of the Arabidopsis mutant tortifolia1 reveals a plant-specific microtubule-associated protein. *Current biology : CB*, **14**, 1515–21.

Carvalho, R.F., Campos, M.L., Pino, L.E., Crestana, S.L., Zsögön, A., Lima, J.E., Benedito, V.A. and Peres, L.E. (2011) Convergence of developmental mutants into a single tomato model system: "Micro-Tom" as an effective toolkit for plant development research. *Plant methods*, **7**, 18.

Catherine A. Konopka, Justin B. Schleede, A.R.S. and S.Y.B. (2006) Dynamin and Cytokinesis. *Traffic*, **7**, 239–247.

Cebolla, A., Vinardell, J.M., Kiss, E., Oláh, B., Roudier, F., Kondorosi, A. and Kondorosi, E. (1999) The mitotic inhibitor ccs52 is required for endoreduplication and ploidy-dependent cell enlargement in plants. *The EMBO journal*, **18**, 4476–84.

Chakrabarti, M., Zhang, N., Sauvage, C., *et al.* (2013) A cytochrome P450 regulates a domestication trait in cultivated tomato. *Proceedings of the National Academy of Sciences of the United States of America*, **110**, 17125–30.

Chan, F.L., Vinod, B., Novy, K., *et al.* (2017) Aurora Kinase B, a novel regulator of TERF1 binding and telomeric integrity. *Nucleic Acids Research*, **45**, 12340–12353.

Chan, Y.-K., Tsai, M.-H., Huang, D.-C., Zheng, Z.-H. and Hung, K.-D. (2010) Leukocyte nucleus segmentation and nucleus lobe counting. *BMC bioinformatics*, **11**, 558.

Cheniclet, C., Rong, W.Y., Causse, M., Frangne, N., Bolling, L., Bordeaux, V.S. and Ornon, V. (2005) Cell Expansion and Endoreduplication Show a Large Genetic Variability in Pericarp and Contribute Strongly to Tomato Fruit Growth 1. *Plant physiology*, **139**, 1984–1994.

Chevalier, C., Bourdon, M., Pirrello, J., Cheniclet, C., Gévaudant, F. and Frangne, N. (2014) Endoreduplication and fruit growth in tomato: evidence in favour of the karyoplasmic ratio theory. *Journal of experimental botany*, **65**, 2731–46.

Chevalier, C., Nafati, M., Mathieu-Rivet, E., Bourdon, M., Frangne, N., Cheniclet, C., Renaudin, J.-P., Gévaudant, F. and Hernould, M. (2011) Elucidating the functional role of endoreduplication in tomato fruit development. *Annals of botany*, **107**, 1159–69.

Chouinard, L. (1951) *Nuclear Differences in Allium Cepa Root Tissues*, University of Wisconsin, Thesis work

Churchman, M.L., Brown, M.L., Kato, N., *et al.* (2006) SIAMESE, a plant-specific cell cycle regulator, controls endoreplication onset in Arabidopsis thaliana. *The Plant cell*, **18**, 3145–57.

Clough, S.J. and Bent, A.F. (1998) Floral dip: a simplified method for Agrobacterium-mediated transformation of Arabidopsis thaliana. *The Plant journal : for cell and molecular biology*, **16**, 735–43.

Cockcroft, C.E., Boer, B.G.W. den, Healy, J.M.S. and Murray, J.A.H. (2000) Cyclin D control of growth rate in plants. *Nature*, **405**, 575–579.

Cong, B., Barrero, L.S. and Tanksley, S.D. (2008) Regulatory change in YABBY-like transcription factor led to evolution of extreme fruit size during tomato domestication. *Nature Genetics*, **40**, 800–804.

Cong, B., Liu, J. and Tanksley, S.D. (2002) Natural alleles at a tomato fruit size quantitative trait locus differ by heterochronic regulatory mutations. *Proceedings of the National Academy of Sciences of the United States of America*, **99**, 13606–11.

Cong, B. and Tanksley, S.D. (2006) FW2.2 and cell cycle control in developing tomato fruit: a possible example of gene co-option in the evolution of a novel organ. *Plant Molecular Biology*, **62**, 867–880.

Cookson, S.J., Radziejwoski, A. and Granier, C. (2006) Cell and leaf size plasticity in Arabidopsis: what is the role of endoreduplication? *Plant, Cell and Environment*, **29**, 1273–1283.

Cools, T., Iantcheva, A., Weimer, A.K., *et al.* (2011) The Arabidopsis thaliana checkpoint kinase WEE1 protects against premature vascular differentiation during replication stress. *The Plant cell*, **23**, 1435–48.

Coombe, B.G. (1976) THE DEVELOPMENT OF FLESHY FRUITS. *Ann. Rev. Plant Physiol.*, **27**, 507–528.

Cortina, C. and Culiáñez-Macià, F.A. (2004) Tomato Transformation and Transgenic Plant Production. *Plant Cell, Tissue and Organ Culture*, **76**, 269–275.

Czerednik, A., Busscher, M., Angenent, G.C. and Maagd, R.A. de (2015) The cell size distribution of tomato fruit can be changed by overexpression of *CDKA1*. *Plant Biotechnology Journal*, **13**, 259–268.

Czerednik, A., Busscher, M., Bielen, B.A.M., Wolters-Arts, M., Maagd, R.A. de and Angenent, G.C. (2012) Regulation of tomato fruit pericarp development by an interplay between CDKB and CDKA1 cell cycle genes. *Journal of experimental botany*, **63**, 2605–17.

Dahan, Y., Rosenfeld, R., Zadiranov, V. and Irihimovitch, V. (2010) A proposed conserved role for an avocado fw2.2-like gene as a negative regulator of fruit cell division. *Planta*, **232**, 663–676.

Damme, D. Van (2009) Division plane determination during plant somatic cytokinesis. *Current Opinion in Plant Biology*, **12**, 745–751.

Damme, D. Van, Coutuer, S., Rycke, De R., Bouget, FY., Inze, D. and Geelen, D. (2006) Somatic cytokinesis and pollen maturation in Arabidopsis depend on TPLATE, which has domains similar to coat proteins. *The Plant Cell,* **18**, 3502-3518

Damme, D. Van, Rybel, B. De, Gudesblat, G., Demidov, D., Grunewald, W., Smet, I. De, Houben, A., Beeckman, T. and Russinova, E. (2011) Arabidopsis α Aurora kinases function in formative cell division plane orientation. *The Plant cell*, **23**, 4013–24.

Damme, D. Van, Vanstraelen, M. and Geelen, D. (2007) Cortical division zone establishment in plant cells. *Trends in Plant Science*, **12**, 458–464.

Demidov, D., Damme, D. Van, Geelen, D., Blattner, F.R. and Houben, A. (2005) Identification and dynamics of two classes of aurora-like kinases in Arabidopsis and other plants. *The Plant cell*, **17**, 836–48.

Dewitte, W., Riou-Khamlichi, C., Scofield, S., Healy, J.M.S., Jacqmard, A., Kilby, N.J. and Murray, J.A.H. (2003) Altered cell cycle distribution, hyperplasia, and inhibited differentiation in Arabidopsis caused by the D-type cyclin CYCD3. *The Plant cell*, **15**, 79–92.

Dubois, K.N., Alsford, S., Holden, J.M., *et al.* (2012) NUP-1 is a large coiled-coil nucleoskeletal protein in trypanosomes with lamin-like functions. *PLoS Biology*, **10**.

Ebel, C., Mariconti, L. and Gruissem, W. (2004) Plant retinoblastoma homologues control nuclear proliferation in the female gametophyte. *Nature*, **429**, 776–780.

El-Assal, S.E.D., Le, J., Basu, D., Mallery, E.L. and Szymanski, D.B. (2004) Distorted2 encodes an ARPC2 subunit of the putative Arabidopsis ARP2/3 complex. *Plant Journal*, **38**, 526–538.

Emmanuel, E. and Levy, A.A. (2002) Tomato mutants as tools for functional genomics. *Current Opinion in Plant Biology*, **5**, 112–117.

Fabian-Marwedel, T., Umeda, M. and Sauter, M. (2002) The rice cyclin-dependent kinase-activating kinase R2 regulates S-phase progression. *The Plant cell*, **14**, 197–210.

Fauser, F., Schiml, S. and Puchta, H. (2014) Both CRISPR/Cas-based nucleases and nickases can be used efficiently for genome engineering in *Arabidopsis thaliana*. *The Plant Journal*, **79**, 348–359.

Fernandez, L., Torregrosa, L., Terrier, N., Sreekantan, L., Grimplet, J., Davies, C., Thomas, M.R., Romieu, C. and Ageorges, A. (2007) Identification of genes associated with flesh morphogenesis during grapevine fruit development. *Plant Molecular Biology*, **63**, 307–323.

Forster, F., Paster, W., Supper, V., *et al.* (2017) Guanylate Binding Protein 1 – Mediated Interaction of T Cell Antigen Receptor Signaling with the Cytoskeleton. *The Journal of Immunology*, **192**, 771-781

Fox, D.T., Gall, J.G. and Spradling, A.C. (2010) Error-prone polyploid mitosis during normal Drosophila development. *Genes and Development*, **24**, 2294–2302.

Francis, D. (2007) The plant cell cycle -15 years on. *New Phytol*, **174**, 261–278.

Frary, A., Nesbitt, T.C., Grandillo, S., *et al.* (2000) fw2.2: a quantitative trait locus key to the evolution of tomato fruit size. *Science*, **289**, 85–8.

Fujimoto, M. and Tsutsumi, N. (2014) Dynamin-related proteins in plant post-Golgi traffic. *Frontiers in plant science*, **5**, 408.

Gady, A.L., Hermans, F.W., Wal, M.H. Van de, Loo, E.N. van, Visser, R.G. and Bachem, C.W. (2009) Implementation of two high through-put techniques in a novel application: detecting point mutations in large EMS mutated plant populations. *Plant methods*, **5**, 13.

Garcia, V., Bres, C., Just, D., *et al.* (2016) Rapid identification of causal mutations in tomato EMS populations via mapping-by-sequencing. *Nature protocols*, **11**, pages 2401–2418

Geelen, D.N. V and Inze, D.G. (2001) A Bright Future for the Bright Yellow-2 Cell Culture 1. *Plant physiology*, **127**, 1375–1379.

Geitler, L. (1948) Ergebnisse und Probleme der Endomitoseforschung. *Österreichische Botanische Zeitschrift*, **95**, 277–299.

Gendreau, E., Traas, J., Desnos, T., Grandjean, O., Caboche, M. and Höfte, H. (1997) Cellular basis of hypocotyl growth in Arabidopsis thaliana. *Plant physiology*, **114**, 295–305.

Gillaspy, G., Ben-David, H. and Gruissem, W. (1993) Fruits: A Developmental Perspective. *The Plant cell*, **5**, 1439–1451.

Giovannoni, J., Nguyen, C., Ampofo, B., Zhong, S. and Fei, Z. (2017) The Epigenome and Transcriptional Dynamics of Fruit Ripening. *Annual Review of Plant Biology*, **68**, 61–84.

Giovannoni, J.J. (2007) Fruit ripening mutants yield insights into ripening control. *Current Opinion in Plant Biology*, **10**, 283–289.

Gonzalez, N., Gévaudant, F., Hernould, M., Chevalier, C. and Mouras, A. (2007) The cell cycle-associated protein kinase WEE1 regulates cell size in relation to endoreduplication in developing tomato fruit. *The Plant Journal*, **51**, 642–655.

Grandillo, S., Ku, H.M. and Tanksley, S.D. (1999) Identifying the loci responsible for natural variation in fruit size and shape in tomato. *Theoretical and Applied Genetics*, **99**, 978–987.

Guo, M., Rupe, M.A., Dieter, J.A., Zou, J., Spielbauer, D., Duncan, K.E., Howard, R.J., Hou, Z. and Simmons, C.R. (2010) Cell Number Regulator1 affects plant and organ size in maize: implications for crop yield enhancement and heterosis. *The Plant cell*, **22**, 1057–73.

Gupta, P., Reddaiah, B., Salava, H., *et al.* (2017) Next-generation sequencing (NGS)-based identification of induced mutations in a doubly mutagenized tomato (*Solanum lycopersicum*) population. *The Plant Journal*, **92**, 495–508.

Gutierrez, C., Ramirez-Parra, E., Castellano, M.M. and Pozo, J.C. del (2002) G1 to S transition: more than a cell cycle engine switch. *Current Opinion in Plant Biology*, **5**, 480–486.

Harashima, H., Shinmyo, A. and Sekine, M. (2007) Phosphorylation of threonine 161 in plant cyclin-dependent kinase A is required for cell division by activation of its associated kinase. *The Plant Journal*, **52**, 435–448.

Hervas, J.P. (1976) Multinucleate plant cells, aneuploidy in a proliferating population. *Experimental Cell research*, **97**, 203-212

Hervas, J.P. (1987) Multinucleate Plant cells, nuclear aneuploidy and mitotic behavior. *Experimental Cell research*, **171**, 436–447.

Hervieux, N., Dumond, M., Sapala, A., Routier-Kierzkowska, A.-L., Kierzkowski, D., Roeder, A.H.K., Smith, R.S., Boudaoud, A. and Hamant, O. (2016) A Mechanical Feedback Restricts Sepal Growth and Shape in Arabidopsis. *Current Biology*, **26**, 1019–1028.

Heyman, J. and Veylder, L. De (2012) The anaphase-promoting complex/cyclosome in control of plant development. *Molecular Plant*, **5**, 1182–1194.

Hörmanseder, K., Obermeyer, G. and Foissner, I. (2005) Disturbance of endomembrane trafficking by brefeldin A and calyculin A reorganizes the actin cytoskeleton of Lilium longiflorum pollen tubes. *Protoplasma*, **227**, 25–36.

Huang, Z., Houten, J. Van, Gonzalez, G., Xiao, H. and Knaap, E. van der (2013) Genome-wide identification, phylogeny and expression analysis of SUN, OFP and YABBY gene family in tomato. *Molecular Genetics and Genomics*, **288**, 111–129.

Huang, Z. and Knaap, E. van der (2011) Tomato fruit weight 11.3 maps close to fasciated on the bottom of chromosome 11. *Theoretical and Applied Genetics*, **123**, 465–474.

Hülskamp, M., Miséra, S. and Jürgens, G. (1994) Genetic dissection of trichome cell development in Arabidopsis. *Cell*, **76**, 555–566.

Hussey, P.J., Ketelaar, T. and Deeks, M.J. (2006) Control of the Actin Cytoskeleton in Plant Cell Growth. *Annual Review of Plant Biology*, **57**, 109–125.

Inzé, D. and Veylder, L. De (2006) Cell cycle regulation in plant development. *Annual review of genetics*, **40**, 77–105.

Isner, J.C., Xu, Z., Costa, J.M., ***et al.*** (2017) Actin filament reorganisation controlled by the SCAR/WAVE complex mediates stomatal response to darkness. *New Phytologist*, **215**, 1059–1067.

Ivakov, A. and Persson, S. (2013) Plant cell shape: modulators and measurements. *Frontiers in plant science*, **4**, 439.

Iwakawa, H., Shinmyo, A. and Sekine, M. (2006) Arabidopsis *CDKA;1* , a *cdc2* homologue, controls proliferation of generative cells in male gametogenesis. *The Plant Journal*, **45**, 819–831.

Joubès, J. and Chevalier, C. (2000) Endoreduplication in higher plants. *The Plant Cell Cycle*, 735–745.

Joubès, J., Lemaire-Chamley, M., Delmas, F., Walter, J., Hernould, M., Mouras, A., Raymond, P. and Chevalier, C. (2001) A new C-type cyclin-dependent kinase from tomato expressed in dividing tissues does not interact with mitotic and G1 cyclins. *Plant physiology*, **126**, 1403–15.

Joubes, J., Phan, T.H., Just, D., Rothan, C., Bergounioux, C., Raymond, P. and Chevalier, C. (1999) Molecular and biochemical characterization of the involvement of cyclin-dependent kinase A during the early development of tomato fruit. *Plant Physiol*, **121**, 857–869.

Just, D., Garcia, V., Fernandez, L., *et al.* (2013) Micro-Tom mutants for functional analysis of target genes and discovery of new alleles in tomato. *Plant Biotechnology*, **30**, 225–231.

Kalve, S., Fotschki, J., Beeckman, T., Vissenberg, K. and Beemster, G.T.S. (2014) Three-dimensional patterns of cell division and expansion throughout the development of Arabidopsis thaliana leaves. *Journal of Experimental Botany*, **65**, 6385–6397.

Katagiri, Y., Hasegawa, J., Fujikura, U., Hoshino, R., Matsunaga, S. and Tsukaya, H. (2016) The coordination of ploidy and cell size differs between cell layers in leaves. *Development (Cambridge, England)*, **143**, 1120–5.

Kawabe, A., Matsunaga, S., Nakagawa, K., Kurihara, D., Yoneda, A., Hasezawa, S., Uchiyama, S. and Fukui, K. (2005) Characterization of plant Aurora kinases during mitosis. *Plant Molecular Biology*, **58**, 1–13.

Keeling, K.M., Lanier, J., Du, M., Salas-Marco, J., Gao, L., Kaenjak-Angeletti, A. and Bedwell, D.M. (2004) Leaky termination at premature stop codons antagonizes nonsense-mediated mRNA decay in S. cerevisiae. *RNA (New York, N.Y.)*, **10**, 691–703.

Keijzer, J. de, Mulder, B.M. and Janson, M.E. (2014) Microtubule networks for plant cell division. *Systems and synthetic biology*, **8**, 187–94.

King, M.C., Raposo, G. and Lemmon, M.A. (2004) Inhibition of nuclear import and cell-cycle progression by mutated forms of the dynamin-like GTPase MxB. *Proceedings of the National Academy of Sciences of the United States of America*, **101**, 8957–62.

Klee, H.J. and Giovannoni, J.J. (2011) Genetics and Control of Tomato Fruit Ripening and Quality Attributes. *Annual Review of Genetics*, **45**, 41–59.

Knaap, E. van der, Chakrabarti, M., Chu, Y.H., *et al.* (2014) What lies beyond the eye: the molecular mechanisms regulating tomato fruit weight and shape. *Frontiers in Plant Science*, **5**, 227.

Knaap, E. van der and Østergaard, L. (2018) Shaping a fruit: Developmental pathways that impact growth patterns. *Seminars in Cell and Developmental Biology*, **79**, 27–36.

Knaap, E. van der, Sanyal, A., Jackson, S.A. and Tanksley, S.D. (2004) High-resolution fine mapping and fluorescence in situ hybridization analysis of sun, a locus controlling tomato fruit shape, reveals a region of the tomato genome prone to DNA rearrangements. *Genetics*, **168**, 2127–40.

Knaap, E. van der and Tanksley, S.D. (2003) The making of a bell pepper-shaped tomato fruit: identification of loci controlling fruit morphology in Yellow Stuffer tomato. *Theoretical and Applied Genetics*, **107**, 139–147.

Kojo, Kei H., Higaki, T., Kutsuna, N., Yoshida, Y.,Yasuhara, H. and Hasezawa, S. (2013) Roles of Cortical Actin Microfilament Patterning in Division Plane Orientation in Plants. *Plant and Cell Physiology,* **54**, 1491-1503.

Konopka, C., Schleede, J., Skop, A. and Bednarek, S. (2006) Dynamin and cytokinesis, *Traffic*, **7**, 239-247.

Kost, B. and Chua, N.H. (2002) The Plant Cytoskeleton: Vacuoles and Cell Walls Make the Difference. *Cell*, **108**, 9–12.

Krieger, U., Lippman, Z.B. and Zamir, D. (2010) The flowering gene SINGLE FLOWER TRUSS drives heterosis for yield in tomato. *Nature Genetics*, **42**, 459–463.

Kurihara, D., Matsunaga, S., Kawabe, A., Fujimoto, S., Noda, M., Uchiyama, S. and Fukui, K. (2006) Aurora kinase is required for chromosome segregation in tobacco BY-2 cells. *The Plant Journal*, **48**, 572–580.

Kurihara, D., Matsunaga, S., Uchiyama, S. and Fukui, K. (2008) Live cell imaging reveals plant aurora kinase has dual roles during mitosis. *Plant and Cell Physiology*, **49**, 1256–1261.

Lammens, T., Li, J., Leone, G. and Veylder, L. De (2009) Atypical E2Fs: new players in the E2F transcription factor family. *Trends in cell biology*, **19**, 111–8.

Łangowski, Ł., Stacey, N. and Østergaard, L. (2016) Diversification of fruit shape in the Brassicaceae family. *Plant Reproduction*, **29**, 149–163.

Lee, S.H. and Dominguez, R. (2010) Regulation of actin cytoskeleton dynamics in cells. *Molecules and cells*, **29**, 311–325.

Leiva-Neto, J.T., Grafi, G., Sabelli, P.A., Dante, R.A., Woo, Y., Maddock, S., Gordon-Kamm, W.J. and Larkins, B.A. (2004) A dominant negative mutant of cyclin-dependent kinase A reduces endoreduplication but not cell size or gene expression in maize endosperm. *The Plant cell*, **16**, 1854–69.

Leysi-Derilou, Y., Robert, A., Duchesne, C., Garnier, A., Boyer, L. and Pineault, N. (2010) Polyploid megakaryocytes can complete cytokinesis. *Cell Cycle*, **9**, 2589–2599.

Lincoln, S.E., Daly, M.J. and Lander, E.S. (1993) *Mapping genes controlling quantitative traits using MAPMAKER/QTL*. Technical Report. Cambridge, MA: Whitehead Institute for Biomedical Research.

Lipka, E., Herrmann, A. and Mueller, S. (2015) Mechanisms of plant cell division. *Wiley periodicals*, **4**, 391-404.

Lipka, E. and Müller, S. (2014) Nitrosative stress triggers microtubule reorganization in Arabidopsis thaliana. *Journal of Experimental Botany*, **65**, 4177–4189.

Lippman, Z.B. and Zamir, D. (2007) Heterosis: revisiting the magic. *Trends in Genetics*, **23**, 60–66.

Lisenbee, C.S., Karnik, S.K. and Trelease, R.N. (2003) Overexpression and mislocalization of a tail-anchored GFP redefines the identity of peroxisomal ER. *Traffic*, **4**, 491–501.

Liu, J., Cong, B. and Tanksley, S.D. (2003) Generation and Analysis of an Artificial Gene Dosage Series in Tomato to Study the Mechanisms by Which the Cloned Quantitative Trait Locus fw2 . 2 Controls Fruit Size. *Plant physiology*, **132**, 292–299.

Liu, J., Eck, J. Van, Cong, B. and Tanksley, S.D. (2002) A new class of regulatory genes underlying the cause of pear-shaped tomato fruit. *Proceedings of the National Academy of Sciences of the United States of America*, **99**, 13302–6.

Mallm, J.P. and Rippe, K. (2015) Aurora Kinase B Regulates Telomerase Activity via a Centromeric RNA in Stem Cells. *Cell Reports*, **11**, 1667–1678.

Martin, L.B.B., Nicolas, P., Matas, A.J., Shinozaki, Y., Catalá, C. and Rose, J.K.C. (2016) Laser microdissection of tomato fruit cell and tissue types for transcriptome profiling. *Nature protocols*, **11**, 2376-2388.

Martin, L.B.B. and Rose, J.K.C. (2013) There's more than one way to skin a fruit: formation and functions of fruit cuticles. *Journal of Experimental Botany*, **65**, 4639–4651.

Martinez, P., Luo, A., Sylvester, A. and Rasmussen, C.G. (2017) Proper division plane orientation and mitotic progression together allow normal growth of maize. *Proceedings of the National Academy of Sciences of the United States of America*, **114**, 2759–2764.

Matas, A.J., Yeats, T.H., Buda, G.J., *et al.* (2011) Tissue- and cell-type specific transcriptome profiling of expanding tomato fruit provides insights into metabolic and regulatory specialization and cuticle formation. *The Plant cell*, **23**, 3893–910.

Mathieu-Rivet, E., Gévaudant, F., Sicard, A., *et al.* (2010) Functional analysis of the anaphase promoting complex activator CCS52A highlights the crucial role of endo-reduplication for fruit growth in tomato. *The Plant Journal*, **62**, 727–741.

Mathur, J., Mathur, N., Kernebeck, B. and Hülskamp, M. (2003) Mutations in actin-related proteins 2 and 3 affect cell shape development in Arabidopsis. *The Plant cell*, **15**, 1632–1645.

Mayer, K.F.X., Schoof, H., Haecker, A., Lenhard, M., Jürgens, G. and Laux, T. (1998) Role of WUSCHEL in regulating stem cell fate in the Arabidopsis shoot meristem. *Cell*, **95**, 805–815.

Melaragno, J.E., Mehrotra, B. and Coleman, A.W. (1993) Relationship between Endopolyploidy and Cell Size in Epidermal Tissue of Arabidopsis. *The Plant cell*, **5**, 1661–1668.

Menda, N., Semel, Y., Peled, D., Eshed, Y. and Zamir, D. (2004) *In silico* screening of a saturated mutation library of tomato. *The Plant Journal*, **38**, 861–872.

Minoia, S., Boualem, A., Marcel, F., *et al.* (2016) Induced mutations in tomato SlExp1 alter cell wall metabolism and delay fruit softening. *Plant Science*, **242**, 195–202.

Monforte, A.J., Diaz, A., Caño-Delgado, A. and Knaap, E. van der (2013) The genetic basis of fruit morphology in horticultural crops: lessons from tomato and melon. *Journal of Experimental Botany*, **65**, 4625–4637.

Müller S., **Han S., Smith L, G.** (2006) Two novel kinesins, POK1 and POK2 play a role in spatial control of cytokinesis. *Current Biol.* **16**: 888-894.

Muños, S., Ranc, N., Botton, E., *et al.* (2011) Increase in tomato locule number is controlled by two single-nucleotide polymorphisms located near WUSCHEL. *Plant physiology*, **156**, 2244–54. A

Murashige, T. and Skoog, F. (1962) A Revised Medium for Rapid Growth and Bio Assays with Tobacco Tissue Cultures. *Physiologia Plantarum*, **15**, 473–497.

Musseau, C., Just, D., Jorly, J., Gévaudant, F., Moing, A., Chevalier, C., Lemaire-Chamley, M., Rothan, C. and Fernandez, L. (2017) Identification of Two New Mechanisms That Regulate Fruit Growth by Cell Expansion in Tomato. *Frontiers in Plant Science*, **8**, 1–15.

Nafati, M., Cheniclet, C., Hernould, M., Do, P.T., Fernie, A.R., Chevalier, C. and Gévaudant, F. (2011) The specific overexpression of a cyclin-dependent kinase inhibitor in tomato fruit mesocarp cells uncouples endoreduplication and cell growth. *The Plant Journal*, **65**, 543–556.

Nagata, Y., Muro, Y. and Todokoro, K. (1997) Thrombopoietin-induced polyploidization of bone marrow megakaryocytes is due to a unique regulatory mechanism in late mitosis. *The Journal of cell biology*, **139**, 449–57.

Nowack, M.K., Grini, P.E., Jakoby, M.J., Lafos, M., Koncz, C. and Schnittger, A. (2006) A positive signal from the fertilization of the egg cell sets off endosperm proliferation in angiosperm embryogenesis. *Nature Genetics*, **38**, 63–67.

Ostler, N., Britzen-laurent, N., Liebl, A., *et al.* (2014) Gamma Interferon-Induced Guanylate Binding Protein 1 Is a Novel Actin Cytoskeleton Remodeling Factor. *Molecular and Cellular Biology*, **34**, 196–209.

Otero, S., Helariutta, Y. and Benitez-Alfonso, Y. (2016) Symplastic communication in organ formation and tissue patterning. *Current Opinion in Plant Biology*, **29**, 21–28.

Pascual, L., Desplat, N., Huang, B.E., *et al.* (2015) Potential of a tomato MAGIC population to decipher the genetic control of quantitative traits and detect causal variants in the resequencing era. *Plant Biotechnology Journal*, **13**, 565–577.

Petit, J., Bres, C., Just, D., *et al.* (2014) Analyses of tomato fruit brightness mutants uncover both cutin-deficient and cutin-abundant mutants and a new hypomorphic allele of GDSL lipase. *Plant physiology*, **164**, 888–906.

Petit, J., Bres, C., Mauxion, J.-P., *et al.* (2016) The Glycerol-3-Phosphate Acyltransferase GPAT6 from Tomato Plays a Central Role in Fruit Cutin Biosynthesis. *Plant physiology*, **171**, 894–913.

Petrovská, B., Cenklová, V., Pochylová, Ž., Kourová, H., Doskočilová, A., Plíhal, O., Binarová, L. and Binarová, P. (2012) Plant Aurora kinases play a role in maintenance of primary meristems and control of endoreduplication. *New Phytologist*, **193**, 590–604.

Pitrat, M. (2008) Melon. *Biotechnology in Agriculture and Forestry*, 209-240.

Porceddu, A., Stals, H., Reichheld, J.P., *et al.* (2001) A Plant-specific Cyclin-dependent Kinase Is Involved in the Control of G2/M Progression in Plants. *Journal of Biological Chemistry*, **276**, 36354–36360.

Potter, C.J. and Xu, T. (2001) Mechanisms of size control. *Current Opinion in Genetics & Development*, **11**, 279–286.

Pound, M.P., French, a. P., Wells, D.M., Bennett, M.J. and Pridmore, T.P. (2012) CellSeT: Novel Software to Extract and Analyze Structured Networks of Plant Cells from Confocal Images. *The Plant Cell*, **24**, 1353–1361.

Praefcke, G.J.K. and Mcmahon, H.T. (2004) The dynamin superfamily : universal membrane tubulation and fission molecules ? *Nature Reviews*, **5**, 133-147.

Renaudin, J.-P., Deluche, C., Cheniclet, C., Chevalier, C. and Frangne, N. (2017) Cell layer-specific patterns of cell division and cell expansion during fruit set and fruit growth in tomato pericarp. *Journal of Experimental Botany*, **68**, 1613–1623.

Reyes, C., Serrurier, C., Gauthier, T., Gachet, Y. and Tournier, S. (2015) Aurora B prevents chromosome arm separation defects by promoting telomere dispersion and disjunction. *Journal of Cell Biology*, **208**, 713.

Ringli, C., Baumberger, N., Diet, A., Frey, B. and Keller, B. (2002) ACTIN2 is essential for bulge site selection and tip growth during root hair development of Arabidopsis. Plant physiology, **129**, 1464-1472.

Roberts, S.E. and Gladfelter, A.S. (2015) Nuclear autonomy in multinucleate fungi. *Current opinion in microbiology*, **28**, 60–5.

Rodríguez-Leal, D., Lemmon, Z.H., Man, J., Bartlett, M.E. and Lippman, Z.B. (2017) Engineering Quantitative Trait Variation for Crop Improvement by Genome Editing. *Cell*, **171**, 470–480.e8.

Rodríguez, G.R., Muños, S., Anderson, C., Sim, S.-C., Michel, A., Causse, M., Gardener, B.B.M., Francis, D. and Knaap, E. van der (2011) Distribution of SUN, OVATE, LC, and FAS in the tomato germplasm and the relationship to fruit shape diversity. *Plant physiology*, **156**, 275–85.

Roeder, A.H.K., Chickarmane, V., Cunha, A., Obara, B., Manjunath, B.S. and Meyerowitz, E.M. (2010) Variability in the control of cell division underlies sepal epidermal patterning in Arabidopsis thaliana. *PLoS biology*, **8**, e1000367.

Rothan, C., Just, D., Fernandez, L., Atienza, I., Ballias, P. and Lemaire-Chamley, M. (2016) Culture of the Tomato Micro-Tom Cultivar in Greenhouse. In Humana Press, New York, NY, pp. 57–64.

Sabine Mueller, S.H. and Smith, and L.G. (2006) Two Kinesins Are Involved in the Spatial Control of Cytokinesis in Arabidopsis thaliana. *Current Biology*, 888–894.

Sablowski, R. (2016) Coordination of plant cell growth and division: collective control or mutual agreement? *Current Opinion in Plant Biology*, **34**, 54–60.

Saedler, R., Mathur, N., Srinivas, B.P., Kernebeck, B., Hülskamp, M. and Mathur, J. (2004) Actin control over microtubules suggested by DISTORTED2 encoding the Arabidopsis ARPC2 subunit homolog. *Plant and Cell Physiology*, **45**, 813–822.

Saito, T., Ariizumi, T., Okabe, Y., *et al.* (2011) TOMATOMA: a novel tomato mutant database distributing Micro-Tom mutant collections. *Plant & cell physiology*, **52**, 283–96.

Samaj, J., Baluska, FrantisekVoigt, B., Schlicht, M., Volkmann, D. and Menzel, D. (2004) Endocytosis, Actin Cytoskeleton, and Signaling1. *Plant physiology*, **135**, 1150–1161.

Sambade, A., Findlay, K., Schaffner, A.R., Lloyd, C.W. and Buschmann, H. (2014) Actin-Dependent and -Independent Functions of Cortical Microtubules in the Differentiation of Arabidopsis Leaf Trichomes. *The Plant Cell*, **26**, 1629–1644.

Savaldi-Goldstein, S., Peto, C. and Chory, J. (2007) The epidermis both drives and restricts plant shoot growth. *Nature*, **446**, 199–202.

Schaefer, E., Belcram, K., Uyttewaal, M., *et al.* (2017) The preprophase band of microtubules controls the robustness of division orientation in plants. *Science (New York, N.Y.)*, **356**, 186–189.

Schnittger, A., Schöbinger, U., Stierhof, Y.D. and Hülskamp, M. (2002) Ectopic B-type cyclin expression induces mitotic cycles in endoreduplicating Arabidopsis trichomes. *Current Biology*, **12**, 415–420.

Schnittger, A., Weinl, C., Bouyer, D., Schobinger, U. and Hulskamp, M. (2003) Misexpression of the Cyclin-Dependent Kinase Inhibitor ICK1/KRP1 in Single-Celled Arabidopsis Trichomes Reduces Endoreduplication and Cell Size and Induces Cell Death. *the Plant Cell Online*, **15**, 303–315.

Schoof, H., Lenhard, M., Haecker, A., Mayer, K.F.., Jürgens, G. and Laux, T. (2000) The Stem Cell Population of Arabidopsis Shoot Meristems Is Maintained by a Regulatory Loop between the CLAVATA and WUSCHEL Genes. *Cell*, **100**, 635–644.

Schutter, K. De, Joubès, J., Cools, T., *et al.* (2007) Arabidopsis WEE1 kinase controls cell cycle arrest in response to activation of the DNA integrity checkpoint. *The Plant cell*, **19**, 211–25.

Schwab, B., Mathur, J., Saedler, R., Schwarz, H., Frey, B., Scheidegger, C. and Hülskamp, M. (2003) Regulation of cell expansion by the DISTORTED genes in Arabidopsis thaliana: Actin controls the spatial organization of microtubules. *Molecular Genetics and Genomics*, **269**, 350–360.

Serrani, J.C., Fos, M., Atarés, A. and García-Martínez, J.L. (2007) Effect of gibberellin and auxin on parthenocarpic fruit growth induction in the cv Micro-Tom of tomato. *Journal of Plant Growth Regulation*, **26**, 211–221.

Shan Wu, Han Xiao, Antonio Cabrera, Tea Meulia, and E. van der K. (2011) SUN Regulates Vegetative and Reproductive Organ Shape. *Plant physiology*, **157**, 1175–1186.

Shi, Q. and King, R.W. (2005) Chromosome nondisjunction yields tetraploid rather than aneuploid cells in human cell lines. *Nature*, **437**, 1038–1042.

Shoji, T., Narita, N.N., Hayashi, K., Hayashi, K., Asada, J., Hamada, T., Sonobe, S., Nakajima, K. and Hashimoto, T. (2004) Plant-specific microtubule-associated protein SPIRAL2 is required for anisotropic growth in Arabidopsis. *Plant physiology*, **136**, 3933–44.

Smith, L.G., Gerttula, S.M., Han, S. and Levy, J. (2001) Tangled1: a microtubule binding protein required for the spatial control of cytokinesis in maize. *The Journal of cell biology*, **152**, 231–6.

Soyk, S., Lemmon, Z.H., Oved, M., *et al.* (2017) Bypassing Negative Epistasis on Yield in Tomato Imposed by a Domestication Gene. *Cell*, **169**, 1142–1155.e12.

Spinner, L., Gadeyne, A., Belcram, K., *et al.* (2013) A protein phosphatase 2A complex spatially controls plant cell division. *Nature Communications*, **4**, 1863.

Steele, N.M., McCann, M.C. and Roberts, K. (1997) Pectin Modification in Cell Walls of Ripening Tomatoes Occurs in Distinct Domains. *Plant physiology*, **114**, 373–381.

Storchova, Z. and Pellman, D. (2004) From polyploidy to aneuploidy, genome instability and cancer. *Nature Reviews Molecular Cell Biology*, **5**, 45–54.

Su'udi, M., Cha, J.-Y., Jung, M.H., Ermawati, N., Han, C., Kim, M.G., Woo, Y.-M. and Son, D. (2012) Potential role of the rice OsCCS52A gene in endoreduplication. *Planta*, **235**, 387–397.

Sugimoto-Shirasu, K. and Roberts, K. (2003) "Big it up": endoreduplication and cell-size control in plants. *Current Opinion in Plant Biology*, **6**, 544–553.

Szymanski, D. and Staiger, C.J. (2018) The Actin Cytoskeleton: Functional Arrays for Cytoplasmic Organization and Cell Shape Control. *Plant physiology*, **176**, 106–118.

Szymanski, D.B. and Cosgrove, D.J. (2009) Dynamic Coordination of Cytoskeletal and Cell Wall Systems during Plant Cell Morphogenesis. *Current Biology*, **19**, R800–R811.

Szymanski, D.B., Marks, M.D. and Wick, S.M. (1999) Organized F-actin is essential for normal trichome morphogenesis in Arabidopsis. *The Plant cell*, **11**, 2331–2347.

Tanksley, S.D. (2004) The Genetic , Developmental , and Molecular Bases of Fruit Size and Shape Variation in Tomato. *the Plant Cell*, **16**, 181–189.

Tomato Genome Consortium (2012) The tomato genome sequence provides insights into fleshy fruit evolution. Supp data. *Nature*, **485**, 635–41.

Umeda, M., Umeda-Hara, C. and Uchimiya, H. (2000) A cyclin-dependent kinase-activating kinase regulates differentiation of root initial cells in Arabidopsis. *Proceedings of the National Academy of Sciences of the United States of America*, **97**, 13396–13400.

Valente, P., Tao, W. and Verbelen, J.P. (1998) Auxins and cytokinins control DNA endoreduplication and deduplication in single cells of tobacco. *Plant Science*, **134**, 207–215.

Vandepoele, K., Raes, J., Veylder, L. De, Rouzé, P., Rombauts, S. and Inzé, D. (2002) Genome-wide analysis of core cell cycle genes in Arabidopsis. *The Plant cell*, **14**, 903–16.

Verkest, A., Manes, C.-L. de O., Vercruysse, S., *et al.* (2005) The cyclin-dependent kinase inhibitor KRP2 controls the onset of the endoreduplication cycle during Arabidopsis leaf development through inhibition of mitotic CDKA;1 kinase complexes. *The Plant cell*, **17**, 1723–36.

Vestal, D.J. and Jeyaratnam, J.A. (2011) The guanylate-binding proteins: emerging insights into the biochemical properties and functions of this family of large interferon-induced guanosine triphosphatase. *Journal of interferon & cytokine research : the official journal of the International Society for Interferon and Cytokine Research*, **31**, 89–97.

Veylder, L. De, Beeckman, T., Beemster, G.T., *et al.* (2001) Functional analysis of cyclin-dependent kinase inhibitors of Arabidopsis. *The Plant cell*, **13**, 1653–68.

Veylder, L. De, Beeckman, T., Beemster, G.T.S., *et al.* (2002) Control of proliferation , endoreduplication and differentiation by the Arabidopsis E2Fa ± DPa transcription factor. *EMBO Journal*, **21**, 1360-1368.

Vieira, P. and Almeida Engler, J. de (2017) Plant Cyclin-Dependent Kinase Inhibitors of the KRP Family: Potent Inhibitors of Root-Knot Nematode Feeding Sites in Plant Roots. *Frontiers in plant science*, **8**, 1514.

Vieira, P., Engler, G. and Almeida Engler, J. de (2012) Whole-mount confocal imaging of nuclei in giant feeding cells induced by root-knot nematodes in Arabidopsis. *New Phytologist*, **195**, 488–496.

Vitrat, N., Cohen-Solal, K., Pique, C., Couedic, J.-P. Le, Norol, F., Larsen, A.K., Katz, A., Vainchenker, W. and Debili, N. (1998) Endomitosis of Human Megakaryocytes Are Due to Abortive Mitosis. *Blood*, **85**, 402–13.

Walker, J.D., Oppenheimer, D.G., Concienne, J. and Larkin, J.C. (2000) SIAMESE, a gene controlling the endoreduplication cell cycle in Arabidopsis thaliana trichomes. *Development*, **127**, 3931–3940.

Wang, H., Zhou, Y., Gilmer, S., Whitwill, S. and Fowke, L.C. (2000) Expression of the plant cyclin-dependent kinase inhibitor ICK1 affects cell division, plant growth and morphology. *The Plant Journal*, **24**, 613–623.

Weimer, A.K., Demidov, D., Lermontova, I., Beeckman, T. and Damme, D. Van (2016) Aurora Kinases Throughout Plant Development. *Trends in Plant Science*, **21**, 69–79.

Wu, S., Xiao, H., Cabrera, A., Meulia, T., Van der Knaap, E. (2011) SUN regulates vegetative and reproductive organ shape by changing cell division patterns. *Plant physiology,* **157**, 1175-86.

Xiao, H., Jiang, N., Schaffner, E., Stockinger, E.J. and Knaap, E. van der (2008) A retrotransposon-mediated gene duplication underlies morphological variation of tomato fruit. *Science (New York, N.Y.)*, **319**, 1527–30.

Xu, C., Liberatore, K.L., MacAlister, C.A., *et al.* (2015) A cascade of arabinosyltransferases controls shoot meristem size in tomato. *Nature Genetics*, **47**, 784–792.

Yanagisawa, M., Desyatova, A.S., Belteton, S.A., Mallery, E.L., Turner, J.A. and Szymanski, D.B. (2015) Patterning mechanisms of cytoskeletal and cell wall systems during leaf trichome morphogenesis. *Nature Plants*, **1**, 15014.

Yu, Y., Steinmetz, A., Meyer, D., Brown, S. and Shen, W.-H. (2003) The tobacco A-type cyclin, Nicta;CYCA3;2, at the nexus of cell division and differentiation. *The Plant cell*, **15**, 2763–77.

Zhang, D. and Yang, L. (2014) Specification of tapetum and microsporocyte cells within the anther. *Current Opinion in Plant Biology*, **17**, 49–55.

Zhang, N., Brewer, M.T. and Knaap, E. van der (2012) Fine mapping of fw3.2 controlling fruit weight in tomato. *Theoretical and Applied Genetics*, **125**, 273–284.

Zhang, T., Wang, X., Lu, Y., Cai, X., Ye, Z. and Zhang, J. (2013) Genome-wide analysis of the cyclin gene family in tomato. *International journal of molecular sciences*, **15**, 120–40.

Zhu, G., Wang, S., Huang, Z., *et al.* (2018) Rewiring of the Fruit Metabolome in Tomato Breeding. *Cell*, **172**, 249–261.e12.

Zimmermann, I., Saedler, R., Mutondo, M. and Hulskamp, M. (2004) The Arabidopsis GNARLED gene encodes the NAP125 homolog and controls several actin-based cell shape changes. *Molecular Genetics and Genomics*, **272**, 290–296.

Zou, Z., Meng, Z., Ma, C., Liang, D., Sun, R. and Lan, K. (2017) Guanylate-Binding Protein 1 Inhibits Nuclear Delivery of Kaposi's Sarcoma-Associated Herpesvirus Virions by Disrupting Formation of Actin Filament. *Journal of Virology*, **91**, e00632-17.

A B S T R A C T TOWARDS THE IDENTIFICATION AND CHARACTERIZATION OF NEW NEGULATORS OF FRUIT TISSUE MORPHOLOGY

Fruit size and morphology are key characters defining the final fruit quality. Among the large fruit diversity observed in the nature, human domestication and selection has induced changes in fruit size and tissue morphology. Only a few genetic regulators have been identified so far, thus cellular and molecular mechanisms by which fruit tissue morphology is defined remain incomplete. In this context, the aim of my thesis is to identify and characterize new regulators of fruit tissue morphology. For this purpose, I used a collection of tomato EMS mutants as a source of genetic and phenotypic diversity. I selected two mutants presenting opposite trends of pericarp thickness. Through a mapping-by-sequencing strategy, I identified a genetic region on chromosome 10, associated with an extreme thick pericarp phenotype. I also investigated the role of the Guanylate Binding Protein (GBP) at the origin of a thin pericarp phenotype. The GBP is a large GTP binding protein that was never characterized in plants so far. In order to go deeper into its functional characterization in plants, I studied in parallel the role of the protein in tomato and *Arabidopsis thaliana* models. I showed that both homolog proteins are localized at the nucleus. Mutation of GBP in tomato induced strong alterations in cell division and cell expansion inside the pericarp and altered lateral root growth in tomato and *Arabidopsis*, a classical feature for mutants impaired in mitosis. This study suggests a role for the GBP in the fine control of cell division in the tomato pericarp.

Key words: fruit, tomato, tissue morphology, cell division, mutant, forward genetics

R E S U M E VERS L'IDENTIFICATION ET LA CARACTERISATION DE NOUVEAUX REGULATEURS DE LA MORPHOLOGIE DES TISSUS DU FRUIT

La taille du fruit et la morphologie des tissus du fruit sont des caractères clés définissant la qualité finale du fruit. Parmi la grande diversité de fruits observée dans la nature, la domestication et la sélection ont entraîné d'importantes modifications de la taille et de la morphologie des tissus du fruit. Jusqu'à présent, seuls quelques régulateurs génétiques ont été identifiés, et les mécanismes cellulaires et moléculaires par lesquels la morphologie des tissus du fruit est définie restent imprécis. Dans ce contexte, l'objectif de ma thèse est d'identifier et de caractériser de nouveaux régulateurs impliqués dans la morphologie des tissus du fruit. Pour cela, j'ai utilisé une collection de mutants EMS de tomate comme source de diversité génétique et phénotypique et j'ai sélectionné deux mutants présentant des tendances opposées et extrêmes d'épaisseur du péricarpe. Grâce à une stratégie de cartographie par séquençage, j'ai identifié une région génétique du chromosome 10, associée au phénotype péricarpe épais. J'ai également étudié le rôle de la Guanylate Binding Protein (GBP) à l'origine du phénotype péricarpe fin chez la tomate. La GBP est une grosse GTP binding protein qui n'a jamais été caractérisée chez les plantes. Afin d'approfondir l'étude de cette protéine, j'ai étudié en parallèle son rôle dans les modèles tomate et *Arabidopsis thaliana*. J'ai démontré que les deux protéines homologues sont localisées dans le noyau. La mutation de la GBP chez la tomate induit de fortes altérations de la division et de l'expansion cellulaire à l'intérieur du péricarpe ainsi qu'une altération de la croissance des racines latérales chez la tomate et *Arabidopsis*, une caractéristique classiquement retrouvée chez les mutants altérés dans la mitose. Cette étude suggère que le GBP joue un rôle dans le contrôle précis des divisions cellulaires dans le péricarpe de tomate.

Mots clés : fruit, tomate, morphologie des tissus, division cellulaire, mutant, génétique directe